University of Hyderabad

DOCTORAL THESIS

Structural and Magnetic Properties of Some Ferrite Nanoparticles and Study of Magneto-viscosity of Corresponding Ferrofluids

A thesis submitted in partial fulfillment of the award of the degree of Doctor of Philosophy



By

Nisha Gautam

School of Physics University of Hyderabad Hyderabad- 500 046 Telangana, INDIA

July, 2021



DECLARATION

I hereby declare that the matter embodied in this thesis entitled, "Structural and Magnetic Properties of Some Ferrite Nanoparticles and Study of Magneto-viscosity of Corresponding Ferrofluids", is the result of investigations carried out by me in the School of Physics, University of Hyderabad, Hyderabad, India under the supervision of Professor Rajender Singh and Dr. V. Ashok.

Place: Hyderabad

Date: 13/07/2021

Nisha Gazitam

Nisha Gautam

Reg. No. 14PHPH01



CERTIFICATE

This is to certify that the thesis entitled, "Structural and Magnetic Properties of Some Ferrite Nanoparticles and Study of Magneto-viscosity of Corresponding Ferrofluids", submitted by Ms. Nisha Gautam bearing Reg. No. 14PHPH01 in partial fulfillment of the requirements for the award of Doctor of Philosophy in the School of Physics is a bonafide work carried out by her under my direct supervision.

This thesis is free from plagiarism and has not been submitted previously in part or in full to this or any other University or Institution for the award of any degree or diploma.

Further, the student has the following publications and conference proceedings before the submission of the thesis for adjudication.

Papers in Refereed Journals

1. Magneto Magneto-viscosity of stable colloidal solutions of Barium-strontium hexaferrite ferrofluid

Nisha Gautam and R. Singh

Materials Research Express 6 (2019).

2. Magnetoviscosity of Hydrothermal synthesized Cu-Zn ferrite ferrofluids

Nisha Gautam, Gadipally Tirupathi and Rajender Singh

AIP Advances, 7 (2017).

3. Magnetoviscosity of Paraffin based barium Ferrite Ferrofluid

Nisha Gautam, Gadipally Tirupathi and Rajender Singh

Conference Proceeding

1. Magneto-viscosity of platelets shaped Ba-Sr Ferrite nanoparticles based Ferrofluid in different", colloids

Nisha Gautam and R. Singh

AIP Conference Proceedings **2115**, 030153 (**2019**).

2. Effect of Zn-doping on structural and magnetic properties of copper ferrite nanoparticles

Nisha Gautam, Gadipally Tirupathi and Rajender Singh

AIP Conference Proceeding 1731, 050099 (2016).

3. Magneto-viscosity of platelet shaped Ba-Sr ferrite nanaoparticles based ferrofluid in different colloids

Nisha Gautam and Rajender Singh

AIP Conference Proceeding 2115, 030153 (2019).

Manuscripts under preparation

1. Structure, magnetic and magneto-viscosity study of Fe₃O₄ nanoparticles and ferrofluids.

Nisha Gautam and Rajender Singh

(To be communicated)

2. Magneto-viscosity of Cu-Zn ferrite based ferrofluids

Nisha Gautam and Rajender Singh

(To be communicated)

Presentations at Conferences

1. National Conference on Frontiers in Physics (FIP) held at University of Hyderabad, Hyderabad during 17th -18th October 2014, participated.

- 25th National Symposium on Cryogenics (NSC-2014) held at School of Physics, University of Hyderabad, Hyderabad during 8th – 10th December 2014, participated.
- 3. 1st National Conference on Advanced Nanomaterials(CAN-2015) held at Department of Physics, Nirmalagiri college, Kannur, Kerala-670701 during 1st and 2nd October 2015, Poster Presentation "Magnetic And Structural Properties of Cu-Zn ferrite Nanoparticles".
- 4. International Conference on Magnetic Materials and Applications (ICMAGMA-2015) held at School of Advanced Sciences, VIT University, Vellore during 2nd-4th December 2015, <u>Poster Presentation</u> "Magneto-viscosity of Water Based Cu-Zn Ferrite Ferrofluid."
- 5. 60th National DAE Solid State Physics Symposium (DAE SSPS-2015) held at Amity University, Uttar Pradesh, Noida during 21-25 2015, <u>Poster Presentation</u>, "Effect of Zn-doping on Structural and Magnetic Properties of Copper Ferrite Nanoparticles".
- 6. 60th Annual Conference on Magnetism and Magnetic Materials (MMM-2015), <u>Poster Presentation</u> on "Magneto-viscosity of Paraffin Based Barium Ferrite Ferrofluid".
- 7. National Conference on Frontiers in Physics (FIP) held at University of Hyderabad, Hyderabad during 28th -29th March 2016, <u>Poster Presentation</u> "Magneto-viscosity of Hydrothermal Synthesized Cu-Zn Ferrite Ferrofluid" (got best poster award).
- 8. 61st Annual Conference on Magnetism and Magnetic Materials (MMM-2016) held at New Orleans, LA, USA during 31st October -4th November, 2016, Poster Presentation "Magneto-viscosity of Hydrothermal Synthesized Cu-Zn Ferrite Ferrofluids".

- 9. International Conference on Complex Fluids (COM-FLU 2016), held at IIIT, Hyderabad during 12th 14th December 2016, Poster Presentation on "Magnetic field dependent Particle Tracking Micro rheology of the Cu-Zn Ferrite Ferrofluids".
- 10. International Conference on Magnetic Materials and Applications (ICMAGMA-2017) held at Leonia, Shameerpet, Hyderabad during 1st-3rd February 2017, Poster Presentation "Synthesis and Magneto- viscosity of Paraffin based Cu-Zn Ferrite Ferrofluid".
- 11. National Conference on 'Physics at Small Scales and Advanced Materials' 2017 held at University of Hyderabad during 8th to 9th September 2017, Poster Presentation "Structural and Magneto-viscosity of Water and Silica oil based Ba-Sr Ferrite Ferrofluids".
- 12. 62nd Annual Conference on Magnetism and Magnetic Materials (MMM-2017) held at Pittsburg, USA during 6th to 10th November 2017, <u>Poster Presentation</u> "Magneto-viscosity of Ba-Sr Ferrite Ferrofluid in different Colloids".
- 13. Workshop on "Processing and Characterization of Thin Films" organized by University of Hyderabad, Hyderabad India, 3rd -9th January 2018, (participated).
- 14. Workshop on " Functional Magnetic Materials" organized by University of Hyderabad, Hyderabad India 26th February 3rd March 2018, (participated).
- 15. International Conference on Magnetic Materials and Applications (ICMAGMA-2018) held at School of Physical Sciences, National Institute of School Education and Research (NISER), Bhubaneswar, Odisha-India during 9th-13th December 2018, Poster Presentation "Magneto-viscosity of Platelets Shaped Nanoparticles Based Ferrofluid in different Colloids".
- 16. Workshop on "Soft and active matter" organized by University of Hyderabad, Hyderabad India 11th to 17th February, 2018, (participated).

- 17. 63rd DAE Solid State Physics Symposium (DAE SSPS-2018) held at Guru Jambheshwar University of Science and Technology, Hisar, India during 18-22 December, 2018, <u>Poster Presentation</u>, "Magneto-viscosity of platelet shaped Ba-Sr ferrite nanoparticles based ferrofluid in different colloids" (got best poster award).
- 18. 5th International Conference on Nano science and Nanotechnology (ICONN-2019) to be held at SRM IST during Jan 28-30, 2019, <u>Poster Presentation</u> "Magneto-viscosity of Stable colloidal solutions of Barium-Strontium Hexaferrite Ferrofluid".
- 19. 6th International Conference on Nanoscience and Nanotechnology (Virtual Conference) to be held at SRM IST during February 1st -3rd, 2021, <u>Poster Presentation</u> "Magneto-viscosity of Cu-Zn ferrite based ferrofluid".



Further, the student has passed the following courses towards the fulfillment of course-work required for Ph.D.

S. No.	Course code	Name	Credits	Pass/Fail
1	PY801	Advanced quantum mechanics	4	Pass
2	PY803	Advanced Statistical mechanics	4	Pass
3	PY804	Advanced electromagnetic theory	4	Pass
4	PY821	Research Methodology	4	Pass

Dean

School of Physics

DEAN

School of Physics University of Myderabad HYDERABAD - 500 046. Professor Rajender Singh Thesis Supervisor

School of Physics

HYD-46 CO

Dr. V. Ashok

Thesis Supervisor School of Physics

Ashok Vudayagiri
School of Physics
University of Hyderabad
Central University P.O.
Hyderabad-500 046.

ACKNOWLEDGEMENTS

First of all, I would like to express my deepest appreciation to my adviser, Professor Rajender Singh. Without his enormous support and valuable guidance, I can hardly imagine that I would have learnt so much during the past six years. He is one of the smartest persons and the kindest human beings, I wish, I could be as energetic and enthusiastic as him. Dr. Rajender has provided insightful discussions about research regarding my thesis but also has given me freedom to pursue various experiments that really enhanced my knowledge in magnetism and rheology of ferrofluids fields. In addition, I am very grateful to Professor Rajender's help and suggestions on my future career.

I would like to give my great thanks to Dr. V. Ashok for supporting me in many ways. I am especially thankful to him for his important role in my Ph.D. career. He is an extremely knowledgeable, wonderful and warm person.

I would like to thank my doctoral committee members of my Ph.D. committee, Professor S. V. S. Nageswara Rao and Dr. Venkataiah Gorige for their helpful discussions and advice. I am grateful to Prof. Surajeet Dhara for allowing me to use Rheometer in carrying out the rheology measurements.

I wish to thank Mr. Sudhakar and Ms. Joyti for X-Ray Diffraction (XRD) measurements, Mrs. Arundhathi and Ms. Sunitha for Field Emission Scanning Electron Microscopy (FESEM) measurements, and Mr. Drugaprasad and Mr. Pankaj for Transmission Electron Microscopy (TEM) measurements. I would like to thank Mr. T. Abraham, Mrs. Deepika, Mr. Sudarshan, Mrs. Shailaja, Mr. Prasad, and other non-teaching staff. I would like to thank CIL staff Dr. Manjunath, Mr. Suresh, Dr. Ahmed, Mr. Sudhakar, Mr. Mantoo, Mr. Giri and Mr. Sai for the technical support.

I would like to thank UGC-RGNF and University of Hyderabad, India for the financial relief.

I express my gratitude to my lab mates Dr. Ramesh, Dr. Padmawati, Dr. Jasmeet, Dr. Ravi and Dr. Atiya for their amusing company and support. I would like to give special thanks to my senior lab mate as well as brother Dr. G. Tirupathi for his brilliant ideas and discussions which were beneficial to drive my PhD and made me learn many things in my research area. I express my gratitude to Dr. Lakshun Naidu for his valuable enormous support and deep knowledge. I am also grateful to Dr. Rasmita Sahoo for rheology measurements and Dr. Binoy Krishna Hazra and Dr. Joshi for their help in magnetic measurements.

I would like to thanks my friends at the School of Physics, Dr. Shantanu, Dr. Dharunjay, Dr. Pundareekam, Mr. Mahender, Mr. Pradeep, Dr. Junaid, Dr. Chakradhara, Mr. Prakash, Mr Avisek, Mr. Naresh, Ms. Manasa, Ms. Leelashree, Mr. Praveen, Mr. Dinesh, Mr. Vinod, Ms. Aishwarya and all other SoP friends. I especially thank my friends Dr. Anupama, Dr. Atiya, Ms. Pooja, Ms. Atasi, Ms. Jhansi, Ms. Poonam and Ms. Arti for their joyful company, friendship and support. I would specially like to thank Mr. Gopi Swamy for his care and enormous support in many ways. I would like to thank Mr. Sreenu and Mr. Sohail for their care and support.

Above all, I would like to thank my parents Mrs. Shashi Gautam (mother) and Mr. Bhagwaan Deen Gautam (father), my elder brothers Mr. Anil Kumar-Mrs. Soni (sister in law) and Jitender Kumar, my sister Mrs. Shikha-Mr. Sujeet (Brother in law) and all other family members for their constant support and blessings. Their never-ending love, constant care, encouragement and enough freedom to acquire knowledge made me free from agonize and gave me strength to pursue me in my PhD as well as throughout my entire life. I would like to thank Mr. Sanjay for his constant support and encouragement during tough times of my Ph.D. duration.

Dedicated to

My Family Members

[Mrs. Shashi Gautam, Mr. Bhagwan Deen Gautam &

Mr. Ramesh Chandra, Mrs. Meenu Chandra and other family members]

Abstract

The magnetic materials are massively used for different purpose and applications. Spinel ferrite is most extensively used ferrite due to its large electrical resistivity and low eddy current. Superparamagnetic nanoparticles easily demagnetize with field. The superparamagnetic type of spinel ferrites made a large enhancement in ferrofluids based technologies such as contrast MRI, drug delivery, hyperthermia and biosensors etc. The objective of the present work is to synthesis magnetic nanoparticles and study their structural and magnetic properties. The second part is to prepare ferrofluids in various media using the synthesised nanoparticles.

Three different types of ferrite (Fe₃O₄, Cu-Zn ferrite and Ba-Sr ferrite) nanoparticles are synthesized. The structural properties are measured by X-ray diffraction, field emission scanning electron microscope, transmission electron microscope and particle size analyser. The results demonstrated the formation of spinel and hexaferrite structure with different shape and particle size distribution of the nanoparticles. The magnetic behaviour of nanoparticle investigated by the DC-magnetization vs. magnetic field and magnetization vs temperature measurements.

Ferrofluid is the combination of colloidal suspension of magnetic nanoparticles in a liquid media which responds to the external applied magnetic field. It has the quality to change the physical properties in the presence of external magnetic field i.e magneto viscosity effect (MVE). The surfactant is used to coat the nanoparticles to prevent the agglomeration and cluster formation. The viscosity of ferrofluid is controlled by applying magnetic force. The results clearly indicate that the viscosity variation with magnetic field is strongly dependent on the nature of carrier fluid and the shear rates. The flow curves show the power law behaviour of viscosity vs shear rate or non- Newtonian behaviour for all ferrofluids in the absence as well as in the presence of magnetic field. The yield stress is calculated from the extrapolation of the shear stress vs. shear rate using Herschel-Bulkley model. In shear the stability of

chains of nanoparticles of different shapes and sizes is different. So, no general conclusion can be made about the influence of the geometric shape of nanoparticles on the MVEs in ferrofluids. The concentrated ferrofluid based on platelet BSM nanoparticles gives much higher MVE compared to other ferrofluids.

The present study can serve as the basis for selecting a ferrofluid for a particular type of application; particularly, when a ferrofluid with a high MVE is needed.

Contents

CHAPTEK-1	1
Introduction	1
1.1 Magnetic materials	1
1.1.1 Diamagnetic materials:	1
1.1.2 Paramagnetic materials:	1
1.1.3 Ferromagnetic materials:	2
1.1.4 Antiferromagnetic materials:	2
1.1.5 Ferrimagnetic materials	2
1.1.6 Superparamagnetic materials:	2
1.1.7 Spin glasses	2
1.2 Ferrites and their Applications	3
1.3 Nanoparticles	7
1.3.1 Fe ₃ O ₄ Nanoparticles	7
1.4 Rheology	8
1.5 Properties of ferrofluids and their applications	8
1.5.1 Surfactant	9
1.6 Types of fluids: There are different types of fluids based on their	properties.
	10
1.6.1 Ideal fluid:	10
1.6.2 Newtonian and Non Newtonian behaviour:	11
1.6.3 Bingham plastic (BP) and Herschel –Bulkley (HB) fluid	11
1.6.4 Thixotropic & Rheopectic Fluid	12

1.7 Flow Models:	12
1.7.1 Bingham plastic model	13
1.7.2 Power law behaviour for fluids:	13
1.7.3 Herschel-Bulkley model for fluids:	14
1.8 "Magneto viscosity" in Ferrofluids	15
1.9 Aim	16
1.10 Objectives of the present work:	16
1.11 Thesis Organization	17
References:	18
CHAPTER-2	25
Material Preparation and Experimental Techniques	25
2.1 Synthesis methods of ferrite nanoparticles	25
2.1.1 Synthesis procedure for magnetite "nanoparticles":	26
2.1.2 Synthesis of Cu _{1-x} Zn _x Fe ₂ O ₄ (CZF) nanoparticles:	26
2.1.3 Synthesis of Hydrothermalized CZF nanoparticles:	28
2.1.4 Synthesis of Ba _{1-x} Sr _x Fe ₁₂ O ₁₉ (x=0, 0.05, 0.1, 0.2, and 0.5) Nanoparti	icles:
	29
2. 2 X'-ray Powder diffraction	31
2. 2. 1 X-rays:	31
2. 2. 2 Rietveld refinement:	32
2. 3 "Field Emission – Scanning Electron Microscope" (FE-SEM)	33
2.4 "High Resolution - Transmission Electron Microscopy" (HR-TEM)	34
2. 5 Particle Size Analyzer:	36

2.6 "Physical Property Measurement System" - Vibrati	ng Sample
Magnetometer (PPMS -VSM):	37
2. 6. 1 Working principle of VSM	37
2. 7 Ferromagnetic resonance (FMR)	38
2.7.1 Experimental Set-Up for FMR	38
2. 7. 2 Microwave Unit	39
2.7.3 The "Cavity"	39
2.7.4 Signal Channel	40
2.7.5 "Magnetic Field Controller"	40
2.7.6 The User (operator) Interface:	40
2.8 Rheometer:	40
References:	43
CHAPTER-3	45
Studies on Fe ₃ O ₄ nanoparticles and ferrofluids	45
3.1 Studies on Fe ₃ O ₄ nanoparticles	45
3.1.1 Structural Studies	45
3.1.2 Morphological Studies	46
3.1.3 Particle size distribution and zeta potential	47
3.1.4 Magnetization studies	48
3.2 Studies on ferrofluids	49
3.2.1 Magneto-viscosity of water based ferrofluid	50
3.2. 2 Toluene based Ferrofluid	51
3 2 3 Paraffin oil based Ferrofluid	.51

3.2.4 Silicone oil based Ferrofluid	51
3.3 Flow Curves of Fe ₃ O ₄ Ferrofluids	54
3.4 Shear stress of different Fe ₃ O ₄ Ferrofluids:	56
References:	59
CHAPTER-4	61
Studies on Cu-Zn (CZF) Ferrite nanoparticles and ferrofluids	61
4.1 Study of Co-precipitated CZF (C-CZF) nanoparticles	61
4.1.1 "Structural studies":	61
4.1.2 Morphological Analysis	63
4.1.3 TEM Analysis	64
4.1.4 Particle size distribution and zeta potential	66
4.1.5 Magnetization Studies of C-CZF nanoparticles:	68
4.1.6 Rheological study of C-CZF based ferrofluids:	72
4.2: Study of hydrothermalized (H- CZF) nanoparticles:	77
4.2.1 "XRD" results:	77
4.2.2 FESEM Results	79
4.2.3 TEM Analysis	80
4.2.4 Particle size distribution and zeta potential	83
4.2.5 Magnetization Studies	84
4.3 Study H-CZF based ferrofluids	87
4.3.1 Magneto-viscosity plots of water based H- CZF ferrofluids:	87
4.3.2 "Magneto-viscosity" plots of "paraffin" based H- CZF ferrofluid	s:90
4 3 3 Shear Stress in Paraffin oil based ferrofluids:	9/1

References:
CHAPTER-510
Studies on Ba-Sr ferrite (BSM) nanoparticles and ferrofluids10
5.1 Study of Ba-Sr ferrite nanoparticles
5.1.1 "Structural" studies:
5.1.2 Morphological study:
5.1.3 Magnetic Properties
5.2 Study of Ba-Sr ferrofluids:
5.2.1 Magneto-viscosity of BaFe ₁₂ O ₁₉ ferrofluids:
5.2.2 Magneto-viscosity of Ba _{0.95} -Sr _{0.05} Fe ₁₂ O ₁₉ ferrofluids in different colloids
11
5.2.3 "Magneto-viscosity" of Ba _{0.9} -Sr _{0.1} Fe ₁₂ O ₁₉ ferrofluids in different colloids
5.2.4 Magneto-viscosity of Bao.8-Sro.2Fe12O19 Ferrofluids in different solvents
5.2.5 Magneto-viscosity of Ba _{0.5} -Sr _{0.5} Fe ₁₂ O ₁₉ Ferrofluids:12
5.2.6 Herschel-Bulkley behaviour in ferrofluids:
5.2.7 Magneto Sweep
5.2.8 Inverse Ferrofluids
References:
CHAPTER-614
Summary and Conclusions14
Summary

6.1 Important Conclusions on Studies on Nanoparticles	141
6.2 Important Conclusions on Studies on Ferrofluids	.143
6.3 Future Scope	.145

List of Figures:

Figure 1. 1 Schematic diagrams for spinel ferrite.	4
Figure 1. 2 Spikes formation in ferrofluid with applied magnetic field.	9
Figure 1. 3 Surfactant coated magnetic nanoparticles with and without field	10
Figure 1. 4 Hydrophilic and Hydrophobic behaviour	10
Figure 1. 5 General flow actions	11
Figure 1. 6 Types of flow for fluids.	12
Figure 1. 7 Thixotropic and rheopectic fluid	12
Figure 1. 8 Bingham plastic flows.	13
Figure 2. 1Schematic methods for synthesize different ferrites ferrofluid	25
Figure 2. 2Diffraction from Bragg's equation.	32
Figure 2. 3Atomic form factor for X-ray (and neutron) against angle.	32
Figure 2. 4 Schematic diagram of FESEM	34
Figure 2. 5 TEM schematic diagram.	35
Figure 2. 6 Schematic diagram of the interaction between electron beam and san	nple
surface	36
Figure 2. 7 Schematic diagram for an X-band EPR spectrometer	39
Figure 2. 8 MCR 501 rheometer	41
Figure 3. 1 XRD pattern of Fe ₃ O ₄ nanoparticles	46
Figure 3. 2FESEM micrograph of Fe ₃ O ₄ nanoparticles.	47
Figure 3. 3Fe ₃ O ₄ nanoparticles distribution (a) and zeta potential (b)	48

Figure 3. 4 Magnetization curve for Fe ₃ O ₄ nanoparticles
Figure 3. 5 ESR signals for Fe ₃ O ₄ nanoparticles
Figure 3. 6 Magneto-viscosity plots of water, toluene, paraffin and "silicone oil" based
ferrofluids51
Figure 3. 7 Colloidal effect in water, toluene, paraffin and silicone oil based ferrofluids
at zero field55
Figure 3. 8 Flow curves of different Fe ₃ O ₄ ferrofluids at various magnetic fields55
Figure 3. 9 Shear stress vs. shear rate at various fields
Figure 4. 1 XRD spectra of C-CZF nanoparticles62
Figure 4. 2 FESEM images of C-CZF nanoparticles
Figure 4. 3 "TEM micrographs" for C-CZF nanoparticles66
Figure 4. 4 Particle size distribution of C-CZF nanoparticles67
Figure 4. 5 Zeta potential of C-CZF nanoparticles
Figure 4. 6 Magnetization curves for C-CZF nanoparticles
Figure 4. 7 Magnetization vs. Zn-content of C-CZF nanoparticles70
Figure 4. 8 FC and ZFC curves of C-CZF nanoparticles at applied field of 100 Oe71
Figure 4. 9 Effect of composition of CZF on viscosity of toluene based ferrofluids at
H=0
Figure 4. 10 Flow curves of CZF toluene based ferrofluids respectively73
Figure 4. 11 Magneto-viscosity of $Cu_{1-x}Zn_xFe_2O_4$ (x= 0.2, 0.4, 0.6) toluene based
ferrofluids respectively
Figure 4. 12 Effect of composition of CZF paraffin based ferrofluids at H=0

Figure 4. 13 Flow curves of $Cu_{1-x}Zn_xFe_2O_4$ (x= 0.2, 0.4, 0.6) paraffin oil based ferm	ofluids
respectively	76
Figure 4. 14 Magneto-viscosity of CZF paraffin oil based ferrofluids	77
Figure 4. 15 XRD images of H-CZF.	78
Figure 4. 16 FESEM images of H- CZF	80
Figure 4. 17 TEM micrographs of H- CZF nanoparticles.	82
Figure 4. 18 Particle size distribution of H- CZF respectively	83
Figure 4. 19 Zeta potential of H-CZF nanoparticles	84
Figure 4. 20 Magnetization curves of H-CZF nanoparticles	85
Figure 4. 21 M (H) loops parameters for H- CZF nanoparticles	86
Figure 4. 22 FC and ZFC curves of H-CZF nanoparticles	87
Figure 4. 23 Effect of colloid in H-CZF water based ferrofluids at H=0	88
Figure 4. 24 Flow curves of H-CZF water based ferrofluids at H=0 to 1.33T	88
Figure 4. 25 Magneto-viscosity of H-CZF water based ferrofluids	90
Figure 4. 26 Effect of colloid in H-CZF paraffin oil based ferrofluids at H=0	91
Figure 4. 27 Flow curves of paraffin oil based H-CZF ferrofluids	92
Figure 4. 28 Magneto-viscosity of paraffin oil based H-CZF ferrofluids	93
Figure 4. 29 H-B model fit	95
Figure 5. 1 XRD of BSM nanoparticles.	101
Figure 5. 2 FESEM images of BSM nanoparticles	103
Figure 5.3 TEM micrographs of BSM nanoparticles	106
Figure 5.4 Particle size distribution of BSM nanoparticles.	107

Figure 5.5 Zeta Potential of BSM nanoparticles
Figure 5.6 Magnetization curves of BSM nanoparticles
Figure 5.7 FC and ZFC curves of BSM nanoparticles at 100 Oe110
Figure 5.8 Solvent and Colloidal effect in BSM ferrofluids at H=0113
Figure 5.9 Viscosity vs. shear rate of BMW, BMP and BMS ferrofluids114
Figure 5.10 Magneto-viscosities of water, paraffin and silicone oil based BSM ferrofluids
Figure 5.11 Magneto-viscosity of paraffin BM based FF117
Figure 5.12 Viscosity vs. shear rate for BMP ferrofluids
Figure 5.13 Viscosity vs. shear rate of BSM5W, BSM5P and BSM5S ferrofluids118
Figure 5.14 Magneto-viscosity at 1 and 10 s ⁻¹ of BSM ferrofluids120
Figure 5.15 Flow curves of paraffin and silicone oil based BSM ferrofluids121
Figure 5.16 Magneto-viscosity of paraffin and silicone oil based BSM ferrofluids123
Figure 5.17 Flow curves of water, paraffin and silicone oil based BSM ferrofluids124
Figure 5.18 Magneto-viscosity of water, paraffin and silicone oil based BSM ferrofluids of 1 and $10~{\rm s}^{\text{-1}}$ respectively.
Figure 5.19 Flow curves of water, paraffin and silicone oil based BSM ferrofluids126
Figure 5.20 Magneto-viscosity at 1 and 10 s ⁻¹ of water, paraffin and silicone oil based BSM50 ferrofluids.
Figure 5.21 H-B model fit for BMW, BSM5W and BSM50W ferrofluids129
Figure 5.22 H-B model fit for BMP and BSM10P ferrofluids
Figure 5.23 H-B model fit for BSM20S and BSM50S ferrofluids
Figure 5.24 Storage moduli (a) and loss moduli (b) of BMW and BSM5W ferrofluids

Figure 5.25 Schematic image of an inverse ferrofluids	.134
Figure 5.26 Viscosity vs. magnetic field of BSM10S ferrofluid	.135
Figure 5.27 Flow curve of BSM10S ferrofluid.	.135
Figure 5.28 Flow curve of shear rate of BSM10S ferrofluid.	.136

List of Tables:

Table 1.1: Classification of ferrite materials	3
Table 2.1: Fe ₃ O ₄ ferrofluids in various colloidal media.	26
Table 2.2: Properties of colloidal media.	27
Table 2.3: C-CZF ferrofluids in various colloidal media.	28
Table 2.4: H-CZF ferrofluids in various colloidal media.	28
Table 2.5: BSM ferrofluids in various colloidal media	29
Table 3.1: Fe ₃ O ₄ ferrofluid in different colloids.	50
Table 3.2: The fitting parameters of power law	55
Table 3.3: H-B model fitting parameters for FW ferrofluid.	57
Table 4.1: Crystallographic parameters for C- CZF nanoparticles	62
Table 4.2: Average particles size, particle distribution and zeta potential par	ameters.
	66
Table 4.3: M (H) parameters for C- CZF nanoparticles.	69
Table 4.4: Crystallographic parameters for H- CZF nanoparticles	78
Table 4.5: Average particle size, distribution and zeta potential parameters fo	
nanoparticles:	84
Table 4.6: Magnetization parameters of H- CZF nanoparticles	85
Table 4.7: Power-law fitting parameters for water based H-CZF ferrofluids	89

Table 4.8: The fitting parameters of power law for H-CZF ferrofluids are tabulated
below: 92
Table 4.9: H-B model fitting parameters95
Table 5.1: Crystallographic parameters for BSM nanoparticles
Table 5.2: Average particles size, hydrodynamic particle distribution and zeta
potential parameters106
Table 5.3: M (H) parameters for BSM nanoparticles
Table 5.4: Physical properties of colloidal
Table 5.5: The fitting parameters of power law for BM ferrofluids are tabulated below:
114
Table 5.6: The fitting parameters of power law for BSM5 ferrofluids119
Table 5.7: Fitting parameters of power law for BSM10 ferrofluids
Table 5.8: The fitting parameters of power law for BSM20 ferrofluids
Table 5.9: The fitting parameters of power law for BSM50 ferrofluids are tabulated
below:
Table 5.10: Shear stress, consistency and power index values for water based
ferrofluids129
Table 5.11: Shear stress, consistency and power index values for paraffin based
ferrofluid
Table 5.12: Shear stress, consistency and power index values for BSM20S and BSM50S
EE 122



CHAPTER-1

Introduction

1.1 Magnetic materials

Magnetic materials are massively used for different purpose and applications. Many years back the mankind understood the significance of the magnetic materials in their life. Since 1930, the studies of various properties of magnetic materials have been done extensively by many groups. The magnetic materials are useful in several applications" like; permanent magnets, "magnetic recording media", sensors, memory chips, activators and in biomedical applications such as hyperthermia, drug delivery and catalyst etc. [1-3]. The electrons and the magnetic dipoles present in magnetic material are the consequences of the magnetic properties with the applied magnetic field. Therefore, based on response to the external magnetic field materials "diamagnetic", "paramagnetic", are categorized into antiferromagnetic, "ferromagnetic" and "ferrimagnetic" materials [4].

1.1.1 Diamagnetic materials:

Usually, these types of materials are hardly magnetized when they come under the magnetic field. At given field the magnetic dipoles line up opposite to the field direction. Therefore, the induce magnetic field repels the applied field and the material oppose the field around it. It has a negative susceptibility which is independent to temperature. e.g.: water, inert gases, and "transition metals".

1.1.2 Paramagnetic materials:

When the field is present, these materials get magnetized due to the tendency of dipole moments alignment towards applied field direction. These materials follow

Chapter-1: Introduction

Curie's law with small and positive magnetic susceptibility. e.g.: Pt, Al and Copper sulphate.

1.1.3 Ferromagnetic materials:

These materials exhibit very strong magnetic nature. The interactions between magnetic dipoles are extremely strong and align parallel at given magnetic field. Alignment of magnetic dipoles in one direction is known as Weiss domain. The spontaneous magnetization is found in the ferromagnetic system even at zero applied field. e.g.: Ni, Gd, Fe, and Dy.

1.1.4 Antiferromagnetic materials:

These materials show the antiparallel arrangement of the neighboring atoms which is the cause of zero net magnetization. This order exists below Neel temperature (T_N) and the material is paramagnetic above T_N. e.g.: Zinc ferrite, hematite, metals, alloys and oxides.

1.1.5 Ferrimagnetic materials

These materials exhibit the imbalanced atoms or spin in the anti-parallel way due to that the net magnetic moment is non-zero. These materials show the extraordinary resistivity and anisotropic properties. They are ferromagnetic below Tc and paramagnetic above T_c. e.g.: ferrites and magnetic garnets.

1.1.6 Superparamagnetic materials:

The superparamagnetism is generated when the multi domains are transformed into single domain of a critical size. The thermal energy at room temperature overwhelm the "magneto static energy" of domain wall resulting in zero hysteresis. This phenomenon is known as superparamagnetism.

1.1.7 Spin glasses

The spin glass is formed when there is disordered in the alignment of unequal spins of the component of the atoms. The net magnetization disappears because of random orientation of spins in the system. This magnetic state is normally observed at low temperatures.

1.2 Ferrites and their Applications

The classification of ferrite structure depends on the crystal structure. The properties are given in the table 1.1:

Table 1. 1: "Classification of ferrite materials"

Ferrite	Crystal structure	General formula
Spinel	Cubic	$M^2Fe_2^{3+}O_4$ $M^{2+} = Ni^{2+}, Mn^{2+},$ $Zn^{2+},Mg^{2+}, Cu^{2+} ions or a$ mixture of mentioned ions
Garnet	Cubic	$R^{3+}Fe_5^{3+}O_{12}$ $R=Y^{3+}, Gd^{3+}$
Hexaferrite	Hexagonal magnetoplumbite	AFe ₁₂ O ₁₉ M-type AM ₂ Fe ₁₆ O ₂₇ W-type AM ₂ Fe ₂₃ O ₄₆ X-type A ₂ M ₂ Fe ₁₆ O ₂₇ Y-type A ₃ M ₂ Fe ₂₄ O ₄₁ Z-type

		A ₄ M ₂ fe ₃₆ O ₆₀ U-type
		$M^{2+} = Fe^{2+}, Ni^{2+}, Mn^{2+}$
		Zn ²⁺ , Mg ²⁺ ions or a
		mixture of mentioned
		ions
Orthoferrite	Orthorhombic	$R^{3+}Fe^{3+}O_3$
	Perovskite	$R^{3+} = Gd^{3+}, Y^{3+}, Nd^{3+},$
		Sm ³⁺ , Lu ³⁺

The spinel ferrite is most extensively used ferrite because of large "electrical resistivity" and low "eddy current". Spinel ferrite is simple class of material having cubic close packed crystal structure. The metal ions generally occupy the "tetrahedral" and "octahedral" sites in the oxygen layers as shown in Fig. 1.1.

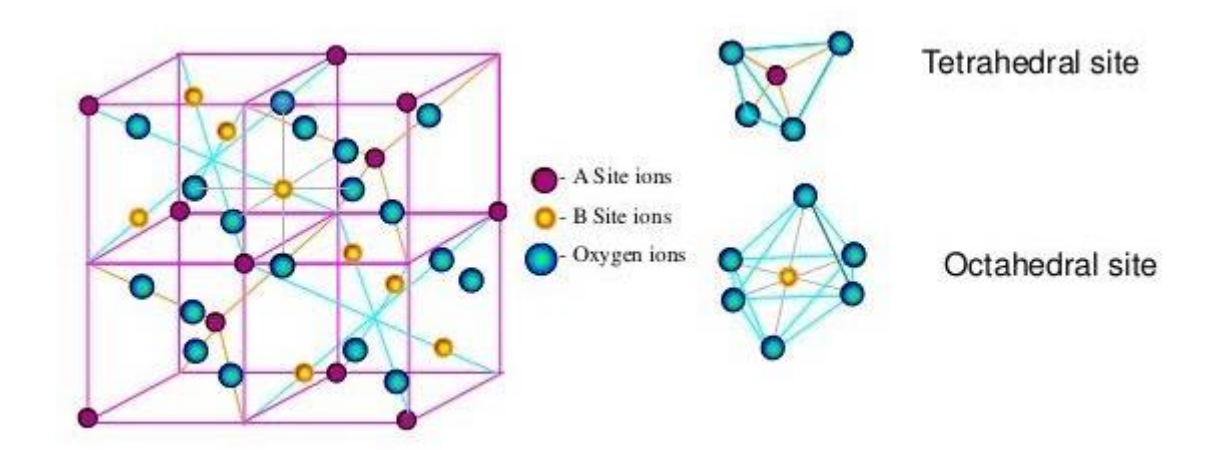
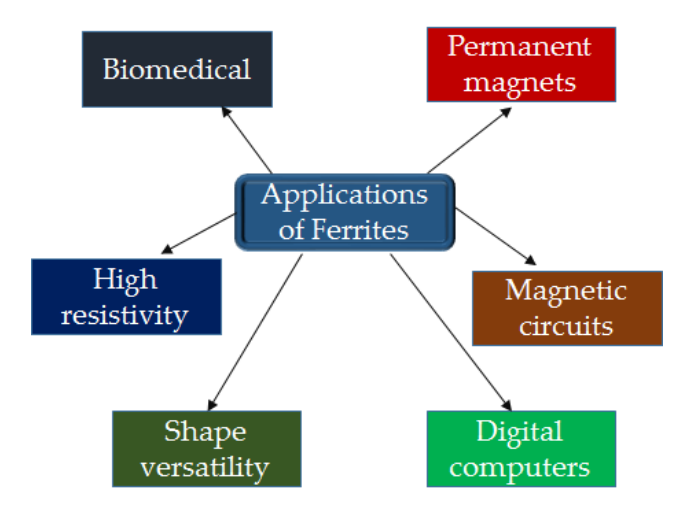


Figure 1. 1 Schematic diagrams for spinel ferrite.

Fig. 1.1 shows the tetrahedral and octahedral sites of metal ions and oxygen ions in spinel lattice structure. The main reason for cation distribution is structural disorder, composition, ion size and deficiency of oxygen in spinel ferrite system. The

general formula for spinel ferrite is $(Me_{1-i}Fe_i)$ $[Me_iFe_{2-i}]$ O_4 where i=0 stand for "normal spinel", i=1 for "inverse spinel" and 0 < i < 1 for mixed spinel. The structural, magnetic and electrical properties can be changed by changing the cation distribution.

The main components of ferrites are iron oxide and metal oxide [5-6]. Basically the super exchange interaction is as a result of placement of magnetic ion among the "high electrical resistivity", "high saturation metal ions. Ferrites possess magnetization", high permeability, less "eddy current" losses and low "dielectric losses" [7-8]. Among all the magnetic materials, ferrite is the highest demandable magnetic material in large number of applications [9]. The change in properties of ferrite can be due to change in synthesis method, quantity of essential metal oxides, sintering, sensitivity and different amount of dopants and impurities which change the area of applications [10]. The ferrites are found to be mostly used in permanent magnets, magnetic recording media, sensors, memory chips and activators etc. In other way ferrites are also used in biomedical applications like hyperthermia, drug delivery, as catalyst and magnetic resonance imaging (MRI) etc. [11-12]. Soft ferrite shows the great performance at less cost because of their "high resistivity" [13]. The superparamagnetic type of spinel ferrites made a large enhancement in ferrofluids based technologies such as contrast MRI, drug delivery, hyperthermia and biosensors etc. [14-15].



Chapter-1: Introduction

When ferrite is exposed to higher frequency microwaves, the eddy current becomes a main problem and reduces the performance of the material. The high frequency problem is reduced by increasing resistivity. The resistivity value in ferrites is of the order of $10^7 \Omega$ m compared to the value for iron which is $10^{-7} \Omega$ m. The reason for decrease in resistivity or increase in conductivity is due to change in conduction mechanism from free electron conduction to electron hopping. Ferrite show the importance at high frequency for electromagnetic applications [16]. The efficiency can be increased by using ferrite nanoparticles. The "Cu-Zn ferrite" is widely used due to its large initial permeability, high resistivity, high dielectric constant, saturation magnetization and low power loss etc. Many group have tried to improve the magnetic properties in various ways such as different synthesis method, heat treatment, substitutions etc. [17]. Some reports show the substitution of Zn in Cu ferrites, regulate the size of the particle and improvement in the structural and magnetic properties [18-19].

The hexagonal ferrites are represented as MaFe₁₂O₁₉ where Ma denotes here "Ba", "Pb", "Sr". They exhibit magnetoplumbite structure and demanded in various applications due to low cost of production. Hexaferrites are massively used as permanent magnets [20-21]. In hexagonal ferrites oxygen ion exhibit closed packed structure. These ferrites show large coercivity and large frequency range of application [22]. The lattice of hexagonal ferrite is matching with the spinel structure with closely packed oxygen ion.

At few layers some metal ions show the same ionic radii as the oxygen ion. These hexagonal ferrites contain large ions and can be produced by replacing the oxygen ion.

The magnetic moment in ferrite is the additions of the particular magnetic moment of the specific sub lattice as explained by Neel. In spinel ferrites the "exchange interaction" among the electrons of ions does not having the similar values on A-site and B-site. Since the interaction among A and B-site or AB-site interaction known as the strongest whereas interaction between AA-site is very weak as compared to A-B site interaction and B-B site is the weakest among all interactions. The strongest interaction is the cause for ferrimagnetism and having the highest "exchange energy" due to which antiparallel arrangement of cation is formed.

1.3 Nanoparticles

The properties of bulk are very different as compared to nanoparticles. Basically the range of the nanoparticles is 1 -100 nm. The properties of material change drastically when the grain or particle size changes from micrometer to Angstrom scale. The nanoparticles have practical application in various fields which covers biomedical and engineering. The nanoparticles can be divided in various type based on their shape, size and properties. The first group includes gold, quantum dots and polymer. The second group contains semiconducting and ceramic. The silica is known as hard nanoparticle. The classification of nanoparticles depends on their demand and can be synthesized in various ways according to their use. The nanoparticles are used to increase the efficiency, speed and sustainability. The nanoparticle finds application in aerosol, suspension and emulsion. The surfactant coating modifies the nanoparticle surface properties to avoid the cluster and agglomeration in the liquids. The coated magnetic nanoparticles are used to make stable ferrofluids, colloidal dispersion, cosmetics and lubricants.

1.3.1 Fe₃O₄ Nanoparticles

Fe₃O₄ (magnetite) is an important member of spinel ferrite family and is known for its excellent properties useful in various applications such as recording material, storage devices, heat transfer, sensors, mineral separation and bio-medical applications etc. [23-26]. It possesses the super paramagnetic behaviour and low Curie temperature. Fe₃O₄ nanoparticles are biocompatible and non- toxic and thus they are useful in biomedical applications. Magnetite has face-centered cubic spinel structure.

Chapter-1: Introduction

The structure formula for magnetite is represented as [Fe³+] A [Fe³+, Fe²+] B O₄. In magnetite crystal structure "oxygen ions" closely organized in the "cubic arrangement", small Fe ion blocks the gap. On "tetrahedral (A) site" Fe ion bounded via four oxygen whereas "octahedral (B) site" bounded by six oxygen. A site shows the anti-parallel arrangement towards B site. There are several synthesis methods for preparing the uniform Fe₃O₄ nanoparticles such as sol-gel, microwave-hydrothermal, co-precipitation, thermal decomposition, micro emulsion etc. [27-28].

1.4 Rheology

Rheology is considered as the deformation of the solids and flow of fluids. Basically the study is to understand the deformation of the matter under stress or in other words to develop the relation between stress and viscosity to get the information about the flow type i.e. Newtonian or non-Newtonian nature of the fluids.

1.5 Properties of ferrofluids and their applications

Ferrofluid is the combination of "colloidal suspension" of magnetic "nanoparticles" in a solvent which responds to the external "applied magnetic field". Ferrofluid was discovered by NASA research center in 1960s in U.S. The scientists were investigating the method of controlling the liquid in space. In the absence of gravity in space, the ferrofluid flow was managed through the "applied magnetic field" [32]. Fig. 1.2 shows the formation of spikes as a result of ferrofluid response towards external applied field. Spikes are formed towards high magnetic field direction.

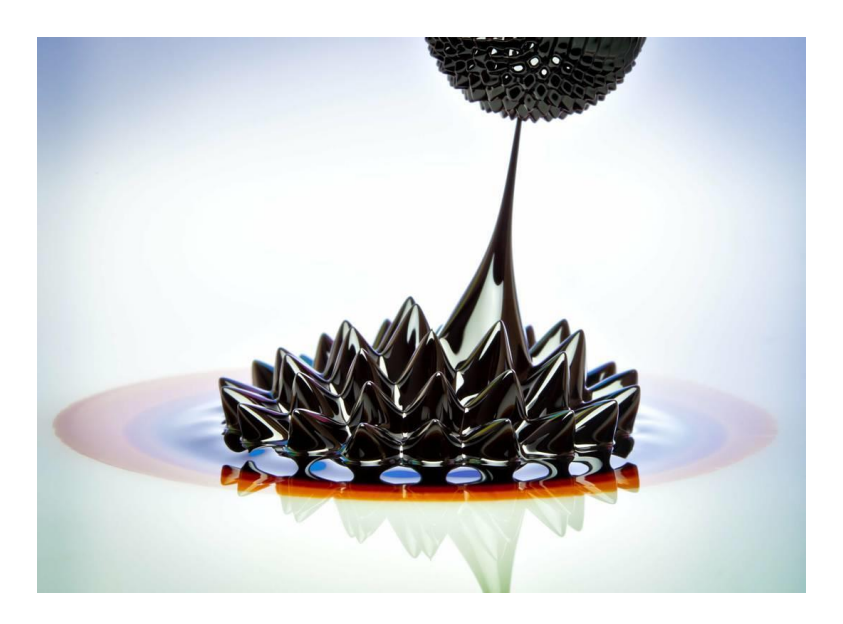


Figure 1. 2 Spikes formation in ferrofluid with applied magnetic field.

In the past decades, several groups have prepared ferrofluid for study of their properties and applications [33]. The size of the magnetic nanoparticle need to be below the critical limit so that due to gravity the Brownian motion of particles is not restricted and no sedimentation takes place. The "nanoparticles" are typically < 10 nm and coated with surfactant such as oleic acid to avoid cluster formation and sedimentation [34]. Cluster or agglomeration happens due to magnetic dipole interaction and Van der Waals forces. The typical solvent used to prepare ferrofluid is water or oil. The ferrofluids are useful in various application such as magnetic sensors, "clutches", lubricants, tunable dampers, defect "sensors", optical grating, magnetic resonance imaging, hyperthermia, drug delivery, cell separation, biosensors and magneto-mechanical applications etc. [29-37].

1.5.1 Surfactant

Surfactant is used to prevent the nanoparticles from clumping and restrict to form agglomeration and settle down in liquid. The tiny magnetic particles interact with each other and form a large dense cluster which leads to sedimentation. The "ideal ferrofluid", does not settle down when magnetic field is applied. The Surfactant can be of hydrophilic or hydrophobic nature as shown in Fig. 1.3.

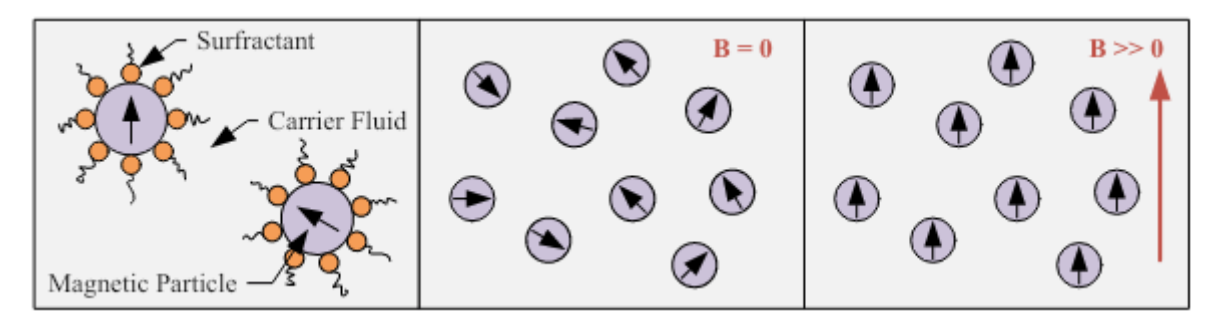


Figure 1. 3 Surfactant coated magnetic nanoparticles with and without field.

Polar surfactant has the property to absorb the nanoparticle whereas non-polar surfactant sticks out to the solvent and forms the regular or irregular layer around the particle. The electrostatic repulsion prevents the particles from agglomeration [38-39]. Apart from preventing the cluster formation in ferrofluids, surfactant improves the fluid's magnetic response or saturation.

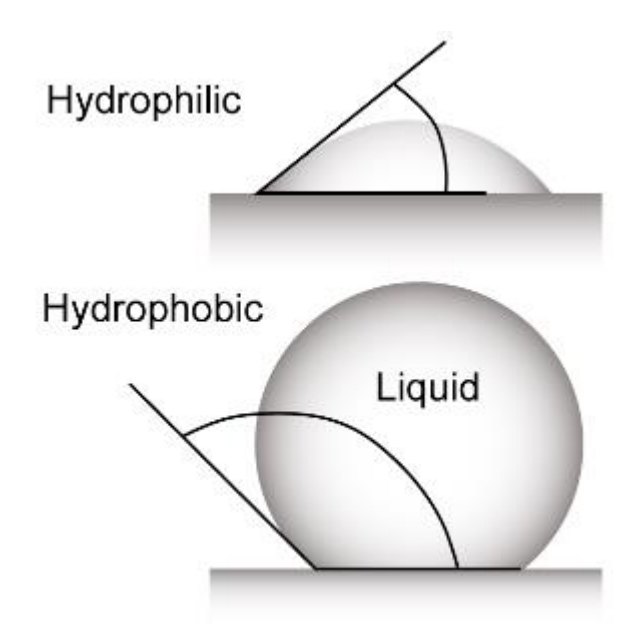


Figure 1. 4 Hydrophilic and Hydrophobic behaviour.

1.6 Types of fluids: There are different types of fluids based on their properties.

1.6.1 Ideal fluid:

A fluid is called ideal when it shows the zero viscosity, incompressible, no shear stress and shows the constant normal stress.

1.6.2 Newtonian and Non Newtonian behaviour:

When the viscosity does not change and remains constant when subject to increase in pressure or temperature, then it is known as the Newtonian behaviour of the fluid. The fluid which obeys the Newton's law is known as Newtonian fluids.

Ex: water and chloroform

$$Viscosity (\eta) = \frac{stress (\tau)}{shear \, rate(\dot{\gamma})}$$
 (1.1)

The fluid which does not follow the Newton' law is known as non-Newtonian fluid or when the shear rate is not equal to shear stress. The viscosity is not constant for the non-Newtonian fluids. Ex: Toothpaste, suspensions, blood, shampoo etc. Fig. 1.5 shows the common flow behaviour of fluids.

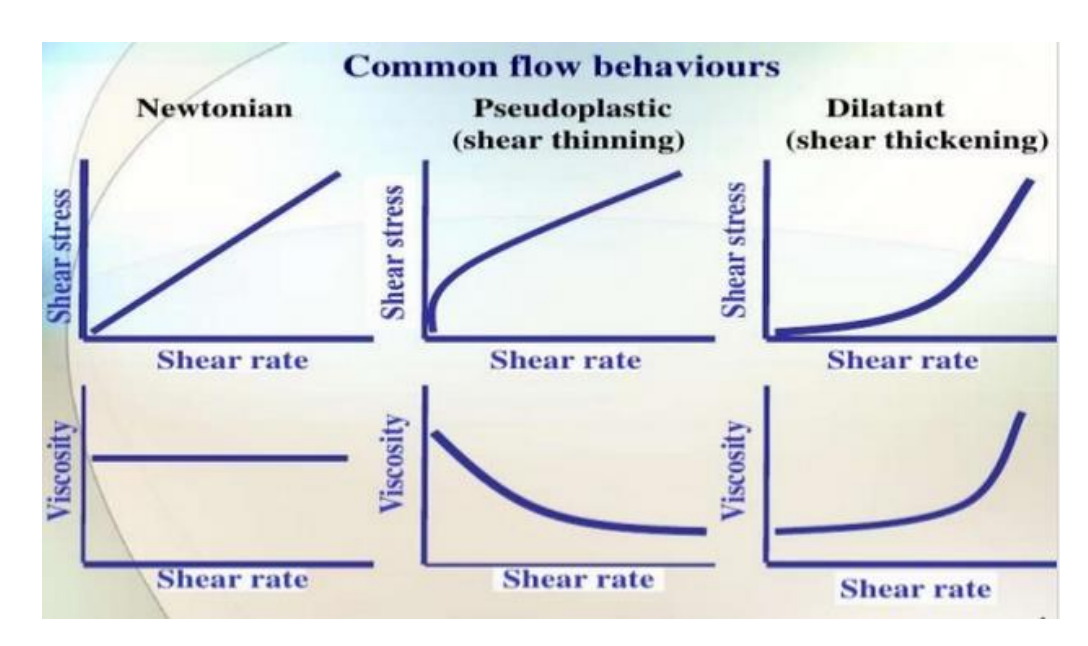


Figure 1. 5 General flow actions.

1.6.3 Bingham plastic (BP) and Herschel -Bulkley (HB) fluid

BP fluids are those fluids which behave like Newtonian fluid when shear is applied as shown in Fig. 1.6.

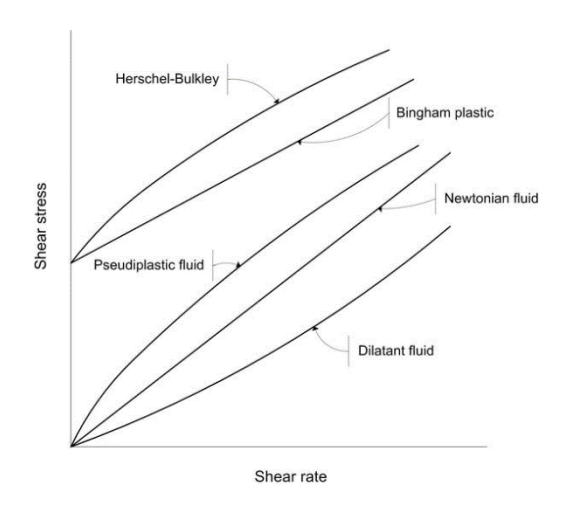


Figure 1. 6 Types of flow for fluids.

If a fluid needs small stress to starts flow then after applying the stress fluid behave as non-Newtonian or flow in the same way then these fluids are known as Herschel-Bulkley fluids.

1.6.4 Thixotropic & Rheopectic Fluid

The viscosity of thixotropic materials decreases with increase in time at constant shear rate. Ex: paraffin oil, cream, gel etc.

The viscosity of rheopectic materials increases with decrease in time at constant shear rate. Ex: printer ink. Fig. 1.7 represents the both behaviour of a fluid with time.

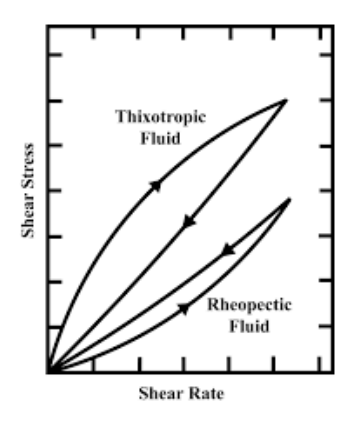


Figure 1. 7 Thixotropic and rheopectic fluid.

1.7 Flow Models:

1.7.1 Bingham plastic model

This model is most general model and useful for drilling engineering. The BP model contains two parameters which are the yield stress and fluid viscosity.

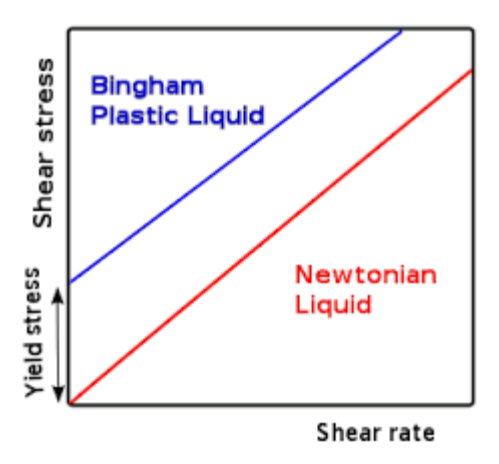


Figure 1. 8 Bingham plastic flows.

In this model at the beginning the fluid resist to flow until shear stress reaches some definite value and once fluid starts to flow the relation between shear rate and shear stress become linear as shown in Fig. 1.8.

$$\tau = YP' + PV' (\gamma) \qquad (1.2)$$
 Here YP' is "yield point", PV' is "plastic viscosity"
$$PV = \theta 600-300\theta$$

$$YP = \theta 300-PV$$

$$YP = (2x \theta 300) - \theta 600 \qquad (1.3)$$

This model is used to calculate the low shear rate and also useful for modeling fluids like toothpaste.

1.7.2 Power law behaviour for fluids:

This law is the simple law to describe the nature of fluid in various range of shear rates on which the coefficients are fitted. It assumes that all fluids are pseudo plastic. This law includes the mathematical prediction and correlates the experimental data [41]. The following equation defines power law behaviour of fluids.

$$\tau = K (\dot{\gamma})^{n-1} \tag{1.4}$$

Here K and n represent consistency' and power index'.

It describes shear thinning part of following curve. If n' = 1, fluid known as Newtonian' fluid whereas if it decreases then it is known as non-Newtonian. The values of power index ranges from 0.2 to 0.6, depends on types of fluid. Power law is useful for modeling the fluids without yield stress at zero shear rates.

Based on power index value the fluid is divided in three types: (i) Pseudo plastic (n<1), (ii) Newtonian fluid (n=1) and (iii) Dilatant (n>1).

1.7.3 Herschel-Bulkley model for fluids:

The generalized model form of non- Newtonian fluid is known as Herschel-Bulkley fluid introduced in 1926 by Winslow Herschel and Ronald Bulkley [42]. Which leads the stress in complex non-linear manner. This law also known as "yield power law model" which pronounces the rheological terms more precisely as compared to other model. There are three parameters defined this model:

$$\tau = \tau_0 + K \dot{\gamma}^n \tag{1.5}$$

Here, consistency (k), flow index (n) and yield stress (τ_0). If n value decreases then it will become more curvature whereas if n increase it become more off curvature as shown in figure 1.6. This law follows two conditions: (i) when n =1, it becomes the Bingham plastic model. (ii) When n=0 and $\tau=\tau_0$, then it describes Newtonian fluid. This law can describe Bingham plastic and power law. Therefore, this model is beneficial over power law in that n and k are not static numbers based on simply two dial reading.

Based on n values shear thinning and shear thickening can be found out while k is the simple proportionality constant. The quantity of stress which the liquid experiences before yield and starts to flow is defined as yield stress.

Some assumptions which all model make:

- The flow is isothermal.
- The drilling fluid is incompressible.
- Workout which model is best Hydraulics analysis.
- Limitation in software and therefore understand where sources of divergence from reality may occur.
- Describe the sources of inaccuracy within these models.

1.8 "Magneto viscosity" in Ferrofluids

When the ferrofluid placed under an external magnetic field then the spike formation starts forming which are nothing but the alignment of the nanoparticles in the field direction and forming the spike structure. These spikes generate due to the interaction between number of forces present in the system such as gravity, Van der Waals force and surface tension etc.[40].

There are some important factors on which magneto-viscosity of ferrofluids depends:

- (i) Synthesis method of nanoparticles and ferrofluids.
- (ii)The stability of the nanoparticles in the ferrofluids.
- (iii) Hydrodynamic response and nanoparticles shape.
- (iv)Proper volume for surfactant, nanoparticles and dispersion media.
- (v) Properties of surfactant and solvent such as viscosity, density, vapor pressure and boiling point.
- (vi)Magnetic response or saturation magnetization of the nanoparticles.
- (vii)Temperature of the ferrofluid.

Several researchers have made effort to improve the stability of ferrofluids by approaching different synthesis methods and other conditions like control

of shape and size of the nanoparticles [43-44]. There is always a challenge to the researchers to produce liquid from a solid through melting the metal magnets because of the property of magnetic materials to loss the magnetic behaviour at high temperature (Neel or Curie temperature).

1.9 Aim

The extraordinary properties of ferrite nanoparticles and ferrofluids are demanded in various applications. The present study is done on the structural and magnetic properties of ferrite nanoparticles. The magneto-viscosity of ferrofluids and their flow properties is also investigated. Synthesis techniques, compositions, shape and size of nanoparticles, surfactant and colloidal media are also discussed. Therefore thesis covers the different properties of three different ferrites (i) Fe₃O₄, (ii) Cu-Zn ferrite, and (iii) Ba-Sr ferrite nanoparticles and their ferrofluid.

1.10 Objectives of the present work:

- 1. To synthesize the Fe₃O₄ nanoparticles and ferrofluid by co-precipitation method.
- 2. To synthesize the $Cu_xZn_{1-x}Fe_2O_4$ (CZF) nanoparticles by using co-precipitation and hydrothermal method.
- 4. To synthesize the Ba_xSr_{1-x}Fe₁₂O₁₉ (BSM) nanoplatelets by using hydrothermal method.
- 5. To study the structural, morphological and stability of all (Fe₃O₄, CZF and Ba-Sr hexaferrite) nanoparticles.
 - 6. To measure the magnetic response for all prepared ferrite nanoparticles.
- 7. To study the rheological properties including flow curves, magneto-viscosity and magneto sweep of the synthesized ferrofluids in different solvents.

1.11 Thesis Organization

- ❖ Chapter 1: This chapter reveals the brief review over ferrite nanoparticles and their applications. Developed structure by doping metal ion in nanostructure spinel ferrite is also discussed. Properties of ferrofluid and their application are also discussed.
- Chapter 2: introduces the synthesis method for preparing the nanoparticles and ferrofluids. The measurements technique briefly described which are used for characterization. The following techniques were used to characterize the all type nanoparticles and their ferrofluids.
 - 1. X-ray diffraction (XRD)
 - 2. Field Emission microscope (FESEM)
 - 3. Transmission electron microscope (TEM)
 - 4. Particle size analyzer
 - 5. Vibrating sample magnetometer (VSM)
 - 6. Electron spin resonance (ESR)
 - 7. Rheometer
- ❖ Chapter-3: This chapter gives the information of structure, magnetic and rheological properties of Fe₃O₄ nanoparticles and ferrofluids.
- Chapter-4: This chapter contains the "structural", "magnetic" and magnetoviscosity of CZF nanoparticles and ferrofluids.
- Chapter-5: This chapter introduces the effect of Sr doping on structural and magnetic and magneto-viscosity of BSM nanoparticles and ferrofluids.
- Chapter-6: This chapter presents the overall thesis summary and future scope.

References:

- [1] O. Shimizu *et al.*, "Development of advanced barium ferrite tape media," *Journal of Magnetism and Magnetic Materials*, vol. 400, pp. 365–369, Feb. 2016.
- [2] K. Shah, R. V. Upadhyay, and V. K. Aswal, "Influence of large size magnetic particles on the magneto-viscous properties of ferrofluid," *Smart Materials and Structures*, vol. 21, no. 7, p. 75005, Jul. 2012.
- [3] N. Gautam, G. Thirupathi, and R. Singh, "Effect of Zn-doping on structural and magnetic properties of copper ferrite nanoparticles," 2016, p. 50099.
- [4] B. Huke and M. Lücke, "Magnetic properties of colloidal suspensions of interacting magnetic particles," *Reports on Progress in Physics*, vol. 67, no. 10, pp. 1731–1768, Oct. 2004.
- [5] L.-Z. Li, L. Peng, X.-X. Zhong, R. Wang, and X.-Q. Tu, "Structural, magnetic and electrical properties of CuZn ferrite nanopowders," *Journal of Magnetism and Magnetic Materials*, vol. 419, pp. 407–411, Dec. 2016.
- [6] A. Gholizadeh, "A comparative study of the physical properties of Cu-Zn ferrites annealed under different atmospheres and temperatures: Magnetic enhancement of Cu0.5Zn0.5Fe2O4 nanoparticles by a reducing atmosphere," *Journal of Magnetism and Magnetic Materials*, vol. 452, pp. 389–397, Apr. 2018.
- [7] M. Gerth-Noritzsch, D. Yu Borin, and S. Odenbach, "Anisotropy of the magnetoviscous effect in ferrofluids containing nanoparticles exhibiting magnetic dipole interaction," *Journal of Physics: Condensed Matter*, vol. 23, no. 34, p. 346002, Aug. 2011.
- [8] M. Manjurul Haque, M. Huq, and M. A. Hakim, "Effect of Zn2+ substitution on the magnetic properties of Mg1–xZnxFe2O4 ferrites," *Physica B: Condensed Matter*, vol. 404, no. 21, pp. 3915–3921, Nov. 2009.

- [9] R. Singh and G. Thirupathi, "Manganese-Zinc Spinel Ferrite Nanoparticles and Ferrofluids," in *Magnetic Spinels Synthesis, Properties and Applications*, M. S. Seehra, Ed. InTech, 2017.
- [10] M. Fang, V. Ström, R. T. Olsson, L. Belova, and K. V. Rao, "Particle size and magnetic properties dependence on growth temperature for rapid mixed coprecipitated magnetite nanoparticles," *Nanotechnology*, vol. 23, no. 14, p. 145601, Apr. 2012.
- [11] Z. M. Wang, R. G. Wu, Z. P. Wang, and R. V. Ramanujan, "Magnetic Trapping of Bacteria at Low Magnetic Fields," *Scientific Reports*, vol. 6, no. 1, Jun. 2016.
- [12] M. Mahdavi et al., "Synthesis, Surface Modification and Characterisation of Biocompatible Magnetic Iron Oxide Nanoparticles for Biomedical Applications," Molecules, vol. 18, no. 7, pp. 7533–7548, Jun. 2013.
- [13] F. Spizzo *et al.*, "Synthesis of Ferrofluids Made of Iron Oxide Nanoflowers: Interplay between Carrier Fluid and Magnetic Properties," *Nanomaterials*, vol. 7, no. 11, p. 373, Nov. 2017.
- [14] J. Drabek and M. Zatloukal, "Influence of long chain branching on fiber diameter distribution for polypropylene nonwovens produced by melt blown process," *Journal of Rheology*, vol. 63, no. 4, pp. 519–532, Jul. 2019.
- [15] D.-H. Kim, S.-H. Lee, K.-N. Kim, K.-M. Kim, I.-B. Shim, and Y.-K. Lee, "Temperature change of various ferrite particles with alternating magnetic field for hyperthermic application," *Journal of Magnetism and Magnetic Materials*, vol. 293, no. 1, pp. 320–327, May 2005.
- [16] A. Goldman, Modern ferrite technology, 2. ed. New York, NY: Springer, 2006.
- [17] T. Prabhakaran, R. V. Mangalaraja, and J. C. Denardin, "Controlling the size and magnetic properties of nano CoFe ² O ⁴ by microwave assisted co-precipitation method," *Materials Research Express*, vol. 5, no. 2, p. 26102, Feb. 2018.

- [18] N. Gautam, G. Thirupathi, and R. Singh, "Magneto-viscosity of hydrothermal synthesized Cu-Zn ferrite ferrofluids," *AIP Advances*, vol. 7, no. 5, p. 56727, May 2017.
- [19] N. Gautam, G. Thirupathi, and R. Singh, "Magneto-viscosity of hydrothermal synthesized Cu-Zn ferrite ferrofluids," *AIP Advances*, vol. 7, no. 5, p. 56727, May 2017.
- [20] R. J. Pandya, U. S. Joshi, and O. F. Caltun, "Microstructural and Electrical Properties of Barium Strontium Titanate and Nickel Zinc Ferrite Composites," Procedia Materials Science, vol. 10, pp. 168–175, 2015.
- [21] X. He, W. Zhong, S. Yan, C.-T. Au, L. Lü, and Y. Du, "The structure, morphology and magnetic properties of Sr-ferrite powder prepared by the molten-salt method," *Journal of Physics D: Applied Physics*, vol. 47, no. 23, p. 235002, Jun. 2014.
- [22] J. Töpfer *et al.*, "Hexagonal ferrites of X-, W-, and M-type in the system Sr–Fe–O: A comparative study," *Journal of Solid State Chemistry*, vol. 226, pp. 133–141, Mar. 2015.
- [23] V. B. Barbeta, R. F. Jardim, P. K. Kiyohara, F. B. Effenberger, and L. M. Rossi, "Magnetic properties of Fe3O4 nanoparticles coated with oleic and dodecanoic acids," *Journal of Applied Physics*, vol. 107, no. 7, p. 73913, Apr. 2010.
- [24] L. F. Gamarra *et al.*, "Magnetic characterization by SQUID and FMR of a biocompatible ferrofluid based on Fe 3 O 4," *Journal of Physics: Condensed Matter*, vol. 21, no. 11, p. 115104, Mar. 2009.
- [25] J. Lu *et al.*, "Solid-state synthesis of monocrystalline iron oxide nanoparticle based ferrofluid suitable for magnetic resonance imaging contrast application," *Nanotechnology*, vol. 17, no. 23, pp. 5812–5820, Dec. 2006.

- [26] M. Imran *et al.*, "Ferrofluid synthesis using oleic acid coated Fe 3 O 4 nanoparticles dispersed in mineral oil for heat transfer applications," *Materials Research Express*, vol. 5, no. 3, p. 36108, Mar. 2018.
- [27] Y. P. He, S. Q. Wang, C. R. Li, Y. M. Miao, Z. Y. Wu, and B. S. Zou, "Synthesis and characterization of functionalized silica-coated Fe ³ O ⁴ superparamagnetic nanocrystals for biological applications," *Journal of Physics D: Applied Physics*, vol. 38, no. 9, pp. 1342–1350, May 2005.
- [28] F. Sayar, G. Güven, and E. Pişkin, "Magnetically loaded poly(methyl methacrylate-co-acrylic acid) nano-particles," *Colloid and Polymer Science*, vol. 284, no. 9, pp. 965–978, Jun. 2006.
- [29] J. M. Linke and S. Odenbach, "Anisotropy of the magnetoviscous effect in a ferrofluid with weakly interacting magnetite nanoparticles," *Journal of Physics: Condensed Matter*, vol. 27, no. 17, p. 176001, May 2015.
- [30] A. Y. Zubarev and L. Y. Iskakova, "Rheological properties of ferrofluids with microstructures," *Journal of Physics: Condensed Matter*, vol. 18, no. 38, pp. S2771–S2784, Sep. 2006.
- [31] R. Müller, R. Hergt, S. Dutz, M. Zeisberger, and W. Gawalek, "Nanocrystalline iron oxide and Ba ferrite particles in the superparamagnetism–ferromagnetism transition range with ferrofluid applications," *Journal of Physics: Condensed Matter*, vol. 18, no. 38, pp. S2527–S2542, Sep. 2006.
- [32] R. Y. Hong, Z. Q. Ren, Y. P. Han, H. Z. Li, Y. Zheng, and J. Ding, "Rheological properties of water-based Fe 3 O 4 ferrofluids," *Chemical Engineering Science*, vol. 62, no. 21, pp. 5912–5924, Nov. 2007.
- [33] S. Odenbach, "Recent progress in magnetic fluid research," *Journal of Physics:* Condensed Matter, vol. 16, no. 32, pp. R1135–R1150, Aug. 2004.

- [34] D. Y. Borin, A. Y. Zubarev, D. N. Chirikov, and S. Odenbach, "Stress relaxation in a ferrofluid with clustered nanoparticles," *Journal of Physics: Condensed Matter*, vol. 26, no. 40, p. 406002, Oct. 2014.
- [35] S. Campelj, D. Makovec, and M. Drofenik, "Preparation and properties of water-based magnetic fluids," *Journal of Physics: Condensed Matter*, vol. 20, no. 20, p. 204101, May 2008.
- [36] N. Gautam, G. Thirupathi, and R. Singh, "Magnetoviscosity of Paraffin-Based Barium Ferrite Ferrofluid," *IEEE Transactions on Magnetics*, vol. 52, no. 7, pp. 1–4, Jul. 2016.
- [37] O. Müller, D. Hahn, and M. Liu, "Non-Newtonian behaviour in ferrofluids and magnetization relaxation," *Journal of Physics: Condensed Matter*, vol. 18, no. 38, pp. S2623–S2632, Sep. 2006.
- [38] A. P. Philipse and D. Maas, "Magnetic Colloids from Magnetotactic Bacteria: Chain Formation and Colloidal Stability," *Langmuir*, vol. 18, no. 25, pp. 9977–9984, Dec. 2002.
- [39] D. Y. Borin *et al.*, "Magnetoviscous effect in ferrofluids with different dispersion media," *Journal of Magnetism and Magnetic Materials*, vol. 416, pp. 110–116, Oct. 2016.
- [40] K. I. Morozov and M. I. Shliomis, "Ferrofluids: flexibility of magnetic particle chains," *Journal of Physics: Condensed Matter*, vol. 16, no. 23, pp. 3807–3818, Jun. 2004.
- [41] Herschel, W.H.; Bulkley, R., "Konsistenzmessungen von Gummi-Benzollösungen", Kolloid Zeitschrift, **39**: 291–300, (1926)
- [42] G. W. Scott Blair et al., J. Phys. Chem., (1939) 43 (7) 853–864.
 Also the de Waele-Ostwald law, e.g Markus Reiner et al., Kolloid Zeitschrift (1933) 65 (1) 44-62

Ostwald called it the de Waele-Ostwald equation: *Kolloid Zeitschrift* (1929) 47 (2) 176-187

- [43] J. de Vicente, F. Vereda, J. P. Segovia-Gutiérrez, M. del Puerto Morales, and R. Hidalgo-Álvarez, "Effect of particle shape in magnetorheology," *Journal of Rheology*, vol. 54, no. 6, pp. 1337–1362, Nov. 2010.
- [44] J. M. Ginder and L. C. Davis, "Shear stresses in magnetorheological fluids: Role of magnetic saturation," *Applied Physics Letters*, vol. 65, no. 26, pp. 3410–3412, Dec. 1994.

CHAPTER-2

Material Preparation and Experimental Techniques

This chapter presents different preparation methods for synthesizing the nanoparticles of various ferrites. The method of preparing stable and uniform ferrofluids in different solvents is also described. Various experimental techniques used for characterization of nanoparticles and ferrofluids are discussed in details.

2.1 Synthesis methods of ferrite nanoparticles

The nanoparticles of Fe₃O₄, CZF and BSM were synthesized by co-precipitation and hydrothermal methods. Fig. 2.1 represents the schematic diagram for preparing the different ferrites nanoparticles.

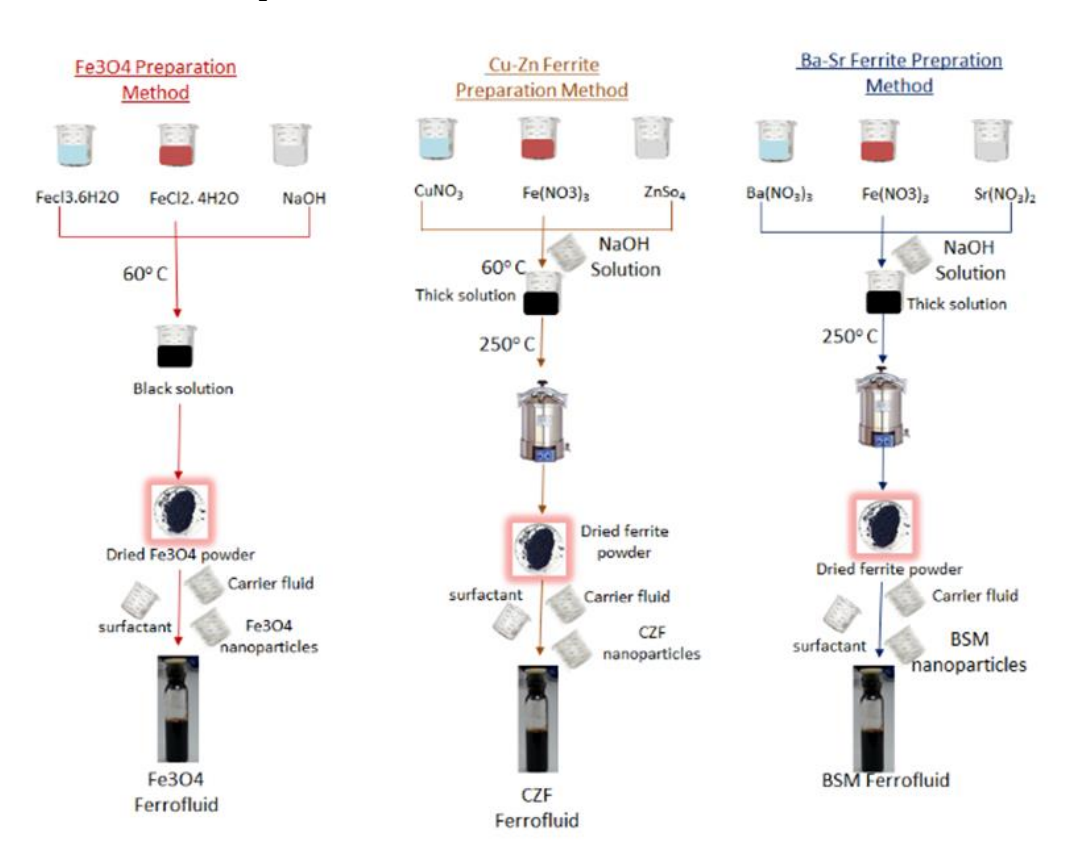


Figure 2. 1Schematic methods for synthesize different ferrites ferrofluid

The synthesis of Fe₃O₄ and CZF nanoparticles was done by co-precipitation method. The hydrothermal method was used to optimize the shape and size of CZF

Chapter 2: Material Preparation and Experimental Techniques

and BSM nanoparticles. The detailed synthesis method for each ferrite is described in the following sections.

2.1.1 Synthesis procedure for magnetite "nanoparticles":

The magnetite nanoparticles were synthesized *via* "co-precipitation method". The FeCl₂·4H₂O, FeCl₃·6H₂O were used as raw materials. Initially, FeCl₃·6H₂O and FeCl₂·4H₂O in (1:2) ratio dissolved in deionized water. The NaOH solution (3 mol) was added in the mixture under constant magnetic stirring until the color of the precipitate changed from brown to black. The prepared nanoparticles were washed several times for maintaining the final pH at 7. The resultant precipitate was dried at 60 °C to obtain nanopowder for characterization. The reaction is represented by the eq.

2.1.1.1 Synthesis of Fe₃O₄′ based ferrofluids:

The Fe₃O₄ nanoparticles coated with "4-Dodecylbenzenesulfonic acid" (DBSA) /oleic acid and dispersed in water', toluene, paraffin' and silicone oil' to prepare ferrofluids as listed in the below table.

Table 2. 1: Fe₃O₄ ferrofluids in various colloidal media.

Ferrofluid Name	Composition	Colloidal	Surfactant
FW	Fe ₃ O ₄	Water	DBSA
FT	Fe ₃ O ₄	Toluene	Oleic acid
FP	Fe ₃ O ₄	Paraffin Oil	Oleic acid
FS	Fe ₃ O ₄	Silicone oil	Oleic acid

2.1.2 Synthesis of Cu_{1-x}Zn_xFe₂O₄ (CZF) nanoparticles:

Co-precipitation method was used to synthesize the nanoparticle of composition Cu_{1-x}Zn_xFe₂O₄ (CZF). Metal salts of Cu²⁺, Zn^{2+'} and Fe^{3+'} were dissolved in distilled water with appropriate ratio. Resultant solution was kept at 80 °C. The following reaction is used for controlling the hydroxide ion in the solution:

$$(1-x)Cu^{2+} + xZn^{2+} + 2Fe^{3+} + nOH^{-} \longrightarrow Cu_{1-x}Zn_xFe_2O_4 + H_2O$$

The distilled water is used for washing the prepared solution to maintain pH at 7. The slurry was heated at 90 °C for 10 hours to dry and obtain CZF nanoparticles.

2.1.2.1 Preparation method of Co-precipitated CZF nanoparticle based ferrofluids:

The hydrodynamic distribution affects the properties of ferrofluid. A number of colloidal were used for synthesizing different CZF based ferrofluids [1-2]. The below table is used to list the properties of "colloidal" for the synthesis of "ferrofluids". From application point of view, stability of ferrofluid is important and it depends on proper selection of colloidal.

Table 2. 2: Properties of colloidal media.

S. No.	"Colloidal"	Dynamic viscosity of colloidal (mPa.s) at 300K	Density (g/ml)	Vapor Pressure(k Pa)
1	Toluene	0.55	0.86	8.7
2	Water'	0.8′	1	4.3
3	Paraffin oil'	25 to 80′	1.1	0.5
4	Silicone oil	10	0.93	0.6

The synthesized ferrofluids are listed in the following table.

Table 2. 3: C-CZF ferrofluids in various colloidal media.

Ferrofluid Name	Composition	Colloidal	Surfactant
CCZF20	Cu _{0.8} Zn _{0.2} Fe ₂ O ₄	Toluene and Paraffin oil	Oleic acid
CCZF40	Cu _{0.6} Zn _{0.4} Fe ₂ O ₄	Toluene and Paraffin oil	Oleic acid
CCZF60	Cu _{0.4} Zn _{0.6} Fe ₂ O ₄	Toluene and Paraffin oil	Oleic acid

2.1.3 Synthesis of Hydrothermalized CZF nanoparticles:

The CZF nanoparticles were synthesized using hydrothermal synthesis route [3]. The salts of Cu²⁺, "Zn²⁺" and "Fe³⁺" were mixed in appropriate mole ratio with water. The resultant mixture was placed in autoclave at 200 °C for 24 hours. The resultant slurry was collected and kept for drying at 80 °C for 12 hours to get the CZF nano powder.

2.1.3.1 Synthesis of Hydrothermalized CZF nanoparticle based Ferrofluids:

The surfactant coated hydrothermalized nanoparticles were dispersed in various solvents to prepare different ferrofluids. The prepared ferrofluids are listed in the table below.

Table 2. 4: H-CZF ferrofluids in various colloidal media.

Ferrofluid Name	Composition	Colloidal	Surfactant
HCZF20W		Water	DBSA
	Cu _{0.8} Zn _{0.2} Fe ₂ O ₄		

HCZF20P		Paraffin oil	Oleic acid
HCZF40W	Cu _{0.6} Zn _{0.4} Fe ₂ O ₄	Water	DBSA
HCZF40P		Paraffin oil	Oleic acid
HCZF60W		Water	DBSA
	Cu _{0.4} Zn _{0.6} Fe ₂ O ₄		
HCZF60P		Paraffin oil	Oleic acid

2.1.4 Synthesis of Ba_{1-x}Sr_xFe₁₂O₁₉ (x=0, 0.05, 0.1, 0.2, and 0.5) Nanoparticles:

The nanoparticles of composition Ba_{1-x}Sr_xFe₁₂O₁₉ were prepared *via* hydrothermal process in an autoclave [4]. The mole ratio of metal nitrates (Ba²⁺/Fe³⁺) 1:4.5 were mixed in distilled water and solution were mixed with sodium hydroxide. The solution was autoclaved for hydrothermal heat treatment at 523K for 24 hours. Finally the solution was washed several times for maintaining the pH at 7. The final paste was dried at 90 °C to obtain ferrite nano powder.

2.1.4.1 Synthesis of Ba_{1-x}Sr_xFe₁₂O₁₉ (x=0, 0.05, 0.1, 0.2, and 0.5) Ferrofluids:

The following table lists various ferrofluids synthesized by dispersing surfactant coated BSM nanoparticles in various solvents. The colors show name of different ferrofluid.

Table 2. 5: BSM ferrofluids in various colloidal media.

Chapter 2: Material Preparation and Experimental Techniques

Ferrofluid name	"Composition" and	Surfactant	"Colloidal "
	nanoparticles magnetic		
	nature		
BMW	BaFe ₁₂ O ₁₉ (FM)	DBSA	Water
ВМР	BaFe ₁₂ O ₁₉ (FM)	Oleic Acid	Paraffin Oil
BMS		Oleic Acid	Silicone Oil
	BaFe ₁₂ O ₁₉ (FM)		
BSM5W	Ba0.95Sr0.05Fe12O19 (FM)	DBSA	Water
BSM5P	Bao.95Sro.05Fe12O19 (FM)	Oleic Acid	Paraffin Oil
BSM5S		Oleic Acid	Silicone Oil
	Bao.95Sro.05Fe12O19 (FM)		
BSM10W	Bao.9Sro.1Fe12O19 (FM)	DBSA	Water
BSM10P	Bao.9Sro.1Fe12O19 (FM)	Oleic Acid	Paraffin Oil
BSM10S		Oleic Acid	Silicone Oil
	Ba _{0.9} Sr _{0.1} Fe ₁₂ O ₁₉ (FM)		
BSM20W	Bao.8Sro.2Fe12O19 (FM)	DBSA	Water
BSM20P	Bao.8Sro.2Fe12O19 (FM)	Oleic Acid	Paraffin Oil
BSM20S		Oleic Acid	Silicone Oil
	Ba _{0.8} Sr _{0.2} Fe ₁₂ O _{19'} (FM)		
BSM5W	Ba0.5Sr0.5Fe12O19' (FM)	DBSA	Water
BSM5P	Bao.5Sro.5Fe12O19 (FM)	Oleic Acid	Paraffin Oil
BSM5S	Bao.5Sro.5Fe12O19 (FM)	Oleic Acid	Silicone Oil

2. 2 X'-ray Powder diffraction

X'-ray diffraction pattern of Fe₃O₄, CZF and BSM nanoparticles were recorded using "Bruker D8 ADVANCE (DAVINCI design) diffractometer" fitted with Cu'-K α ' target for generating X-rays. The "Joint Committee on Powder Diffraction standards (JCPDS)", "PCPDF win" and the National Bureau of Standards data cards are used for comparing the obtained diffraction patterns of the synthesized nanoparticles.

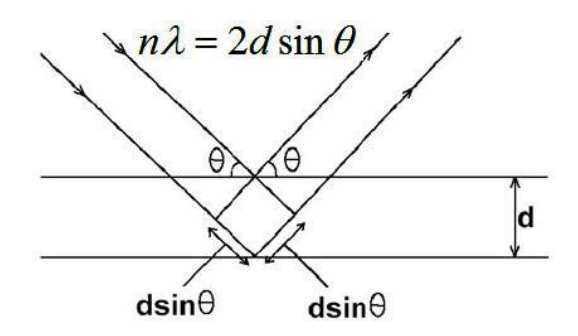
2. 2. 1 X-rays:

The interaction between atom and high energy electrons, generate X-rays. The generated spectrum is electromagnetic spectrum, the spectrum at low tensions shows only continuous spectrum and at high tensions 25 kV or higher discrete sharp lines. In order to confirm the structure of a material refer to its composition at different types of complication, finding the molecular formula to the correct position of all atoms in the molecules. The structural properties massively affect the macroscopic properties of a material. Therefore, structural characteristics play an important role in identifying the structure of a material. XRD and Bragg diffraction are used for morphological and structural information of nanomaterials.

The diffraction from a crystal is shown in Fig. 2.2. For constructive interference the path length difference is given by formula,

$$2d_{hkl} \sin\theta = n\lambda \tag{2.1}$$

The equation (2.1) known as "Bragg's law", where, 'n' represents an "integer", ' λ ' represents "x -ray wavelength" and ' θ ' represents the "Bragg angle".



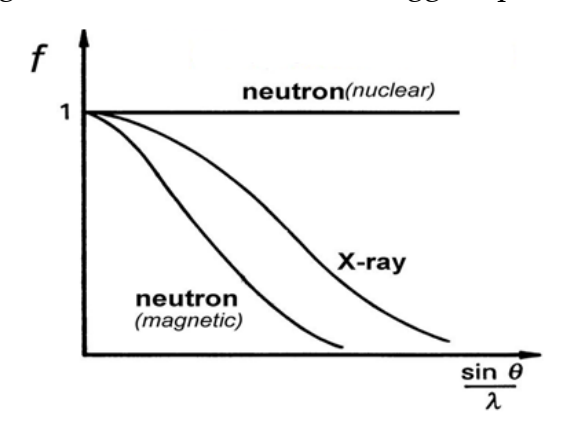


Figure 2. 2Diffraction from Bragg's equation.

Figure 2. 3Atomic form factor for X-ray (and neutron) against angle.

The "structure factor (F_{hkl}) " is an essential parameter in "crystallography" which carries the "atomic structure factor" and "atoms positions" which are defined with the formula

$$F_{hkl} = \sum_{n=1}^{N} f_n \exp(2\pi i (ha_n + kb_n + lc_n))$$
 (2.2)

Where F_{hkl} is structure factor, f_n is atomic scattering factor and a, b and c are atomic positions in unit cell.

In the XRD pattern the intensity of peaks are directed through the crystal structure and diffractometer. The atomic form factor against angle for X-ray is given in Fig. 2.3.

2. 2. 2 Rietveld refinement:

Full Prof Suite program use to perform Rietveld refinement. For profile parameter "Thompson-Cox-Hastings pseudo-Voigt" is used. The crystallite size of the ferrite nanoparticle is estimated from "Williamson-Hall (WH) plot".

"Full Prof Program" is established for "Rietveld analysis of neutron" or XRD data composed at variable or constant step in 2θ . Individually or with powder data the single crystal refinements can also be done with this program.

Some important properties of FullProf are described below:

- XRD contains the laboratory and synchrotron sources.
- With different profile parameters one and two wavelengths can be used.
- The 2θ (scattering variable) in degrees.
- The background can be fixed, refined by Fourier filtering.
- For each phase the peak shape selection can be "Gaussian", "Lorentzian", modified Lorentzian, "pseudo-Voigt", "Pearson-VII" and "Thompson-Cox-Hastings (TCH) pseudo-Voigt".
- Multi-phase can be up to 16 phases.
- Magnetic structure refinement can be done in two way: one is explaining the magnetic structure in magnetic unit cell and the other one is important for unequal magnetic structures.
- The consequence of size and strain is reflected in hkl-dependence of FWHM.

2. 3 "Field Emission – Scanning Electron Microscope" (FE-SEM)

FESEM (Model Ultra55 of Carl Zeiss) was used for capturing images of the nanoparticles with spatial resolution < 2 nm. Electron microscopes are high vacuum instrument. To avoid the electrical mismatch inside the gun, high vacuum is appropriate and allow electrons to move within the apparatus. Several electron emission sources are required for various vacuum stages. Emission sources are classified in two classes: "thermionic emitters" and "field emitters". The first one is used to heat the filament for reduce the work function. The electron beam containing a tungsten filament shield of zirconium oxide from Schottky field emitter. This is mainly worked to minimize the work function for emitter electron from tungsten (4.6 eV to 2.8 eV). The increased thermionic emission field is used at high field gradient to produce the electron in FESEM. The field emission gun generally made by Tungsten wire in which the electron emitters can produce up to 1000x the emission of a tungsten filament. The narrower probing beams which provide by electron gun is result in both improved minimize sample charging and spatial resolution.

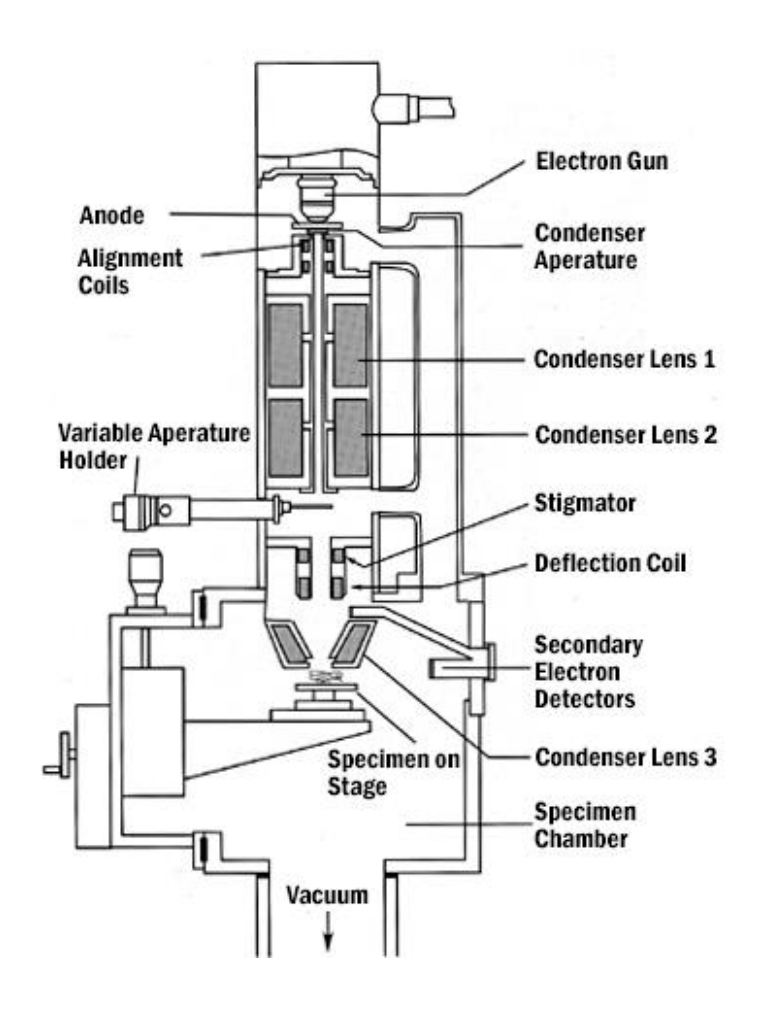


Figure 2. 4Schematic diagram of FESEM.

Fig. 2.4 shows the schematic diagram of FESEM. The primary electron are focused (with 1 to 30 kV) and deflected in the high vacuum column (< 1x10⁻⁷ Torr) by electronic lenses to generate the fine beam for bombardment of the object and the secondary electrons are emitted in every spot. The angle and velocity of "secondary electron" relate with surface structure. The detector is used to capture these electrons and generate the signal. These signals are converted into the video scan image and can be saved which is used to focus the microstructure and cross-sectional mode.

2.4 "High Resolution - Transmission Electron Microscopy" (HR-TEM)

"Transmission electron microscope" (TEM) is extremely useful and multipurpose instrument which is used to characterize the morphology, particle size,

diffraction pattern of materials and elemental analysis. The "spatial resolution" in TEM has ability to confirm the picture and material "diffraction". The bright field and dark field pictures are used to study the defect as well as domain structure. The direct atomic arrangement can be visualized in high resolution imaging mode (HRIM).

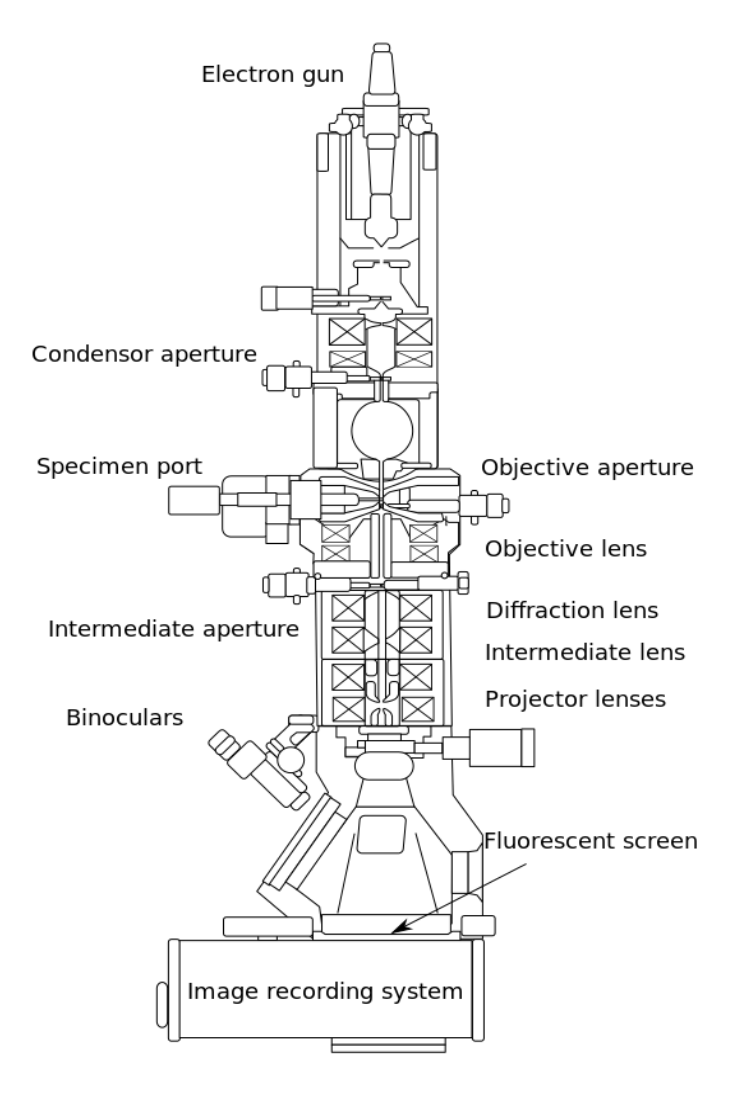


Figure 2. 5 TEM schematic diagram.

Chapter 2: Material Preparation and Experimental Techniques

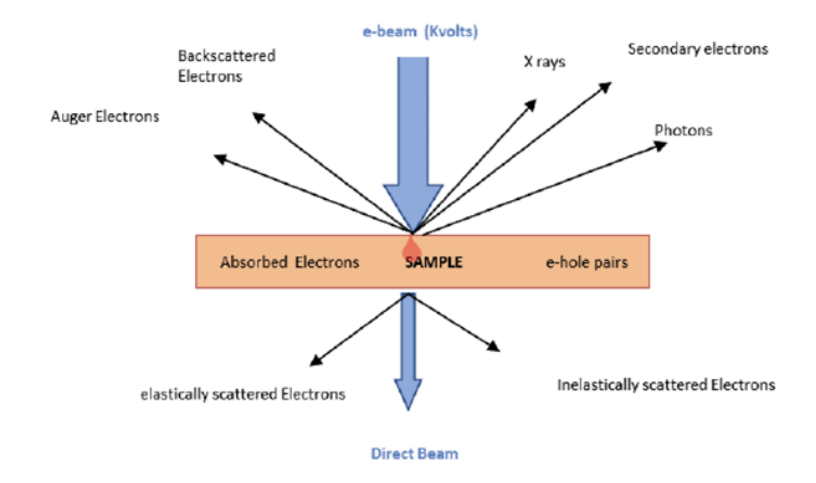


Figure 2. 6 Schematic diagram of the interaction between electron beam and sample surface.

The diffraction mode gives the clear information of crystal structure. TEM schematic diagram presented in Fig.2.6. High energy electrons produced by the accelerating voltage of 300 kV are used in TEM. The electron beam is passed through the sample leading to their scattering. The operating mode is a refined system based on electromagnetic lenses used to focus the electron for picture collection. The mode of image gives the highly magnified vision of the structure. The atomic arrangements are found at HRTEM.

The electron diffraction mode shows the pure information of local crystal structure.

In diffraction mode, an electron diffraction pattern is originated through sample place lightened via "electron beam". The diffraction pattern corresponds to XRD pattern. The particular spot pattern represents single crystal and ring pattern shows the polycrystalline and the series of diffusion rings indicate the amorphous nature of a material.

2. 5 Particle Size Analyzer:

Particle size analyzer (Modal Litisizer[™] 500) is a powerful tool to characterize particles in the liquid media. It determines the "particle size", "zeta potential" and "molecular mass". The cmPALS technology provides the unprecedented accuracy in

ELS measurements. Laser light with wavelength 658 nm is used through an individual frequency laser diode. There are three angle used known as detection angles 15°, 90°, 175° (particle size), 15° (zeta potential) and 90°(molecular mass). The measurement range are 0.3nm -10 μ m (particle size), 3.8nm- 100 μ m (zeta potential) and 980Da-200MDa (molecular mass). The system has the temperature range of 0-90 ° C (32- 194 ° F). The minimum volume of liquid required is 20 μ L for particle size, 350 μ L for zeta potential and 20 μ L for molecular mass. "Dynamic light scattering" (DLS) technique provide the information on average particle size from the average size distribution. Electrophoretic light scattering (ELS) is used for measuring the zeta potential. The speed of particles is measured by ELS in the presence of "electric field". The speed of moving the particle depends on the surface charge (zeta potential)

2.6 "Physical Property Measurement System" - Vibrating Sample Magnetometer (PPMS -VSM):

Physical Property Measurement System (PPMS-6000 Quantum Design) is used for performing the magnetic measurements with the maximum magnetic field of 9T and temperature range of 2- 300 K.

2. 6. 1 Working principle of VSM

The VSM was used for magnetization measurements of the samples sample under the uniform magnetic field. The VSM is based on "Faraday's law of induction". The magnetization depends on the constant field, as much the strongest the constant field, highest will be the magnetization. The magnetic dipole moment creates the magnetic stray as the sample is displaced and can be observed by the pick—up coils.

The voltage is generated in the pick-up coil by varying the magnetic flux. The "time dependent induced voltage" is,

$$Z_{\text{coil}} = \frac{d\varphi}{dt} = \frac{d\varphi}{dz}\frac{dz}{dt}$$
 (2.3)

Chapter 2: Material Preparation and Experimental Techniques

Here, Φ known as "magnetic flux", 'z' shows the "vertical position of the sample", 't' represents "time".

The voltage of "sinusoidal oscillating sample" defined as:

$$Z \text{ coil } = (2\pi f^*C^*m)^*(A \sin(2\pi ft))$$
 (2.4)

Here 'C' refers to "coupling constant", 'm' is "magnetic moment of the sample", 'A' represents "amplitude of oscillation", and 'f' is "frequency of oscillation".

The instrument was calibrated by a cylindrical shaped Ni sample. The magnetization as low as 10-6 emu/gm could be measured.

2. 7 Ferromagnetic resonance (FMR)

It has been used to study magnetic phase transition and anisotropy. The spectra was noted on "JEOL (JES-FA200) ESR spectrometer operating" at "X- band" frequency (ν = 9.16 GHz). Field modulation was adjusted at frequency of 100 kHz and amplitude 10 Oe". The magnetic field was ramped from 0-10 kOe to record the first derivative of the power absorption. The dynamic susceptibility at fixed frequency of the spectrometer was recorded as a function of the magnetic field strength. Resonance field was measured at the field where dP/dH became zero.

2.7.1 Experimental Set-Up for FMR

The standard JEOL (JES-FA200) X-band ESR is describes below:

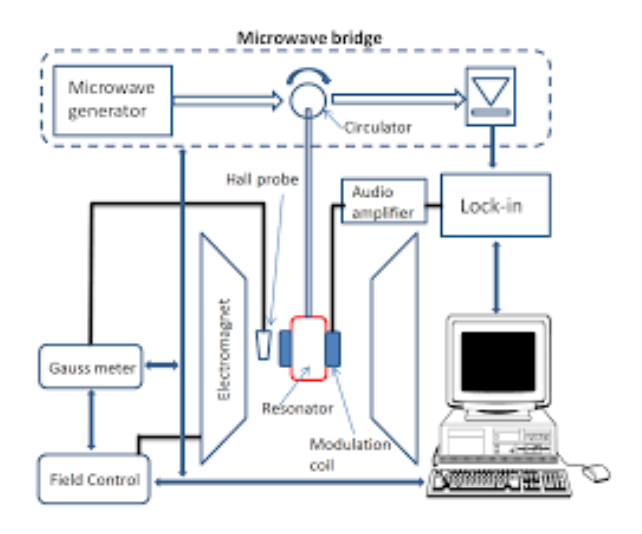


Figure 2. 7 Schematic diagram for an X-band EPR spectrometer.

2. 7. 2 Microwave Unit

The microwave bridge play role in both microwave as well as detector of the transmitted waves. The gun diode was used for create the microwaves with X-band frequencies (v = 9.2 GHz). The waveguide was used to shift the microwave to an attenuator.

The output of the attenuator is transferred with a waveguide to a circulator that forces the waves into the resonator containing the sample and the reflected microwave is directed to the detector, which consists of a diode that converts the microwave power to electric current.

The waveguide is used to transfer the output of the attenuator *via* circulator which directs the waves into the resonator containing the sample and the reflected microwave is directed with detector.

2.7.3 The "Cavity"

"Microwave cavity" is used to keep the sample which aids the amplification of weak signals from the sample. Cavity with high quality factor is required to minimize the energy dissipation and to improve the sensitivity. To achieve this condition the sample is located in least electric field and extreme magnetic field.

2.7.4 Signal Channel

The "phase sensitive detection" is used with necessary electronics to make the signal channel. Basically it Improve the sensitivity in system. At "modulation frequency", "magnetic field" is "modulated" sinusoidally. For comparison the field modulated signal is used as reference. It is delicate to some "modulation frequency" and phase like field modulation. Some signals which do not satisfy the requirements are blocked.

2.7.5 "Magnetic Field Controller"

Magnetic field controller regulates the field sweep. The regulator controller arranges the field values, the sweeping duration and required current to flow in each magnet coil. A Hall probe is placed in between the two magnet poles to sense the field. The controller regulates the field by comparing the Hall probe with the earlier set reference voltage.

2.7.6 The User (operator) Interface:

The JEOL ESR-spectrometer has Acquisition Software configured for different types of measurements. The computer software is active to feed the values. Through the software several parameters are set. The temperature controller is used for cooling and maintaining the sample temperature

2.8 Rheometer:

The rotational rheometer (Anton Paar MCR 501) was used to investigate the magneto-viscosity of various ferrofluids at 25°C. The diameter of the measuring system is 20 mm parallel plate geometry. The gap is 0.1 mm between the plates and rotational which was used to carry out all measurements. The magnetic platform is attached with the rheometer to obtain the "magnetic field" in the vertical direction.



Figure 2. 8 MCR 501 rheometer

The cutting edge technology is used in the MCR rheometer. The low friction bearing, EC motor technique and patented normal force have been optimized. Except rotational, oscillatory mode is also supported in MCR rheometer. The measurements can be performed at various temperature of the sample with specific accessories. The air bearings, high performance synchronous motor and force sensor make the Anton Paar MCR 501 a compact system.

The movement of bearings can be detected from the normal force sensor. The bottom plate is unmovable and is equipped with a Peltier temperature controller unit attached to a hood for maintaining uniform sample temperature. The air bearings and oil free air compressor is used for supplying air at continuous pressure of 5-8 bar to the rheometer. A chiller is used to circulate water to the system. The Rheo Plus

Chapter 2: Material Preparation and Experimental Techniques

software is used for controlled rheological measurements. In rheometer air bearing is one of the most important part which supports the synchronous motor. Two types of air bearings namely radial and axial air bearings are used. The axial air bearing is used to support weight of all the rotating parts. A very small angular displacement (less to $0.1~\mu$ rad) can be measured by using optical encoder. This encoder carries nonconducting light source and photo cell. During the transient and steady state, the normal force sensor which is integrated through the air bearing, is used to measure the normal force in both positive and negative directions. The temperature control unit maintains the uniform temperature all over the sample. The Peltier system carrying an actively controlled lower plate and hood, provides a desired level of temperature directly with 0.02 C accuracy. To determine the gap between the plates the true gap technology based on induction method is used. This technology also supports to suppress the errors in measurements initiated by normal force and thermal expansion. The transponder chip is combined to the geometry which contains all the significant data and communicated to the Rheo Plus software. The measuring geometries are easily attached to the rheometer rotor using a quick-fitting coupling. The equipment is useful in three measuring geometries namely cone –plate, parallel plate and cup-bob.

References:

- [1] R. Singh and G. Thirupathi, "Manganese-Zinc Spinel Ferrite Nanoparticles and Ferrofluids," in *Magnetic Spinels Synthesis, Properties and Applications*, M. S. Seehra, Ed. InTech, 2017.
- [2] N. Gautam, G. Thirupathi, and R. Singh, "Effect of Zn-doping on structural and magnetic properties of copper ferrite nanoparticles," 2016, p. 50099.
- [3] N. Gautam, G. Thirupathi, and R. Singh, "Magnetoviscosity of Paraffin-Based Barium Ferrite Ferrofluid," *IEEE Transactions on Magnetics*, vol. 52, no. 7, pp. 1–4, Jul. 2016.
- [4] N. Gautam and R. Singh, "Magneto-viscosity of stable colloidal solutions of Barium-strontium hexaferrite ferrofluid," *Materials Research Express*, vol. 6, no. 8, p. 84012, Jun. 2019.

<u>Chapter 2: Material Preparation and Experimental Techniques</u>

CHAPTER-3

Studies on Fe₃O₄ nanoparticles and ferrofluids

This chapter contains the details about the structural and magnetic properties of Fe₃O₄ nanoparticles. The XRD, FESEM, DLS, ESR and VSM have been used to characterize the structure, morphology and stability of the magnetic nanoparticles. DBSA\Oleic acid have been used as surfactants to coat the nanoparticles which were dispersed in water, toluene, paraffin and silicone oil for the preparation of ferrofluids. The magneto-viscosity measurements were carried out on the synthesized ferrofluids. The effect of the colloidal on the rheological properties of the ferrofluids is studied.

3.1 Studies on Fe₃O₄ nanoparticles

The less toxic nature of magnetite nanoparticles is make them attractive for biomedical applications. In the recent years, several groups have studied various properties of Fe₃O₄ nanoparticles. The Fe₃O₄ nanoparticles were synthesized via alternating current magnetic field assisted method anticipating improvement in their properties compared with classic co-precipitation method [1]. However not much difference is found in the properties of nanoparticles synthesized by this method. We have followed the simple co-precipitation method described in chapter 2 to synthesize the magnetite nanoparticles. The structural and magnetic properties of the synthesized nanoparticles were studied at room temperature.

3.1.1 Structural Studies

Fig. 3.1 shows the XRD pattern of magnetite (Fe₃O₄) nanoparticles. The XRD pattern confirms the single phase cubic spinel structure (JCPDS No: 01-1111) with space group Fd-3m. All the observed peaks are indexed to Fe₃O₄ crystal structure. There is no impurity phase seen in the data. The most intense peak (311) is described by Gaussian and used to calculate the half - width of reflection.

Chapter 3: Studies on Fe₃O₄ nanoparticles and ferrofluids

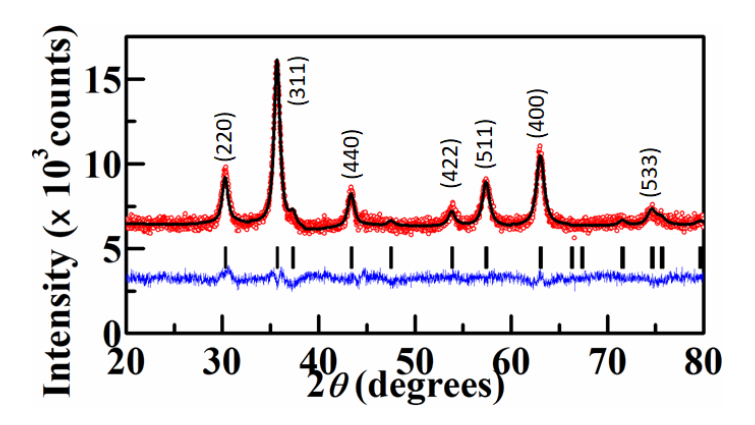


Figure 3. 1 XRD pattern of Fe₃O₄ nanoparticles.

The average crystallite size of Fe₃O₄ nanoparticles is calculated using the Debye-Scherrer formula [2]:

$$D_{hkl} = \frac{K\lambda}{\beta_{hkl}.\cos\theta}$$
 (3.1)

Here K is particle shape factor (0.9), λ is X- ray wavelength, β_{hkl} is half- width of (hkl) reflection,= $\frac{2\theta}{2}$, shows Bragg angle. The average crystallite size of magnetite nanoparticle is estimated by using eq. (3.1) is 13 ±1.5 nm which agrees with FESEM particle size. The equation to find out the lattice parameter (a) in cubic crystal structure is defined as:

$$a = d_{hkl} \sqrt{h^2 + k^2 + l^2}$$
 (3.2)

Here (h,k,l) are Miller indices, dhkl represents inter-planar spacing. The estimated lattice parameter by using eq. (3.2) is 8.384 Å for the spinel structure of Fe₃O₄.

3.1.2 Morphological Studies

Fig. 3.2 shows the FESEM image of Fe₃O₄ nanoparticles. FESEM micrograph confirmed the formation of the agglomeration of nanoparticles as nanostructures. The average estimated particle size is around 15 nm. The particles are mostly spherical in shape.

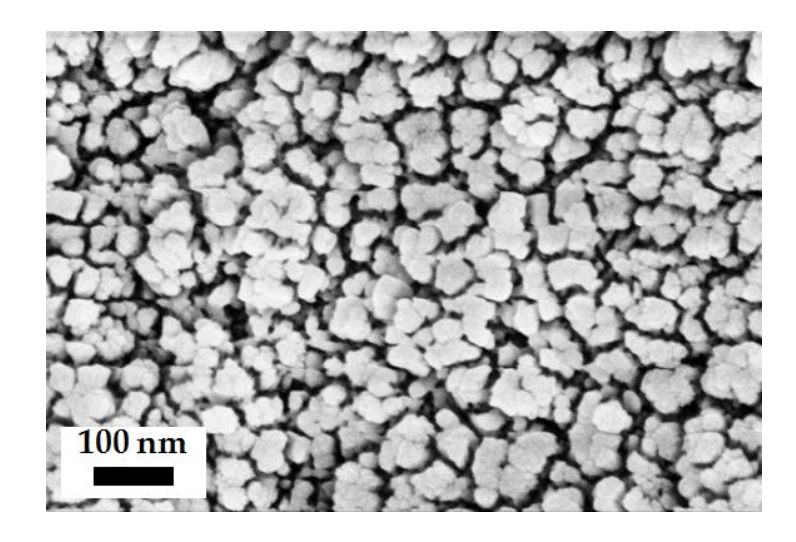


Figure 3. 2FESEM micrograph of Fe₃O₄ nanoparticles.

The particles size from FESEM studies is comparable with that obtained from XRD data.

3.1.3 Particle size distribution and zeta potential

Fig 3.3 (a) shows the particle size distribution of Fe₃O₄ nanoparticles. The estimated hydrodynamic diameter is 206.2 nm. The size distribution is large as compared to FESEM average particle size distribution due to the tendency of magnetic nanoparticles to form cluster or agglomerate in the water media.

The measured value of zeta potential is - 70.2 mV for magnetite nanoparticles which is considered to be the good for the stability of ferrofluid. Zeta potential value depends on the ionic strength of a solution. Zeta potential scan was done to determine the stability of nanoparticles in water. The magnetite nanoparticles dispersed in water to measure the zeta potential is shown in Fig 3.3 (b).

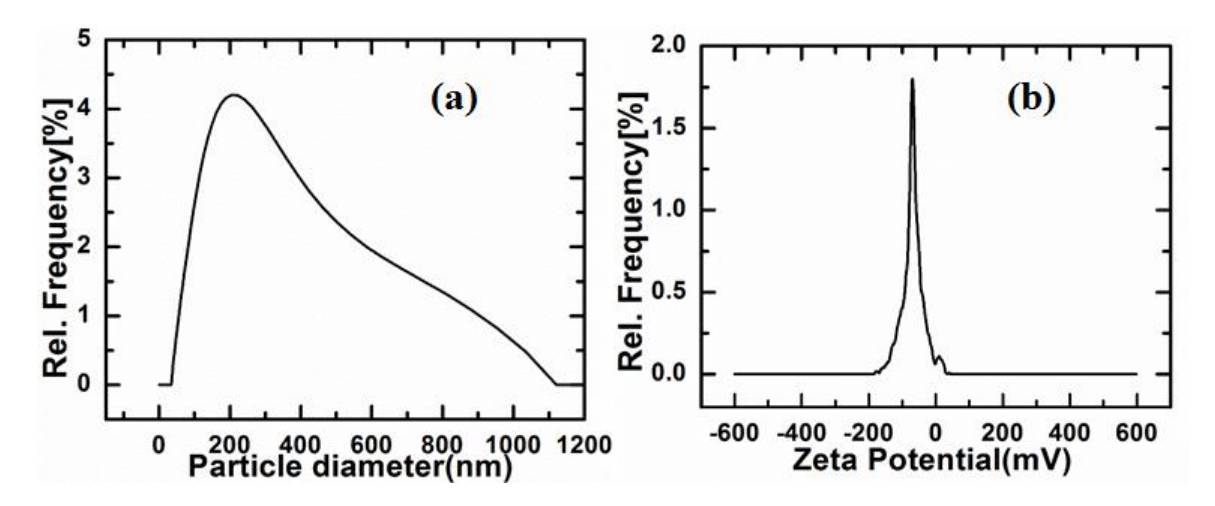


Figure 3. 3Fe₃O₄ nanoparticles distribution (a) and zeta potential (b).

The rise in ionic strength is the cause of compression of the electric double layer which results in reduction in zeta potential and vice versa.

3.1.4 Magnetization studies

M (H) plot at room temperature for Fe₃O₄ nanoparticles is shown in Fig. 3.4. The magnetite nanoparticles show ferrimagnetic behaviour. Similar results for Fe₃O₄ nanoparticles is reported by other group [3]. The saturation magnetization of Fe₃O₄ nanoparticles is 48 emu/g at 1.5 T.

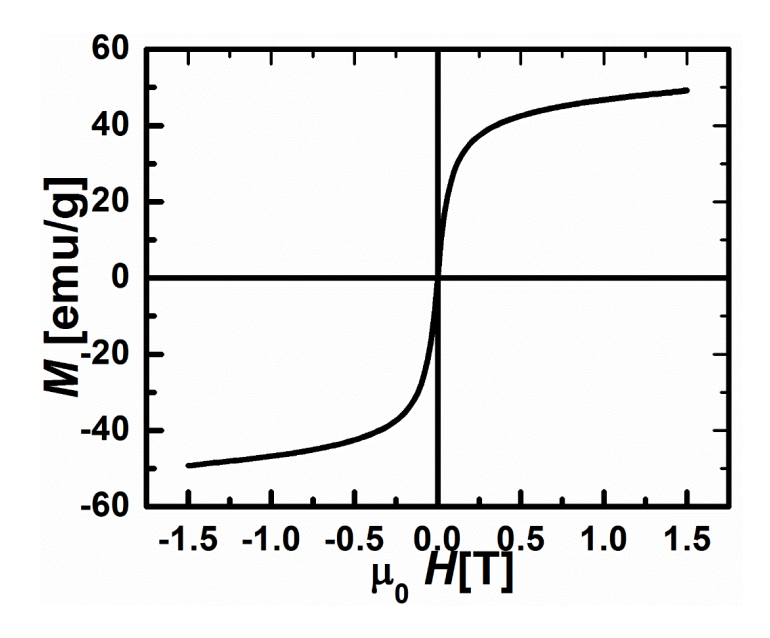


Figure 3. 4Magnetization curve for Fe₃O₄ nanoparticles.

Fig. 3.5 shows the ESR spectra of the nanoparticles. A broad asymmetric ESR signal is observed.

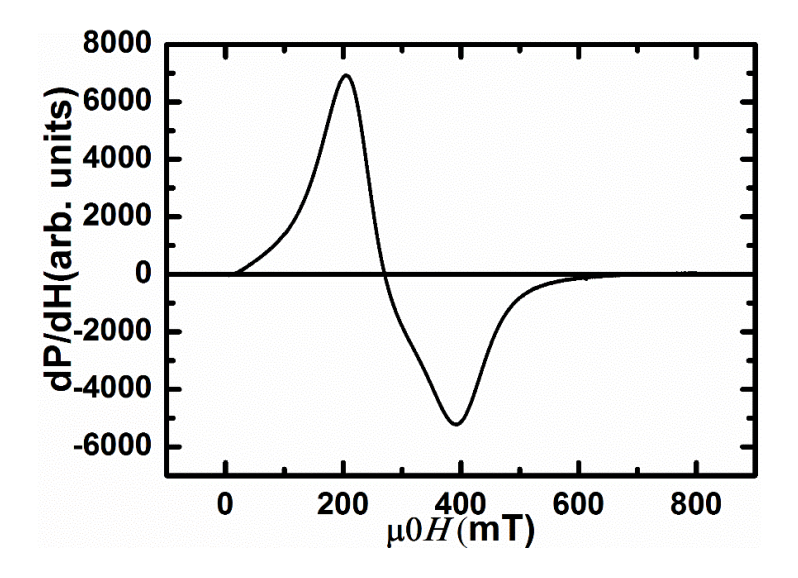


Figure 3. 5ESR signals for Fe₃O₄ nanoparticles.

The estimated g-value is 2.1, which clearly shows the ferrimagnetic nature of the nanoparticles. The magnetic moment of the Fe₃O₄ nanoparticles depends on particle size as well as the spin arrangement at the particle surface. The slightly different magnetic properties may be due to difference in particle size obtained in our synthesis procedure. Similar magnetic properties are reported by other group [4].

3.2 Studies on ferrofluids

The Fe₃O₄ based ferrofluids (FFs) were synthesized by using Fe₃O₄ nanoparticles in various solvents such as water, toluene, paraffin oil and silicone oil. The volume ratio of Fe₃O₄ nanoparticles, "surfactant" (DBSA /oleic acid) and solvent (water, toluene, paraffin or silicone oil in a particular volume) have been taken as 1:0.5:1.5 for preparing the ferrofluids. The Fe₃O₄ nanoparticles were coated with DBSA for the preparation of water (FW) based ferrofluid. Whereas Fe₃O₄ nanoparticles were coated with oleic acid for the toluene (FT), paraffin (FP) and silicone (FS) oil based ferrofluids respectively. The DBSA and oleic acid coating for Fe₃O₄ nanoparticles exhibit large hydrophobic nature which reduce the contact among the layers.

Chapter 3: Studies on Fe₃O₄ nanoparticles and ferrofluids

The list of prepared Fe₃O₄ nanoparticles based different ferrofluids are given below.

Table 3. 1: Fe₃O₄ ferrofluid in different colloids.

Ferrofluid Name	Composition	Solvent	Surfactant
FW	Fe ₃ O ₄	Water	DBSA
FT	Fe ₃ O ₄	Toluene	Oleic acid
FP	Fe ₃ O ₄	Paraffin Oil	Oleic acid
FS	Fe ₃ O ₄	Silicone oil	Oleic acid

3.2.1 Magneto-viscosity of water based ferrofluid

Magneto-viscosity of Fe₃O₄ based ferrofluids is studied in the magnetic field range of 0-1.33 T using a rheometer as described in chapter 2. Most of the magneto-viscosity measurements on Fe₃O₄ water based ferrofluids are reported in the low field range of 0-1 kOe. In this work magneto-viscosity measurements on Fe₃O₄ based ferrofluids in various colloids are carried out in the high magnetic range. Fig. 3.6 shows the magneto-viscosity plots for various Fe₃O₄ based ferrofluid at two shear rates of 1 and 10 s⁻¹. The variation of viscosity with increasing and deceasing field is complex at shear rate of 1 s⁻¹. With increasing field viscosity initially increases rapidly with increasing field and saturates at around 0.25 T field. It decreases with decreasing field with a large hysteresis in viscosity vs. magnetic field curve.

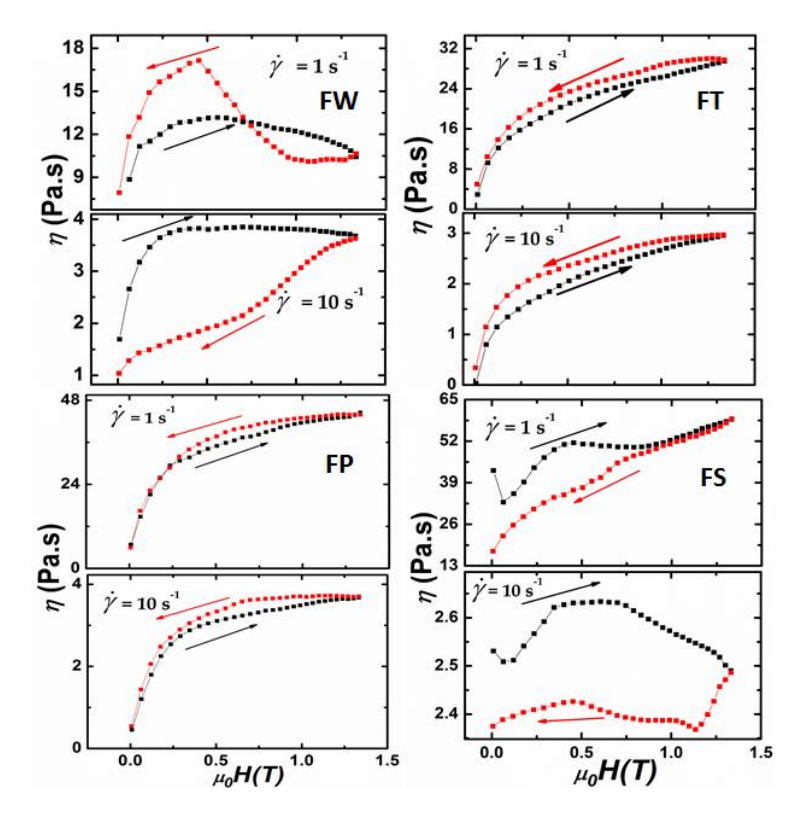


Figure 3. 6Magneto-viscosity plots of water, toluene, paraffin and "silicone oil" based ferrofluids.

3.2. 2 Toluene based Ferrofluid

Fig 3.6 shows Magneto-viscosity of toluene based ferrofluid at shear rate of 1 and 10 s⁻¹. The viscosity increases first rapidly and then slowly increased with increasing field. There is no saturation in viscosity even up to the highest magnetic field. There is small hysteresis in viscosity vs. field plot.

3.2.3 Paraffin oil based Ferrofluid

Fig. 3.6 shows the magneto-viscosity of paraffin oil based Fe₃O₄ ferrofluid at 1 and 10 s⁻¹ shear rates. Paraffin oil based ferrofluid show high viscosity (41 Pas. s) at 1 s⁻¹. The magnetic field of 0.7 T is sufficient for the viscosity to saturate at both shear rates. There is very small hysteresis in viscosity vs. magnetic field curve.

3.2.4 Silicone oil based Ferrofluid

Fig. 3.6 shows the magneto-viscosity of "silicone oil" based Fe₃O₄ ferrofluid at 1 and 10 shear rates respectively. This ferrofluid showed the highest viscosity (59Pa.s) without saturation at higher field. The viscosity vs. field behaviour is complex for increasing as well as decreasing. There is large hysteresis in viscosity vs. field curve at shear rate of $10 \, \text{s}^{-1}$.

The experimental results indicates that the variation in viscosity with magnetic field depends on the nature of carrier fluid and shear rate. The viscosity of liquids is determined by the interaction among the liquid molecules. Whereas for ferrofluids viscosity is due to colloids as well as due to interactions between magnetic nanoparticles. When a magnetic field is applied, the magnetic nanoparticles align in the direction of magnetic field forming drops or linear chains which offer flow resistance leading to increase in ferrofluid viscosity.

The viscosity variations of the FF with magnetic field is shown in Fig. 3.6. For FP and FT FF, when the field is decreasing the viscosity is higher than when field is increasing. Whereas for FW at shear rate 10 s⁻¹ and FS FF when the field is decreasing viscosity is lower than when the field is increasing. At lower fields for FW (shear rate 1 s⁻¹) FF when the field is decreasing, viscosity is higher than when the field is increasing.

As per classical theories with the increase magnetic field, the viscosity of the FF increases due to resistance offered by aggregation and formation of chain-like or drop-like structures [5]. When the field is decreasing the magnetic structures formed could not recover completely [6-8]. The magnetic field could cause, which leads to significant increase of viscosity of the ferrofluid. Computational Studies also confirm the formation of linear chains and bulk drop-like structures in FFs [9-10]. Obviously, the appearance of the chain-like and drop-like structures could affect the magneto-viscous properties of FFs. Several studies has pointed out that dipole–dipole interaction between nanoparticles and shear stress compete and give rise to magneto-viscous

effect [11-15]. Even a small percentage of the nanoparticles forming magnetic structures as dimers is sufficient to affect the flow of ferrofluid [16].

Fig. 3.6 hysteresis curves shows some interesting results.

- The increase in viscosity with increasing magnetic field is due formation of the chain-like and drop-like magnetic structures. It has been pointed out that the polydispersity of nanoparticle size in ferrofluids is necessary for magnetic structure formation [6-7]. At low fields the biggest nanoparticles form the drops
 When the field increases, the drops align in the field direction leading to viscosity saturation. As the magnetic field increases further the relatively small particles also form new chain-like structures and drops leading to further increase in viscosity of the FF. Much higher field is required to observe viscosity saturation due to relatively small particles. So the magneto-viscous effect of the FF at low field is due to the biggest particles and at high magnetic field it is due to relatively small particles.
- 2. The viscosity is higher when the magnetic field is decreased than when magnetic field is increased for FP and FT ferrofluids. This may be due to the reason that the structures do not reach the initial sizes when field is increased. It may also be due to formation of bigger drops than the drop size while increasing the field.

For FW and FS ferrofluids, the higher viscosity of ferrofluid when the field magnetic field is increased than when field is decreased is observed. This may be due to breakup of structures to smaller size due to shear when the field is decreased. The hydrodynamic forces become more dominant than field effects.

The hysteresis phenomenon observed in the magneto-viscosity plots, therefore, can be explained in view of formation and disintegration of the magnetic structures formed during increasing / decreasing of magnetic field.

The dipole-dipole interaction energy between the nanoparticles must be more than the thermal energy to form nanoparticle structures in a magnetic field.

When the magnetic field is applied the structure orient in the direction of field in the form of chains or drops giving rise to increase in viscosity i.e. magneto viscosity effect (MVE). When the shear rate is increased, the chains or drops disintegrate into smaller units leading to decrease in viscosity. The MVE therefore qualitatively as well as quantitatively depends on the competition between magnetic forces and hydrodynamic force (shear flow). The MVE therefore will be higher if magnetic field strength is high and shear rate is low.

3.3 Flow Curves of Fe₃O₄ Ferrofluids

The flow behaviour of the synthesized ferrofluids is investigated from the flow curves at different applied "magnetic fields". Fig. 3.7 shows the effect of solvent of Fe₃O₄ based ferrofluid on viscosity vs. shear rate plots. The FS FF show the highest viscosity. The non –Newtonian behaviour is observed for FW, FS and FT FFs in entire range of shear rate. The FT FF shows Newtonian behaviour above shear rate of 200 s⁻¹. Because of high concentration of magnetic particles, the magnetic structures are formed due to dipole interactions of the nanoparticles. The large distribution in hydrodynamic diameter of the magnetic particles suggest that the drop-like magnetic structures of various sizes are formed in the FF without the application of external magnetic field. The size of the magnetic structures depends on the type of solvent. In the case of FS, FW and FT FFs, these structures are so large in size that the highest shear rate is unable to disintegrate them resulting in Non- Newtonian behaviour of these FFs. These results show a profound effect of solvent on the rheological properties of Fe₃O₄ based.

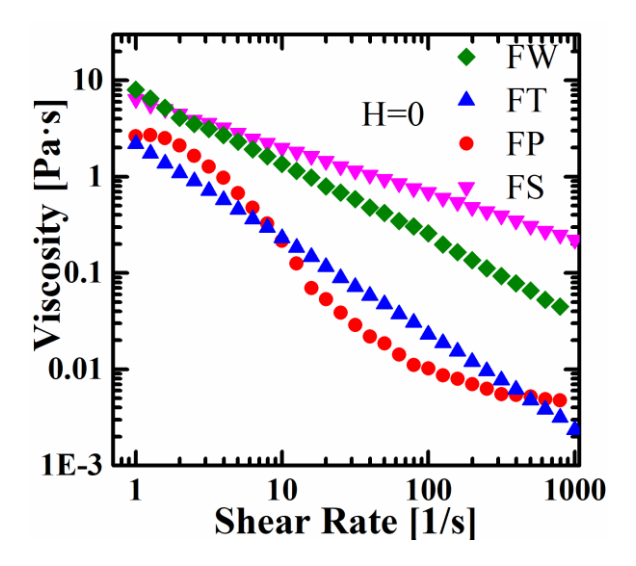


Figure 3. 7 Colloidal effect in water, toluene, paraffin and silicone oil based ferrofluids at zero field

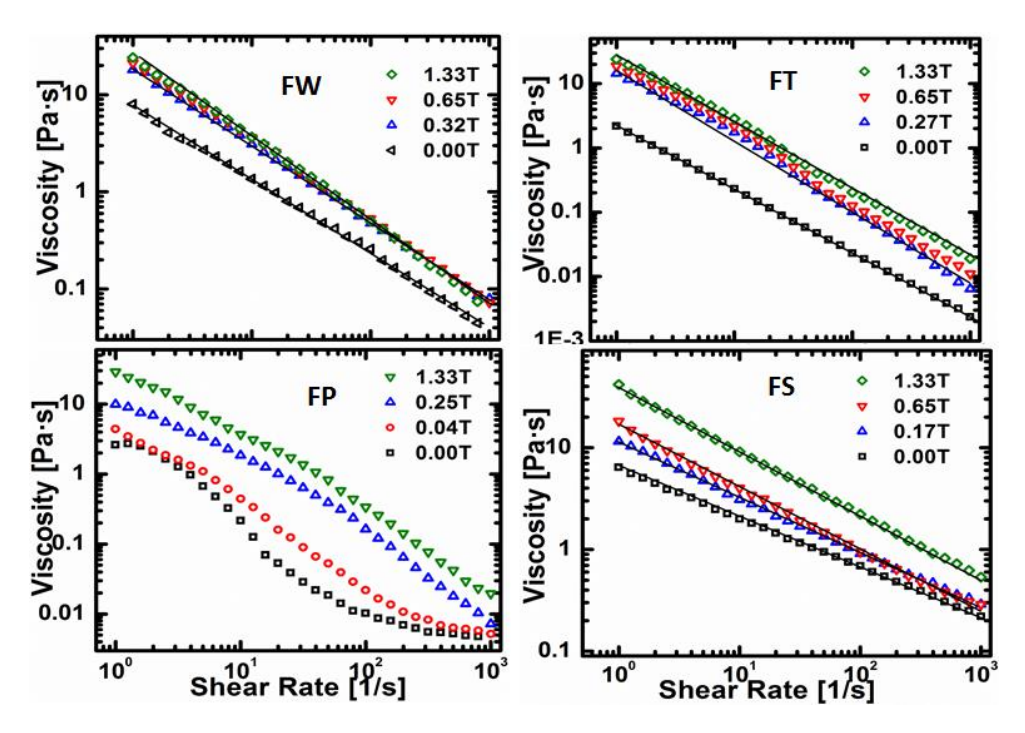


Figure 3. 8 Flow curves of different Fe₃O₄ ferrofluids at various magnetic fields

Table 3. 2: The fitting parameters of power law

Ferrofluid Name	K values	n (power index)	Magnetic field (T)
	7.6	0.22	0.00
FW	23.8	0.19	1.33

Chapter 3: Studies on Fe₃O₄ nanoparticles and ferrofluids

	2.1	0.02	0.00
FT	14	0.08	0.27
	24	0.08	1.33
	6.31	0.5	0.00
FS	17	0.3	0.65
	39	0.3	1.33

Fig. 3.8 shows the flow curves for Fe₃O₄ ferrofluids at different field values between 0 to 1.33 T. The viscosity increases at low shear rate and thus show non-Newtonian behaviour. The similar viscosity vs. shear rate behaviour was observed by other group [17]. Since in low shear regime, the "magnetic force" dominate the "hydrodynamic force" in the ferrofluid leading to magnetic structure formation which hinder the flow and thus lead to increase in viscosity. Due to disordered arrangement of the magnetic nanoparticles at low shear rate they resist to flow so the resultant fluidity decreased [18]. As the shear rate increases the bigger chains were broken into smaller chains which leads to decrease in the viscosity. The hydrodynamic forces dominate in the high shear rate regime and the ferrofluids show the Newtonian behaviour. Similar behaviour is noticed by other group in water based ferrofluid based on surface modified dextran coated magnetic nanoparticles [19]. The power law behaviour is nor observed for FP FF.

3.4 Shear stress of different Fe₃O₄ Ferrofluids:

The FW ferrofluid data is analyzed in view of H-B model. Fig.3.8 shows the shear stress verses shear rate for water based ferrofluid (FW). At higher magnetic field the stress is increasing due to magnetized saturation of the magnetic nanoparticles (Fe₃O₄) in the external magnetic field direction. This phenomenon is described through

Herschel-Bingham (H-B) model: $\tau = \tau_0 + K \dot{\gamma}^{n-1}$, where τ_0 shows the yield stress of the Fe₃O₄ nanoparticle, τ is shear stress. The yield stress values are calculated via extrapolation of the shear stress plot by "H-B model fit" at zero field as well as "applied magnetic fields". This model is derived using the power law with the inclusion of "yield stress"

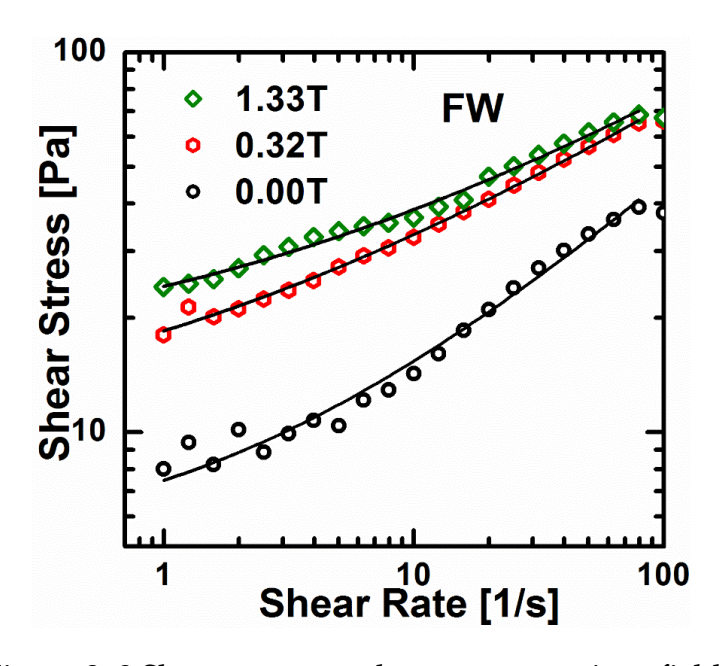


Figure 3. 9 Shear stress vs. shear rate at various fields

The increase in yield stress value from 4 to 15 Pa with applied field from 0 to 1.33 T is observed. With increasing field the chain formation occurs leading to increase in yield stress.

Table 3. 3: H-B model fitting parameters for FV	V:	ferrofluid.
---	----	-------------

Ferrofluid Name	K values	n (power index)	Magnetic field (T)	Yield stress($ au_0$ (Pa)
	2.7	1.58	0.0	4.70
FW	8.90	1.42	0.32	9.5
	9.10	1.4	1.33	15

Chapter 3: Studies on Fe₃O₄ nanoparticles and ferrofluids

Many research group have worked on synthesize the stable ferrofluid from different method and in different colloidal media [21]. Recently, the rheological properties of water based Fe₃O₄ ferrofluids was reported [22]. The flow curves follow the Newtonian behaviour and H-B model at different fields. Similarly, other group reported that the water based ferrofluids exhibit the non-Newtonian behaviour at different magnetic field[23]. Most of the studies are on dilute ferrofluids. In this work concentrated Fe₃O₄ based ferrofluid in water is synthesized and got high viscosity as compared to other reports. The toluene and paraffin oil based ferrofluids show low hysteresis in viscosity vs. field plots which is promising for applications.

In summary, the nanoparticles of Fe₃O₄ were successfully prepared by coprecipitation method. The XRD data analysis confirmed the cubic spinel structure with Fd-3m space group. The microstructural study is confirmed the spherical shaped nanoparticles. The magnetization results showed the ferrimagnetic behaviour. The magneto-viscosity of ferrofluids determined through the interaction among molecules of the solvent, between the magnetic nanoparticles and the applied magnetic field. Silicone oil based ferrofluid showed the highest magneto-viscosity at 1 s⁻¹ whereas the toluene based and paraffin oil based ferrofluids found to be more stable fluids with the application of applied field. The flow curves showed the non-Newtonian behaviour for all synthesized ferrofluids. The yield stress values are calculated via extrapolation of the shear stress plot by "H-B model fit" at zero field as well as "applied magnetic fields".

References:

- [1] Y. Li *et al.*, "Fe3O4@PSC nanoparticle clusters with enhanced magnetic properties prepared by alternating-current magnetic field assisted co-precipitation," *Colloids and Surfaces A: Physicochemical and Engineering Aspects*, vol. 520, pp. 348–354, May 2017.
- [2] A. O. Bokuniaeva and A. S. Vorokh, "Estimation of particle size using the Debye equation and the Scherrer formula for polyphasic TiO ² powder," *Journal of Physics: Conference Series*, vol. 1410, p. 12057, Dec. 2019.
- [3] Y. Wei, B. Han, X. Hu, Y. Lin, X. Wang, and X. Deng, "Synthesis of Fe3O4 Nanoparticles and their Magnetic Properties," *Procedia Engineering*, vol. 27, pp. 632–637, 2012.
- [4] O. M. Lemine *et al.*, "Sol–gel synthesis of 8nm magnetite (Fe3O4) nanoparticles and their magnetic properties," *Superlattices and Microstructures*, vol. 52, no. 4, pp. 793–799, Oct. 2012.
- [5] M. A. Martsenyuk, Yu. L. Raikher, and M. I. Shliomis,"On the kinetics of magnetization of suspensions of ferromagnetic particles", *Sov. Phys.-JETP*, vol. 38, No.2, February 1974.
- [6] A. Y. Zubarev, J. Fleischer, and S. Odenbach, "Towards a theory of dynamical properties of polydisperse magnetic fluids: Effect of chain-like aggregates," *Physica A: Statistical Mechanics and its Applications*, vol. 358, no. 2–4, pp. 475–491, Dec. 2005.
- [7] A. Y. Zubarev and L. Y. Iskakova, "To the theory of rheological properties of ferrofluids: influence of drop-like aggregates," *Physica A: Statistical Mechanics and its Applications*, vol. 343, pp. 65–80, Nov. 2004.
- [8] S. Masoud Hosseini, A. Fazlali, E. Ghasemi, H. Ahmadi Moghaddam, and M. Salehi, "Rheological properties of a γ-Fe2O3 paraffin-based ferrofluid," *Journal of Magnetism and Magnetic Materials*, vol. 322, no. 23, pp. 3792–3796, Dec. 2010.
- [9] E. Krutikova and A. O. Ivanov, "The role of van der Waals forces in ferrofluid phase separation," *Physics Procedia*, vol. 9, pp. 49–53, 2010.
- [10] A. Yu Zubarev and L. Y. Iskakova, "Condensation phase transitions in bidisperse colloids," *Physica A: Statistical Mechanics and its Applications*, vol. 349, no. 1–2, pp. 1–10, Apr. 2005.
- [11] S. Odenbach and K. Raj, "The Influence of Large Particles And Agglomerates On The magnetoviscous Effect In Ferrofluids", *Magnetohydrodynamics*, vol. 36, No. 4, 2000.

- [12] S. Odenbach and S. Thurm, "Magnetoviscous Effects in Ferrofluids," in *Ferrofluids*, vol. 594, S. Odenbach, Ed. Berlin, Heidelberg: Springer Berlin Heidelberg, 2002, pp. 185–201.
- [13] Stefan Odenbach, Thomas Rylewicz, Michael Heyen,"A rheometer dedicated for the investigation of viscoelastic effects in commercial magnetic Fluids", *Journal of Magnetism and Magnetic Materials* 201 (1999) 155-158.
- [14] S. Odenbach, H. Stork," Shear dependence of field-induced contributions to the viscosity of magnetic fluids at low shear rates", *Journal of Magnetism and Magnetic Materials* 183 (1998) 188-194.
- [15] S. Odenbach, "Ferrofluids—magnetically controlled suspensions," *Colloids and Surfaces A: Physicochemical and Engineering Aspects*, vol. 217, no. 1–3, pp. 171–178, Apr. 2003.
- [16] L. Mao, S. Elborai, X. He, M. Zahn, and H. Koser, "Direct observation of closed-loop ferrohydrodynamic pumping under traveling magnetic fields," *Physical Review B*, vol. 84, no. 10, Sep. 2011.
- [17] G. Wang, Y. Ma, Y. Tong, and X. Dong, "Synthesis, characterization and magnetorheological study of 3-aminopropyltriethoxysilane-modified Fe ³ O ⁴ nanoparticles," Smart Materials and Structures, vol. 25, no. 3, p. 35028, Mar. 2016.
- [18] Y.-H. Son, Y. Jung, H. Roh, and J.-K. Lee, "Enhanced viscoelastic property of iron oxide nanoparticle decorated organoclay fluid under magnetic field," *Nano Convergence*, vol. 4, no. 1, Dec. 2017.
- [19] A. Józefczak, T. Hornowski, Z. Rozynek, A. Skumiel, and J. O. Fossum, "Rheological Study of Dextran-Modified Magnetite Nanoparticle Water Suspension," *International Journal of Thermophysics*, vol. 34, no. 4, pp. 609–619, Apr. 2013.
- [20] H. Gu *et al.*, "Ubbelohde viscometer measurement of water-based Fe3O4 magnetic fluid prepared by coprecipitation," *Journal of Magnetism and Magnetic Materials*, vol. 348, pp. 88–92, Dec. 2013.
- [21] N. S. Asri *et al.*, "Syntheses of ferrofluids using polyethylene glycol (PEG) coated magnetite (Fe3O4), citric acid, and water as the working liquid in a cylindrical heat pipe," *Nano-Structures & Nano-Objects*, vol. 25, p. 100654, Feb. 2021.
- [22] R. Y. Hong, Z. Q. Ren, Y. P. Han, H. Z. Li, Y. Zheng, and J. Ding, "Rheological properties of water-based Fe 3 O 4 ferrofluids," *Chemical Engineering Science*, vol. 62, no. 21, pp. 5912–5924, Nov. 2007.
- [23] M. E. Khosroshahi and L. Ghazanfari, "Preparation and rheological studies of uncoated and PVA-coated magnetite nanofluid," *Journal of Magnetism and Magnetic Materials*, vol. 324, no. 24, pp. 4143–4146, Dec. 2012

CHAPTER-4

Studies on Cu-Zn (CZF) Ferrite nanoparticles and ferrofluids

This chapter is on the studies of structure, magnetic and magneto-viscosity of Zn doped Cu-ferrite nanoparticles synthesized by two different preparation methods. The chapter is divided in two sub-sections. First section describes the structural, magnetic and magneto-viscosity of co-precipitated "Cu_{1-x}-Zn_xFe₂O₄" (C-CZF) (x= 0, 0.2, 0.4, 0.6) nanoparticles and ferrofluids. Second section describes structural, magnetic and magneto viscosity of hydrothermalized "Cu_{1-x}-Zn_xFe₂O₄" (H-CZF) (x= 0, 0.2, 0.4, 0.6) nanoparticles and ferrofluids. The XRD, FESEM, DLS and VSM were used to characterize the nanoparticles. The DBSA and oleic acid were used as the surfactants. The C-CZF nanoparticles were dispersed in toluene and paraffin oil and the H-CZF nanoparticles were dispersed in water and paraffin oil for the preparation of ferrofluids. The effect of colloidal on magneto-viscosity is studied for the synthesized ferrofluids.

4.1 Study of Co-precipitated CZF (C-CZF) nanoparticles

4.1.1 "Structural studies":

Fig. 4.1 shows the XRD of Cu-Zn (Zn=0, 0.2, 0.4, 0.6) ferrite. Rietveld analysis is used to fit the XRD pattern and two phases are observed in the structure. The cubic spinel is the main phase which has Fd-3 m space group and the other one is CuO phase with C12/c1 space group. Spinel phase percentage is found to be increased from 74% to 100% as x increases from 0 to 0.4 respectively. The CuO phase vanishes at x = 0.4 and again appears at x = 0.6. These results show the instability in the structure formation. The Debye Scherrer formula is used to calculate the crystallite size as described in chapter 3. The average crystallite sizes (d), lattice parameters (a, b, c) for all phases are tabulated in the Table 4.1.

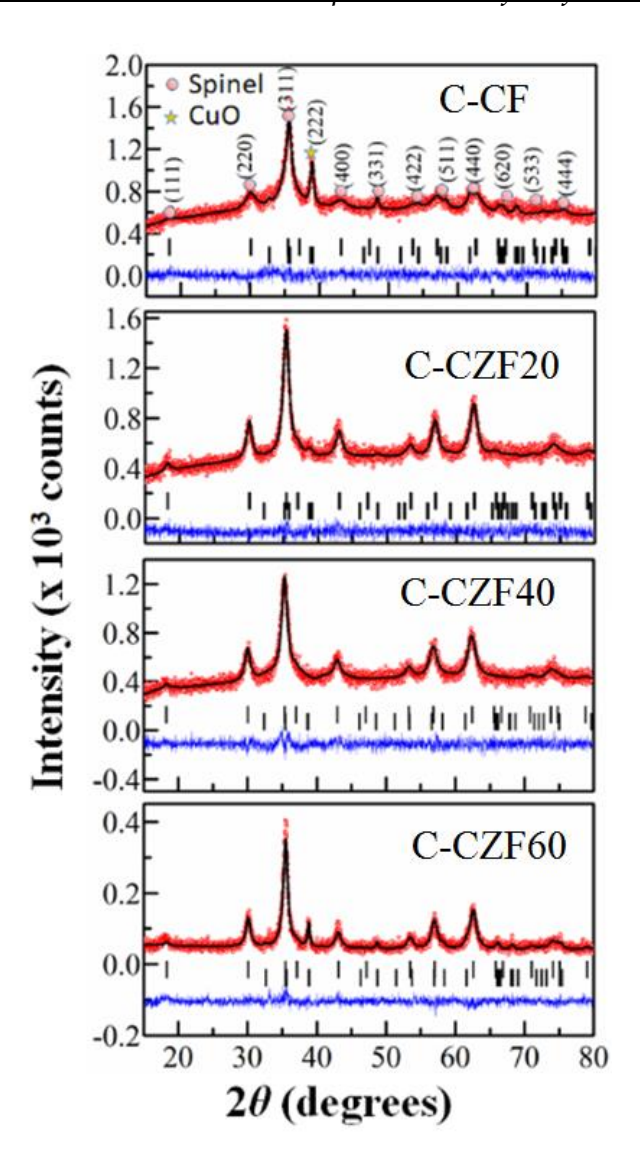


Figure 4. 1 XRD spectra of C-CZF nanoparticles.

Table 4. 1: Crystallographic parameters for C- CZF nanoparticles.

Sample	CuO phase	Crystallite	Lattice	Spinel	Lattice
Name	(%)	Size (nm)	parameters for	phase	parameters
		(d)	CuO (Å)	(%)	(Á)
CCF	25	8	a=4.73,b=3.38, c	75	a=b=c=8.39
			=5.13,β=99.94		α= β=γ= 90

CCZF20	5	9	a =4.78,b= 3.47, c	95	a=b=c=8.40
			= 4.96, β=100.33		α= β=γ= 90
CCZF40	_	7	a =4.70,b= 3.47, c =	100	a=b=c=8.41
			4.96, β=99.55		α= β=γ= 90
CZF60	8	10	a=4.68, b=3.38, c	92	a=b=c=8.38
			=5.13, β=99.57		α= β=γ= 90

4.1.2 Morphological Analysis

The FESEM micrographs for CZF nanoparticles of various compositions are shown in Fig.4.2. The acquired micrographs reveal that the particles are almost spherical in shape but not uniform in size. It is observed that the particles are forming bigger cluster with increasing Zn content in the Cu ferrite.

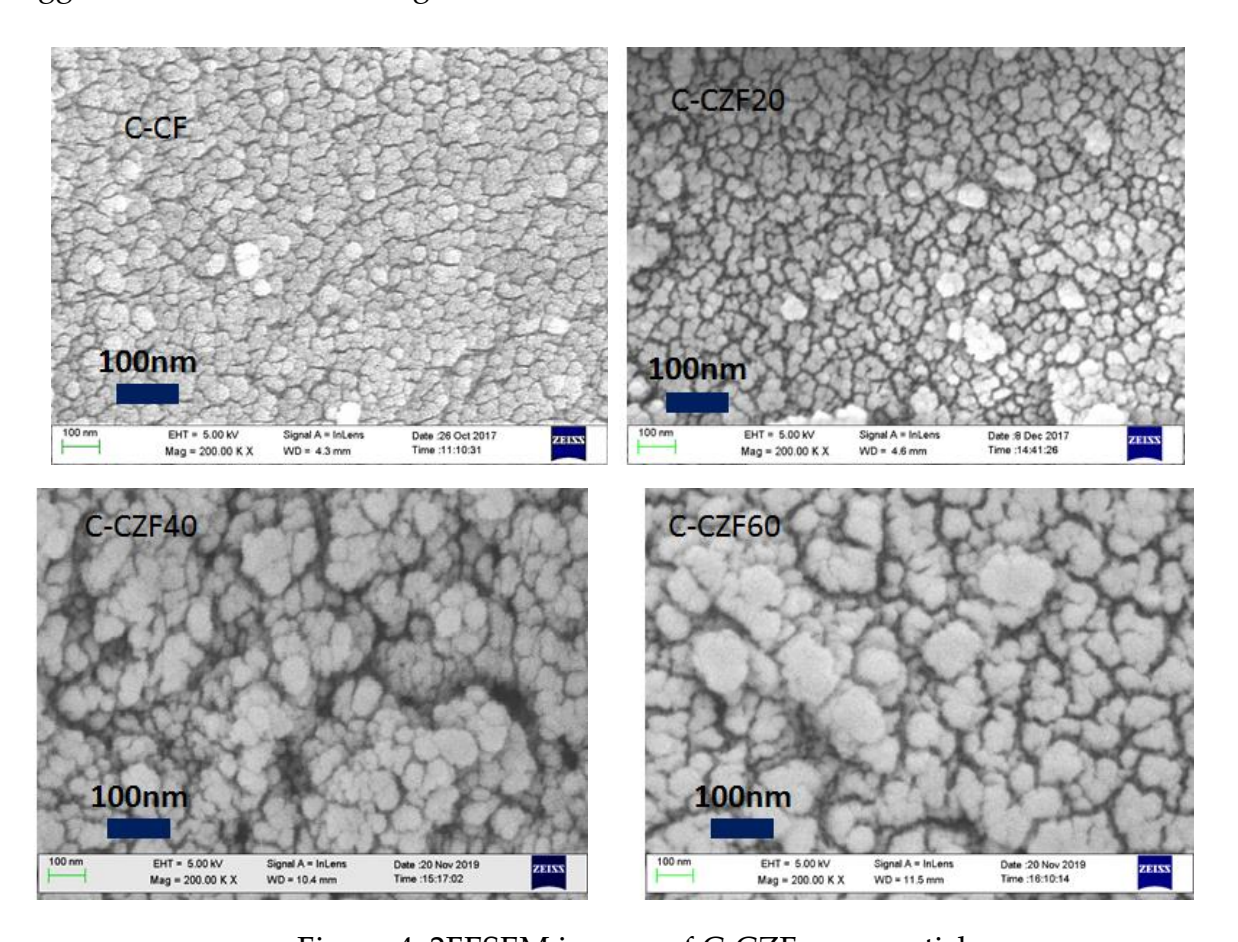
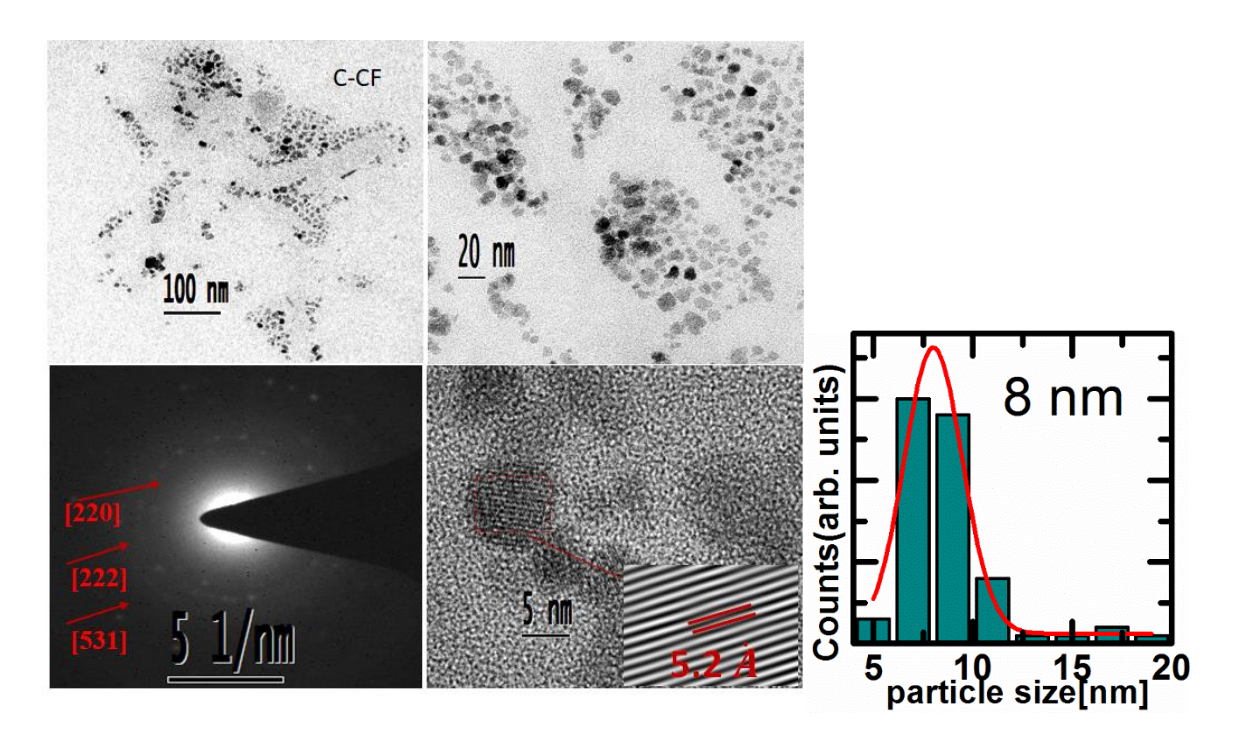
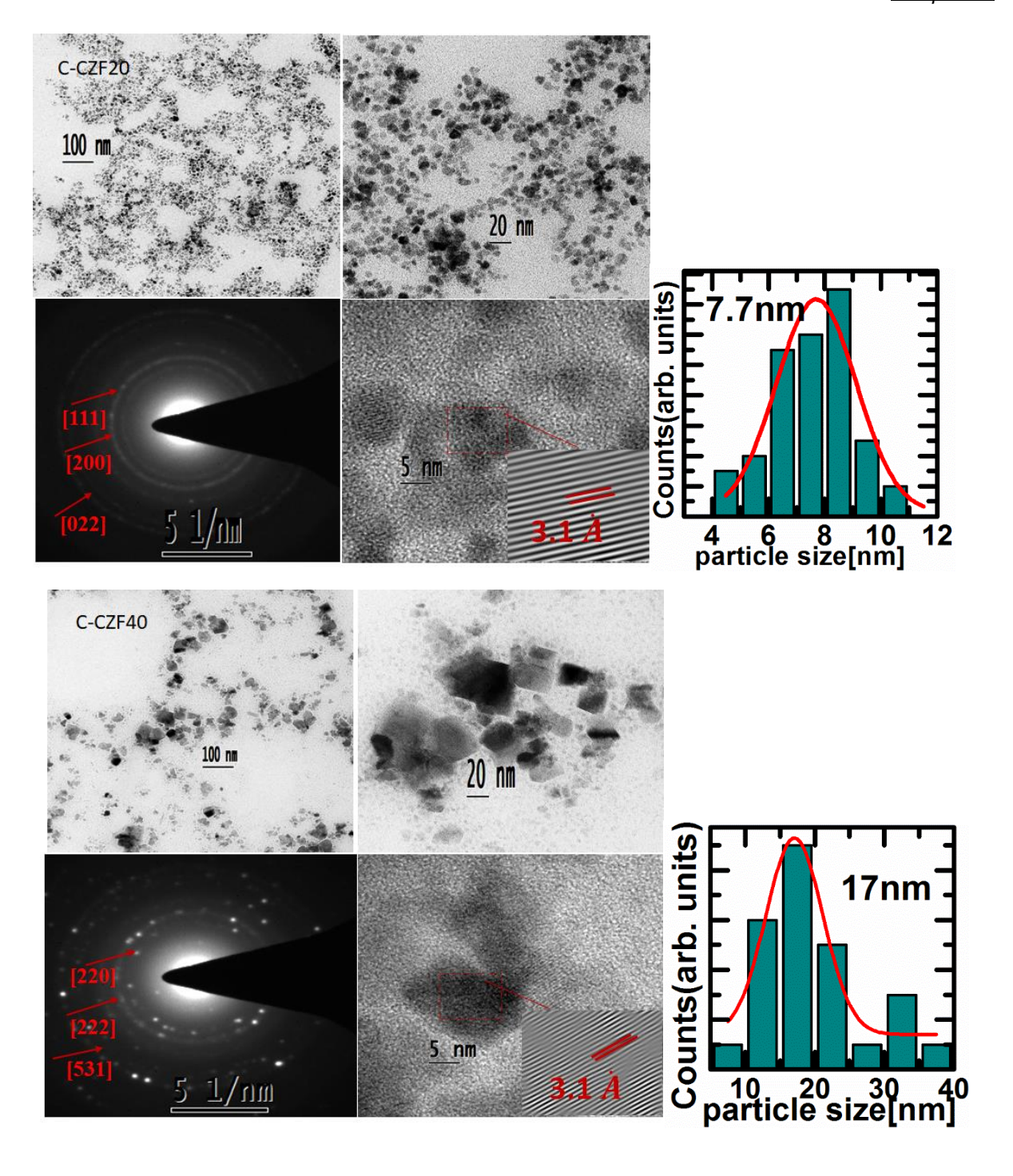


Figure 4. 2FESEM images of C-CZF nanoparticles.

4.1.3 TEM Analysis

Fig. 4.3 represents the TEM images of co-precipitated Cu-Zn (Zn= 0.0, 0.2, 0.4, 0.6) ferrite nanoparticles at different magnifications. For each composition (CCF, CCZF20, CCZF40, CCZF60) image are recorded to show the distribution of the nanoparticles, "scattered area electron diffraction (SAED) pattern" and "high resolution transmission electron microscopy" (HR-TEM). The images show mixture of spherical as well as cubic shape nanoparticles. The average particle sizes are listed in Table 4.2.





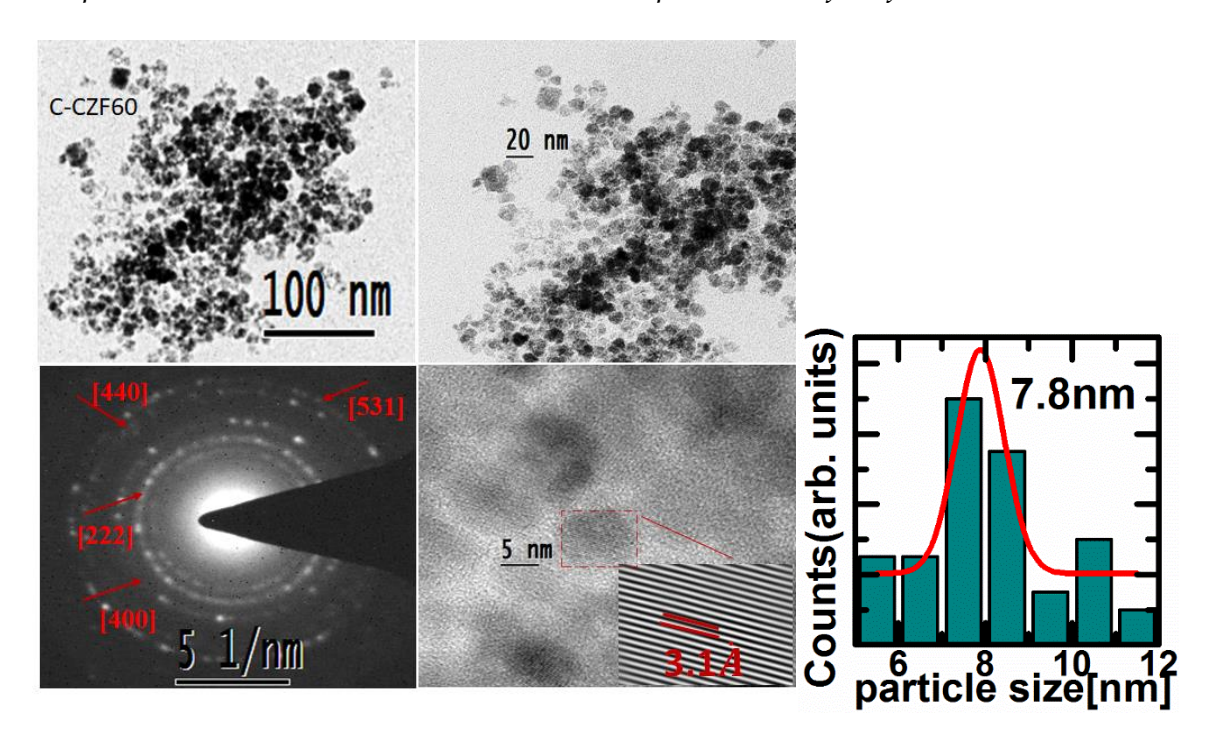


Figure 4. 3 "TEM micrographs" for C-CZF nanoparticles.

Table 4. 2: Average particles size, particle distribution and zeta potential parameters.

Sample Name	Average Particles Size (± 1 nm)	Hydrodynamic diameter (±5 nm)	Zeta Potential (mV)
C-CF	8	161	-63.7
C-CZF20	7.7	169	-71.8
C-CZF40	17	171	-81.8
C-CZF60	7.8	195	-80.2

4.1.4 Particle size distribution and zeta potential

 $\label{eq:Fig. 4.4} \textbf{Fig. 4.4} \ \textbf{represents} \ \textbf{the hydrodynamic particle size distribution of C-CZF} \\ \textbf{nanoparticles}.$

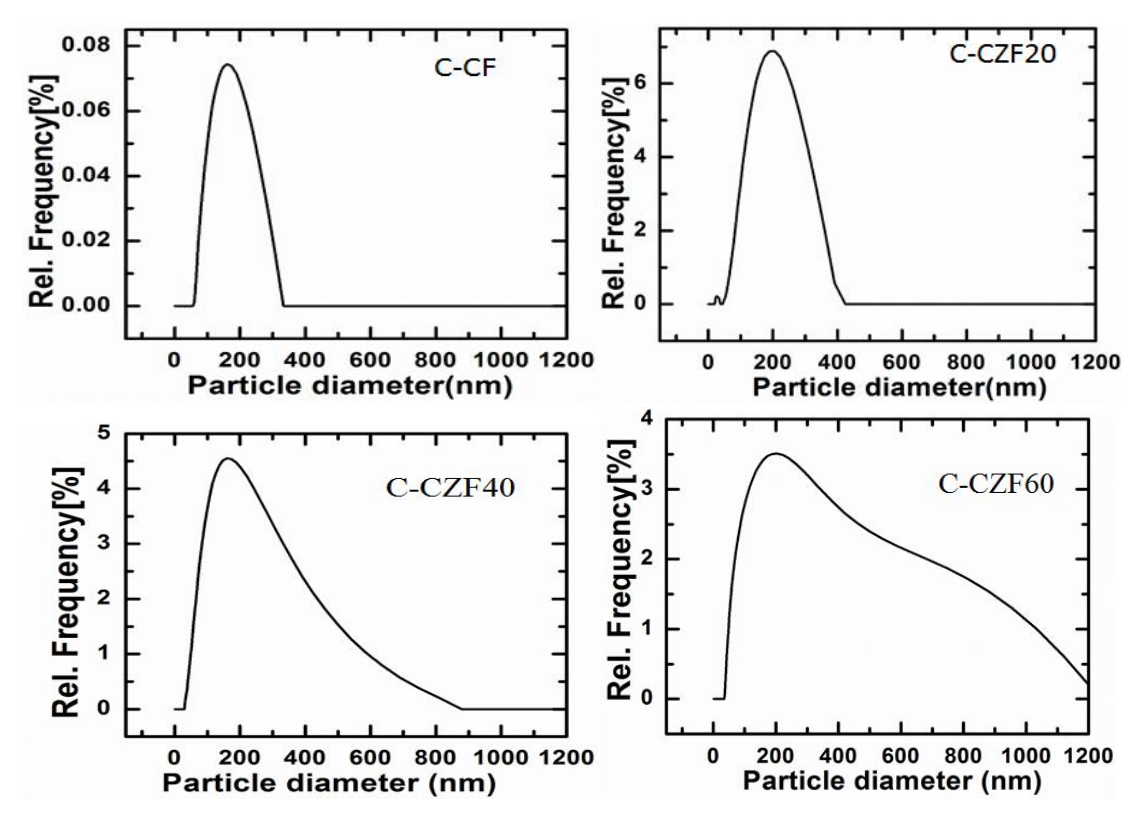


Figure 4. 4Particle size distribution of C-CZF nanoparticles.

The quantity of sample taken for measurement is about 0.05%. The hydrodynamic diameter of the nanoparticles is more as compared to TEM results due to the cluster formation of magnetic nanoparticles when mixed in water media. The hydrodynamic size is listed in table 4.2 for various samples. It is found that the hydrodynamic size distribution increases with increase in Zn content. This means that bigger agglomerate formation is taking place with increasing non-magnetic metal ion.

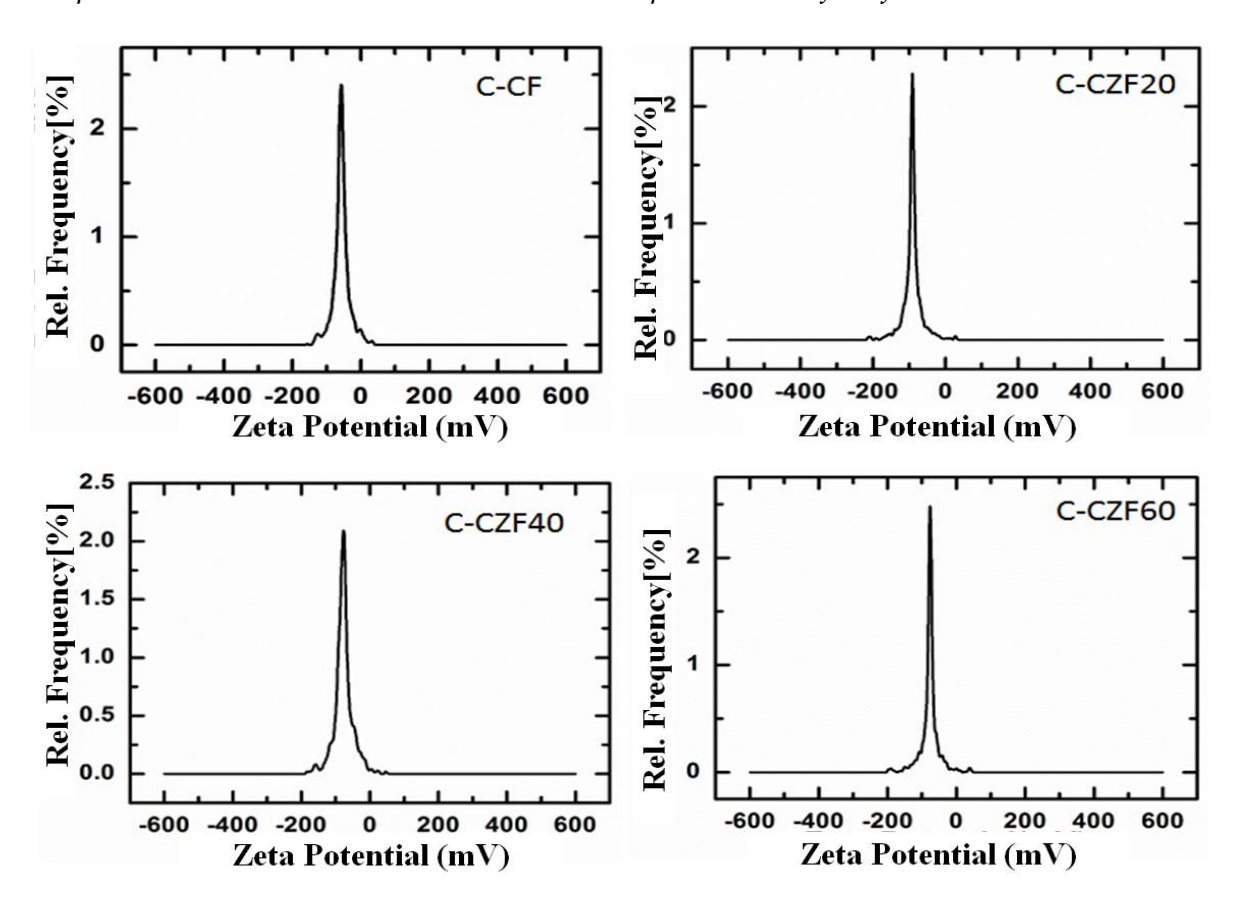


Figure 4. 5 Zeta potential of C-CZF nanoparticles

The Fig 4.5 illustrates the zeta potential which is basically used to predict the suspension stability. The higher "zeta potential" value indicate higher "stability" of the solution. The C-CZF samples show high negative zeta values which contribute to prevent the agglomeration by electrostatic repulsion. The samples show excellent stability.

4.1.5 Magnetization Studies of C-CZF nanoparticles:

Fig. 4.6 shows the magnetization (M (H)) vs. applied magnetic field plots for Cu-Zn (Zn=0.0, 0.2, 0.4, 0.6) nanoparticles at 5K and 300K.

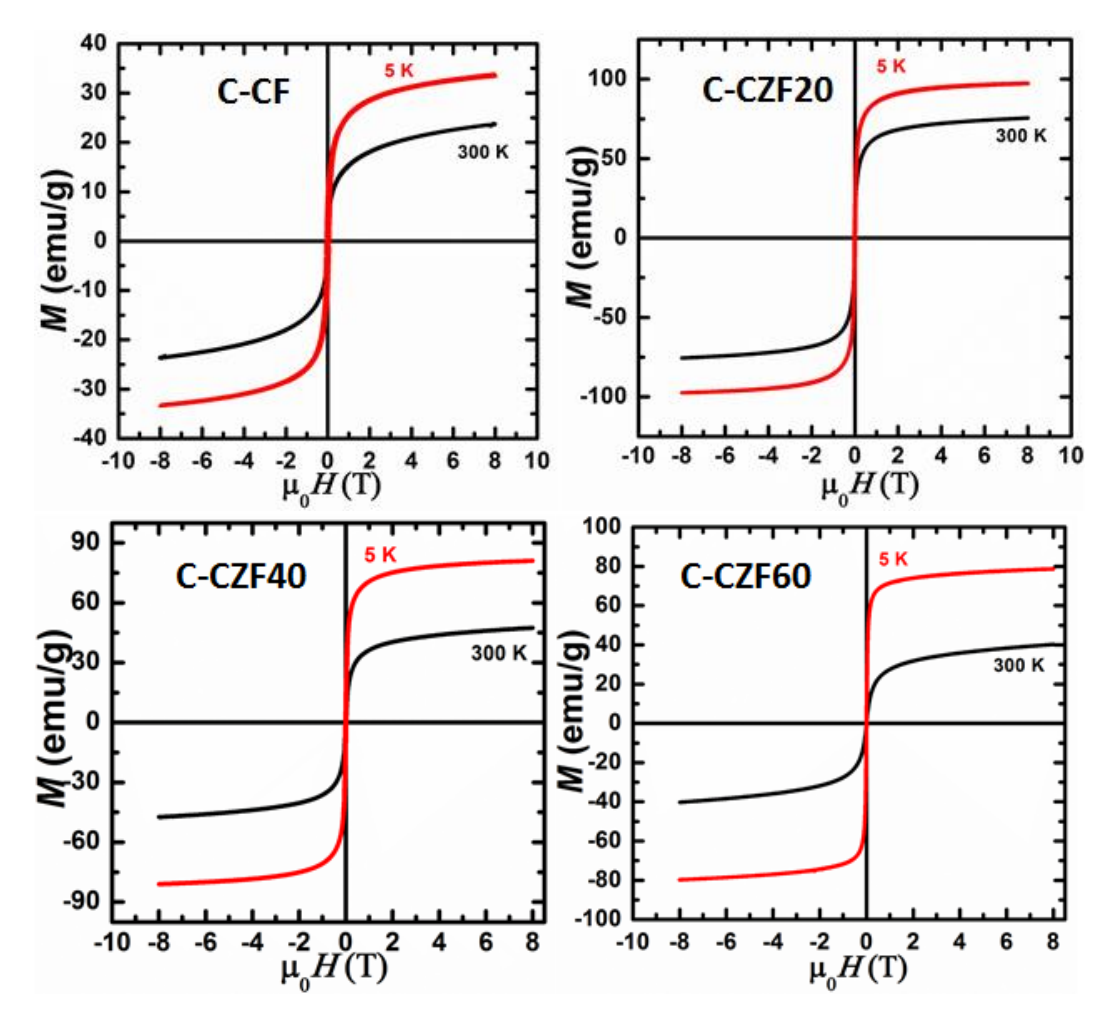


Figure 4. 6 Magnetization curves for C-CZF nanoparticles.

Due to low values of M_R and H_C magnetic, the results confirm the super paramagnetic behaviour of CZF nanoparticles [1-2]. The Ms value increases as Zn content increases to x=0.2 and then followed by decreasing trend for Zn content, x>0.2.

Table 4. 3: M (H) parameters for C- CZF nanoparticles.

Sample Name	Saturation Magnetization (Ms) (emu/g) at 300 K	Saturation Magnetization (Ms))(emu/g) at 5 K
CCF	23	33
CCZF20	75	97
CCZF40	47	81

Chapter 4 Studies on Cu-Zn (CZF) Ferrite nanoparticles and ferrofluids

CZF60 40 78

Fig. 4.7 shows the magnetization vs. Zn content. Magnetic properties of ferrite depend on the composition, particle size and cation distribution. The reduction in lattice parameters with increasing Zn content for x > 0.2 should increases Ms, but it decreases gradually with increase in Zn content as shown in Fig 4.6 and Fig 4.7.

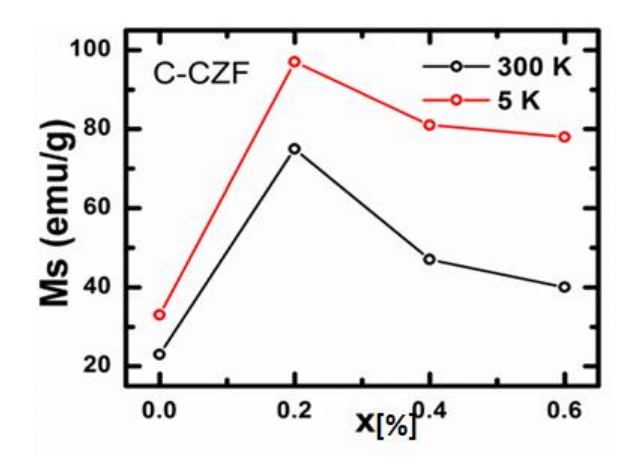


Figure 4. 7 Magnetization vs. Zn-content of C-CZF nanoparticles.

The initial increase in Ms can be described on the basis of "Neel's sub-lattice model theory". The increment in magnetization is resultant of drop of "MA" with "Zn" content because of non-magnetic Zn^{+2} ions in spinel ferrite acquire the A site and replaces Fe^{+3} from A site to B site. The Cu-Zn ferrite has cubic spinel structure. The cations "super exchange interaction" (A-B) is highly stronger as compared to "(A-A)" or "(B-B)" interactions. Therefore, the cation distributions over A and B sites and particles size has strong effect on magnetic properties. The super exchange interaction between two magnetic cations through oxygen ion can be as a result of "intra sub lattice" "AA" and "BB" and inter-sublattice "AB" interactions. The bond angle and distance between two metal cations determine the superexchange interaction strength between them. The "AB" interaction is known as the strongest interaction among all other interactions, whereas AA and BB interaction are weak interactions. So the "AB" interaction become weak for x > 0.2 due to reduction in number of magnetic ions at A site as Zn content increases.

The temperature dependence of magnetization of CZF nanoparticles in temperature range of 2 to 375 K was studied under "applied magnetic field" of 100 Oe in "zero-field cooling" (ZFC) and "field cooling" (FC) modes. In ZFC mode the sample was cooled from 375 to 2 K without field. The magnetization measurement was performed with increasing temperature by applying 100 Oe magnetic field. The sample was cooled under field in FC mode and magnetization data was noted. The magnetization increases with decreasing temperature in ZFC mode. After reaching a maximum value it decreases rapidly with decreasing temperature. Magnetization vs. temperature plot for C-CZF nanoparticles is shown in Fig. 4.8.

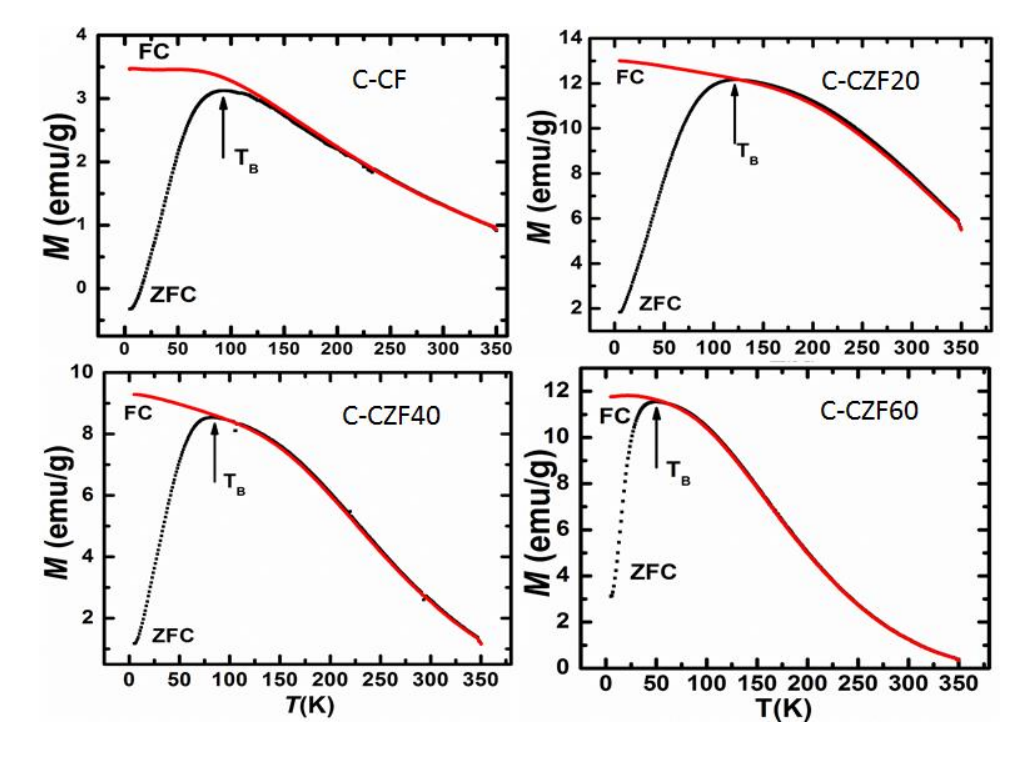


Figure 4. 8FC and ZFC curves of C-CZF nanoparticles at applied field of 100 Oe.

The magnetization achieved maximum value at "blocking temperature (T_B)" where the "relaxation time" is equivalent to time scale of magnetic measurements. Therefore, as temperature decreases, under FC mode magnetization continues to increase approaching towards a saturation value. The FC and ZFC curves separation elucidate the non-equilibrium magnetization. Two phenomenon have been noticed for the superparamagnetic system: First is the paramagnetic nature at high

temperatures for all the samples and second is the curved maxima in ZFC curves at temperature T_{max} . This is related to the magnetic moment distribution of nanoparticles. The curve separation temperature, $T_B = 91$, 113, 89, 51 K for CCF, CCZF20, CCZF40 and CCZF60 samples, respectively. The results clearly show the irreversibility continuing below T_B . This is related to the blocking temperature of the bigger particles.

4.1.6 Rheological study of C-CZF based ferrofluids:

4.1.6.1 Flow curves and magneto-viscosity plots of toluene based Cu-Zn ferrite ferrofluids

Toluene has low viscosity and used as most common dispersing solvent for ferrofluid preparation. Fig. 4.9 shows the effect of composition for toluene based CZF ferrofluids without any external magnetic field. The C-CZF20 FF show high viscosity as compared to C-CZF40 and C-CZF60 FF due to high magnetization. All ferrofluids follow Newtonian behaviour at shear rate $> 50 \, \text{s}^{-1}$ and non-Newtonian behaviour at shear rate $< 50 \, \text{s}^{-1}$.

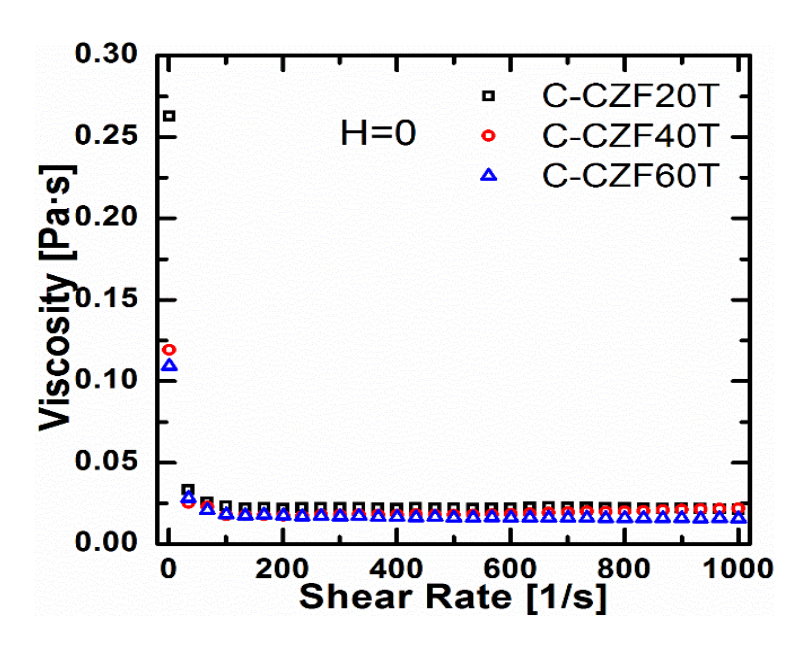


Figure 4. 9 Effect of composition of CZF on viscosity of toluene based ferrofluids at H=0.

Fig. 4.10 depicts the flow curves of toluene based ferrofluids at various magnetic field values. All the ferrofluids show "non-Newtonian" behaviour at low shear rate <

100 s⁻¹. The flow curves approach "Newtonian" behaviour at high "shear rate". These flow curves exhibit the power law behaviour.

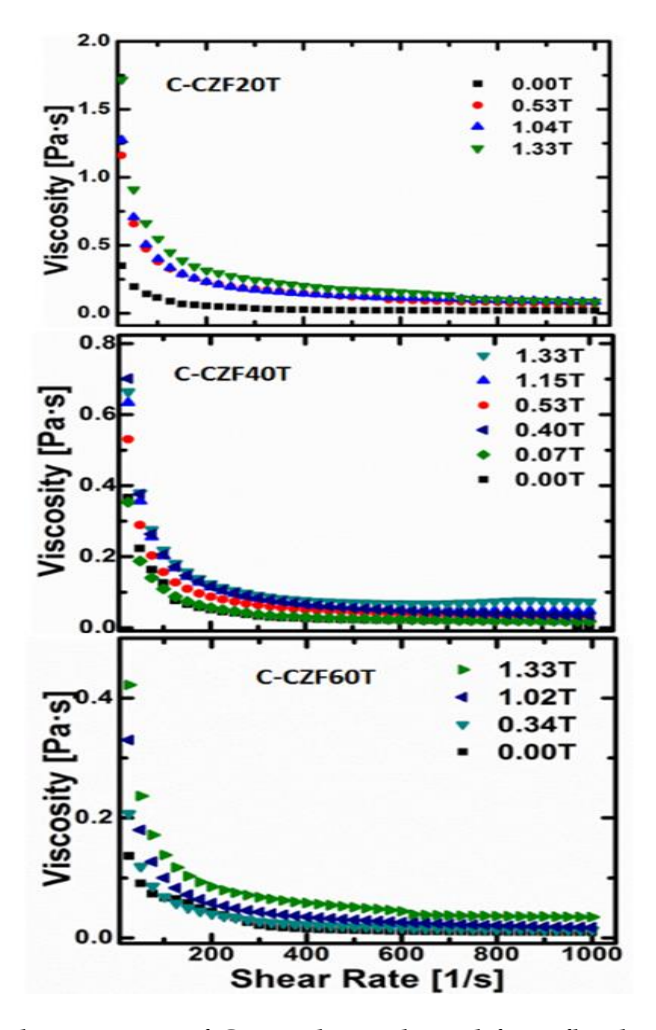


Figure 4. 10 Flow curves of CZF toluene based ferrofluids respectively.

The ferrofluid show "non-Newtonian" behaviour even without external applied field at low shear rates indicating the formation of magnetic structures like drops or chains due to dipole-dipole interactions. The large hydrodynamic diameter and its dispersion indicates the formation of magnetic drops of various sizes. These magnetic drops consisting of nanoparticles align in chains when an external magnetic field is applied and thus give rise to magneto viscous effect (MVE). Fig. 4.11 shows the magneto-viscosity of toluene based CZF FF ferrofluids at 1 and 10 s⁻¹shear rates.

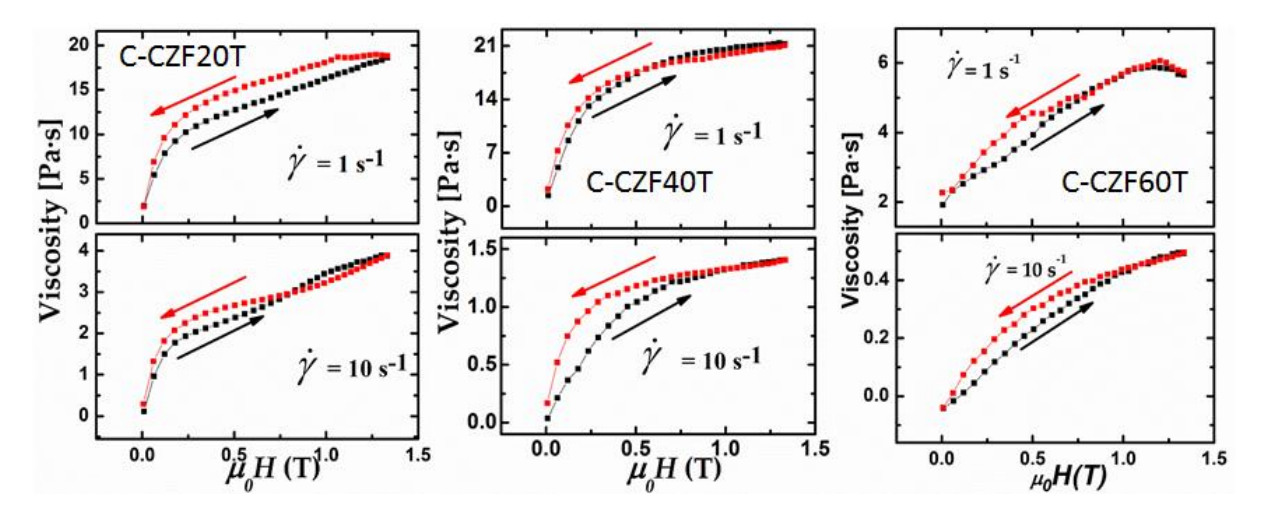


Figure 4. 11 Magneto-viscosity of toluene based C-CZF ferrofluids.

The hysteresis is observed in magneto-viscosity curves. The viscosity increases sharply as magnetic field is applied for CZF20T, CZF40T FFs and appears to approach saturation value with increasing field. For CZF60T the viscosity increases with increasing field with no sign of approaching saturation value. For all samples the viscosity is lower for increasing magnetic field stage than for decreasing magnetic stage. This means that magnetic structures, chains and drops formed while increasing magnetic field do not relax back to their original shapes when magnetic field is removed. This is due to domination of magnetic force over hydrodynamic force in the ferrofluid. The maximum MVE with minimum hysteresis is observed for CZF40T at shear rate of 1 s⁻¹. This sample therefore can find application as flow controller by applying magnetic field.

4.1.6.2 Flow curves and "magneto-viscosity" plots of "paraffin" based CZF ferrofluids

The CZF20P, CZF40P and CZF60P ferrofluids were prepared by dispersing coated CZF nanoparticles with oleic acid in paraffin oil. As from magnetization study the CZF (Zn=0.2, 0.4 and 0.6) nanoparticles exhibit the super paramagnetic nature. Fig. 4.12 represents the effect of composition on viscosity vs. shear rate plot at zero applied field for CZF paraffin based ferrofluids. The C-CZF20 FF show high viscosity as compared to other FF due to high magnetization. All ferrofluids follow the non-

Newtonian behaviour below shear rate $< 100 \text{ s}^{-1}$ and approach Newtonian behaviour above shear rate of $> 100 \text{ s}^{-1}$.

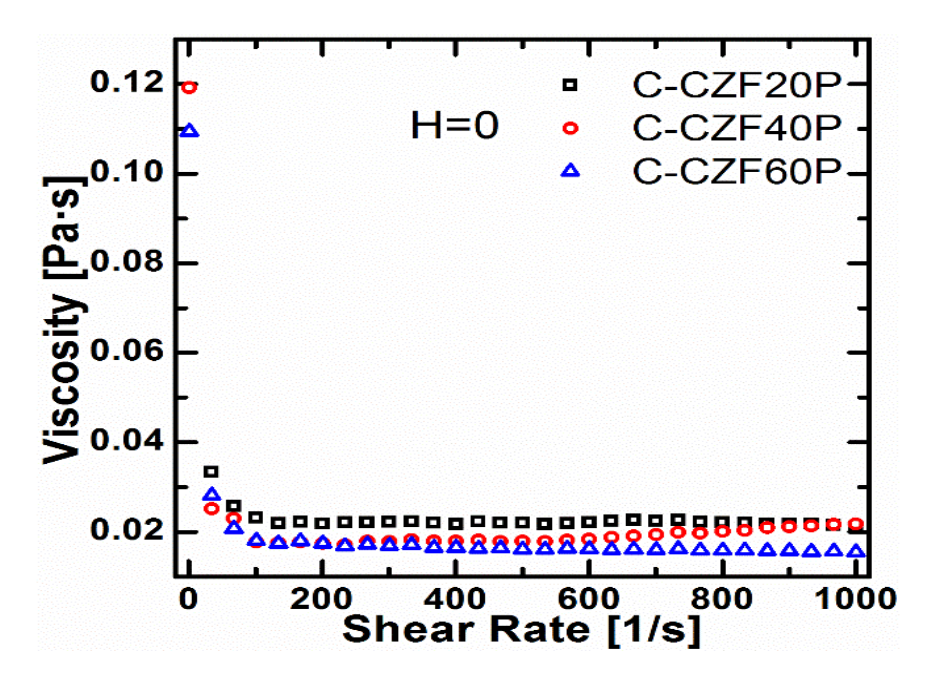


Figure 4. 12 Effect of composition of CZF paraffin based ferrofluids at H=0.

Fig. 4.13 presents the viscosity vs. shear rate at different magnetic fields (0 to 1.33T). The viscosity decreases non-linearly with shear rate. The ferrofluids approach Newtonian behaviour above shear rate of 500 s⁻¹ when magnetic field is applied. This is due to alignment of preexisting magnetic structures as linear chains in the applied magnetic field direction. The CZF40P ferrofluid exhibits the maximum magneto viscosity effect at low shear rate as compared to the other ferrofluids. These may be due to large dispersion in hydrodynamic diameter compared to other FFs.

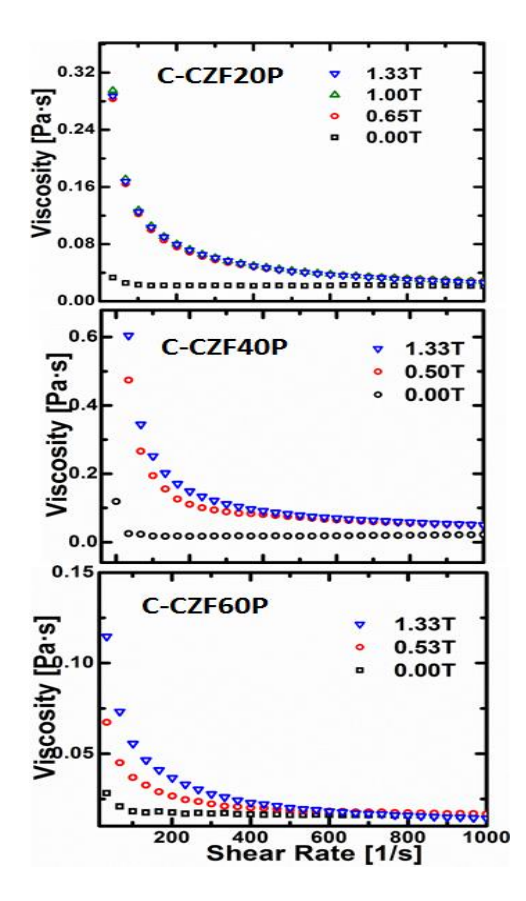


Figure 4. 13 Flow curves of paraffin oil based C-CZF ferrofluids.

Fig. 4.14 represents the magneto-viscosity of CZF nanoparticles dispersed in paraffin oil at shear rate 1 and $10~\rm s^{-1}$ for CZF20P, CZF40P and CZF60P respectively. The CZF40P shows the highest change in viscosity with applied magnetic field. This may be due to wider distribution in hydrodynamic diameters of magnetic structures consisting of nanoparticles preformed in the absence of applied field. When the field is applied the bigger particles as well as tiny particles generate the aggregation in the field direction as chains or drops. All the ferrofluids show the magnetic hysteresis. The maximum MVE with minimum hysteresis is observed for CZF40T at shear rate of $1~\rm s^{-1}$.

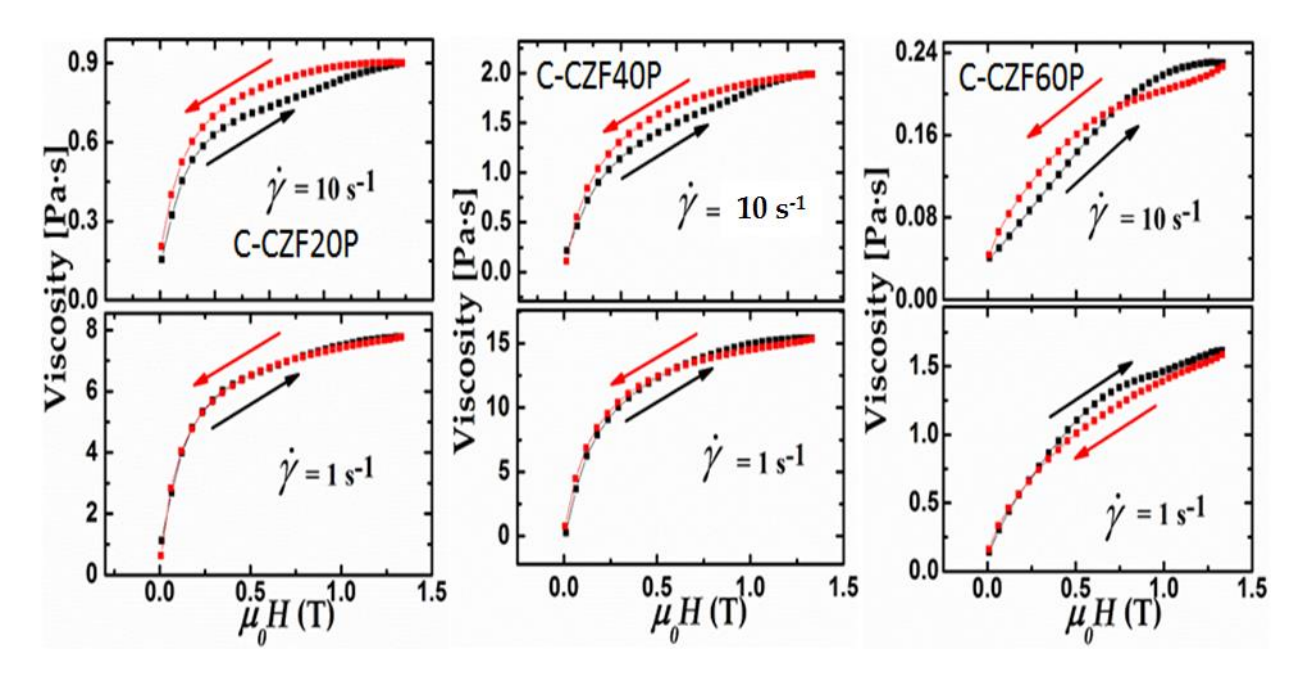


Figure 4. 14 Magneto-viscosity of CZF paraffin oil based ferrofluids.

This sample therefore can find application as flow controller by applying magnetic field. The magnetic hysteresis is much lower as compared to toluene based FFs

4.2: Study of hydrothermalized (H- CZF) nanoparticles:

4.2.1 "XRD" results:

Fig. 4.15 shows the "XRD pattern" of hydrothermalized CZF samples. The XRD pattern is fitted with the three phase structures confirmed by "Rietveld analysis". The cubic spinel is main the phase with space group Fd-3m. The second phase is CuO with space group "C12/c1" and third is confirmed as orthorhombic phase with the "space group" "R -3 c". The orthorhombic phase is 41% for x=0.0 composition and with substituting of Zn it disappeared.

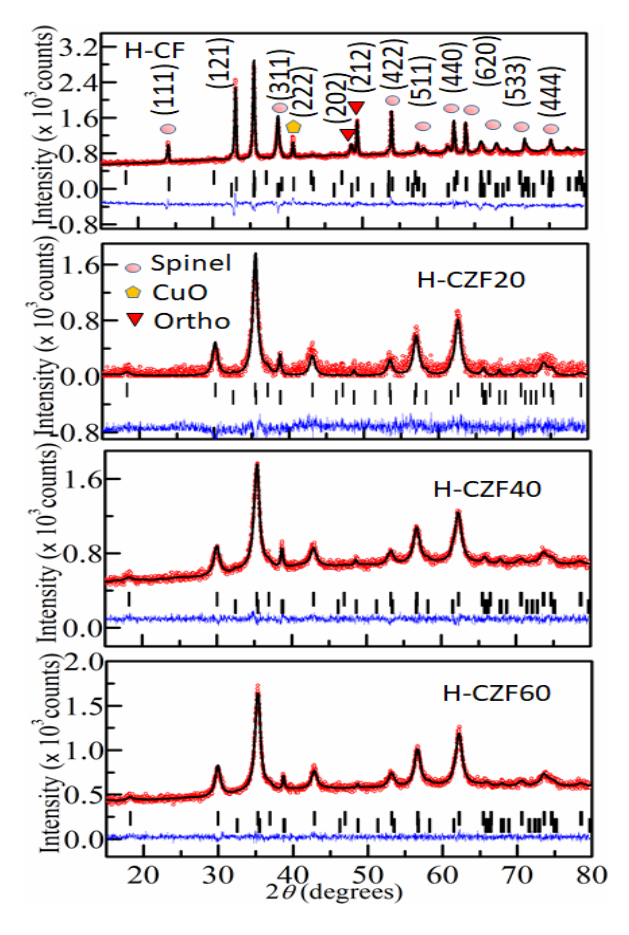


Figure 4. 15 XRD images of H-CZF.

The lattice parameters for orthorhombic phase are a=b=5.04 c=13.78 Å and $\alpha=\beta=90$, $\gamma=120$. The average crystallite size and lattice parameters of hydrothermal CZF nanoparticles are mentioned in the Table 4.4. After hydrothermal treatment the phases are stabilized. Increase in lattice parameter is noticed due to the difference in ionic sizes of Cu⁺² and Zn⁺² with increase in Zn content. The ionic radius of Zn is more as compared to Cu⁺² and when doping happen on A-site then Fe⁺³ ion are displaced from A- site to B-site [3].

Table 4. 4: "Crystallographic parameters" for H- CZF nanoparticles.

Sample	Crystallite	CuO	Lattice	Spinel	Lattice parameters
Name	Size (nm)	phase	parameters for	phase	for Spinel phase (Á)
		(%)	CuO phase (Å)	(%)	
HCF	28	56	a=4.698,b=3.416,	3	a=b=c = 8.391 α=β=γ=
			c =5.11,β=99.61		90
HCZF20	13	8	a=4.698,b=	92	a=b=c = 8.385
			3.416, c =5.11		α=β=γ= 90
			β=99.59		
HCZF40	10	1	a =4.709,b=	99	a=b=c = 8.432
			3.429, c = 5.136		α=β=γ= 90
			β=99.55		
HCZF60	11	0.5	a=4.697,b=	99.5	a=b=c = 8.441
			3.427, c =5.140		α=β=γ= 90
			β=99.53		

4.2.2 FESEM Results

The FESEM micrographs for H-CZF nanoparticles are presented in Fig. 4.16. The non- uniform particle size distribution of nearly spherical in the shape is observed. The images show particle agglomeration for all the CZF samples.

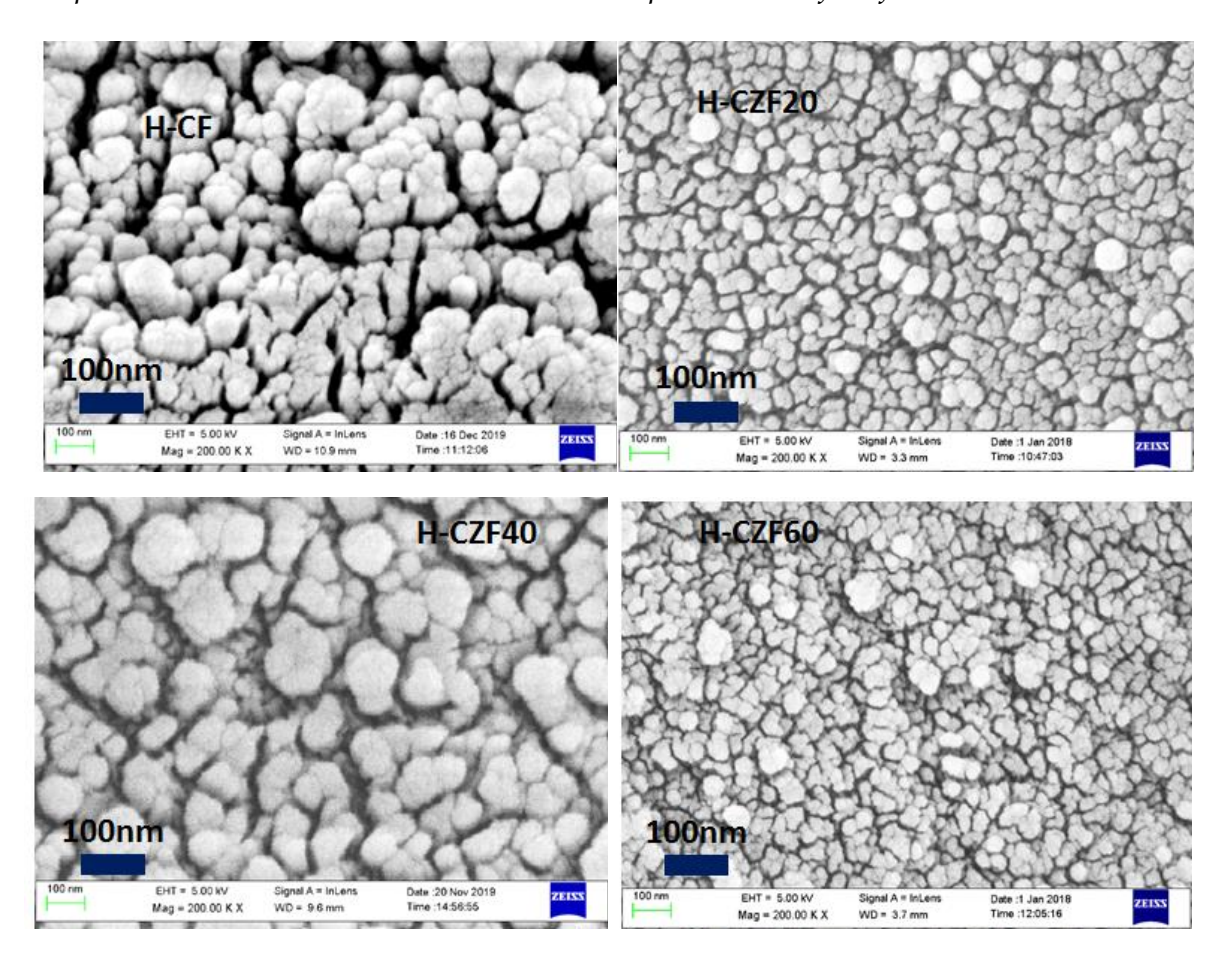
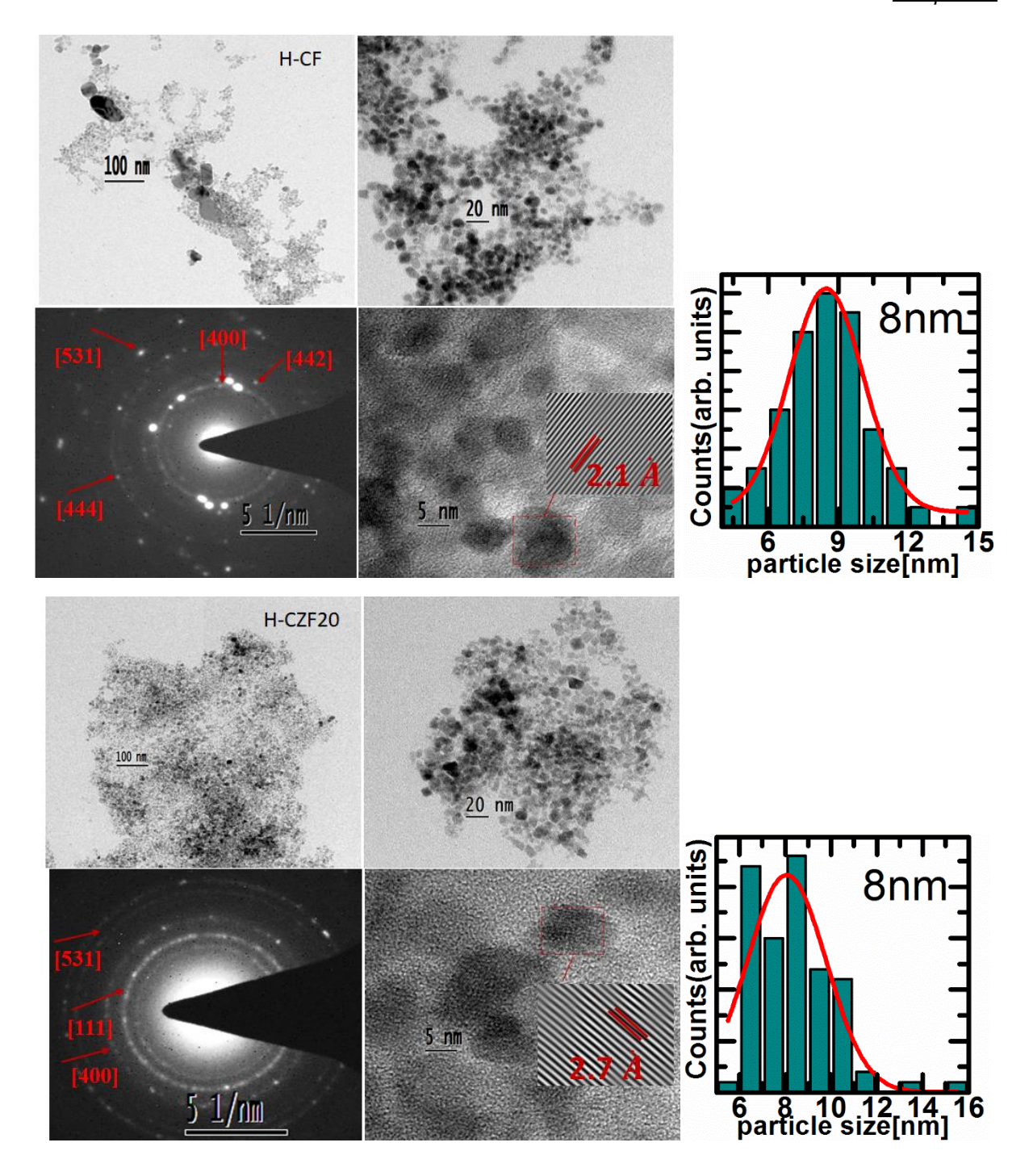


Figure 4. 16 FESEM images of H- CZF

4.2.3 TEM Analysis

Fig. 4.17 shows the TEM images of H-CZF (Zn= 0.0, 0.2, 0.4, 0.6) ferrite nanoparticles at different magnifications.



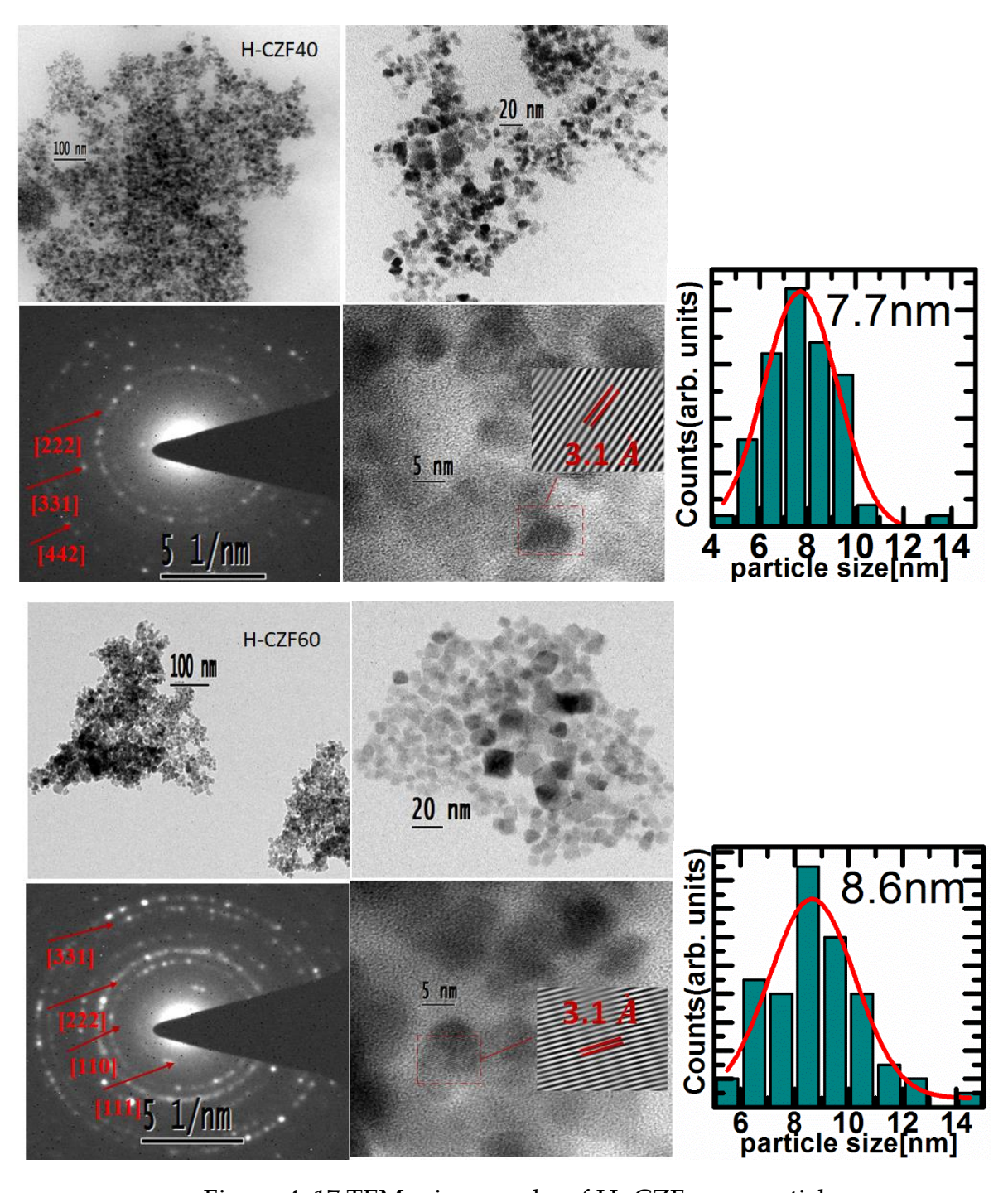


Figure 4. 17 TEM micrographs of H- CZF nanoparticles.

In Fig. 4.17 each composition (HCF, HCZF20, HCZF40, HCZF60) have four images together: two micrographs show the distribution of the nanoparticles, third show the scattered "area electron diffraction" (SAED) pattern and fourth represent "high resolution transmission electron microscopy" (HR-TEM) respectively. The H-CZF samples show increase in crystallite size. The analysis concluded that particles size is enlarged and the shape changes from spherical to cubic after heat treatment of

the nanoparticles [4-5]. Particle size and distribution along with zeta potential for CZF nanoparticles are is listed in Table 4.5.

4.2.4 Particle size distribution and zeta potential

Fig. 4.18 shows the size distribution H-CZF nanoparticles. The hydrodynamic diameter of the nanoparticles is more as compared to TEM results due to the cluster formation of magnetic nanoparticles when put into the water media. The hydrodynamic sizes are listed in Table 4.5 for various samples. The hydrodynamic diameter increases with increase Zn content which clarifies the particle cluster formation is taking place with increasing of non-magnetic metal ion.

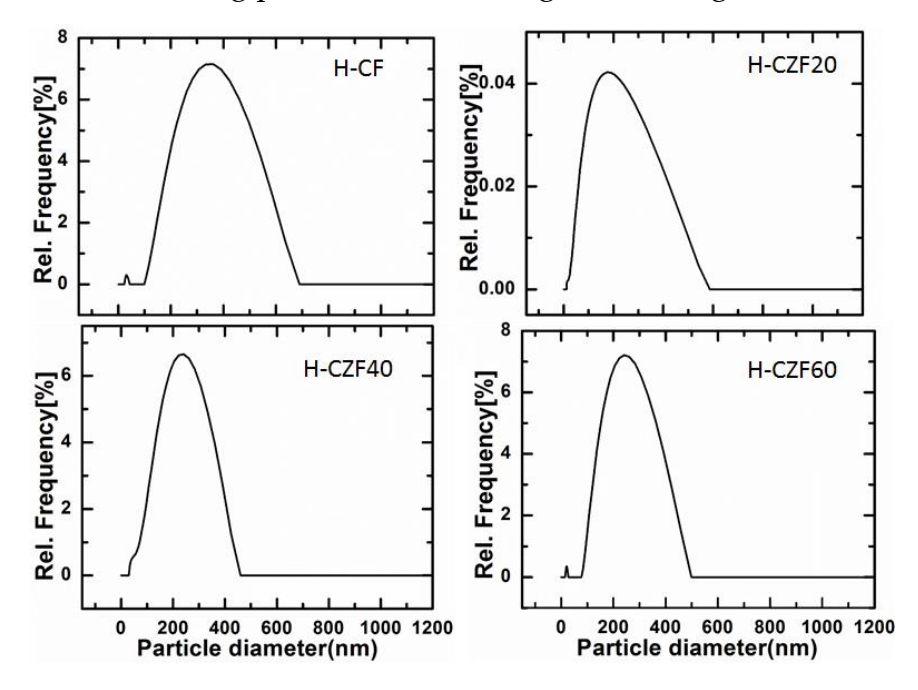


Figure 4. 18 Particle size distribution of H- CZF nanoparticles.

The Fig 4.19 shows the zeta potential which is basically used to predict the suspension stability. Higher the "zeta potential" value, higher will the stability / strength of the solution. The higher negative zeta values (Table 4.5) contribute towards preventing the cluster formation by electrostatic repulsion in liquid solvent. The hydrothermal samples show excellent stability.

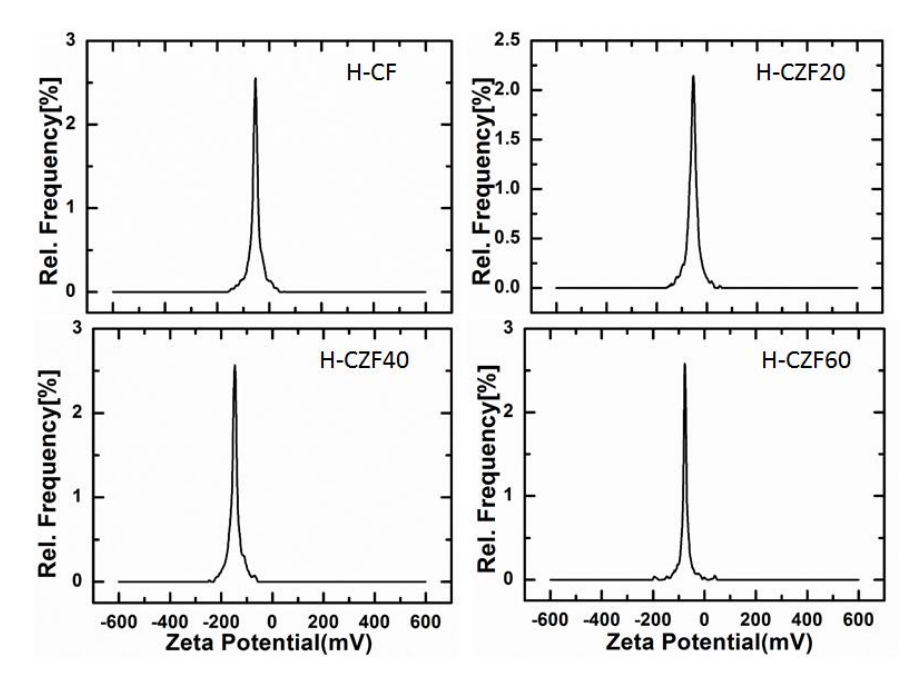


Figure 4. 19 Zeta potential of H-CZF nanoparticles.

Table 4. 5: Average particle size, distribution and zeta potential parameters for H-CZF nanoparticles:

Sample Name	Particles Size (nm)	Hydrodynamic particles Size (nm)	Zeta Potential (mV)
H-CF	8	299	-60.5
H -CZF20	8	178	-59.8
H -CZF40	7.7	191	-151.4
H -CZF60	8.6	215	-79.5

4.2.5 Magnetization Studies

Fig. 4.20 shows the (M (H)) plots of H-CZF (Zn = 0.0, 0.2, 0.4, 0.6) nanoparticles at 5K and 300K respectively.

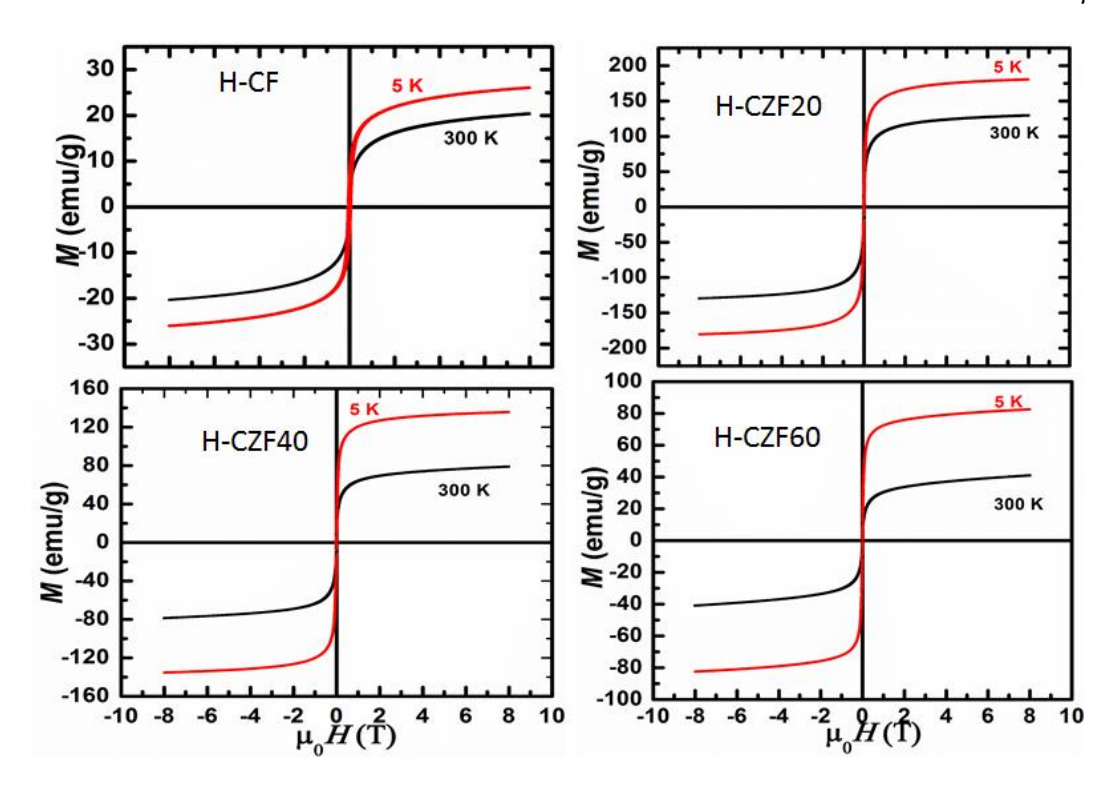


Figure 4. 20 Magnetization curves of H-CZF nanoparticles.

Table 4. 6: Magnetization parameters of H- CZF nanoparticles.

Sample Name	Ms (emu/g) at 300 K	Ms (emu/g) at 5 K
HCF	20	26
HCZF20	130	180.5
HCZF40	78.7	135
HCZF60	41	82.5

Fig. 4.21 shows the saturation magnetization of H- CZF nanoparticles vs. Zn content. The samples show high magnetization values and exhibit superparamagnetic behaviour. All H-CZF samples have higher magnetization as compared to C-CZF samples. The magnetization increases as Zn content increase to x = 0.2 followed by a decreasing trend for Zn content x > 0.2.

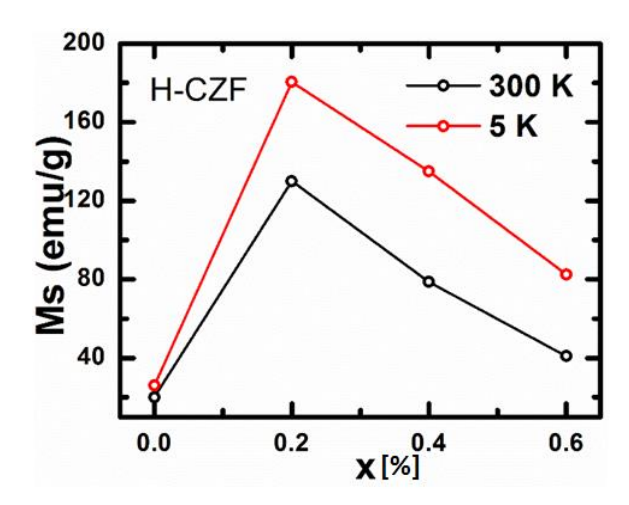


Figure 4. 21 M (H) loops parameters for H- CZF nanoparticles.

The magnetic parameters are listed in Table 4.6. As explained above the "AB" interaction become weak for x> 0.2 due to reduction in number of magnetic ions at A site as Zn content increases.

Fig. 4.22 shows the M (T) plots of H-CZF nanoparticles under FC and ZFC modes under applied "magnetic field" of 100 Oe. The results show the superparamagnetic behaviour of the nanoparticles. In FC mode magnetization decreases with increasing temperature. In ZFC curves, the "magnetic moment" of nanoparticles is frozen below blocking temperature. Apparently with increasing "temperature", the magnetization increases till T_B , and then overlaps with FC mode curve. The measured T_B values are 139, 155, 129, 102 K for x= 0.0, 0.2, 0.4, 0.6 H-CZF nanoparticles respectively.

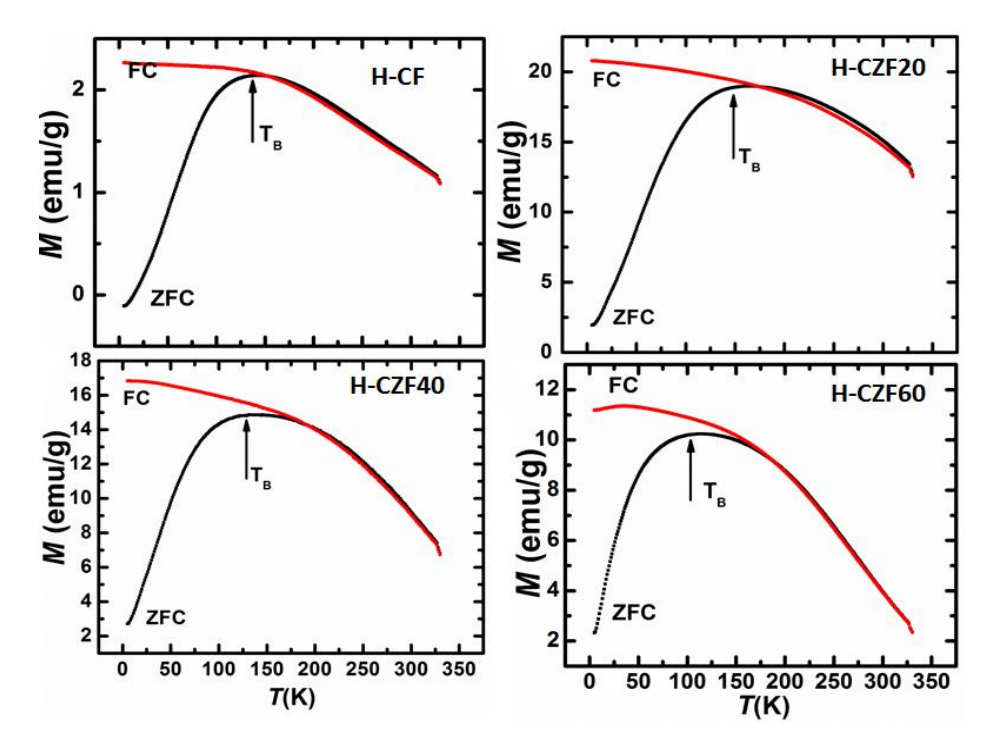


Figure 4. 22 FC and ZFC curves of H-CZF nanoparticles

4.3 Study H-CZF based ferrofluids

4.3.1 Magneto-viscosity plots of water based H- CZF ferrofluids:

The volume ratio of nanoparticles, DBSA and water is 1:0.5:1.5 for different composition of CZF. The nanoparticles coated with DBSA surfactant were used for the preparation of water based ferrofluids. Fig. 4.23 shows the effect of colloidal in H-CZF water based ferrofluids at zero field. The H-CZF20W FF show the highest viscosity as compared to other FF at zero field and non -Newtonian behaviour up to shear rate of $1000 \, \text{s}^{-1}$. H-CZF40W and H-CZF60W FF show non -Newtonian behaviour below shear rate of $100 \, \text{s}^{-1}$ and Newtonian behaviour above $100 \, \text{s}^{-1}$. Power law behaviour is not observed for the FFs at H = 0.

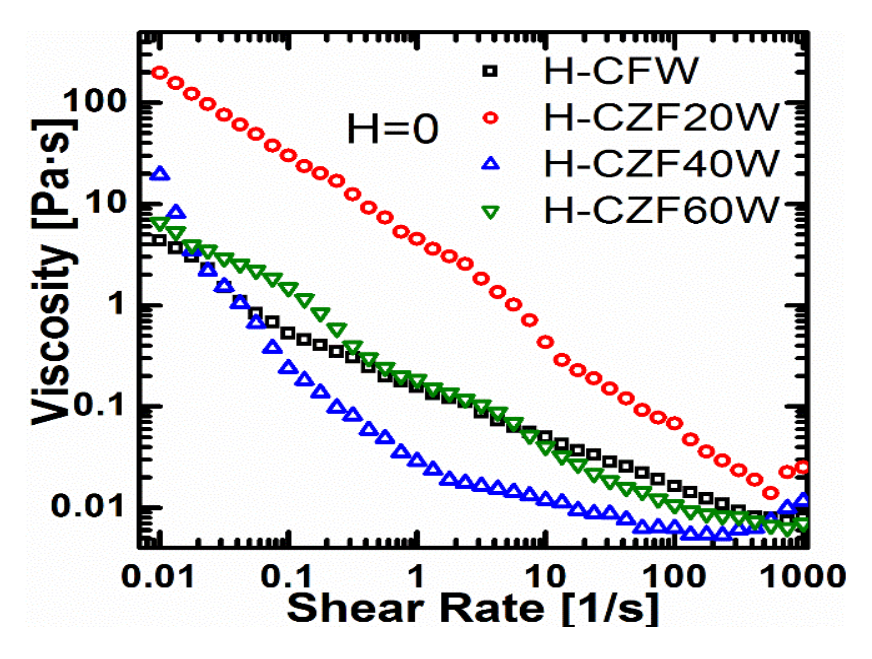


Figure 4. 23 Effect of colloid in H-CZF water based ferrofluids at H=0.

Flow curves of H-CZF ferrofluids in the presence of magnetic field are shown in Fig. 4.24.

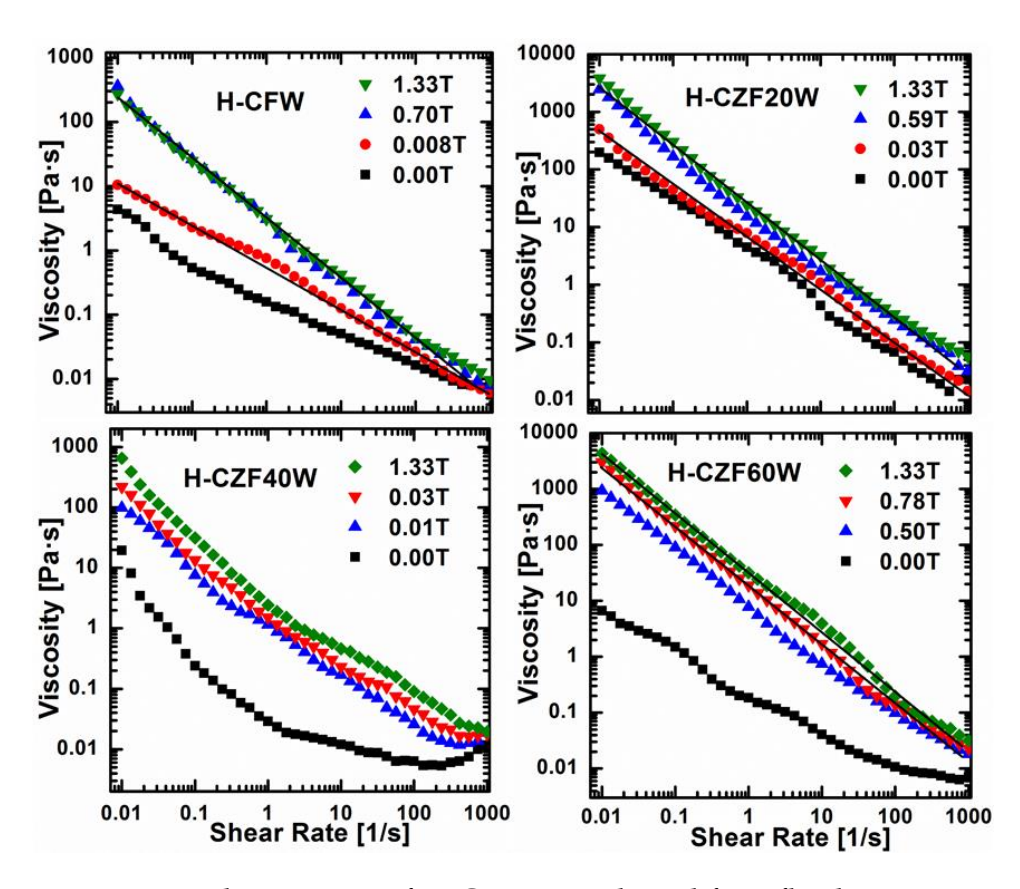


Figure 4. 24 Flow curves of H-CZF water based ferrofluids at H=0 - 1.33T.

All ferrofluids show the "non-Newtonian" behaviour at low shear rate and Newtonian behaviour at shear rates above $100 \, \rm s^{-1}$. The Power law fittings are obtained for some FFs. The fitting parameters are listed in table 4.7

Table 4. 7: Power-law fitting parameters for water based H-CZF ferrofluids.

Ferrofluid Name	K values	n (power index)	Magnetic field (T)
	0.58	0.37	0.008
H-CFW	1.9	0.06	1.33
	2.3	0.16	0.008
H-CZF20W	24	0.10	1.33
	8.7	0.01	0.50
H-CZF60W	29	0.08	1.33

Fig. 4.25 shows viscosity vs. applied magnetic field of CZF ferrofluids at shear rate of 10 and 100 s⁻¹. "Magneto viscosity" plots show a linear behaviour with increasing applied magnetic fields and do not saturate even up to highest applied field. When the "applied field" is reduced to "zero", viscosity value remains high due to the persistence of magnetic structure during increasing magnetic field stage. The viscosity continuously increases with increasing magnetic field stage. When the magnetic field is decreasing, the viscosity is higher than the increasing magnetic field. This indicates that the magnetic structures formed do not relax to initial shape on removal of magnetic field. So magnetic force is dominating over hydrodynamic force in water based ferrofluid.

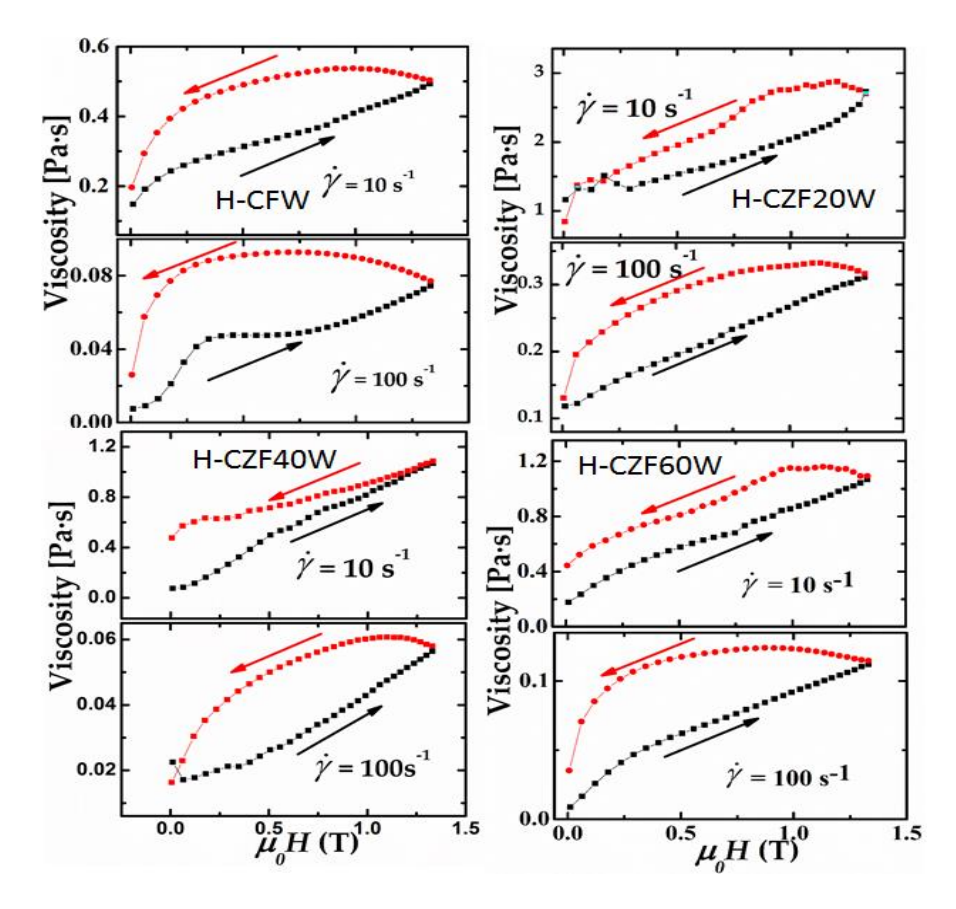


Figure 4. 25 Magneto-viscosity of H-CZF water based ferrofluids

4.3.2 "Magneto-viscosity" plots of "paraffin" based H- CZF ferrofluids:

Oleic acid was used as the "surfactant" to coat nanoparticles for preparing "paraffin" based ferrofluid. The ratio of nanoparticles, oleic acid and water by volume is 1:0.5:1.5 for different composition of CZF respectively. Fig. 4.26 shows the direct observation of colloidal effect on the H-CZF ferrofluids at zero field. The H-CZF40P FF shows the higher viscosity at zero field.

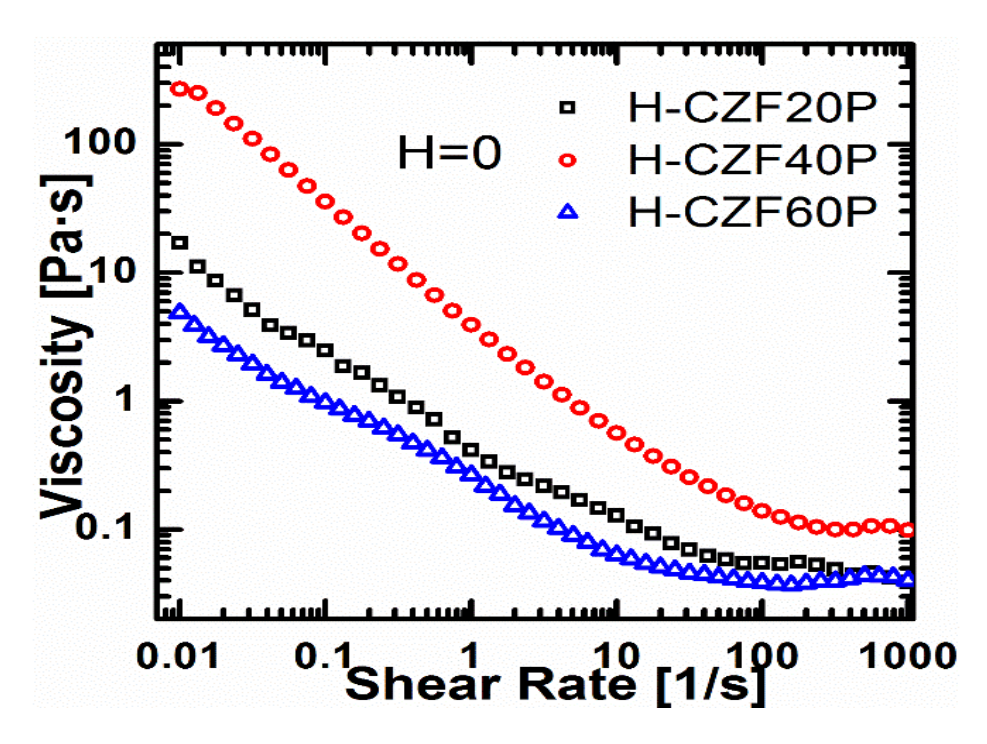


Figure 4. 26 Effect of colloid in H-CZF paraffin oil based ferrofluids at H=0

Fig. 4.27 shows flow curves (viscosity vs. shear rate) of H-CZF ferrofluids. The viscosity is found to decrease with increase in "shear rate" non-linearly following a power law behaviour of viscosity vs. shear rate for all samples. The magneto-viscosity effect is highest for HCZF40 ferrofluid at low shear rates. All ferrofluids exhibit shear thinning behaviour i.e. the viscosity decreases with increase in the shear rate.

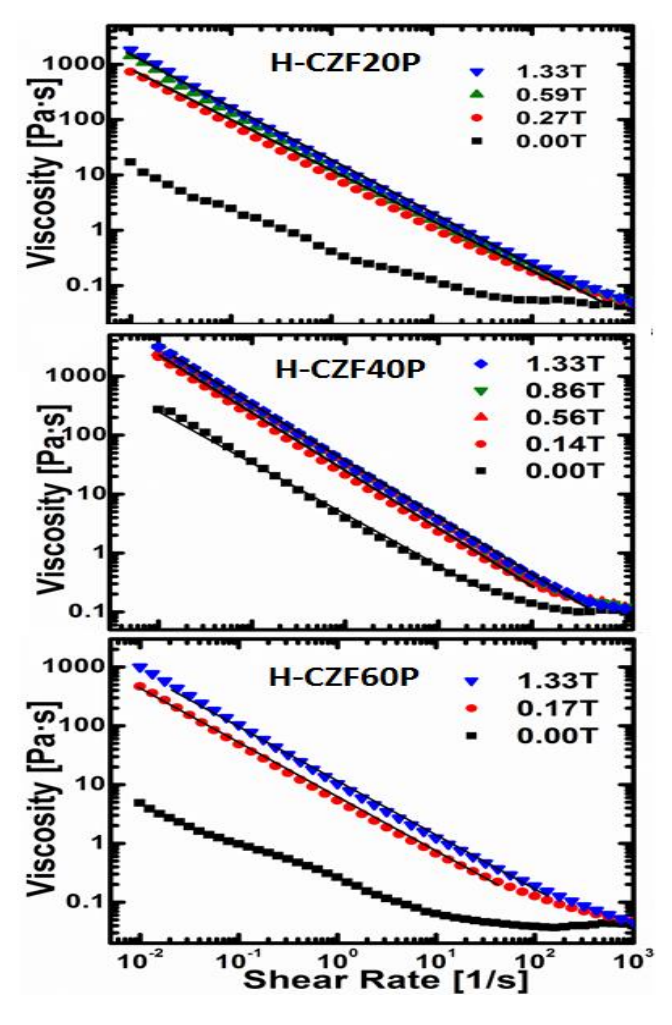


Figure 4. 27 Flow curves of paraffin oil based H-CZF ferrofluids.

When shear stress is applied, the dipole interactions between particles are broken and particles are separated leading to gradual decrease in viscosity. The concentrated ferrofluids show shear thinning behaviour more readily than the dilute ferrofluids.

Table 4. 8: The fitting parameters of power law for H-CZF ferrofluids are tabulated below:

Ferrofluid Name	K values	n (power index)	Magnetic field (T)
	9.6	0.56	0.27
H-CZF20P	14.7	0.04	1.33

	20.4	0.005	0.14
H-CZF40P	31.4	0.002	1.33
	5	0.023	0.17
H-CZF60P	11	0.020	1.33

Fig. 4.28 shows the variation of viscosity with applied magnetic field for CZF ferrofluids at "1" and "10" s⁻¹. The increase in the viscosity of the fluid when magnetic field is applied is due to formation of magnetic structure like chains and drops as discussed in chapter 3 [6-7]. The length of chains increases with increase in magnetic field leading to significant increase in viscosity of the ferrofluid. With the reduction in magnetic field, the formed chains may disintegrate into original particles or different magnetic structures depending on the competition between magnetic interactions and hydrodynamic force. If the magnetic structure do not come back to original state, then hysteresis is observed in viscosity vs. magnetic field plots.

The magneto viscosity plots show almost negligible hysteresis for CZF20P and CZF60P FFs compared to CZF40P FF. The CZF40P show the highest magnetoviscosity effect.

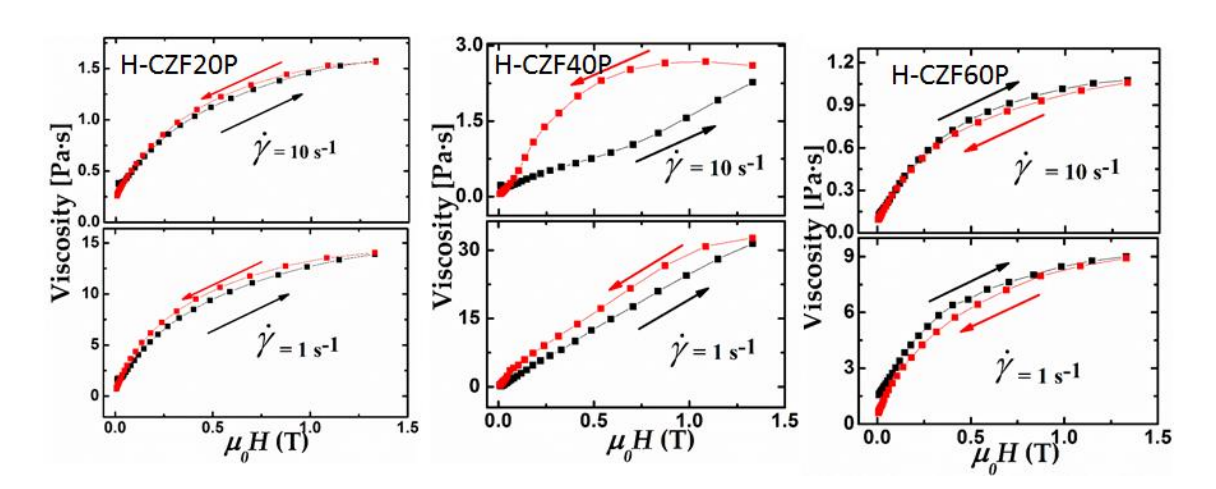


Figure 4. 28 Magneto-viscosity of paraffin oil based H-CZF ferrofluids

Chapter 4 Studies on Cu-Zn (CZF) Ferrite nanoparticles and ferrofluids

The viscosity for CZF40P increases linearly with increasing stage of magnetic field. The magnetic structures formed revert back for shear rate of 1 s⁻¹, giving the minimum hysteresis. However, for shear rate of 10 s⁻¹ structures formed do not disintegrate and hinder the flow of fluid and thus give rise to high viscosity compared increasing magnetic stage. These structures start disintegrating as the field is reduced to zero leading to decreasing trend in viscosity.

4.3.3 Shear Stress in Paraffin oil based ferrofluids:

The shear thinning behaviour and magneto-viscosity of the FF is explained by "Herschel-Bulkley (H-B) model", in this model shear stress is related to shear strain by the equation given as:

$$\tau = \tau_0 + K \dot{\gamma}^{n,}$$

Where τ_0 and τ are yield stress and shear strain of the ferrofluid respectively.

Fig. 4.29 shows the plots of shear stress vs. shear rate for H-CZF ferrofluids.

The change in the variation of shear stress vs. shear rate above 200 s⁻¹ indicates that there is a yield stress associated with the ferrofluid. This yield stress arises due to the interactions between nanoparticles. The interactions between nanoparticles is strong in concentrated ferrofluids leading to a strong initial resistance to fluid flow. With the increase in shear rate, the resistance is ultimately overcome leading to more free flow of the ferrofluid. The flow curves are analysed using Herschel–Bulkley (H-B) model developed for suspensions [6-8].

Fig. 4.29 shows the plots of "shear stress" vs. "shear rate" at various magnetic fields for paraffin based ferrofluids (H-CZF20P HCZF40Pand HCZF60P). It is observed that the shear rate starts to speed up above a particular stress value, which is known as the yield stress(τ_0) of the sample. The shear stress and shear rate curves are fitted to the B-H model equation.

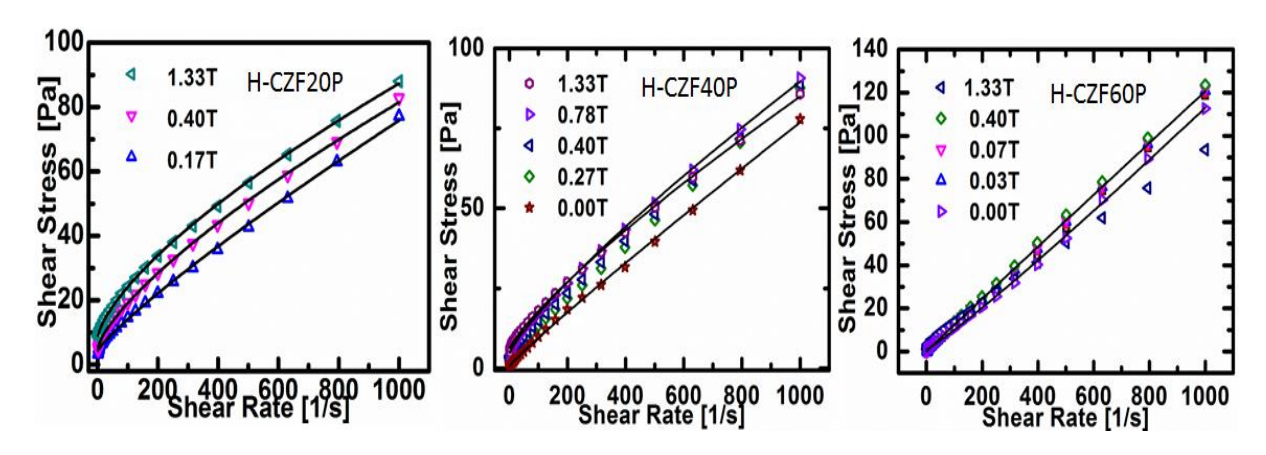


Figure 4. 29 H-B model fit.

The solid lines is Fig. 4.29 are the fitting curves as per above equation. The fitting is good and table 4.7 lists the estimated H-B model parameters. The yield stress increases monotonically with increase in applied "magnetic field" because of chain-type structure formation of the nanoparticles. The Yield stress is highest for H-CZF20 sample and minimum for H-CZF60 sample. The n value is < 1 for H-CZF20 and H-CZF 40 sample.

Table 4. 9: H-B model fitting parameters.

Ferrofluid Name	K values	n (power index)	Magne tic field	Yield Shear stress(τ_0)
	0.1	0.7	0.17	4.2
H-CZF20P	.3	0.76	0.4	5.07
	.6	0.8	1.33	8.4
	0.8	0.8	0.0	0.6
II 677 10D	0.1	0.82	0.2	0.8
H-CZF40P	0.12	0.85	0.4	2
	0.17	0.86	0.78	4

Chapter 4 Studies on Cu-Zn (CZF) Ferrite nanoparticles and ferrofluids

	.2	0.9	1.33	5
	0.6	1	0.0	0.1
II CZE(OD	2	1.2	0.03	0.3
H-CZF60P	4.5	1.6	0.07	0.4
	7	1.8	0.40	0.6
	9	2	1.33	0.8

indicating Pseudo plastic flow for these fluids. Whereas for H-CZF60 sample n > 1 indicating Dilatant flow for the fluid.

The synthesis of Zn- Cu ferrite nanoparticles have been reported by several groups by using different synthesis method [9-14]. In all these studies the synthesized nanoparticles are spherical in shape. Whereas, synthesized CZF nanoparticles via coprecipitation method in the present study are mixture of spherical as well as cubic shape nanoparticles. The synthesized CZF nanoparticles by hydrothermal method are cubic shaped. The synthesized nanoparticles are more stable with improved magnetic properties. The synthesized CZF nanoparticles were used to prepare the water, toluene, paraffin oil and silicone oil based ferrofluids. The ferrofluids were studied to understand the effect of nanoparticle shape and nature of colloid on the magnetoviscosity effect in ferrofluids.

In summary, the nanoparticles of Cu-Zn ferrite were prepared by coprecipitation and hydrothermal methods. The Rietveld analysis confirmed the twophase (spinel and CuO phase) for co-precipitated samples whereas for hydrothermalized samples, three phases (spinel, CuO and orthorhombic phase) are confirmed. The orthorhombic phase disappeared after Zn doping in Cu ferrite. The microstructural studies confirmed the spherical and cube shaped nanoparticles. The broad distribution of nanoparticles and good stability were estimated from the particles size analyzer analysis. The magnetization results show zero corecivity at room temperature. The saturation magnetization increases after heat treatment. The co-precipitated CZF nanoparticles were dispersed in toluene and paraffin oil; while hydrothermalized CZF nanoparticles were dispersed in water and paraffin oil for the preparation of ferrofluids. The flow curves show non-Newtonian power law behaviour at low shear rates for all ferrofluids. At shear rates of > 400 all ferrofluid show Newtonian behaviour. All of the ferrofluids exhibit a shear thinning behaviour. The maximum MVE with minimum hysteresis is observed for C-CZF40T Toluene and Paraffin based ferrofluids at shear rate of 1 s⁻¹. The maximum MVE with minimum hysteresis is observed for H-CZF40T Paraffin based ferrofluids at shear rate of 1 s⁻¹. The shear stress and shear rate curves for Paraffin oil based H-ZCF ferrofluids follow the "Herschel-Bulkley (H-B) model", these ferrofluids therefore can find application as flow controller by applying magnetic field.

References:

- [1] N. Gautam, G. Thirupathi, and R. Singh, "Effect of Zn-doping on structural and magnetic properties of copper ferrite nanoparticles," 2016, p. 50099.
- [2] A. Gholizadeh, "A comparative study of the physical properties of Cu-Zn ferrites annealed under different atmospheres and temperatures: Magnetic enhancement of Cu0.5Zn0.5Fe2O4 nanoparticles by a reducing atmosphere," *Journal of Magnetism and Magnetic Materials*, vol. 452, pp. 389–397, Apr. 2018.
- [3] M. Manjurul Haque, M. Huq, and M. A. Hakim, "Effect of Zn2+ substitution on the magnetic properties of Mg1–xZnxFe2O4 ferrites," *Physica B: Condensed Matter*, vol. 404, no. 21, pp. 3915–3921, Nov. 2009.
- [4] N. Gautam, G. Thirupathi, and R. Singh, "Magneto-viscosity of hydrothermal synthesized Cu-Zn ferrite ferrofluids," *AIP Advances*, vol. 7, no. 5, p. 56727, May 2017.
- [5] G. Thirupathi and R. Singh, "Study of Magnetoviscosity of Ferromagnetic MnZn-Ferrite Ferrofluid," *IEEE Transactions on Magnetics*, vol. 51, no. 11, pp. 1–4, Nov. 2015.
- [6] "S. Odenbach and K. Raj," The Influence of Large Particles and Agglomerates On The Magnetoviscous Effect In Ferrofluids" *Magnetohydrodynamics*, Vol. 36, No. 4, 2000.
- [7] "M.Tamilmagan, D. Easu, Baskarlal V.P.M, V.Andal," Synthesis, characterisation, design and study of magnetorheological property of nano fe2O3.", Int.J. ChemTech Res. 2015,8(5),pp 65-69.
- [8] "By Eugene C. Bingham, "An Investigation of the Laws of Plastic Flow"vol.13.
- [9] C. Murugesan, N. Kambhala, S. Angappane, and G. Chandrasekaran, "Influence of Zn concentration on the structural and magnetic properties of nanocrystalline Cu 1–x Zn x Fe 2 O 4 mixed ferrites synthesized using novel combustion method," *Journal of Magnetism and Magnetic Materials*, vol. 443, pp. 334–342, Dec. 2017.
- [10] L.-Z. Li, L. Peng, X.-X. Zhong, R. Wang, and X.-Q. Tu, "Structural, magnetic and electrical properties of CuZn ferrite nanopowders," *Journal of Magnetism and Magnetic Materials*, vol. 419, pp. 407–411, Dec. 2016.
- [11] Y. Liu, J. Hsu, Y. Fu, and K. Tsai, "Preparation of Cu–Zn ferrite photocatalyst and it's application," *International Journal of Hydrogen Energy*, vol. 41, no. 35, pp. 15696–15702, Sep. 2016.
- [12] C. Hasirci, O. Karaagac, and H. Köçkar, "Superparamagnetic zinc ferrite: A correlation between high magnetizations and nanoparticle sizes as a function of reaction time via hydrothermal process," *Journal of Magnetism and Magnetic Materials*, vol. 474, pp. 282–286, Mar. 2019.

- [13] S. Akhter *et al.*, "Magnetic and magnetocaloric properties of Cu1–xZnxFe2O4 (x=0.6, 0.7, 0.8) ferrites," *Journal of Magnetism and Magnetic Materials*, vol. 367, pp. 75–80, Oct. 2014.
- [14] A. Tony Dhiwahar, M. Sundararajan, P. Sakthivel, C. S. Dash, and S. Yuvaraj, "Microwave-assisted combustion synthesis of pure and zinc-doped copper ferrite nanoparticles: Structural, morphological, optical, vibrational, and magnetic behavior," *Journal of Physics and Chemistry of Solids*, vol. 138, p. 109257, Mar. 2020.

Chapter 4 Studies on Cu-Zn (CZF) Ferrite nanoparticles and ferrofluids

CHAPTER-5

Studies on Ba-Sr ferrite (BSM) nanoparticles and ferrofluids

This chapter describes the properties of "Ba_{1-x}Sr_xFe₁₂O₁₉" (x = 0.0, 0.05, 0.1, 0.2, 0.5) nanoparticles and the corresponding ferrofluids. The magneto-viscosity, flow curves and magneto sweep studies were carried out on Ba-Sr ferrite based ferrofluids prepared in different solvents. The XRD, FESEM, DLS and VSM techniques were used to characterize the nanoparticles. The DBSA and oleic acid were used as the surfactants.

5.1 Study of Ba-Sr ferrite nanoparticles

5.1.1 "Structural" studies:

Fig. 5.1 shows the XRD pattern of $Ba_{1-x}Sr_xFe_{12}O_{19}$ (x =0.0, 0.2, 0.4, and 0.6) hexaferrite nano powder synthesized by the method described in chapter 2.

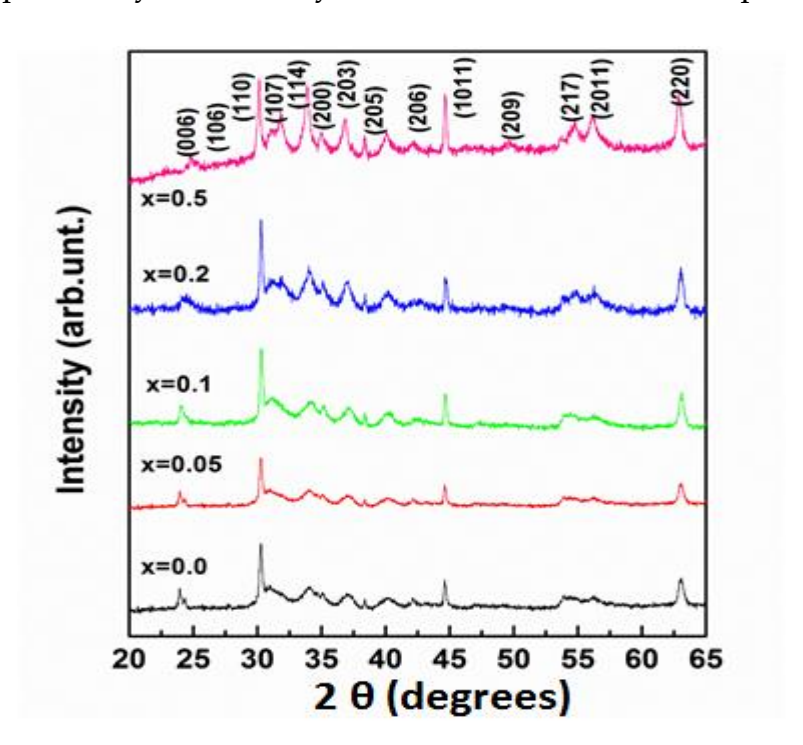


Figure 5. 1 XRD of BSM nanoparticles (x=0, 0.05, 0.1, 0.2, 0.5) respectively.

Chapter-5: Studies on Ba-Sr ferrite (BSM) nanoparticles and ferrofluids

The "single-phase" hexagonal "magnetoplumbite" structure for BaFe₁₂O₁₉ with "space group" ("P63/mmc") (No.194 JCPDS" data file is confirmed. The Ba-Sr ferrite phase was confirmed and compared with other reports in the literature on hexagonal platelet nanoparticles. The "lattice parameters" and crystallite sizes are listed in Table 5.1. For reducing the formation of intermediate phases like α - Fe₂O₃ and BaFe₂O₃, the Fe/Ba ratio was optimized.

The observed broad peaks in XRD pattern are due to the small sized particles. The XRD peak (311) was considered for calculating the crystallite size using the Debye-Scherer equation, as discussed in chapter 3.

Table 5. 1: "Crystallographic parameters" for BSM nanoparticles.

Sample Name	Crystallite size(nm)	Lattice
		Parameter(Å)
ВМ	51	a=b=6.801 and c=17.669
BSM5	74	a=b=6.809 and c=17.691
BSM10	47	a=b=6.802 and c=17.671
BSM20	49	a=b=6.805 and c=17.680
BSM50	57	a=b=6.841 and c=17.773

5.1.2 Morphological study:

Fig. 5.2 shows FESEM micrographs for all compositions of BSM nanoparticles. The particles size distribution, thickness and uniformity are affected by the change in Sr concentration. The large hexagonal platelet-shaped structures are formed. All the changes are due to the quantity of hydroxide ions taken for synthesis. The hydroxide ions are absorbed on the surface and prevent the crystal growth in (100) direction.

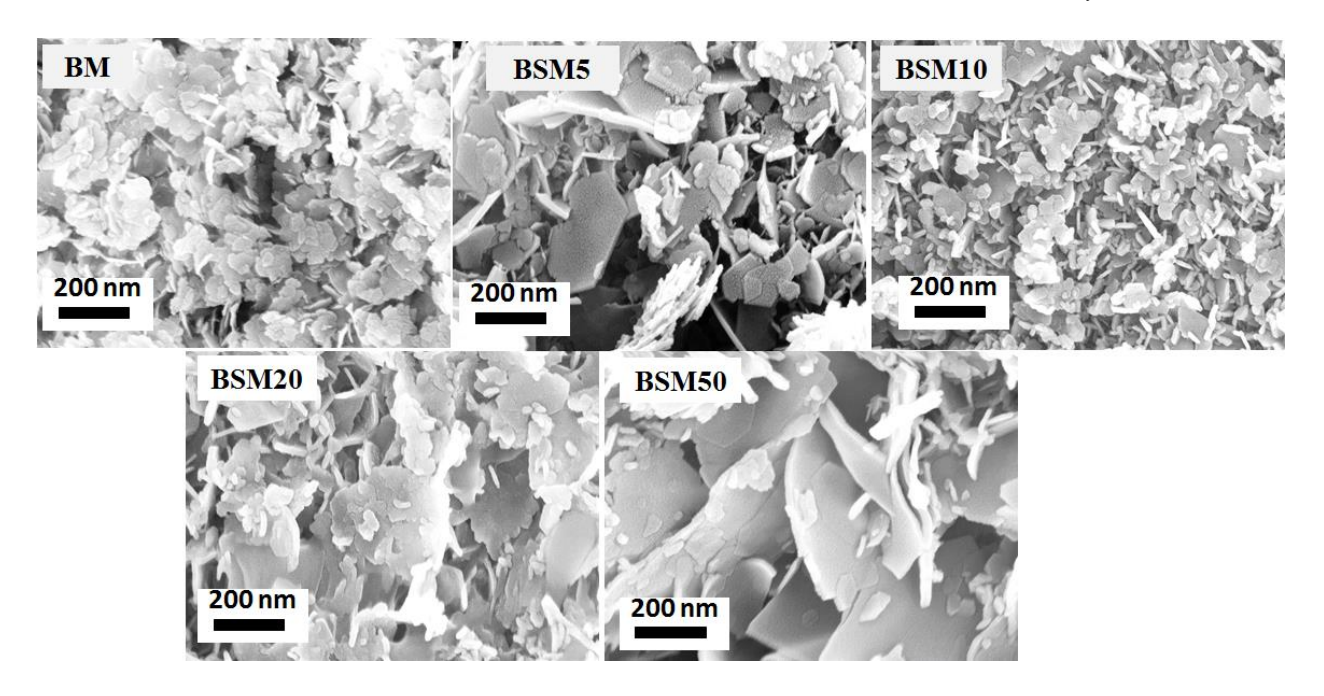
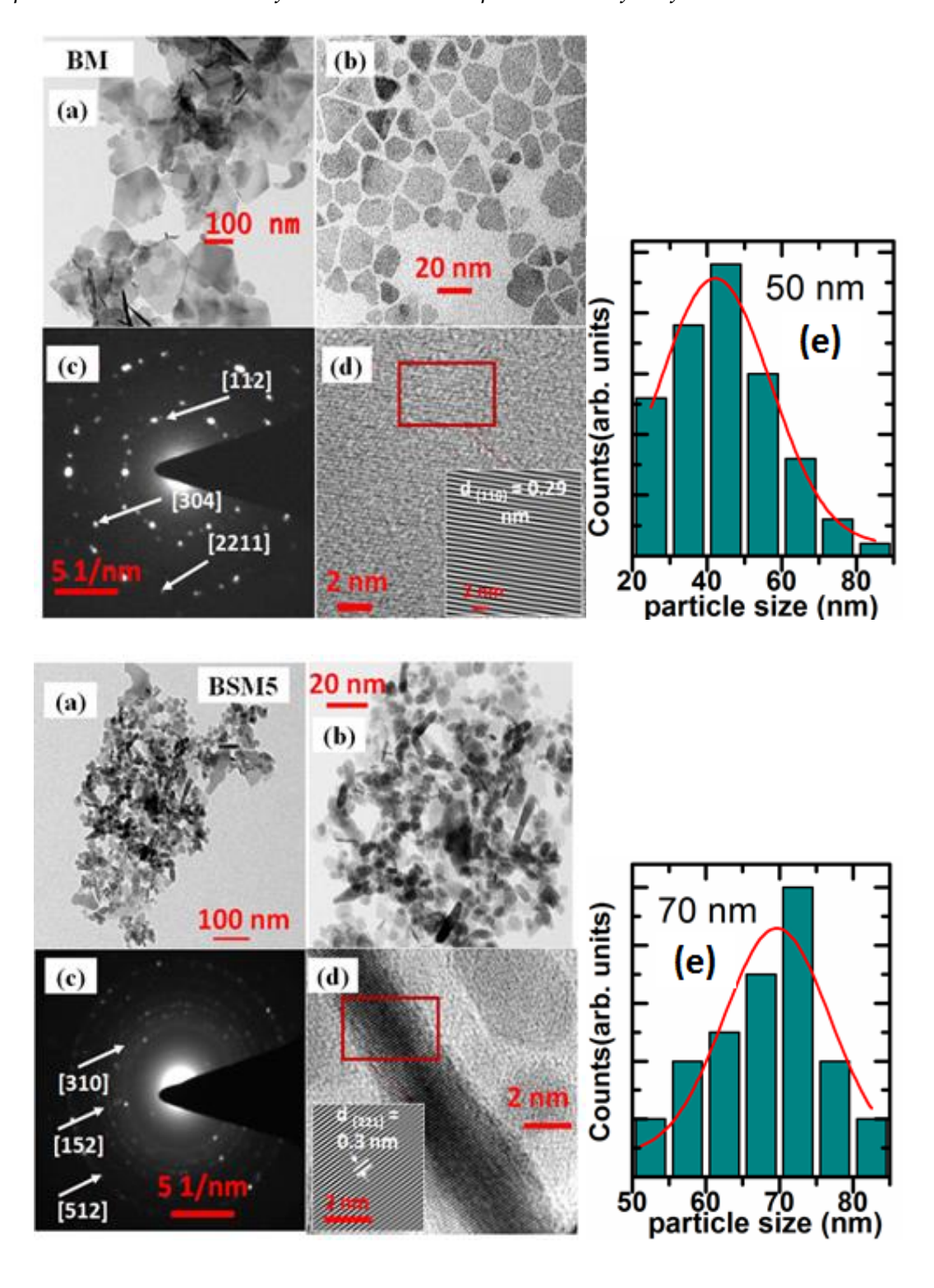


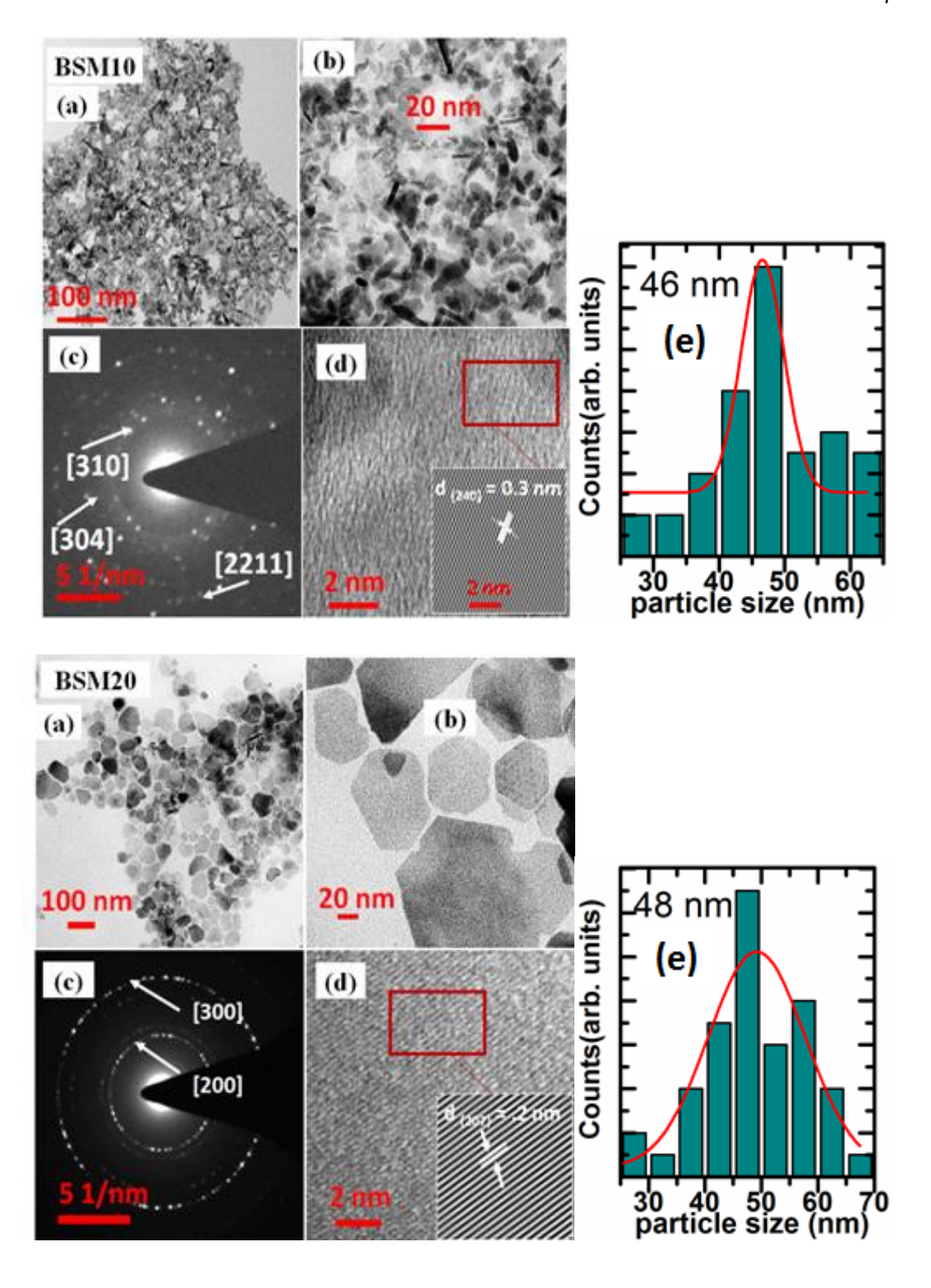
Figure 5. 2 FESEM images of BSM particles (x=0.0, 0.05, 0.1, 0.2, 0.5) respectively.

The hydroxide ion dosage is important to form hexagonal-shaped nanoparticles. Finally, the result shows that the particles are nanometer in size and hexagonal shaped, similar to as reported by other group [1].

Fig. 5.3 shows the TEM images of BSM (Sr = 0.0, 0.2, 0.4, 0.6) ferrite nanoparticles. The images show the size distribution of the nanoparticles, "scattered area electron diffraction (SAED) pattern" and HR-TEM micrographs respectively. The particles are "hexagonal" in shape with average sizes 50, 70, 48, 46, and 56 nm for BM, BSM5, BSM10, BSM20, and BSM50 samples from the micrographs respectively.

Chapter-5: Studies on Ba-Sr ferrite (BSM) nanoparticles and ferrofluids





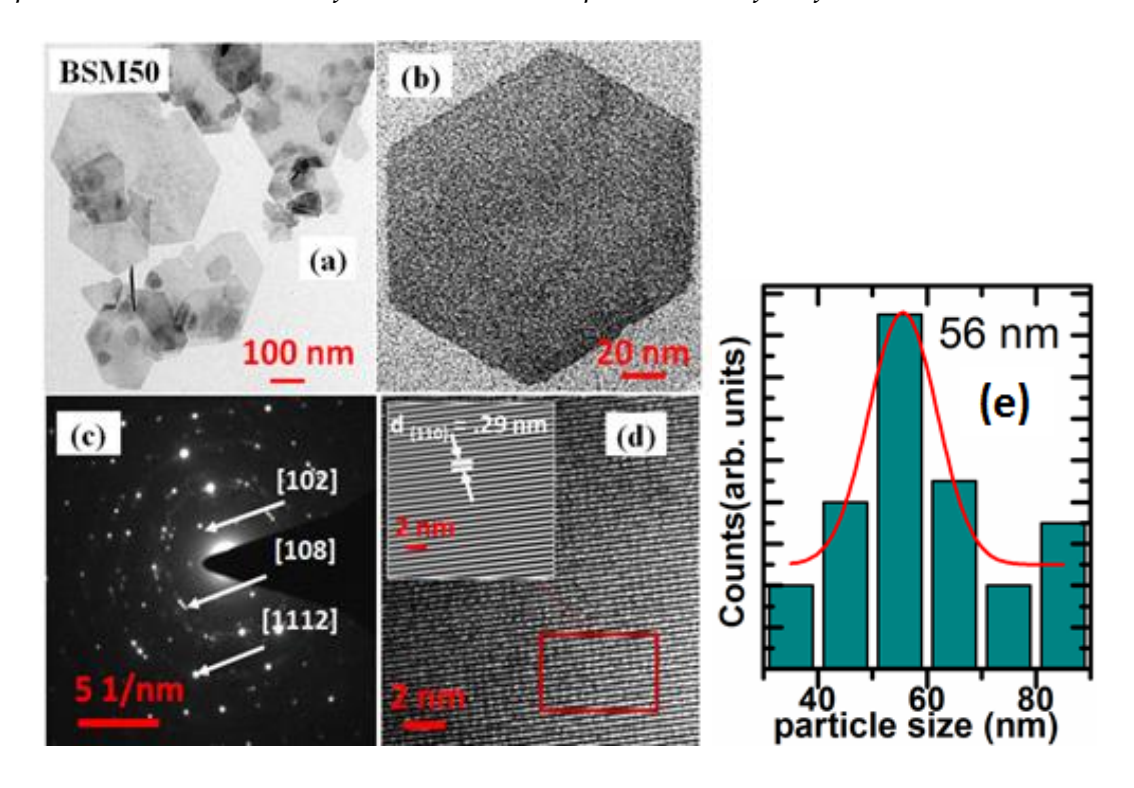


Figure 5. 3 TEM particle distribution (a) & (b), Electron diffraction pattern (c), "HR-TEM" micrographs (d) and Average particle distribution (e) of samples BM, BSM5, BSM10, BSM20 and BSM50 respectively.

Table 5. 2: Average particles size, hydrodynamic particle distribution and zeta potential parameters.

Sample Name	Average Particles Size (nm)	Hydrodynamic particles Size distribution (nm)	Zeta Potential (mV) (PSA)
	(TEM)	(PSA)	
ВМ	50	121.2	-58.8
BSM5	70	287	-71.8
BSM10	48	209.8	-58.9

BSM20	46	256.2	-59.8
BSM50	56	425.5	-88

The hydrodynamic distribution of BSM ferrofluid is shown in Fig. 5.4.

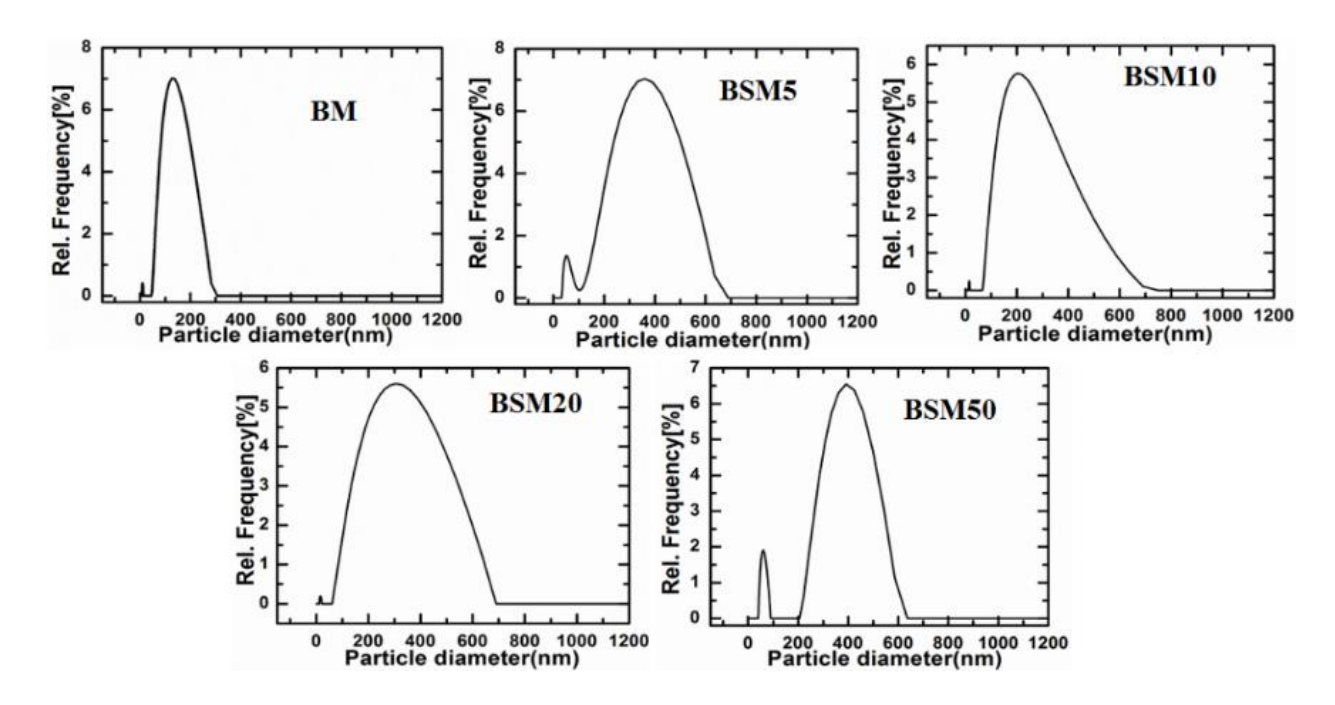


Figure 5. 4 Particle size distribution of BM, BSM5, BSM10, BSM20 and BS50 nanoparticles.

Two "hydrodynamic distributions" are found for "BSM" nanoparticles. Hydrodynamic diameters of nanoparticles are listed in Table 5.2. The first peak shows the thickness distribution and the second shows the size distribution of the platelet-shaped nanoparticles. The hydrodynamic particle size is found to be more than that estimated by TEM due to cluster formation in water.

Chapter-5: Studies on Ba-Sr ferrite (BSM) nanoparticles and ferrofluids

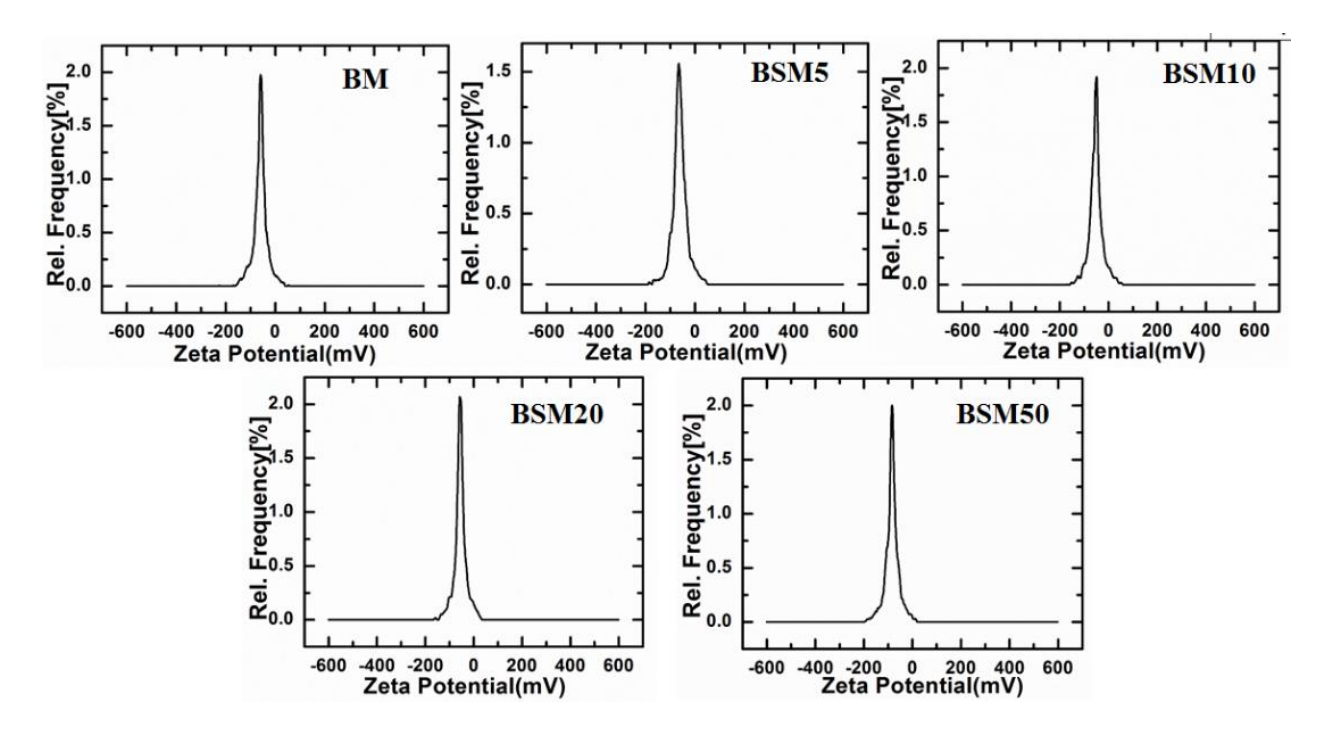


Figure 5. 5 Zeta Potential of BM, BSM5, BSM10, BSM20 and BSM50 nanoparticles respectively.

The zeta potential of BSM ferrofluid is given in Fig. 5.5. For "zeta potential" measurement the BSM nanoparticles were dispersed in water and the values are given in Table 5.2.

5.1.3 Magnetic Properties

Fig. 5.6 shows the plots of magnetization vs. applied magnetic field plots for BSM (BM, BSM5, BSM10, BSM20, and BSM50) nanoparticles at 5K and 300K. The magnetic results indicate a drop in "saturation magnetization" because of the creation of a nonmagnetic or amorphous phase in BSM samples. The saturation magnetization for pure barium ferrite is reported to be 17 emu/g. The hysteresis loop shows a ferrimagnetic behaviour. The remanence and coercivity parameters estimated from the magnetic hysteresis are listed in Table 5.3.

Table 5. 3: M (H) parameters for BSM nanoparticles.

Sample	Mr	Ms	Hc	Mr	Ms	Hc
Name	(emu/g)	(emu/g)	(G)	(emu/g)	(emu/g)	(G)
	300K	300K	300K	5K	5K	5K
BM	3	17	360	9	25	888
BSM5	6	28	345	15	40	887
BSM10	7	28	464	16	42	948
BSM20	6	25	558	14	37	1090
BSM50	9	25	895	15	37	1436

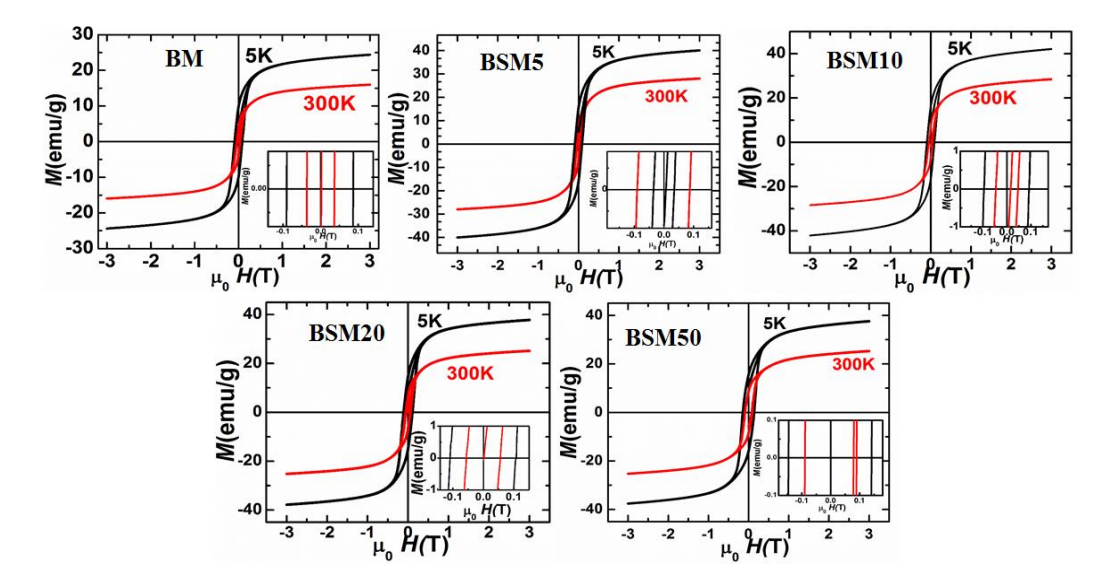


Figure 5. 6 Magnetization curves *M* (H) of Ba_{1-x}Sr_xFe₁₂O₁₉.

Fig 5.7 depicts the M-T (FC and ZFC) plots for $Ba_{1-x}Sr_xFe_{12}O_{19}$ (0.0, 0.05, 0.1, 0.2, 0.5) nanoparticles in the temperature range of 2 to 325K under magnetic field of 100 Oe.

Chapter-5: Studies on Ba-Sr ferrite (BSM) nanoparticles and ferrofluids

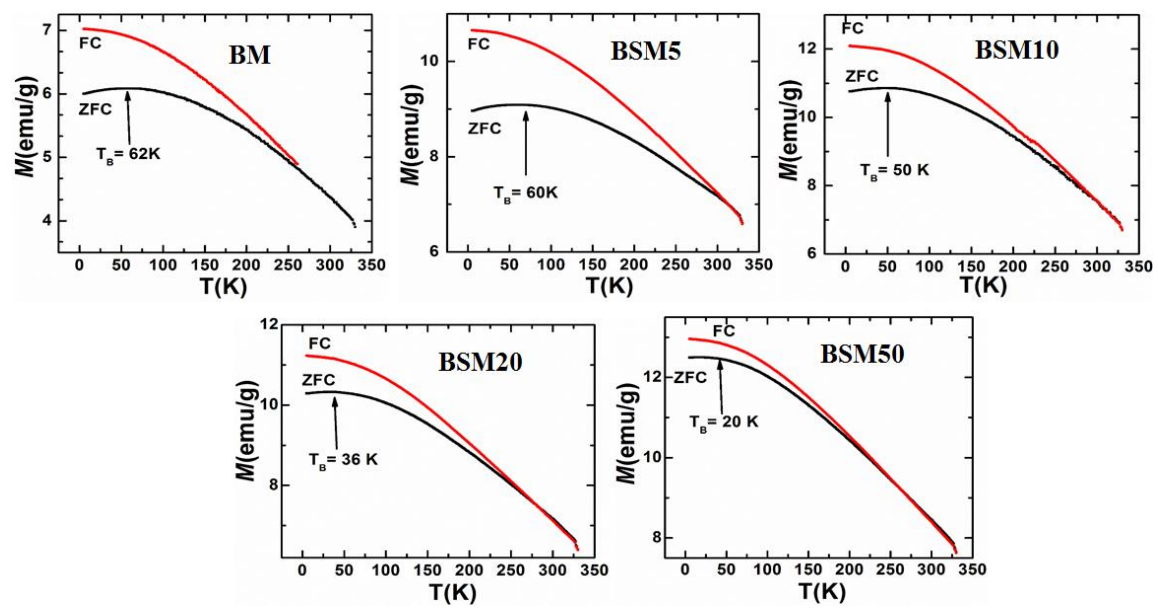


Figure 5. 7 FC and ZFC curves of BSM nanoparticles at 100 Oe.

The FC and ZFC curves are found to merge in the higher temperature region. In ZFC mode the magnetization appears with a broad peak which vanishes with increasing Sr content. The broad peak in ZFC curve can be due to "pinning of domain walls" with decreasing temperature. The magnetic domains are oriented randomly at high temperatures. The domains are aligned in the field direction when the sample is cooled under the magnetic field. Due to microstructural defects, some domain wall stay pinned in opposite direction to the field. As a result the net magnetization increasing trend slows down and gives rise to a broad peak with decreasing temperature.

5.2 Study of Ba-Sr ferrofluids:

The compositions of Ba_{1-x}Sr_xFe₁₂O₁₉ (BM, BSM5, BSM10, BSM20 and BSM50) were used for preparing ferrofluids. The ferrofluids were prepared in different solvents to compare the stability and understand the solvent's effect on their magneto viscosity. The physical properties of solvents used for synthesis of ferrofluid are given in Table 5.4.

Table 5. 4: Physical properties of colloidal.

S. No.	"Colloidal"	"Dynamic Viscosity" of colloidal (mPa. s) at 300K	"Density" (g/ml)	"Vapor pressure" (k Pa)
1	Water	0.8	1	4.3
2	Paraffin Oil	25 to 80	1.1	0.5
3	Silicone oil	1	0.971	0.6

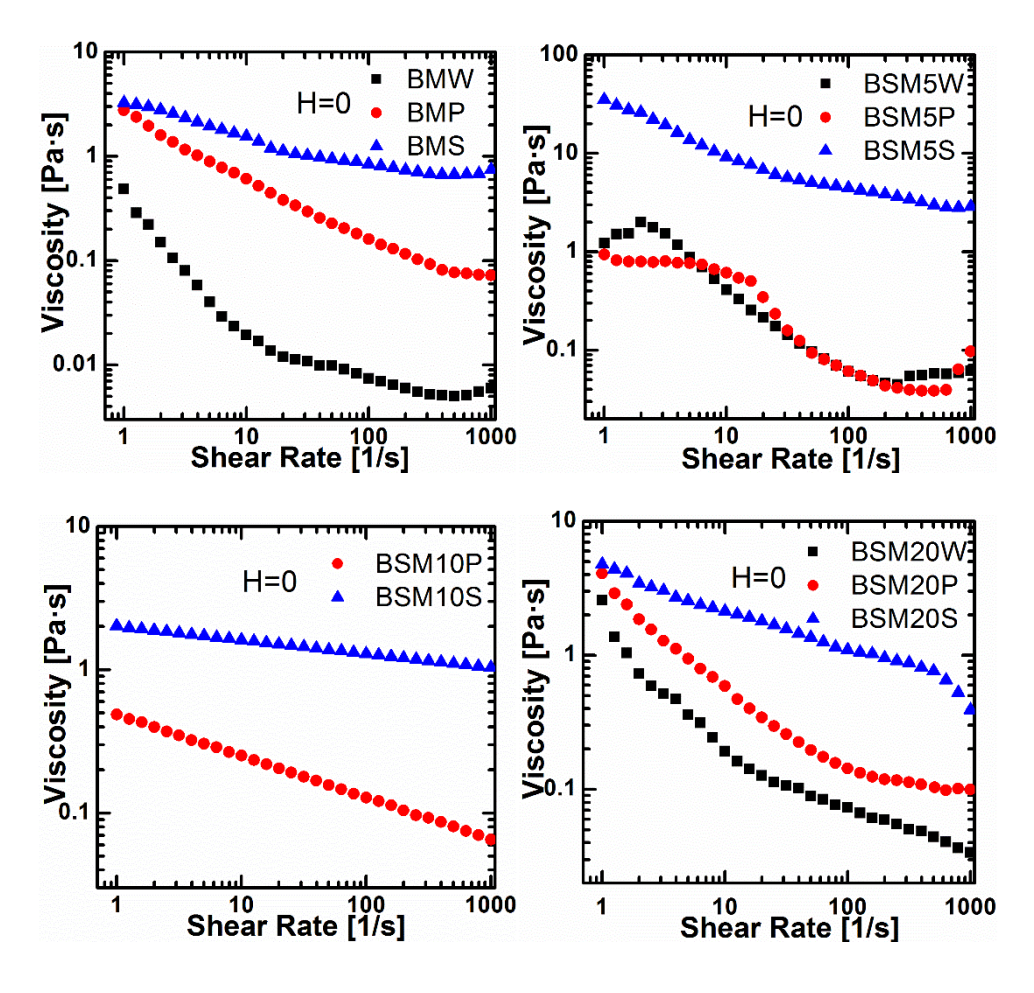
The below table lists the prepared ferrofluids (color used to identify the different sections):

Ferrofluids	Composition	Surfactant	Solvent
BMW	BaFe ₁₂ O ₁₉	DBSA	Water
BMP	BaFe ₁₂ O ₁₉	Oleic Acid	Paraffin Oil
BMS	BaFe ₁₂ O ₁₉	Oleic Acid	Silicone Oil
BSM5W	Ba _{0.95} Sr _{0.05} Fe ₁₂ O ₁₉	DBSA	Water
BSM5P	Ba _{0.95} Sr _{0.05} Fe ₁₂ O ₁₉	Oleic Acid	Paraffin Oil
BSM5S	Ba _{0.95} Sr _{0.05} Fe ₁₂ O ₁₉	Oleic Acid	Silicone Oil
BSM10W	Ba _{0.9} Sr _{0.1} Fe ₁₂ O ₁₉	DBSA	Water
BSM10P	Ba _{0.9} Sr _{0.1} Fe ₁₂ O ₁₉	Oleic Acid	Paraffin Oil
BSM10S	Ba _{0.9} Sr _{0.1} Fe ₁₂ O ₁₉	Oleic Acid	Silicone Oil

Chapter-5: Studies on Ba-Sr ferrite (BSM) nanoparticles and ferrofluids

BSM20S	Ba _{0.8} Sr _{0.2} Fe ₁₂ O ₁₉ Ba _{0.8} Sr _{0.2} Fe ₁₂ O ₁₉	DBSA	Water
BSM20P	Ba _{0.8} Sr _{0.2} Fe ₁₂ O ₁₉	Oleic Acid	Paraffin Oil
BSM20S		Oleic Acid	Silicone Oil
BSM50S	Ba _{0.5} Sr _{0.5} Fe ₁₂ O ₁₉ Ba _{0.5} Sr _{0.5} Fe ₁₂ O ₁₉	DBSA	Water
BSM50P	Ba _{0.5} Sr _{0.5} Fe ₁₂ O ₁₉	Oleic Acid	Paraffin Oil
BSM50S		Oleic Acid	Silicone Oil

Fig. 5.8 shows the effect of solvent on viscosity for various colloids based ferrofluids at zero applied magnetic field. Shear thinning is observed for all the ferrofluids. The maximum viscosity is observed for Silicone based ferrofluids for each composition of the nanoparticles.



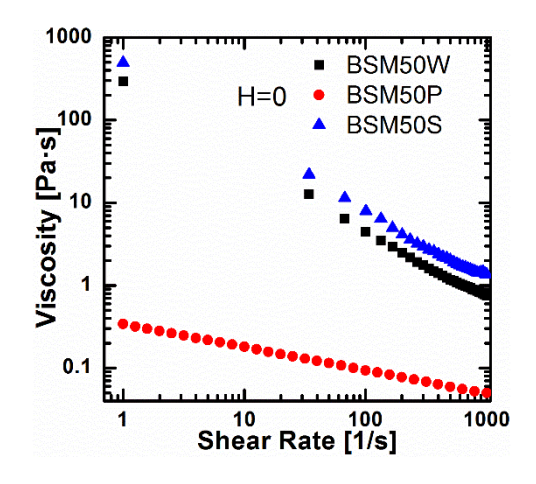


Figure 5. 8 Solvent and Colloidal effect in BSM ferrofluids at H=0.

The shear thinning effect is lowest for BSM10S and highest for BSM50S ferrofluid. The flow remains Non-Newtonian up to shear rate of 1000 s⁻¹ for all ferrofluids except for BM, BSM5, and BSM20P which show Newtonian behaviour above the shear rate of 200 s⁻¹. These results show that magnetic structures in the form of drops and chains are formed in the ferrofluid due to dipole-dipole interactions.

5.2.1 Magneto-viscosity of BaFe₁₂O₁₉ ferrofluids:

Ba-Fe₁₂O₁₉ (BM) nanoparticles were "dispersed" in "water", paraffin and "silicone oil" for synthesizing the BMW, BMP and BMS ferrofluids respectively. The "volume ratio" of the nanoparticles, surfactant and "solvent" is taken as 1:0.5:1.5 respectively.

The "viscosity" vs. shear rate with various "magnetic fields" are shown in Fig. 5.9.

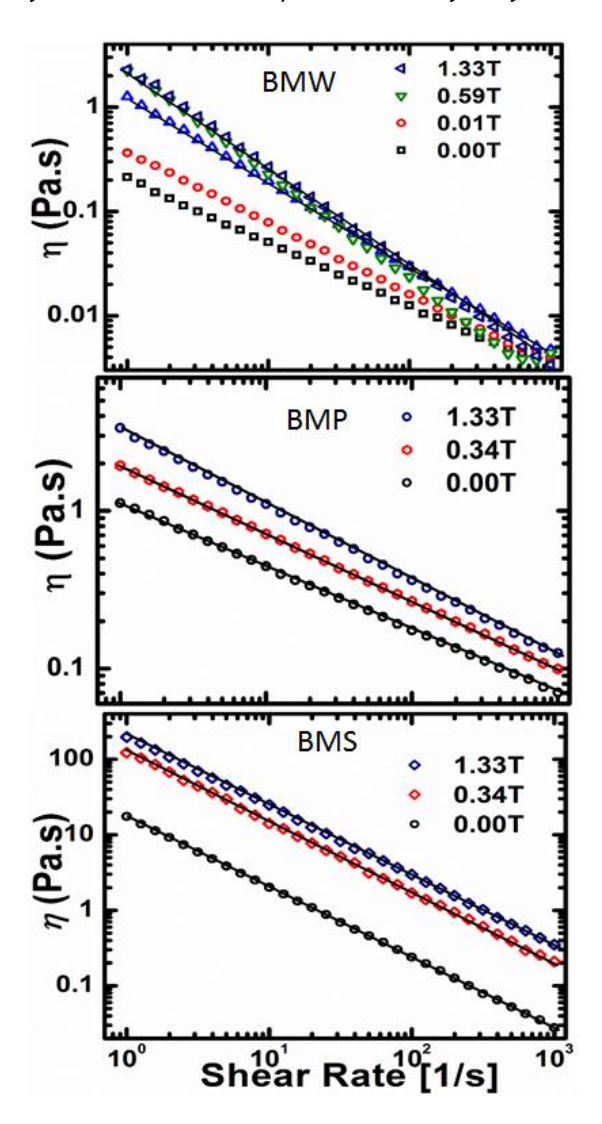


Figure 5. 9 Viscosity vs. shear rate of BMW, BMP and BMS ferrofluids.

The viscosity vs. shear rate plots indicate non-Newtonian behaviour for all the ferrofluids. The BMS ferrofluid show the highest viscosity (200 Pa.s) at 1.33 T applied magnetic field. The shear thinning behaviour for these ferrofluid similar to Cu-Zn and Fe₃O₄ based ferrofluids described in chapter 3 and 4 is observed. Fig. 5.9 shows Viscosity vs. shear rate at some selected applied magnetic field. The plot show that the "power law" behaviour is observed in all ferrofluids [3]. The n-value decreases from 0.68 to 0.58 as magnetic field increases from 0.17 to 1.33 T. The small *n*-value indicates higher shear thinning at different applied magnetic field.

Table 5. 5: The fitting parameters of power law for BM ferrofluids are tabulated below:

Ferrofluid	K values	n (power	Magnetic
Name		index)	field (T)
	0.2	0.3	0.00
BMW	0.3	0.3	0.01
	2.26	0.01	1.33
	1.92	0.57	0.34
ВМР	3.3	0.51	1.33
	17.3	0.06	0.00
BMS	125.4	0.09	0.34
	200	0.08	1.33

The decrease in *n*-value with an increase in the applied field reveals that the viscosity is influenced more by applied magnetic field at low shear rates than at higher shear rates. This behaviour at lower and higher shear rates appears due to the competition between the flow field and the applied magnetic field. The chain formation increases in viscosity when the magnetic field is applied perpendicular to the shear flow. The chains are broken in to small units with an increase in shear rate. The dominance of viscous forces over magnetic forces causes the chains to break. Fig. 5.10 illustrates the variation in "viscosity" curves at 1 and 10 s⁻¹ of BMW, BMP and BMS ferrofluids respectively. The following points are to be noted from the plots.

Chapter-5: Studies on Ba-Sr ferrite (BSM) nanoparticles and ferrofluids

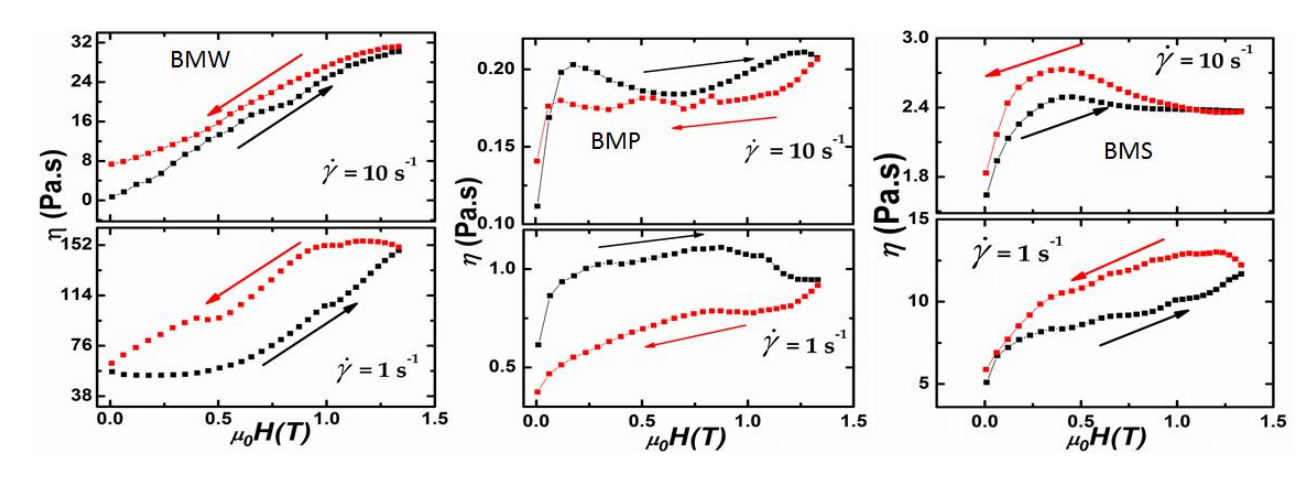


Figure 5. 10 magneto-viscosities of water, paraffin and silicone oil based BSM ferrofluids.

(1)The plate shaped particle are structurally more anisotropic than the other geometric shapes. (2) When the magnetic field is applied, the plate magnets will stack into long chains along the magnetic field due to high initial susceptibility. (3) With further increase in field, the viscosity increases and the plots for BMP and BMS. (4) In the present case, the stacked plate magnets forming long chains show slow mechanical relaxations with flow fields. The stacked plates in the field direction will be saturated after a specific field. But, instead of the viscosity increasing with magnetic field, the mechanical relaxation of the stacked plate structure takes place in the constant shear rate. The observed viscosity plots are attributed to the competition between the applied magnetic field and the relaxation of the plate magnets due to the shear rate. The oil based ferrofluids show saturation with the increase in applied magnetic field whereas the water based FF show linear behaviour. The BMW viscosity at shear rate 1s⁻¹ shows the highest value at 1.33 T. These results show that variation of viscosity with magnetic field is strongly dependent on the nature of the solvent.

The magneto-viscosity of BMP FF at constant shear rate of 50 and 150 s $^{-1}$ are shown in Fig. 5.11. The viscosity initially increases with the applied magnetic field, followed by a cusp and show the saturation at a high field. The maxima are noticed in the magneto-viscosity plots. The platelets are stacked in the field direction due to high initial susceptibility. The resultant viscosity curves confirm the competition between

field and relaxation of magnetic platelets due to shear. It is noticed that the hysteresis is decreasing with the increase in shear rate. This means the smaller magnetic structures follow the variation in magnetic field and thus give rise to lower hysteresis in the viscosity vs. field plots.

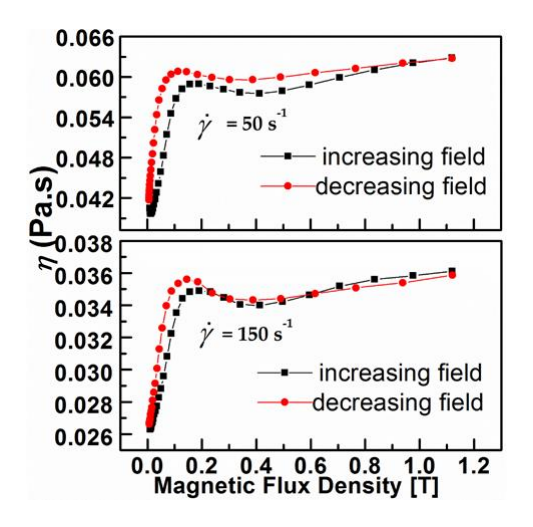


Figure 5. 11 Magneto-viscosity of paraffin BM based FF.

Fig. 5.12 ((a) & (b)) show the flow curves for paraffin based ferrofluids. The plots (Fig. 5.12 (a)) are fitted with power law equation as shown in chapter 3. The calculated K values are 0 .2-0.3 at the different fields from 0.17-1.33T.

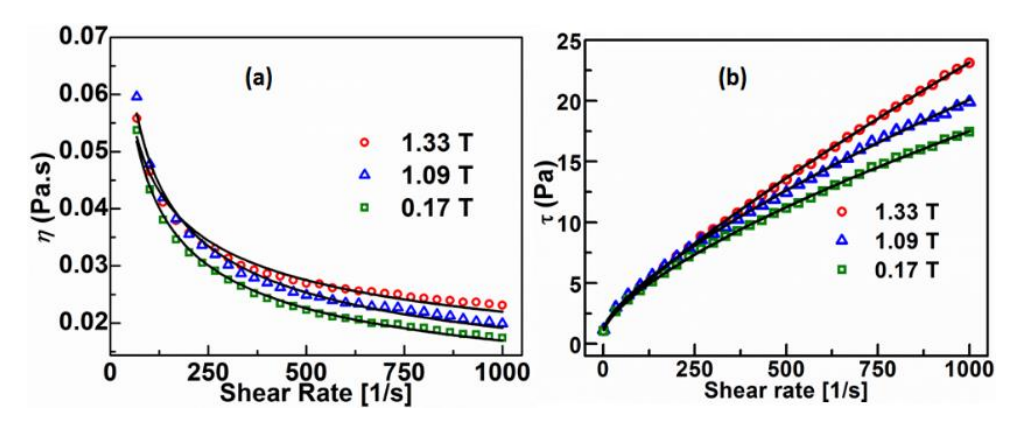


Figure 5. 12 viscosity vs. shear rate (a), shear stress vs. shear rate (b) for BMP ferrofluids.

The n value reduces from 0.68 to 0.58, clearly showing the shear thinning behaviour at different fields. Fig. 5.12 (b) shows the shear stress vs. shear rate. The H-B model fit is carried out for zero and applied fields as done in chapter 3 and 4. The yield stress is positive so the power index (n) is more as compared to the power law.

The range of n parameter is 0.72-0.82, K is 0.04-0.14 for magnetic field 0.17, 1.09 and 1.33T.

5.2.2 Magneto-viscosity of Ba_{0.95}-Sr_{0.05}Fe₁₂O₁₉ ferrofluids in different colloids:

Fig. 5.13 shows the viscosity vs. shear rate for BSM 5 based FF at various magnetic fields.

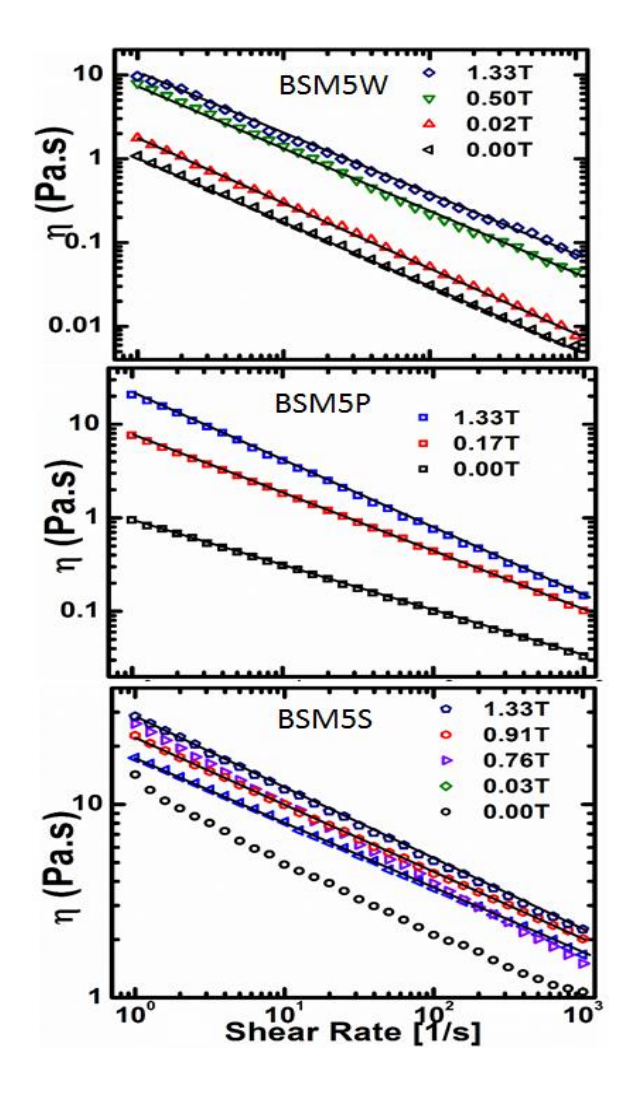


Figure 5. 13 Viscosity vs. shear rate of BSM5W, BSM5P and BSM5S ferrofluids.

The shear thinning behaviour for these ferrofluid similar to BM described in the above section is observed. The power law behaviour is observed for these ferrofluids.

The viscosity of most ferrofluid decrease and fluid show the field induced structure formation by the applied shear force. The field induced structure show alignment along the shear flow direction also reduces the fluid viscosity. This has been

confirmed through Small-angle Neutron Scattering (SANS)[4]. The particles are aligned towards the field in low shear. When shear increases, the deviation of chains from the field direction becomes more prominent and chains break into small particles. In another words, there is a race between the "hydrodynamic force" and "magnetic force". At the low "shear rate" the "magnetic force" dominates the "hydrodynamic force" and chain formation happen. Whereas at high "shear rate" the hydrodynamic force governs to the magnetic force and chain becomes weaker or break into individual particle.

Table 5. 6: The fitting parameters of power law for BSM5 ferrofluids.

-			, ,
Ferrofluid	K values	n	Magnetic field
Name		(power index)	(T)
	0.59	0.57	0.00
BSM5W	1.19	0.42	0.02
	10.5	0.27	1.33
	0.93	0.51	0.00
BSM5P	7.5	0.38	0.17
	21	0.2	1.33
	13	0.59	0.00
BSM5S	22.4	0.64	0.17
	28.5	0.62	1.33

Chapter-5: Studies on Ba-Sr ferrite (BSM) nanoparticles and ferrofluids

For more understanding of the relationship between magnetic force and hydrodynamic force and defined by a dimensionless quantity called Mason number which is an important term in magneto-rheological analysis. Mason number is as given by:

$$Mn = \frac{\eta_c \dot{\gamma}}{2\mu_0 \mu_c \beta^2 H^2} \tag{5.1}$$

Where μ_0 is the permeability of the vacuum, μ_c the relative permittivity of carrier liquid and " β " is "contrast factor" defined as:

$$\beta = \frac{\mu_p - \mu_c}{\mu_p + \mu_c} \tag{5.2}$$

 μ_p , is the relative permeability of the particles.

The degree of "shear thinning" rises as the "magnetic field" increases. Many groups report this.

Fig. 5.14 shows the viscosity as a function of magnetic field (from 0.0 to 1.33 T) at 1 and $10 \, s^{-1}$ for BSM5W, BSM5P and BSM5S ferrofluids, respectively. The magnetoviscosity rapidly increases with increasing field.

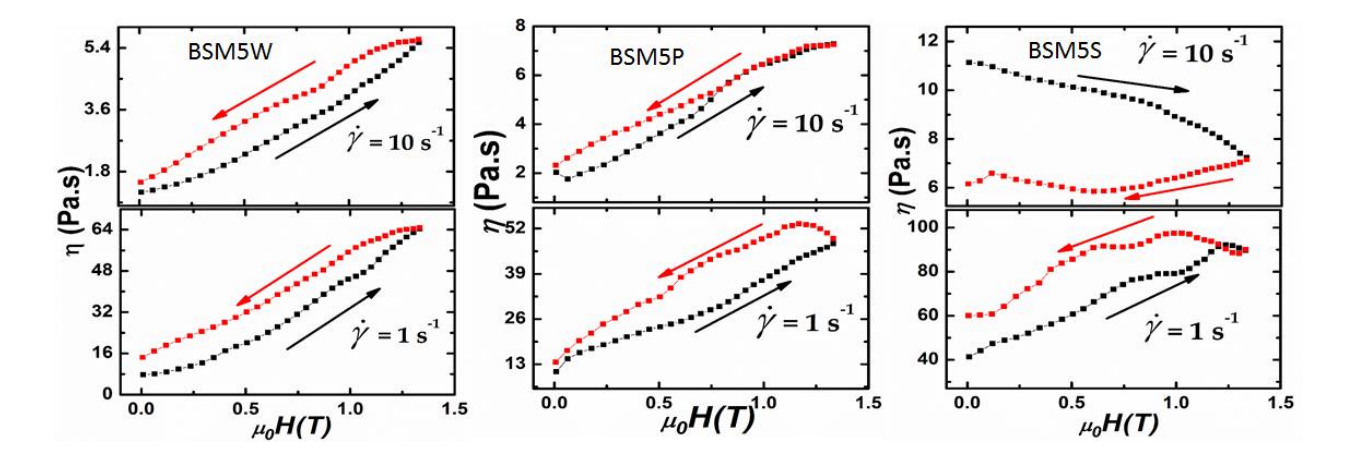


Figure 5. 14 Magneto-viscosity at 1 and 10 s⁻¹ of BSM ferrofluids.

In BSM5W and BSM5P ferrofluids there is no saturation up to high field (1.33T), still need high magnetic field >1.33T which is similar to our earlier report [5]. The

BSM5S ferrofluid shows a large viscosity among all other ferrofluids at 1 s⁻¹ and 10 s⁻¹. The BSM5S ferrofluid shows the open hysteresis loop at 1 and 10 s⁻¹. This is attributed to the situation where chains are not broken completely and magnetic structures are not returning toward the original position. Therefore, the viscosity is high for this ferrofluid at both shear rate (1s⁻¹ &10s⁻¹).

5.2.3 "Magneto-viscosity" of Ba_{0.9}-Sr_{0.1}Fe₁₂O₁₉ ferrofluids in different colloids:

The coated Ba-Sr ferrite nanoparticles were mixed in paraffin (BSM10P) and "silicone oil" (BSM10S) for the preparation of ferrofluids. Fig. 5.15 shows flow curves of BSM10P and BSM10S ferrofluids. The ferrofluids show non-Newtonian behaviour at various magnetic fields. The BSM10S ferrofluid show higher viscosity (4.8Pa.s) as compared to the BSM10P ferrofluid.

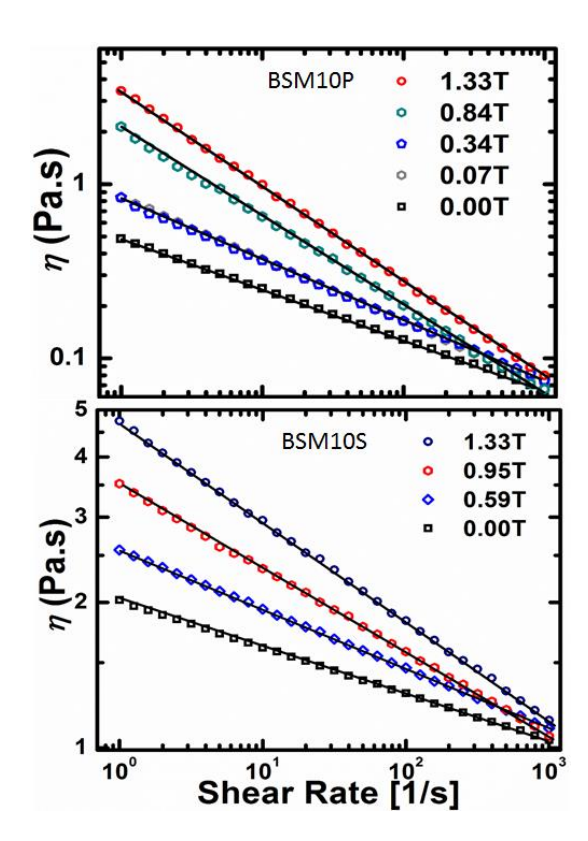


Figure 5. 15 Flow curves of paraffin and silicone oil based BSM ferrofluids.

Table 5. 7: Fitting parameters of power law for BSM10P and BSM20S ferrofluids.

Chapter-5: Studies on Ba-Sr ferrite (BSM) nanoparticles and ferrofluids

Ferrofluid	K values	n (power	Magnetic
Name		index)	field (T)
	0.48	0.7	0.00
BSM10P	0.8	0.64	0.34
	2.07	0.49	0.84
	3.4	0.45	1.33
	2	0.003	0.00
	2.5	0.87	0.59
BSM10S	3.4	0.82	0.95
	4.7	0.79	1.33

Fig. 5.16 represents the magneto-viscosity curves of BSM10P and BSM10S ferrofluids at a shear rate "1" and "10" s^{-1} respectively.

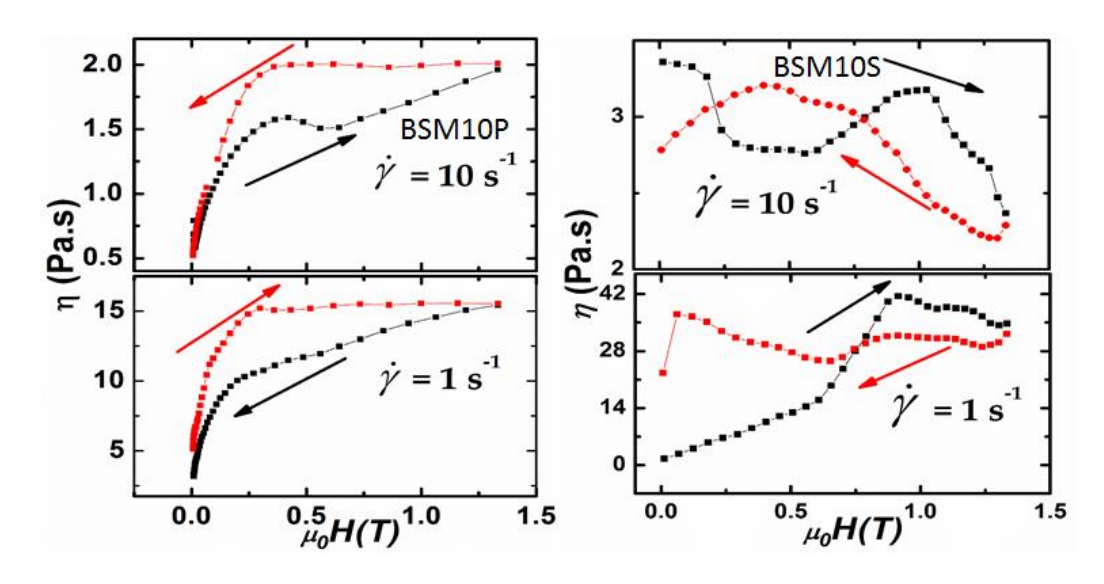


Figure 5. 16 Magneto-viscosity of paraffin and silicone oil based BSM ferrofluids.

In BSM10P ferrofluid "viscosity" increased rapidly with an increase in the field and saturated at 0.25T for both shear rates (1 & 10s⁻¹). Whereas BSM10S ferrofluid reaches the highest viscosity values (42Pa.s) at around 0.8 T and saturates with further increase in field. The behaviour of viscosity vs. field at a shear rate of 1s ⁻¹ and 10 s⁻¹ are just the opposite.

5.2.4 Magneto-viscosity of Ba_{0.8}-Sr_{0.2}Fe₁₂O₁₉ Ferrofluids in different solvents:

The coated Ba_{0.8}-Sr_{0.2}Fe₁₂O₁₉ "nanoparticles were dispersed in water" (BSM20W), paraffin (BSM20P) and "silicone oil" (BSM20S) for preparation of BSM20W, BSM20P, and BSM20S ferrofluids respectively. Fig. 5.17 shows the flow curves at some selected fields.

The non-Newtonian behaviour is observed for ferrofluids. The shear thinning behaviour for these ferrofluid similar to BM described in above section is observed. The power law behaviour has been observed for these ferrofluids.

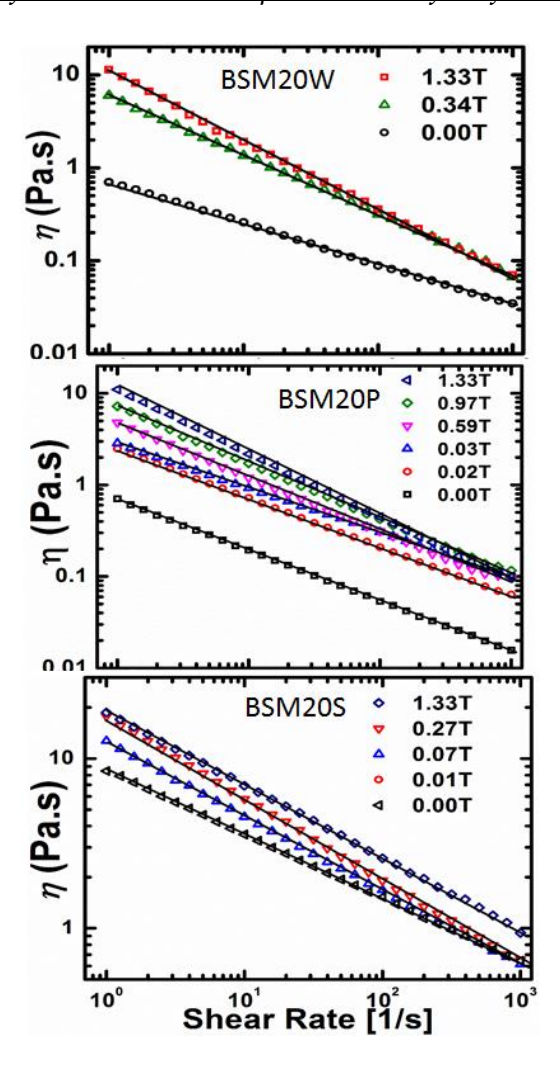


Figure 5. 17 Flow curves of water, paraffin and silicone oil based BSM ferrofluids.

Table 5. 8: The fitting parameters of power law for BSM20 ferrofluids

Ferrofluid Name	K values	n (power index)	Magnetic field (T)
	0.48	0.7	0.00
BSM20W	5.9	0.36	0.34
	11.4	0.21	1.33
	0.69	0.44	0.00

201111	2.4	0.46	0.02
BSM20P	2.8	0.51	0.03
	4.7	0.4	0.59
	7.2	0.37	0.97
	11	0.3	1.33
	8	0.62	0.00
BSM20S	12	0.55	0.07
	18.7	0.57	1.33

The magneto-viscosity data comparison between water, paraffin and silicone oil based ferrofluid are as follows:

- (i) "Viscosity" increases almost linearly in water and paraffin based ferrofluids and ends up with hysteresis loop with higher viscosity in decreasing field stage.
 - (ii) BSM20S ferrofluid shows the saturation at applied magnetic field 0.25T.

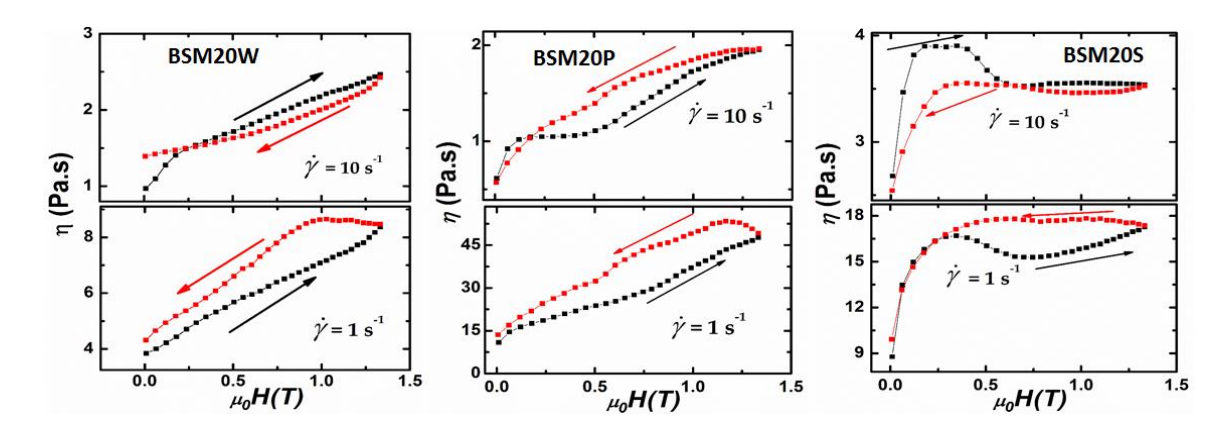


Figure 5. 18 Magneto-viscosity of water, paraffin and silicone oil based BSM ferrofluids of 1 and $10 \, s^{-1}$ respectively.

5.2.5 Magneto-viscosity of Ba_{0.5}-Sr_{0.5}Fe₁₂O₁₉ Ferrofluids:

The coated Ba_{0.5}-Sr_{0.5}Fe₁₂O₁₉ "nanoparticles were dispersed in water", paraffin and "silicone oil" to prepare BSM50W, BSM50P, and BSM50S ferrofluids respectively. Fig. 5.19 presents the flow curves at different applied magnetic fields.

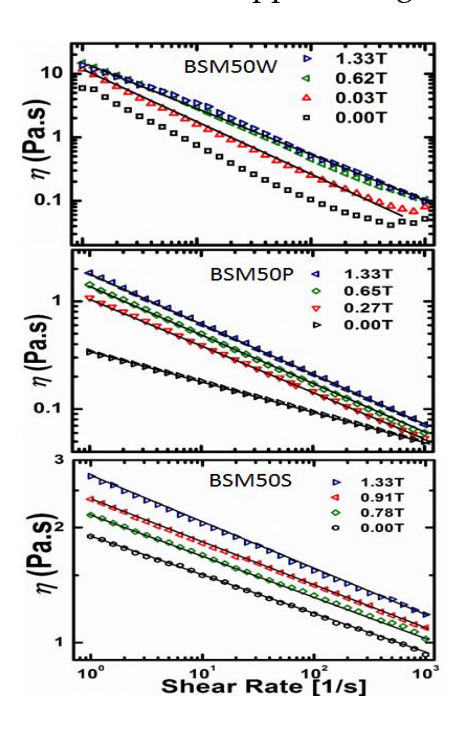


Figure 5. 19 Flow curves of water, paraffin and silicone oil based BSM ferrofluids.

The flow curves show the "decrease in viscosity with increase in shear rate". All ferrofluids undergo "non-Newtonian" to "Newtonian" transition without magnetic field as well as with magnetic field. The shear thinning behaviour for these ferrofluid is similar to the BM described in the above section. The power law behaviour is observed for all these ferrofluids.

Table 5. 9: The fitting parameters of power law for BSM50 ferrofluids are tabulated below:

Ferrofluid Name	K values	n (power index)	Magnetic field (T)
	6.3	0.0004	0.00

BSM50W	11.7	0.11	0.03
	14	0.29	1.33
	0.69	0.44	0.00
DCI (TOD	2.4	0.46	0.02
BSM50P	2.8	0.51	0.03
	4.7	0.4	0.59
	7.2	0.37	0.97
	11	0.3	1.33
	0.3	0.72	0.00
BSM50P	1	0.56	0.27
	1.4	0.54	0.65
	1.8	0.53	1.33
	1.89	0.894	0.00
DCMEOC	2.1	0.898	0.78
BSM50S	2.3	0.887	0.91
	2.7	0.87	1.33

Fig. 5.20 shows the "magneto-viscosity" as a function of the magnetic field at "1" and "10" s⁻¹ for water (BSM50W), paraffin oil (BSM50P) and silicone oil (BSM50S) based ferrofluid respectively. The viscosity response is quite different in different solvents with applied magnetic field. In the presence of a magnetic field, nanoplatelets try to align toward the "field direction" which leads to "chain formation" in the ferrofluids. Here the BSM50S ferrofluid show the highest change in viscosity at "1" and "10" s⁻¹ with the increase in the magnetic field.

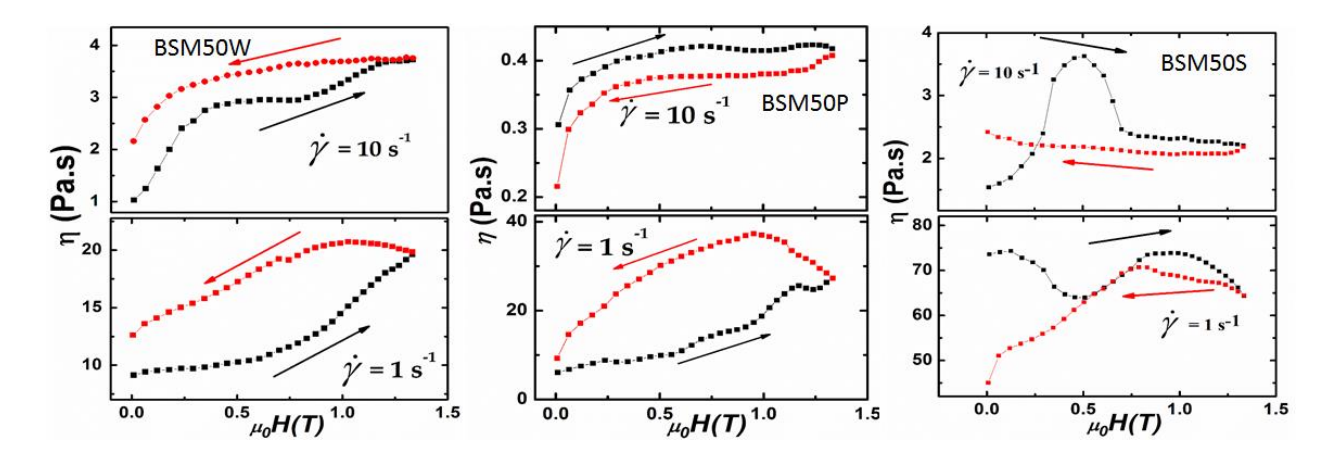


Figure 5. 20 "Magneto-viscosity" at 1 and 10 s⁻¹ of water, paraffin and silicone oil based BSM50 ferrofluids.

The almost linear increase in viscosity with the increasing magnetic field is observed for BSM50W and BSM50P ferrofluid at 1 s⁻¹ and saturating at 10s⁻¹.

The BSM50W and BSM50P ferrofluid show large hysteresis on removing the magnetic field indicating that the formed structure is not coming back to its original position at zero field. The hysteresis plots for BSM50S are complicated and indicates the unstable nature of formed magnetic structures. The nano platelets could slide over each other more easily than cubic and spherical particles. This will affect viscosity variation with increase as well as with a decrease in the magnetic field and thus on hysteresis plots.

5.2.6 Herschel-Bulkley behaviour in ferrofluids:

5.2.6.1 Water Based Ferrofluid

The water based ferrofluid is selected for analysis as per Herschel-Bulkley (H-B) model.

Fig. 5.21 shows shear stress vs. shear rate plots for three water based ferrofluids at different magnetic field. The fits to experimental data are found using the equation: $\tau = \tau_0 + K\dot{\gamma}^n$, Where τ_0 is the "yield stress".

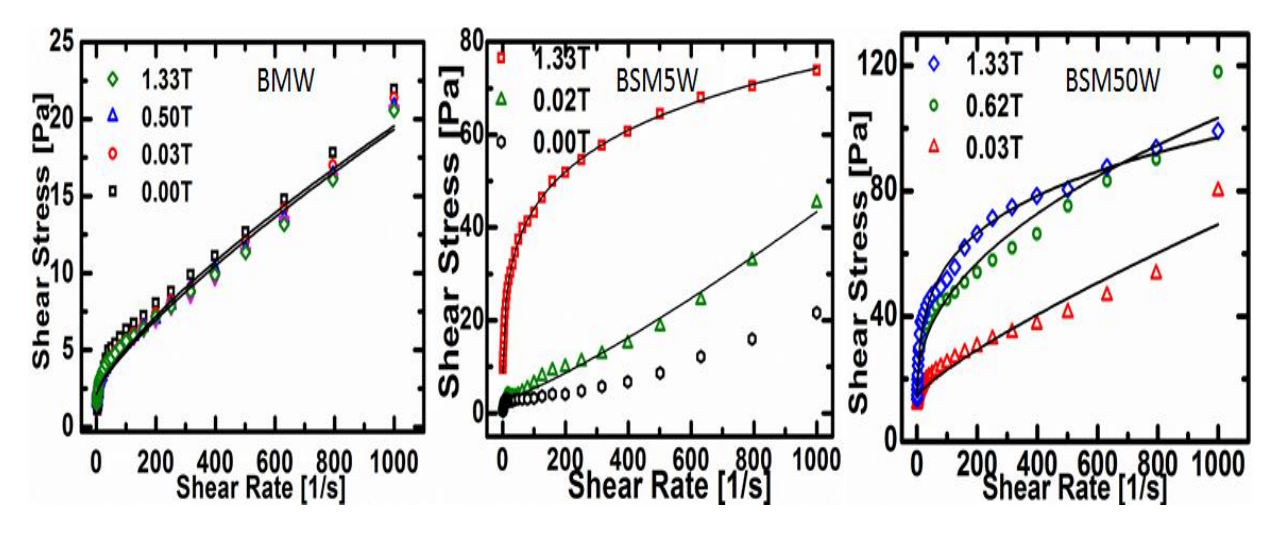


Figure 5. 21 "H-B model fit" for BMW, BSM5W and BSM50W ferrofluids.

The colloidal plays an essential part in the rheological properties of ferrofluids. The nature of colloidal and ratio of surfactant plays a crucial part in the change of viscosity under different conditions except for the magnetic properties of nanoparticles. There is large change in yield stress on application of magnetic field. The value increased from 4 to 60 Pa with field values from 0 to 1.33T. Good H-B fits are obtained for these water ferrofluids at 1.33 T. The H-B model appears to be more suitable to describe the flow curves in the high magnetic field. At a high magnetic field almost all nanoparticles are arranged in long chains at low shear rates. When the shear rate increases, the long chains are broken into smaller units leading to Newtonian behaviour of the ferrofluid.

Table 5. 10: Shear stress, consistency and power index values for water based ferrofluids

Chapter-5: Studies on Ba-Sr ferrite (BSM) nanoparticles and ferrofluids

Ferrofluid	K values	n	Magnetic	Yield stress
Name		(power index)	field (T)	(au_0)
	0.09	0.76	0.5	2.07
BMW	0.07	0.78	1.33	2.1
	0.009	1.2	0.02	2.79
BSM5W	32.3	0.16	1.33	23.6
	0.2	0.81	0.03	14.3
BSM50W	3.3	0.4	0.62	16.3
	24.9	0.2	1.33	9.35

Fig. 5.22 shows the shear stress vs. shear rate plots for paraffin based BSM ferrofluids. All the fitted with the H-B model equation. The yield stress provides the information about the force needed for breaking the large aggregation or formed chains which try to reforms due to magnetic-static force in an applied magnetic field. The BSM10P sample shows a higher stress value than BMP due to their hydrodynamic distribution performance in the solvent. The n-values are in the range of 0.8 to 0.9 and the K-values are in the range of 0.13 to 0.15 for the applied magnetic field range of 0.008 to 0.34 T.

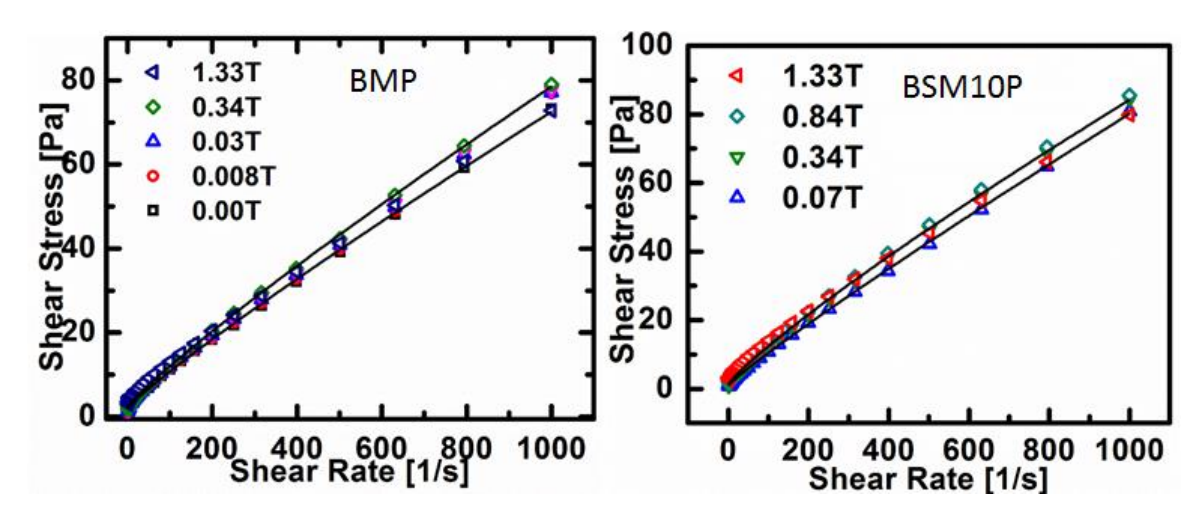


Figure 5. 22 "H-B model fit" for BMP and BSM10P ferrofluids.

Table 5. 11 : Shear stress, consistency and power index values for paraffin based ferrofluid.

Ferrofluid Name	K values	n (power index)	Magnetic field (T)	Yield stress($ au_0$)
	0.13	0.9	0.008	1.9
ВМР	0.15	0.89	1.33	2.2
	0.13	0.92	0.84	0.94
BSM10P	0.2	0.86	1.33	1.19

The yield stress increases as the applied "magnetic field" increases for both the ferrofluids.

Fig. 5.23 shows the shear stress vs. shear rate plots for silicone oil based BSM20S and BSM50S ferrofluids.

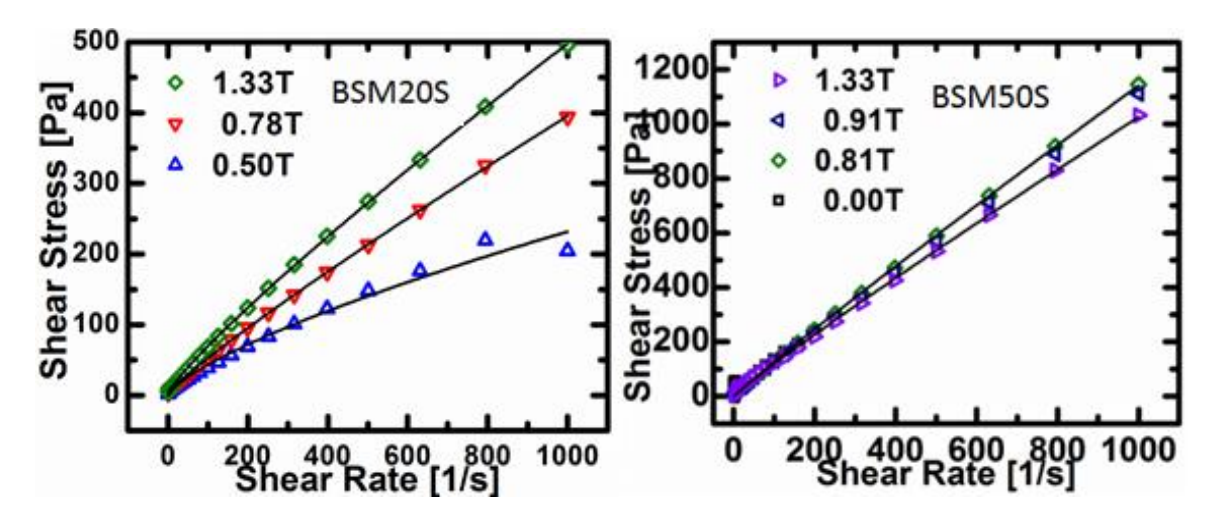


Figure 5. 23 "H-B model fit" for BSM20S and BSM50S ferrofluids.

The yield stress is found to be higher for BSM50S FF compared to other ferrofluids.

Table 5. 12: Shear stress, consistency and power index values for BSM20S and BSM50S FF.

Ferrofluid	K values	n	Magnetic	Yield
Name		(power index)	field (T)	$stress(au_0)$
	0.77	0.9	0.78	3.75
BSM20S	1.1	0.87	1.33	4.4
	0.2	0.81	0.03	14.3
BSM50S	3.3	0.4	0.62	15.3
	24.9	0.2	1.33	16

5.2.7 Magneto Sweep

The oscillatory experiments are helpful to probe the viscoelastic properties of the ferrofluids. The oscillatory test with small amplitudes is used to detect small changes

in the structure due to deformations. The strain amplitude sweep directly affects the formation and destruction of chains in ferrofluids. The elastic behaviour is given by storage modulus G.' The mechanical energy used to destroy the elastic structure is estimated by loss modulus G'.

The "storage modulus" (G') and "loss modulus" (G'') were determined with respect to the magnetic field applied 0 - 1.33 T at a constant strain amplitude γ_0 = 0.01% and $\omega = 10$ rad/sec for two ferrofluids as is illustrated in Fig. 5.24. The difference in the flow magneto sweep curves is observed for ferrofluids (BMW and BM5W) samples at the low field. It is observed from the curves that both show a quite similar trend. Initially when the field is applied the G' and G'' increased rapidly and at some field (0.5T), both samples show the maxima and then decreased at higher field. Loss modulus increases with increasing the field for both samples and showed the maxima and then decreased with increasing field. This is due to the change in microstructure in the ferrofluids, which may be the reason for this phenomenon. The storage modulus is higher than the loss modulus due to internal magnetic field strength. In the applied magnetic field (0 to 1.33T), the particles strongly interact and form the chain-type structure. At 0.5 T field almost all nanoparticles are in long chain structures. The movement of these structures becomes limited. As a result separated liquid flows more easily between these structures leading to a decrease in storage modulus and loss modulus. This is a phase transition in ferrofluid [6].

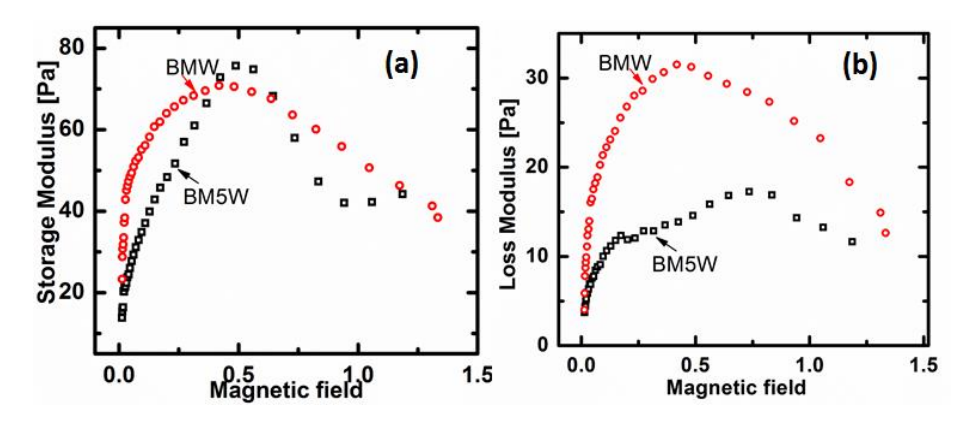


Figure 5. 24 "storage moduli" (a) and "loss moduli" (b) of BMW and BSM5W ferrofluids.

5.2.8 Inverse Ferrofluids

The ferrofluid with nonmagnetic particles dispersed in it is known as inverse ferrofluids (IFF). Mainly silica large size particles are used for creating the matrix in the ferrofluid having long chain order and hydrodynamically continuous medium. The non-magnetic particles are form chains in the field direction, like in normal ferrofluids[7]. IFF shows an increase in shear resistance similar to normal ferrofluids [8-9]. The study of such a system offers the advantage of probing the effects of different particle shapes and sizes. We have focused on the simplest IFF consisting of BSM10S ferrofluid and silica particles volume % of 0.0005 (diameter 2.34 μ m).

Fig 5.25 represents the schematic diagram for inverse ferrofluid.

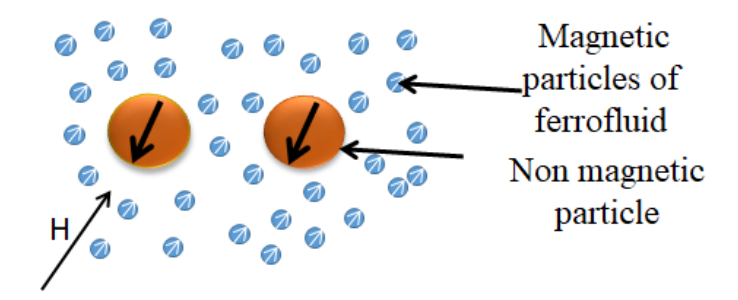


Figure 5. 25 Schematic image of an inverse ferrofluids.

The chain formation on the application of magnetic field in inverse ferrofluids was discovered by Skjeltrop [10]. Inverse ferrofluids originate the viscosity rise comparable to other fluids (MR fluid, ferrofluids). Since the size and shape of the nonmagnetic particles are well defined, inverse ferrofluids also serve as suitable systems for model studies of the magneto rheological effect. The variation of viscosity for an inverse ferrofluid is shown in Fig. 5.26. The viscosity of inverse ferrofluid increases and reaches a saturation value smoothly. This is unlike the erratic variation of BSM10S ferrofluids discussed above.

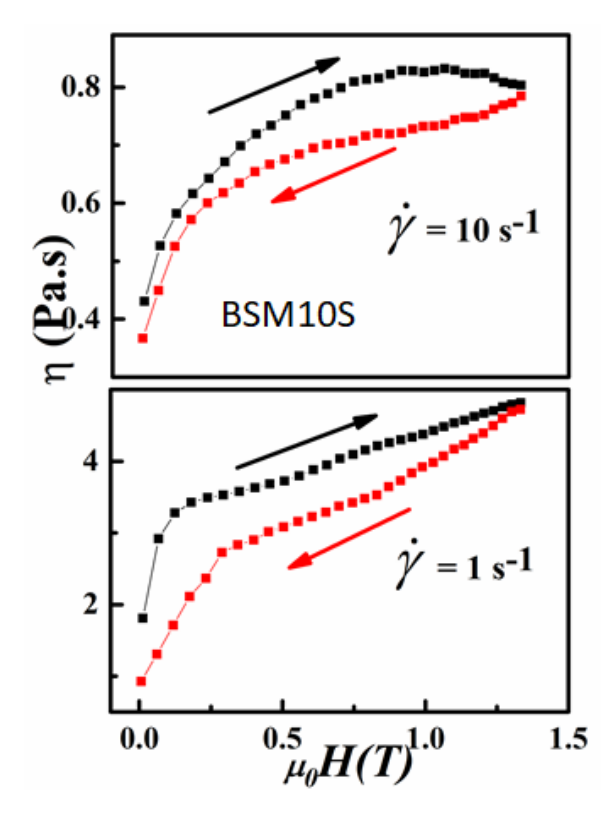


Figure 5. 26 Viscosity vs. magnetic field of BSM10S ferrofluid.

For the decreasing magnetic field stage, the viscosity is lower than the increasing magnetic stage. This indicates that the magnetic structures disintegrate into small units while decreasing the magnetic field.

The viscosity vs. shear rate plot is shown in Fig. 5.27 for inverse ferrofluid with and without magnetic field.

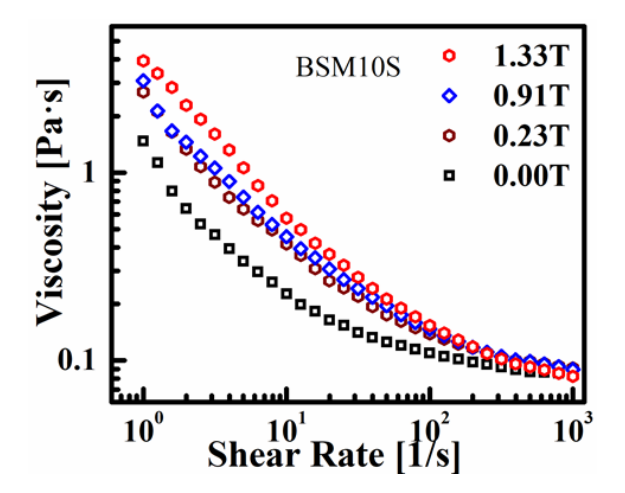


Figure 5. 27 Flow curve of BSM10S ferrofluid.

Chapter-5: Studies on Ba-Sr ferrite (BSM) nanoparticles and ferrofluids

This viscosity at low "shear rates" decreases non-linearly with increasing shear rate. It approaches a constant value at a shear rate greater than around 300 s⁻¹ indicating a transition from "non-Newtonian" to Newtonian behaviour with an increase in shear rate.

The stress dependence on the shear rate at various magnetic fields is shown in Fig. 5.28 for inverse ferrofluid shows that the stress is increasing with field strength due to the strong chain-like structure formation of the magnetic structures. The observed shape of the flow curves from 1 to 3 s⁻¹, is unusual. Indeed, it is known that a decreasing flow curve cannot occur for a homogeneous material. These regions of the flow curve probably arise due to instabilities within the system [11].

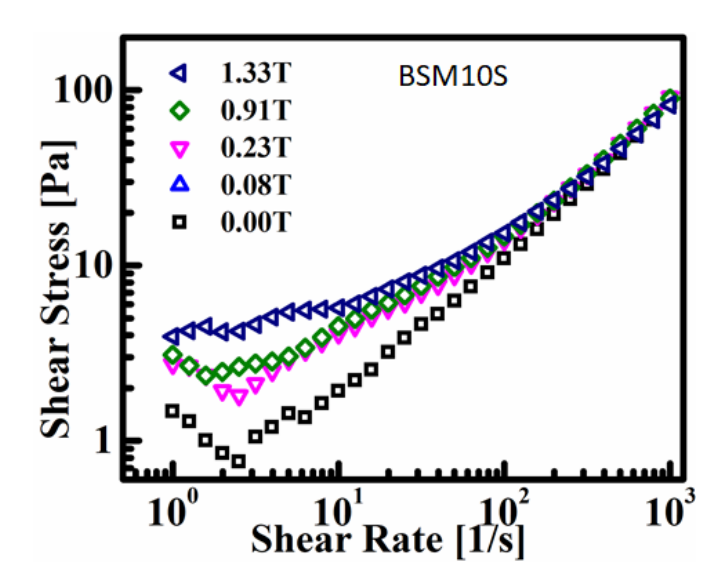


Figure 5. 28 Flow curve of shear rate of BSM10S ferrofluid.

The decreasing flow curves are reported in ERF under dc fields [12]. Observation of such results in the present IFF may be due to the platelet nature of nanoparticles in the ferrofluid. It is not clear what is the nature of the non-homogeneities or instabilities in these flow regimes.

The various synthesis methods have been reported to achieve a single hexagonal phase with better structural and magnetic properties [13-14]. In order to improve the properties, some research groups have tried doping and found doping is useful in removing the magnetic anisotropy required for many applications [15-16]. The Sc-

doping in barium hexaferrite improves the structural and magnetic properties [17]. While increasing the synthesis temperature, structural growth is found to be more stable with uniform particle size.

The Ba-Sr hexaferrite platelets shaped nanoparticles synthesized via hydrothermal route gave the better structural and magnetic response in the present work. These nanoparticles were used to prepare water, paraffin and silicone oil based ferrofluids to study their magneto-viscosity at different applied magnetic field. The studies on Ba-Sr hexaferrite platelets shape based ferrofluids are reported for the first time.

In summary, the Ba_{1-x}-Sr_x Fe₁₂O₁₉ (x=0, 0.05, 0.1, 0.2, 0.5) nanoparticles were successfully synthesized via hydrothermal process. The analysis of XRD data confirmed the single-phase hexagonal magneto-plumbite structure of the nanoparticles. The microstructural study confirmed the hexagonal platelet shaped nanoparticles. The size distribution of nanoparticles and good stability was estimated from the particles size analyzer analysis. The magnetization results reveal the ferromagnetic nature of BSM nanoparticles at room temperature. The Three types of ferrofluid were prepared by dispersing the BSM nanoparticles in water, paraffin and silicone oil. All ferrofluids exhibit the power-law behaviour of viscosity vs. shear rate. water-based BM ferrofluid's viscosity vs. magnetic field plots shows the highest viscosity and linear behaviour with the applied magnetic field. Although the magnetization of the platelet shaped nanoparticles of BSM is less compared to Fe₃O₄ (spherical) and Cu-Zn (cubic) nanoparticles, but the Magneto Viscosity Effect (MVE) of the ferrofluids based on BSM is high. This may be due to the platelet shape of the Herschel-Bulkley's model was found to be applicable in BSM nanoparticles. explaining the MVE of the BSM ferrofluids.

The storage and dissipation moduli measurement indicate the phase separation in ferrofluid. The studies on inverse ferrofluid reveal the phenomenon of decreasing flow curve.

References:

- [1] C. Liu *et al.*, "Microstructure and magnetic properties of M-type strontium hexagonal ferrites with Y-Co substitution," *Journal of Magnetism and Magnetic Materials*, vol. 436, pp. 126–129, Aug. 2017.
- [2] R. J. Pandya, U. S. Joshi, and O. F. Caltun, "Microstructural and Electrical Properties of Barium Strontium Titanate and Nickel Zinc Ferrite Composites," *Procedia Materials Science*, vol. 10, pp. 168–175, 2015.
- [3] N. Gautam, G. Thirupathi, and R. Singh, "Magnetoviscosity of Paraffin-Based Barium Ferrite Ferrofluid," *IEEE Transactions on Magnetics*, vol. 52, no. 7, pp. 1–4, Jul. 2016.
- [4] N. Gautam and R. Singh, "Magneto-viscosity of stable colloidal solutions of Barium-strontium hexaferrite ferrofluid," *Materials Research Express*, vol. 6, no. 8, p. 84012, Jun. 2019.
- [5] N. Gautam and R. Singh, "Magneto-viscosity of platelet shaped Ba-Sr ferrite nanoparticles based ferrofluid in different colloids," *AIP Conference Proceedings* **2115**, 030153 (2019).
- [6] A. Yu Zubarev and L. Y. Iskakova, "Condensation phase transitions in bidisperse colloids," *Physica A: Statistical Mechanics and its Applications*, vol. 349, no. 1–2, pp. 1–10, Apr. 2005.
- [7] Berend-Jan de Gans, Hans Hoekstra and Jorrit Mellema," Non-linear magnetorheological behaviour of an inverse ferrofluid", *Faraday Discuss.*, 1999, 112, 209-224.
- [8] B. J. de Gans, C. Blom, A. P. Philipse and J. Mellema," Linear viscoelasticity of an inverse ferrofluid", *PHYSICAL REVIEW E*, Vol.60, number 4.
- [9] C. C. Ekwebelam and H. See," Determining the flow curves for an inverse ferrofluid" *Korea-Australia Rheology Journal*, vol. 20, no. 1, March 2008 pp. 35-42.
- [10] A. T. Skjeltorp.pdf A. T. Skjeltorp," One- anti Two-Dimensional Crystallization of Magnetic Holes", *Physical Review Letters*, vol. 51, no. 25, Dec. 1983.
- [11] P. C. F. Møller, J. Mewis, and D. Bonn, "Yield stress and thixotropy: on the difficulty of measuring yield stresses in practice," *Soft Matter*, vol. 2, no. 4, p. 274, 2006.
- [12] Howard See, Akiko Kawai, Fumikazu Ikazaki, "The effect of mixing particles of different sizr on the electrheological response under steady shear flow", Rheol Acta (2002) 41, 55-60.
- [13] M. Amini and A. Gholizadeh, "Shape control and associated magnetic and dielectric properties of MFe12O19 (M = Ba, Pb, Sr) hexaferrites," *Journal of Physics and Chemistry of Solids*, vol. 147, p. 109660, Dec. 2020.

- [14] X. Wei, Y. Liu, D. Zhao, X. Mao, W. Jiang, and S. S. Ge, "Net-shaped barium and strontium ferrites by 3D printing with enhanced magnetic performance from milled powders," *Journal of Magnetism and Magnetic Materials*, vol. 493, p. 165664, Jan. 2020.
- [15] R. S. Alam, M. Moradi, M. Rostami, H. Nikmanesh, R. Moayedi, and Y. Bai, "Structural, magnetic and microwave absorption properties of doped Bahexaferrite nanoparticles synthesized by co-precipitation method," *Journal of Magnetism and Magnetic Materials*, vol. 381, pp. 1–9, May 2015.
- [16] B. Grindi, Z. Beji, G. Viau, and A. BenAli, "Microwave-assisted synthesis and magnetic properties of M-SrFe12O19 nanoparticles," *Journal of Magnetism and Magnetic Materials*, vol. 449, pp. 119–126, Mar. 2018.
- [17] M. Hähsler, M. Zimmermann, S. Heißler, and S. Behrens, "Sc-doped barium hexaferrite nanodiscs: Tuning morphology and magnetic properties," *Journal of Magnetism and Magnetic Materials*, vol. 500, p. 166349, Apr. 2020.

<u>Chapter-5: Studies on Ba-Sr ferrite (BSM) nanoparticles and ferrofluids</u>

CHAPTER-6

Summary and Conclusions

Summary

Magnetic materials and ferrofluids have been extensively in demand for various industrial and medical purpose due to their outstanding physical properties which can be controlled by applied magnetic field. During last several years, ferrofluid are being studied for engineering and medical applications. Ferrofluids carry the tunable magnetic field rheological properties useful for number of applications. The microstructural changes in the ferrofluid ("magneto-viscosity") properties have been extensively studied. "Magneto-viscosity" can be improved by changing some parameters like preparation methods, particle morphology, concentration, colloids and "applied external magnetic field". The parameters which can be changed for application demands are viscosity, shear rate, yield stress, magnetic hysteresis and magnetic field. The present work is on studies of "structural" and "magnetic properties" of different ferrite nanoparticles. The magneto-viscosity measurements were carried out on the corresponding ferrofluids. The summary of the thesis is briefly described here:

6.1 Important Conclusions on Studies on Nanoparticles

- The nanoparticles of Fe₃O₄ were synthesized by using co-precipitation method at room temperature. The XRD data analysis shows the single phase "cubic spinel structure" with "Fd-3m" space group by using "Rietveld refinement".
- FESEM micrographs confirmed almost spherical shape of the nanoparticles.

 The "zeta potential" showed the excellent stability of Fe₃O₄ nanoparticles.
- The "magnetization M(H)" plots show the "ferrimagnetic nature" of the "nanoparticles" at room temperature.

Chapter-6: Summary and Conclusions

- The Cu_{1-x}Zn_xFe₂O₄ (x=0.0-0.6) ferrite were synthesized via co-precipitation process. The synthesis process was regulated by suitable ratio of metal and hydroxide ions.
- The effect of Zn substitution on structure and magnetic properties of nanoparticles is investigated. The XRD data is fitted with two-phase structure using Rietveld analysis for all CZF samples with various crystallite size.
- The FESEM micrographs show high grade agglomeration due to internal "magnetic field".
- TEM micrographs show the spherical and cube shape of the nanoparticles. The broad particle distributions is observed from the particle size analyzer data.
 The zeta potential shows the excellent stability.
- The magnetization of CZF (0.0 to 0.6) nanoparticles shows zero hysteresis at room temperature indicating superparamagnetic nature. The Ms decreases gradually with increasing Zn content. The AB interaction becomes weaker when x > 0.2 due to reduction of magnetic ions on A site with increase in Zn content.
- The M (T) plots of CZF nanoparticles elucidates the non-equilibrium magnetization.
- The Cu_{1-x}Zn_xFe₂O₄ (x=0.0-0.6) ferrite were synthesized via hydrothermal method.
- Hydrothermalized CZF samples show the change in particles shape and size. The XRD data are fitted with three phase structure using Rietveld analysis. The stable structure formation and homogeneity is found after hydrothermal treatment of CZF samples. The orthorhombic phase disappeared on Zn doing.
- The TEM micrographs confirm the cubic shape of the nanoparticles.
- The magnetization increases after heat treatment of CZF samples.
- Ba_{1-x}Sr_xFe₁₂O₁₉ (x = 0.0, 0.05, 0.1, 0.2, 0.5) nanoparticles were synthesized by hydrothermal process.

- XRD data show that all peaks correspond to hexagonal phase of M-type hexaferrite.
- FESEM and TEM confirm the hexagonal platelet shape of the nanoparticles.
- The magnetization decreases with increasing Sr content. The magnetic results indicate reduction in saturation magnetization due to the creation of nonmagnetic phase in BSM samples.

6.2 Important Conclusions on Studies on Ferrofluids

- In order to prepare the ferrofluid, the DBSA coated Fe₃O₄ nanoparticles were dispersed in water and oleic acid coated Fe₃O₄ nanoparticles were dispersed in toluene, paraffin oil and silicone oil. The flow curves show the non-Newtonian behaviour in the absence and presence of the magnetic field (0 to 1.33T).
- The magneto-viscosity plots show different behaviour with applied magnetic field at 1 and 10 s⁻¹. The silicone oil based ferrofluid shows the highest magneto-viscosity at 1 s⁻¹. But as the stability point of view the toluene and paraffin oil based ferrofluids show the minimum hysteresis. The chain formation and magnetic hysteresis are observed in the magneto-viscosity curves.
- In magneto-viscosity analysis the water and silicone oil based ferrofluid show higher magnetic hysteresis loop due to the viscosity of solvents and the hydrodynamic size distribution of particles in water and silicone oil. The magnetic structures of nanoparticles do not return to their original shape after removing the magnetic field leading to large magnetic hysteresis.
- The ferrofluids which show less magnetic hysteresis are the most demandable ferrofluids in various applications.
- The toluene and paraffin oil based ferrofluids were found to be more convenient ferrofluids in sensors and heat absorber applications.

Chapter-6: Summary and Conclusions

- For the magneto-viscosity study, two types of ferrofluids were prepared:

 Toluene based and paraffin oil based. The flow curves show the nonNewtonian behaviour at high magnetic field.
- In magneto-viscosity curves show the chain formation which occurs due to bigger aggregation in higher field. The viscosity increases with decrease in the field attribute the magnetic interaction and mechanical alignment of particles and less loss of aggregation of particles. The magneto-viscosity was found to be the same for x=0.2 to 0.4 ferrofluid sample.
- The two types of ferrofluids have been prepared from the hydrothermalized nanoparticles: water based and paraffin oil based CZF ferrofluids. The flow curves show the power law behaviour of viscosity vs. shear rate in zero as well in the presence magnetic field for all ferrofluids. The chain formation oppose the motion of ferrofluid leading to increase in viscosity with increase in magnetic field. The magneto viscosity plots show less hysteresis for ferrofluids with $0.2 \le x \le 0.6$ of Zn content compared to ferrofluid with x = 0.4. The ferrofluid with x = 0.4 show the highest viscosity (2.2Pa.s) under the magnetic field.
- In magneto-viscosity plots show high reversibility with the magnetic field in toluene and paraffin oil based ferrofluids which is an important property for switching application.
- Three types of ferrofluids were prepared by dispersing the BSM nanoparticles in water, paraffin and silicone oil. All ferrofluids exhibit the power law behaviour of viscosity vs. shear rate. The magneto-viscosity plot of the water based BM ferrofluid shows the highest viscosity and linear behaviour with applied magnetic field. Although the magnetization of the platelet shaped nanoparticles of BSM is less compared to Fe₃O₄ (spherical) and Cu-Zn (cubic) nanoparticles, but the Magneto Viscosity Effect (MVE) of the ferrofluids based on BSM is high. This may be due to platelet shape of the BSM nanoparticles.

- Herschel-Bulkley model was found to be applicable in explaining the MVE of the BSM ferrofluids.
- The storage and dissipation moduli measurements indicate the phase separation in ferrofluid. The studies on inverse ferrofluid reveal the phenomenon of decreasing flow curve.
 - The dipole-dipole interaction between magnetic nanoparticles determines the magneto viscous behaviour of ferrofluids.
 - The particle aggregates formed in the ferrofluid may have a different shape than that of the nanoparticles.
 - The flow curve and hysteresis of ferrofluids based on different shapes and sizes of nanoparticles may also be different. So, no general conclusion can be made about the influence of the geometric shape of nanoparticles on the MVEs in ferrofluids.
 - The concentrated ferrofluid based on platelet BSM nanoparticles gives much higher MVE compared to other ferrofluids.
 - The present study is useful for selecting a ferrofluid for a specific application. This is important when a ferrofluid with a high MVE is needed.

6.3 Future Scope

Further work on ferrofluids can be undertaken:

- 1. To improve the synthesis techniques for developing the uniform sized nanoparticles for various applications.
- 2. To modify the ferrofluid with innovative surfactant and colloidal media.
- 3. To study the heating efficiency in ferrofluid hyperthermia using specific absorption (SAR) and intrinsic loss power (ILP) for the efficiency of the ferrofluids.

Chapter-6: Summary and Conclusions

4. To understand the magnetic phenomena at the room temperature using AC-susceptibility.

To study the Faraday rotations in the superparamagnetic ferrofluid at room temperature.

Structural and Magnetic Properties of Some Ferrite Nanoparticles and Study of Magneto-viscosity of Corresponding Ferrofluids

by Nisha Gautam

Submission date: 05-Jul-2021 04:05PM (UTC+0530)

Submission ID: 1615932185

File name: Nisha thesis.pdf (9.46M)

Word count: 21401

Character count: 111299

Structural and Magnetic Properties of Some Ferrite Nanoparticles and Study of Magneto-viscosity of Corresponding Ferrofluids

ORIGINALITY REPORT

7%

SIMILARITY INDEX

INTERNET SOURCES

PUBLICATIONS

STUDENT PAPERS

PRIMARY SOURCES

Nisha Gautam, Gadipelly Thirupathi, Rajender Singh. "Magnetoviscosity of Paraffin-Based Barium Ferrite Ferrofluid", IEEE Transactions on Magnetics, 2016

2%

Publication

Nisha Gautam, Rajender Singh. "Magnetoviscosity of stable colloidal solutions of Barium-strontium hexaferrite ferrofluid", Materials Research Express, 2019

1 %

Publication

www.intechopen.com

Internet Source

<1%

Wang, Shenghai, Chuncheng Yang, and Xiufang Bian. "Magnetoviscous properties of Fe3O4 silicon oil based ferrofluid", Journal of Magnetism and Magnetic Materials, 2012.

< 1%

Publication

5

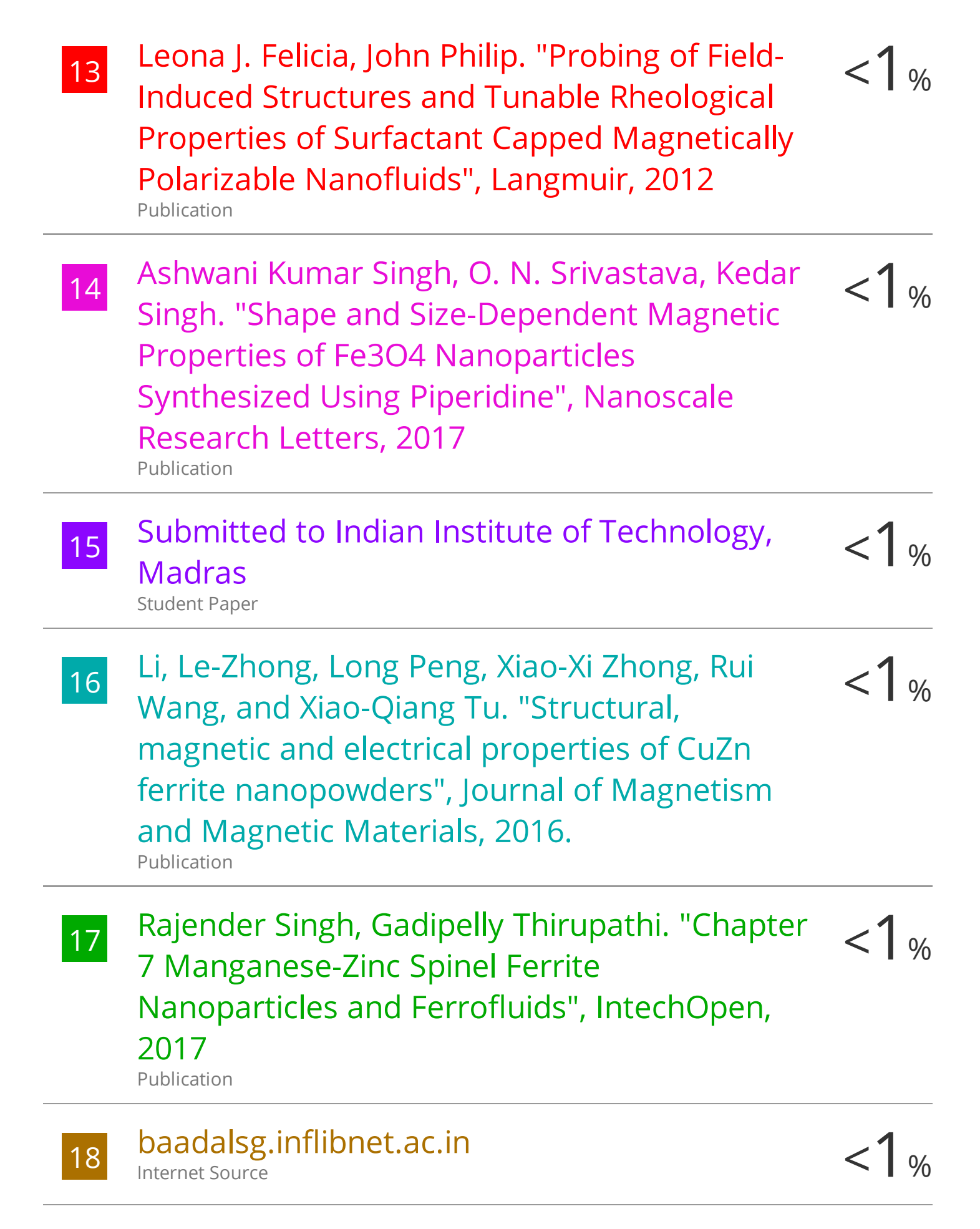
Nisha Gautam, Rajender Singh. "Magnetoviscosity of platelet shaped Ba-Sr ferrite

<1%

nanoparticles based ferrofluid in different colloids", AIP Publishing, 2019

Publication

6	worldwidescience.org Internet Source	<1%
7	Submitted to Higher Education Commission Pakistan Student Paper	<1%
8	Submitted to Jaypee University of Information Technology Student Paper	<1%
9	Jinlong Yang, Yong Huang. "Novel Colloidal Forming of Ceramics", Springer Science and Business Media LLC, 2020 Publication	<1%
10	Rheology of Filled Polymer Systems, 1999. Publication	<1%
11	Nawle, Anant C., Ashok V. Humbe, M.K. Babrekar, S.S. Deshmukh, and K.M. Jadhav. "Deposition, characterization, magnetic and optical properties of Zn doped CuFe2O4 thin films", Journal of Alloys and Compounds, 2016. Publication	<1%
12	Lecture Notes in Physics, 2002. Publication	<1%



19	"Particle Light Scattering Methods and Applications", Encyclopedia of Spectroscopy and Spectrometry, 2009 Publication	<1%
20	A. Sendil Kumar, K Ravinder Reddy, Anil K. Bhatnagar. "Magnetization and ESR studies of La 0.67 (Ca 1– x Mg x) 0.33 MnO 3 systems", Journal of Alloys and Compounds, 2015	<1%
21	M.H. Abdellatif, Claudia Innocenti, Ioannis Liakos, Alice Scarpellini, Sergio Marras, Marco Salerno. "Effect of Jahn-Teller distortion on the short range magnetic order in copper ferrite", Journal of Magnetism and Magnetic Materials, 2017 Publication	<1%
22	Quantitative EPR, 2010. Publication	<1%
23	run.unl.pt Internet Source	<1%
24	Yong Huang, Jinlong Yang. "Novel Colloidal Forming of Ceramics", Springer Nature, 2010 Publication	<1%
25	www.science.gov Internet Source	<1%
26	www.scitechnol.com Internet Source	<1%

27	link.springer.com Internet Source	<1%
28	Gadipelly Thirupathi, Rajender Singh. "Study of Magnetoviscosity of Ferromagnetic MnZn-Ferrite Ferrofluid", IEEE Transactions on Magnetics, 2015 Publication	<1%
29	Gupta, M "Mossbauer, magnetic and electric studies on mixed Rb-Zn ferrites prepared by solution combustion method", Materials Chemistry and Physics, 20111017 Publication	<1%
30	Submitted to North East Wales Institute of Higher Education Student Paper	<1%
31	tel.archives-ouvertes.fr Internet Source	<1%
32	Submitted to Pandit Deendayal Petroleum University Student Paper	<1%
33	Submitted to University of Hyderabad, Hyderabad Student Paper	<1%
34	iopscience.iop.org Internet Source	<1%
35	valmap.dfis.ull.es	

Exclude quotes On Exclude matches < 14 words

Exclude bibliography On

Magneto-viscosity of Paraffin Based Barium Ferrite Ferrofluid

Nisha Gautam, Gadipelly Thirupathi and Rajender Singh

School of Physics, University of Hyderabad, Central University P.O., Hyderabad, Telangana-500046, India

The ferrofluids synthesized from platelet magnets in liquid media are quite interesting due to their shape induced magnetic response. In the present work, the magneto-viscosity of Ba-ferrite, BaFe₁₂O₁₉ (BaM) ferrofluid is studied to understand the magnetic response of BaM platelet particles. The platelet particles were synthesized by hydrothermal method and coated with oleic acid. The X-ray diffraction data confirms the platelets consisting of BaM phase. The field emission scanning electron microscopy and transmission electron microscopy micrographs show hexagonal platelets of 3 to 5 nm thickness and 50 to 250 nm in size. The magnetization vs. magnetic field plot shows hard ferromagnetic behavior of the nanoparticles. The ferrofluid was synthesized by dispersing coated platelets in paraffin. The flow curves of the ferrofluid exhibit shear thinning with power law behavior in the presence of magnetic field. The yield stress values are determined by extrapolating shear stress vs. shear rate plots to zero shear rate at various applied magnetic field values using Hershel-Bulkley equation. The magneto-viscosity, η of the ferrofluid as a function of magnetic field is investigated at various shear rates. The η value increases with increase in magnetic field, reaches a maximum value and then saturates at higher fields. This trend is due to the alignment of platelet shaped magnetic particles along the direction of magnetic field at different shear rates. With increase in magnetic field, the interaction between the magnetic nanoparticles and their arrangement becomes stronger leading to stacked plate chain formation. This shows that the variation of magneto viscosity as a function of shear rate can be controlled by competition between flow field and the magnetic field.

Index Terms—Barium M-ferrite, Ferrofluid, Platelet nanoparticle, Rheological.

I. INTRODUCTION

BARIUM FERRITE (BaM) belongs to a large family of ferromagnetic oxides with a hexagonal close-packed structure. Barium ferrite can be used in permanent magnets due its hard ferromagnetic nature [1]. The study of ferrofluids consisting of platelet shaped magnetic nanoparticles is a new area of research activity due to their structural induced magnetic response. The ferrofluids are useful in applications such as retention of magnetic field, levitation of magnetic and non-magnetic objects, micro magnetics and catalysis associated with small particles, magnetic shielding etc. The most common applications of ferrofluids are in computers, loudspeakers, semiconductors, motion control, sensors etc.

The focus of the present work is on the study of magnetoviscosity of paraffin based BaM ferrofluid synthesized by using oleic acid coated ferromagnetic platelet particles. The behavior of the ferrofluid is similar to the plate shaped magnets dispersed in liquid crystal [2]-[3]. The magnetoviscosity of the ferrofluid is investigated considering the effects of flow field, magnetic field and interactions between the nanoparticles.

II. EXPERIMENTAL

The barium ferrite (BaFe₁₂O₁₉) platelet magnetic nanoparticles were synthesized by hydrothermal method in auto clave as described in ref. [4]. The metal nitrates with the mol ratio (Ba²⁺/Fe³⁺) = 1:4.5 were dissolved in deionized water and co-precipitated with NaOH. The solution was heated hydrothermally in auto clave at 250 °C for 10 hours. The resulting precipitate was washed with deionized water until the pH reached 7, and then dried at 100 °C. The barium-ferrite

Corresponding author: Rajender Singh (e-mail: rssp@uohyd.ernet.in, rsinghsp@gmail.com).

nanoparticles were coated with oleic acid to avoid the agglomeration and cluster formation and dispersed in paraffin to synthesis of Ba-ferrite ferrofluid [5]. The oleic acid adsorbed onto the nanoparticles' surfaces provides their colloidal stability in nonpolar liquids [6] [7]. The oleic acid coated nanoparticles are hydrophobic and can be suspended in nonpolar liquids to get relatively concentrated ferrofluids [8]. The stability of Ba-ferrite nanoparticles for different surfactants is explained in ref. [9]. The X-ray diffraction pattern was recorded using a Bruker powder diffractometer equipped with Cu-Ka source at room temperature to characterize the phases in the samples. The micrographs of the BaM nanoparticles were recorded using a CARL ZEISS field emission scanning electron microscope (FESEM) and FEI Tecnai G2S-Twin 200 kV transmission electron microscope (TEM). The magnetization measurements as a function of applied magnetic field were carried out using the Lakeshore vibrating sample magnetometer (VSM). The magnetorheological data was investigated using oscillatory and rotational Rheometer (Anton-Paar MCR 501) at 303 K. The measuring system was a 20 mm diameter parallel-plate geometry. The gap between the plates was 0.1 mm and rotational mode was used for all measurements. The Rheometer equipped with magnetic stage from Anton-Paar was used for the generation of magnetic field in the vertical direction.

III. RESULTS AND DISCUSSIONS

Figure 1 shows the X-ray diffraction (XRD) pattern of BaM nanoparticles. The XRD pattern indicates a single-phase hexagonal magnetoplumbite structure corresponding to BaFe₁₂O₁₉ with space group (P6₃/mmc) (No.194) referred from standard JCPDS data file. This phase is verified carefully and compared with similar work on the platelet particles of Baferrite [10]. The lattice parameters are 5.896, 5.896 and 23.835

Å. The proper selection of Fe/Ba ratio has helped in suppressing the intermediate phases, such as α - Fe₂O₃ and BaFe₂O₃. The XRD pattern consists of broad peaks and a few sharp peaks which are influenced by small sized particle's thickness similar to the work of other groups [4] [11] [12].

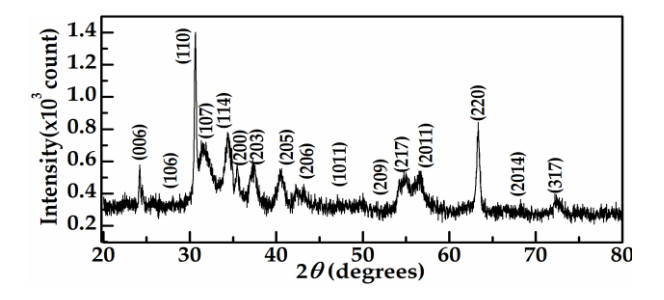


Fig. 1. X-ray diffraction pattern of barium ferrite platelet nanoparticles.

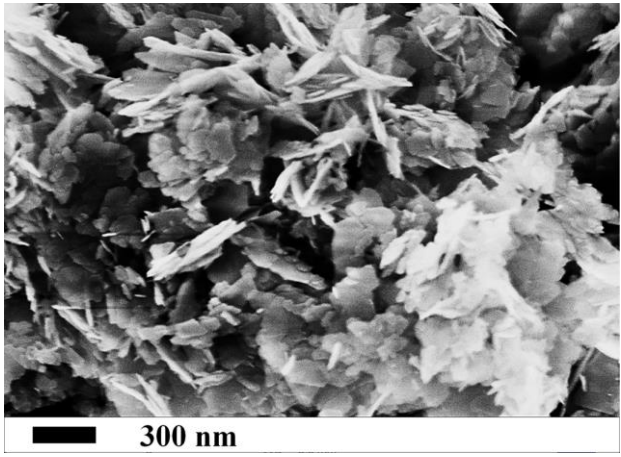


Fig. 2. FESEM micrograph of barium ferrite platelets.

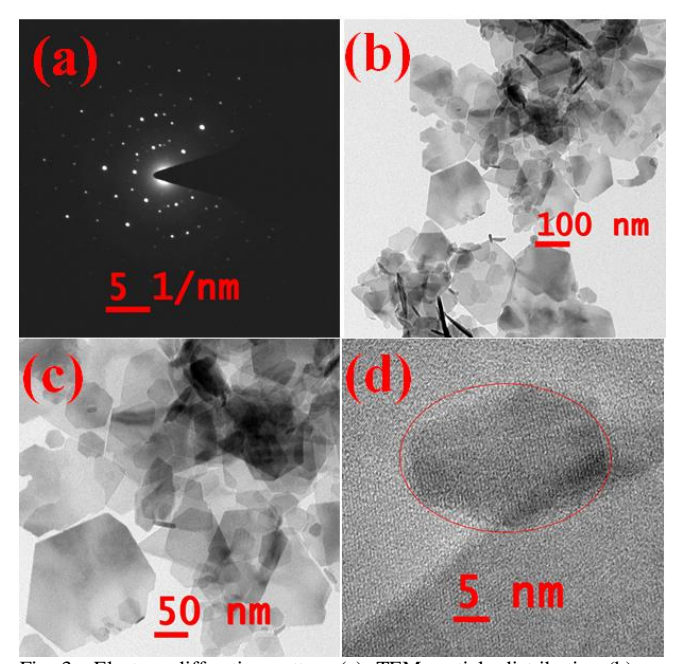


Fig. 3. Electron diffraction pattern (a), TEM particle distribution (b), HR TEM micrographs (c) of Ba-ferrite hexagonal platelet nanoparticles

Figure 2 shows hexagonal disks in the FESEM micrograph

of barium ferrite nanoparticles. The size, thickness and homogeneity of the hexagonal disks are dependent on the dosage of hydroxide ions used during the hydrothermal synthesis. The hydroxide ions are adsorbed on (001) surface and restrict the growth in (100) direction. So the formation of platelets depend on hydroxide ions dosage [3]. The FESEM micrograph in Fig 2 show that the particles are of nanometers size and plate shaped similar to reported by other group [13].

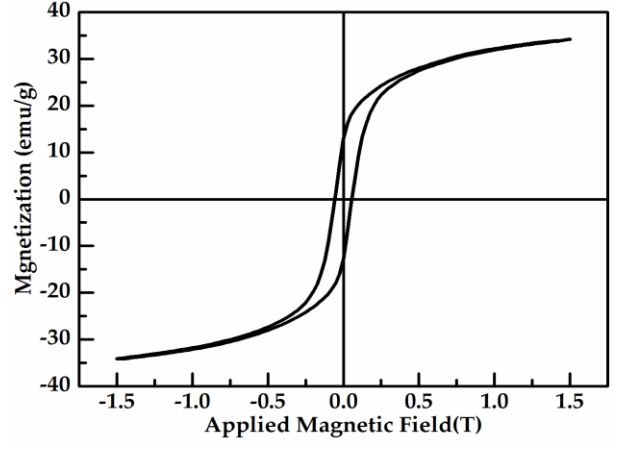


Fig. 4. Magnetization as a function of applied magnetic field of Baferrite nanoparticles.

The TEM micrographs of BaM nanoparticles are shown in Fig 3. The electronic diffraction pattern also reveal the hexagonal (BaFe $_{12}O_{19}$) phase structure of BaM nanoparticles (fig3a). It is clear from this image that the nanoparticles are almost hexagonal in structure [4] [8]. The micrographs show hexagonal platelets of 3 to 5 nm in thickness and 50 to 250 nm in size (fig3b - 3c). The planes shown in HR-TEM micrograph (fig.3d) correspond to hexagonal structure.

Fig. 4 shows the M-H hysteresis loop of BaM nanoparticles. The data reveals the hard ferromagnetic behavior with the saturation magnetization (M_s) of ~ 34 emu/g at applied field of 1.5 T at room temperature. The values of coercivity (H_c) and remanence (M_r) are 0.056 T and 12.6 emu/g respectively. Similar results are reported by other groups [14] [15].

Fig. 5 shows the viscosity plots of the BaM-ferrofluid with increasing and decreasing magnetic field in the range of 0 -1.3 T at shear rates of 10, 50 and 150 s⁻¹. Initially the viscosity increases rapidly with increase in magnetic field, followed by a cusp, and then it saturates with further increase in magnetic field. The magneto viscosity of ferromagnetic ferrofluids containing spherical particles is explained in our earlier work [5]. There was no maxima observed in the magneto viscosity plots of ferrofluid containing spherical particles. The alignment of magnetic nanoparticles takes place along the direction of magnetic field when the magnetic field is applied. With the increase in magnetic field, the interaction between the magnetic nanoparticles becomes stronger and leads them to form chains similar to what is reported in the case of ferromagnetic platelets dispersed in liquid crystals [16]. Increase in viscosity by increase in magnetic field is a consequence of formation and rearrangement of new structures (chain-like or drop-like structures), which are

destroyed by increase in shear rate leading to slower increase in viscosity with magnetic field [5] [17].

The following points are to be noted from the plots in Fig. 5. (1) The plate shaped particle are structurally more anisotropic than the other geometric shapes. (2) When the magnetic field is applied, the plate magnets will stack into long chains along the magnetic field due to high initial susceptibility. (3) With further increase in field, the viscosity should saturate, but a maxima is observed in the plots. (4) In the present case, the stacked plate magnets forming long chains show slow mechanical relaxations with flow fields. The stacked plates in the field direction will be saturated after certain field. But, instead of the viscosity increasing with magnetic field, the mechanical relaxation of the stacked plate structure takes place in the constant shear rate. As a result, the decrease in viscosity takes place giving rise to a maxima in the plot. (5) The slight increase in viscosity takes place with further increase in magnetic field. The observed viscosity plots are attributed to the competition between the applied magnetic field and the relaxation of the plate magnets due to shear rate. The maxima in the plot vanishes at lower shear rate due to the viscosity becoming purely magnetic.

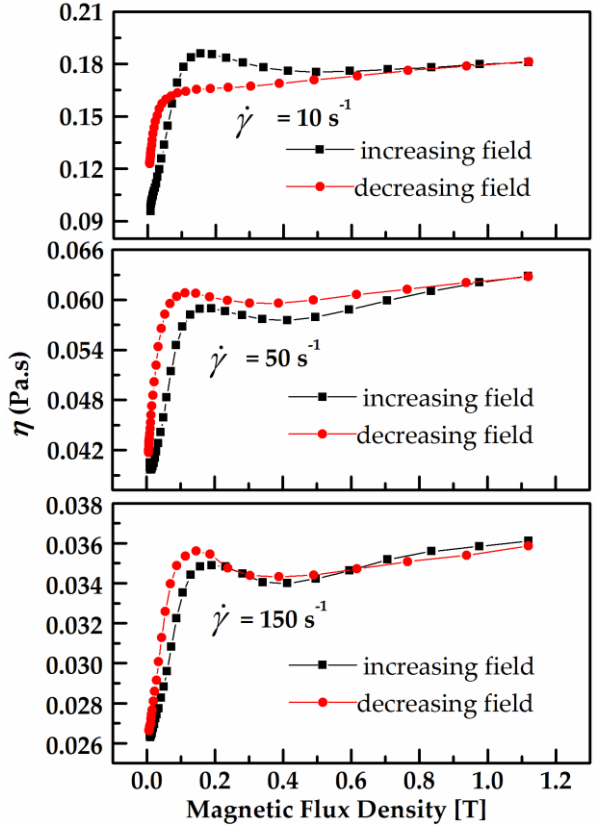


Fig. 5. Magneto viscosity plots at different shear rates of Ba-ferrite ferrofluid with increasing and decreasing magnetic field. Solid lines are guide to the eve.

Fig. 6 shows the Shear rate vs. viscosity (η) plots at some selected magnetic fields (H). These plots are fitted with following power law equation.

$$\eta = K\dot{\gamma}^{n-1} \tag{1}$$

Here K is the consistency coefficient and the exponent n is power law index. The K-value is between 0.2-0.3 for the

various magnetic fields values. The n-value decreases from 0.68 to 0.58 as magnetic field increases from 0.17 to 1.33 T. The small n-value indicates higher shear thinning at different applied magnetic field. The decrease in n-value with increase in applied field reveals that the viscosity is influenced more by applied magnetic field at low shear rates than at higher shear rates. This behavior at lower and higher shear rates appears due to the competition between the flow field and the applied magnetic field. In other words, the flow curves of Fig. 6 can be explained by the non-dimensional parameter, "Mason number". Similar to electro-rheological fluids, the Mason number (Ma) is the ratio of shear forces or hydrodynamic forces ($F_{\rm H}$) to the magnetic forces ($F_{\rm M}$) i.e. Ma= $F_{\rm H}/F_{\rm M}$.

The chain formation leads to increase in viscosity when the magnetic field is applied perpendicular to the shear flow. The chain length decreases with increase in Ma-value. The dominance of viscous forces over magnetic forces causes the chains to break. The viscosity as function of Mason number also follows the power law behaviour. There is a critical value of Mason number that determines the transition from magnetization to hydrodynamic control of the suspension structure [18]-[22].

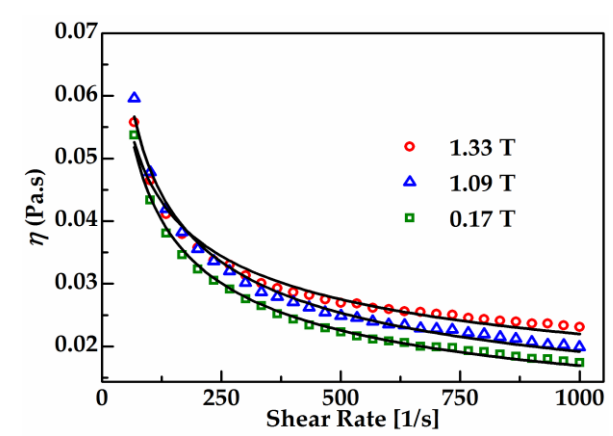


Fig. 6. Viscosity vs. shear rate at various magnetic fields of Ba-ferrite ferrofluid

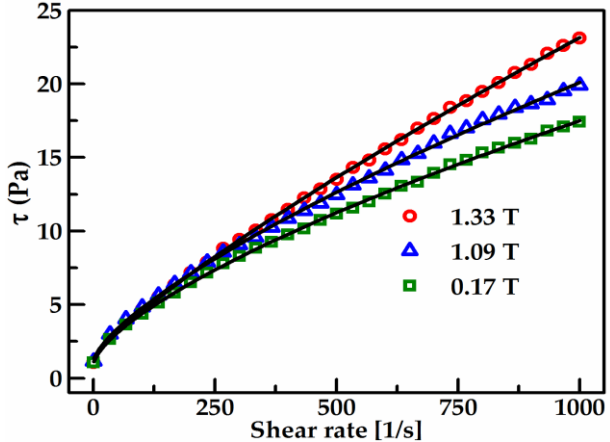


Fig. 7. Shear stress vs. shear rate at various magnetic fields of Baferrite ferrofluid.

Shear stress (τ) as a function of shear rate $(\dot{\gamma})$ plots are shown in fig. 7. Herschel-Bulkley (H-B) model combines the power law model with the yield stress in the following equation.

$$\tau = \tau_0 + K\dot{\gamma}^n \tag{2}$$

The yield stress (τ_0) values are determined by extrapolation of shear stress (τ) vs. shear rate plots with H-B model fit for zero field and applied magnetic fields [23]. The H-B model is derived from the power law by considering yield stress. Here the yield stress is positive, so the n-value is higher than that obtained from power law. The n-value is in the range 0.72 to 0.82, whereas the K-value is in the range 0.04 to 0.14 for various applied fields of 0.17, 1.09 and 1.33 T.

The flow curves show increase in yield stress from 0.796, 0.97, 1.21 and 1.28 Pa for applied field of 0, 0.17, 1.09 and 1.33T respectively. The monotonic increase in yield stress is observed with magnetic field. This is similar to reported by other groups [24].

IV. CONCLUSION

The BaM-ferrite ferrofluid was synthesized by dispersing oleic acid coated Ba-ferrite platelet nanoparticles synthesized by hydrothermal method and dispersed in paraffin. The BaFe₁₂O₁₉ is hexagonal structured hard ferrite belonged to the space group of P63/mmc. The reflections found in the XRD pattern indicates the single phase. This phase is verified carefully with similar work on the platelet particles of Ba-ferrite. The micrographs of FESEM and TEM confirmed the hexagonal platelet structure. The hard ferromagnetic behavior is observed in M(H) plot. The flow curves show the power law behavior at different applied magnetic fields. The magneto viscosity plots show different behavior compared to other ferrofluid reported in the literature due to shape induced magnetic response. The variation in magneto viscosity as a function of shear rate is controlled by competition between flow field and magnetic field.

ACKNOWLEDGEMENTS

NG is grateful for RGNF Fellowship by UGC, India.

REFERENCES

- [1] W. Zhao, "Synthesis of nonstoichiometric M-type barium ferrite nanobelt by spark plasma sintering method," *Chinese Science Bulletin*, vol. 50, no. 13, p. 1404, 2005.
- [2] N. A. Clark, "Soft-matter physics: Ferromagnetic ferrofluids," *Nature*, vol. 504, no. 7479, pp. 229–230, Dec. 2013.
- [3] L. Zhao, X. Lv, Y. Wei, C. Ma, and L. Zhao, "Hydrothermal synthesis of pure BaFe12O19 hexaferrite nanoplatelets under high alkaline system," *Journal of Magnetism and Magnetic Materials*, vol. 332, pp. 44–47, Apr. 2013.
- [4] D. Lisjak and M. Drofenik, "Chemical Substitution—An Alternative Strategy for Controlling the Particle Size of Barium Ferrite," *Crystal Growth & Design*, vol. 12, no. 11, pp. 5174–5179, Nov. 2012.
- [5] G. Thirupathi and R. Singh, "Study of Magneto-Viscosity of Ferromagnetic MnZn-Ferrite Ferrofluid," *IEEE Transactions on Magnetics*, vol. PP, no. 99, pp. 1–1, 2015.

- [6] R. Müller, R. Hiergeist, H. Steinmetz, N. Ayoub, M. Fujisaki, and W. Schüppel, "Barium hexaferrite ferrofluids preparation and physical properties," *Journal of Magnetism and Magnetic Materials*, vol. 201, no. 1–3, pp. 34–37, Jul. 1999.
- [7] R. Müller, R. Hiergeist, W. Gawalek, A. Hoell, and A. Wiedenmann, "Magnetic and structural investigations on barium hexaferrite ferrofluids," *Journal of magnetism and magnetic materials*, vol. 252, pp. 43–45, 2002.
- [8] D. Primc, D. Makovec, D. Lisjak, and M. Drofenik, "Hydrothermal synthesis of ultrafine barium hexaferrite nanoparticles and the preparation of their stable suspensions," *Nanotechnology*, vol. 20, no. 31, p. 315605, Aug. 2009.
- [9] R. B. Jotania, R. B. Khomane, A. S. Deshpande, C. C. Chauhan, and B. D. Kulkarni, "Physical and Magnetic Properties of Barium Calcium Hexaferrite Nano-particles Synthesized by Water-in-oil Reverse Micelle and Co-precipitation Techniques," *Journal of Scientific Research*, vol. 1, no. 1, Dec. 2008.
- [10] L. Jie, Z. Huai-Wu, L. Yuan-Xun, L. Ying-Li, and M. Yan-Bing, "The structural and magnetic properties of barium ferrite powders prepared by the sol?gel method," *Chinese Phys. B*, vol. 21, no. 1, p. 017501, Jan. 2012.
- [11] M. Drofenik, M. Kristl, A. Žnidaršič, D. Hanžel, and D. Lisjak, "Hydrothermal Synthesis of Ba-Hexaferrite Nanoparticles," *Journal of the American Ceramic Society*, vol. 90, no. 7, pp. 2057–2061, Jul. 2007.
- [12] D. Makovec, D. Primc, S. Šturm, A. Kodre, D. Hanžel, and M. Drofenik, "Structural properties of ultrafine Ba-hexaferrite nanoparticles," *Journal of Solid State Chemistry*, vol. 196, pp. 63–71, Dec. 2012.
- [13] D. B. Hovis and K. T. Faber, "Textured microstructures in barium hexaferrite by magnetic field assisted gelcasting and templated grain growth," *Scripta materialia*, vol. 44, no. 11, pp. 2525–2529, 2001.
- [14] S. Castro, M. Gayoso, J. Rivas, J. M. Greneche, J. Mira, and C. Rodríguez, "Structural and magnetic properties of barium hexaferrite nanostructured particles prepared by the combustion method," *Journal of Magnetism and Magnetic Materials*, vol. 152, no. 1–2, pp. 61–69, Jan. 1996.
- [15] S. H. Mahmood, G. H. Dushaq, I. Bsoul, M. Awawdeh, H. K. Juwhari, B. I. Lahlouh, and M. A. AlDamen, "Magnetic Properties and Hyperfine Interactions in M-Type BaFe12-2xMoxZnxO19 Hexaferrites," *Journal of Applied Mathematics and Physics*, vol. 02, no. 05, pp. 77–87, 2014.
- [16] A. Mertelj, D. Lisjak, M. Drofenik, and M. Čopič, "Ferromagnetism in suspensions of magnetic platelets in liquid crystal," *Nature*, vol. 504, no. 7479, pp. 237–241, Dec. 2013.
- [17] G. Thirupathi and R. Singh, "Magneto-viscosity of MnZn-ferrite ferrofluid," *Physica B: Condensed Matter*, vol. 448, pp. 346–348, Sep. 2014
- [18] Juan de Vincente, "Magnetorheology: a review," e-rheo-iba, vol.1, pp 1-18,2013.
- [19] S. G. Sherman, A. C. Becnel, and N. M. Wereley, "Relating Mason number to Bingham number in magnetorheological fluids," *Journal of Magnetism and Magnetic Materials*, vol. 380, pp. 98–104, Apr. 2015.
- [20] S. G. Sherman and N. M. Wereley, "Performance of magnetorheological fluids beyond the chain based shear limit," *Journal of Applied Physics*, vol. 115, no. 17, p. 17B523, May 2014.
- [21] R. Calhoun, A. Yadav, P. Phelan, A. Vuppu, A. Garcia, and M. Hayes, "Paramagnetic particles and mixing in micro-scale flows," *Lab on a Chip*, vol. 6, no. 2, p. 247, 2006.
- [22] K. Shah, R. V. Upadhyay, and V. K. Aswal, "Influence of large size magnetic particles on the magneto-viscous properties of ferrofluid," *Smart Materials and Structures*, vol. 21, no. 7, p. 075005, Jul. 2012.
- [23] J. P. Rich, P. S. Doyle, and G. H. McKinley, "Magnetorheology in an aging, yield stress matrix fluid," *Rheologica Acta*, vol. 51, no. 7, pp. 579–593, Jul. 2012.
- [24] S. S. Deshmukh and G. H. McKinley, "Rheological behavior of magnetorheological suspensions under shear, creep and large amplitude oscillatory shear (LAOS) flow," *Proc. XIV Int. Congr. on Rheology*, 2004.



Magneto-viscosity of hydrothermal synthesized Cu-Zn ferrite ferrofluids

Nisha Gautam, Gadipelly Thirupathi, and Rajender Singh School of Physics, University of Hyderabad, Central University P.O., Hyderabad, Telangana 500 046, India

(Presented 3 November 2016; received 23 September 2016; accepted 25 November 2016; published online 1 March 2017)

The paraffin based ferrofluids were synthesized using the oleic acid coated Cu-Zn ferrite (CZF) nanoparticles of compositions $Cu_{0.6}Zn_{0.4}Fe_2O_4$ (CZF1) and $Cu_{0.4}Zn_{0.6}Fe_2O_4$ (CZF2) synthesized by hydrothermal process. The transmission electron micrographs (TEM) show the cubic shape particles of 4 to 10 nm and 4 to 18 nm size for CZF1 and CZF2 respectively. The nanoparticles show superparamagnetic behaviour. The viscosity increases with increase in magnetic field due to the formation of long chains of magnetic nanoparticles in ferrofluid. At higher flow rate, the magnetic chains break into smaller units and arrange along the flow direction. The flow curves show power law behavior. The size of magnetic nanoparticles influences the magnetoviscosity of the ferrofluids. © 2017 Author(s). All article content, except where otherwise noted, is licensed under a Creative Commons Attribution (CC BY) license (http://creativecommons.org/licenses/by/4.0/). [http://dx.doi.org/10.1063/1.4977759]

I. INTRODUCTION

The ferrofluids find application in fields like magnetic devices, electronic packing, mechanical engineering, aerospace, bioengineering and biomedical treatment etc. The size, shape, functionality and magnetization of the nanoparticles play significant role in the biomedical fields such as hyperthermia and drug delivery. Synthesis of stable magnetic nanofluids is a technological challenge. The nanoparticles synthesized by hydrothermal heating process offers advantage over controlling the particle shape and size distribution. The process reduces the structural disorders such as oxygen deficiency which leads to increase in uniformity and stability. The evolution of microstructures in magnetic particles based ferrofluids affect the viscosity of ferrofluids with increase in magnetic field strength. In this work, we report the magneto viscosity of ferrofluids synthesized by using hydrothermally obtained nanoparticles. The results are discussed considering the effect of size, shape, magnetization, shear rate, interactions between nanoparticles and their aggregation. 1–4

II. EXPERIMENTAL

The nanoparticles with composition $Cu_{0.6}Zn_{0.4}Fe_2O_4$ (CZF1) and $Cu_{0.4}Zn_{0.6}Fe_2O_4$ (CZF2) were synthesized by hydrothermal process in autoclave at 250 °C for 12 hours following the method reported elsewhere.⁵ The CZF nanoparticles were coated with oleic acid to avoid the agglomeration and cluster formation and dispersed in paraffin for the synthesis of Cu-Zn ferrite ferrofluid.⁶ The respective volume ratio of CZF nanoparticles, oleic acid and paraffin was taken as 0.5:0.5:1 to synthesize the ferrofluids.

The X-ray diffraction patterns were recorded using a Bruker powder diffractometer equipped with $\text{Cu-K}\alpha$ source at room temperature to characterize the phases in the samples. The Rietveld refinement was performed using Full prof suite for XRD. The micrographs of the CZF nanoparticles were recorded using FEI Tecnai G2S-Twin 200 kV transmission electron microscope (TEM). The magnetization as a function of applied field was carried out using the Lakeshore vibrating sample magnetometer (VSM). The ferromagnetic resonance spectra were carried out using JEOL JES-FA200 ESR spectrometer at X-band (v = 9.12 GHz) in different static external field directions. The



magnetoviscometer data was investigated using oscillatory and rotational rheometer (Anton-Paar MCR 501) at 303 K. The measuring system was a 20 mm diameter parallel-plate geometry. The gap between the plates was 0.1 mm and rotational mode was used for all measurements. The rheometer equipped with magnetic stage from Anton-Paar was used for the generation of magnetic field in the vertical direction.

III. RESULTS AND DISCUSSION

Fig 1 a,b (left) shows the X-ray diffraction (XRD) patterns which are well fitted with two-phase structure using Rietveld analysis. The major phase is cubic spinel system with space group Fd-3 m and the minor phase is monoclinic crystal system (CuO-phase) with space group C12/c1. The CuO phase fraction is 0. 6% and 0.3% for CZF1 and CZF2 respectively. The average crystallite size of CZF nanoparticles with Zn-content of 40% and 60% are 7 and 31 nm respectively. The lattice parameter are 8.432(2) and 8.441(1) Å for CZF1 and CZF2 nanoparticles respectively. The CuO phase found to be less for high Zn-content in the CZF. The transmission electron micrographs (TEM) micrographs of CZF nanoparticles are shown in Fig. 1. The cubic shaped particles with size distribution of 4 to 10 nm and 4 to 18 nm for CZF1 and CZF2 respectively are observed. The zero corecivity is observed in magnetization plots (Fig. 1(top-right)) at 300 K with the magnetization value (M_s) at 1.5 T of 54.5 and 79.8 emu/g for nanoparticles with composition Cu_{0.6}Zn_{0.4}Fe₂O₄ and Cu_{0.4}Zn_{0.6}Fe₂O₄ respectively. The coating decreases the magnetization of the nanoparticles. The magnetization data of the coated nanoparticle of Cu_{0.4}Zn_{0.6}Fe₂O₄ shown by curve (c) indicates the decrease in magnetization from its original value of 79.8 emu/g to 46 emu/g at 1.5 T. The variation of magnetization of the uncoated nanoparticles is due to variation in the particle size and cation distribution within the nanoparticles. Fig. 1(bottom-right) shows the ferromagnetic resonance (FMR) spectra of CZF ferrofluids. The line shape of the resonance signal give information about the magnetic and electronic state of the paramagnetic centers present in the material.⁸ The resonance in CZF2 is at lower field compared to that in CZF1 ferrofluid. This indicates the magnetic response of CZF2 is more than that of CZF1 ferrofluid.

Fig. 2 (left) shows the magneto-viscosity hysteresis plots of CZF1 and CZF2 at shear rate $(\dot{\gamma})$ of 1 s⁻¹. The viscosity (η) of CZF2 ferrofluid is higher than that of CZF1 ferrofluid at various applied magnetic field. The magneto-viscosity is analogous to the magnetization as a function of magnetic

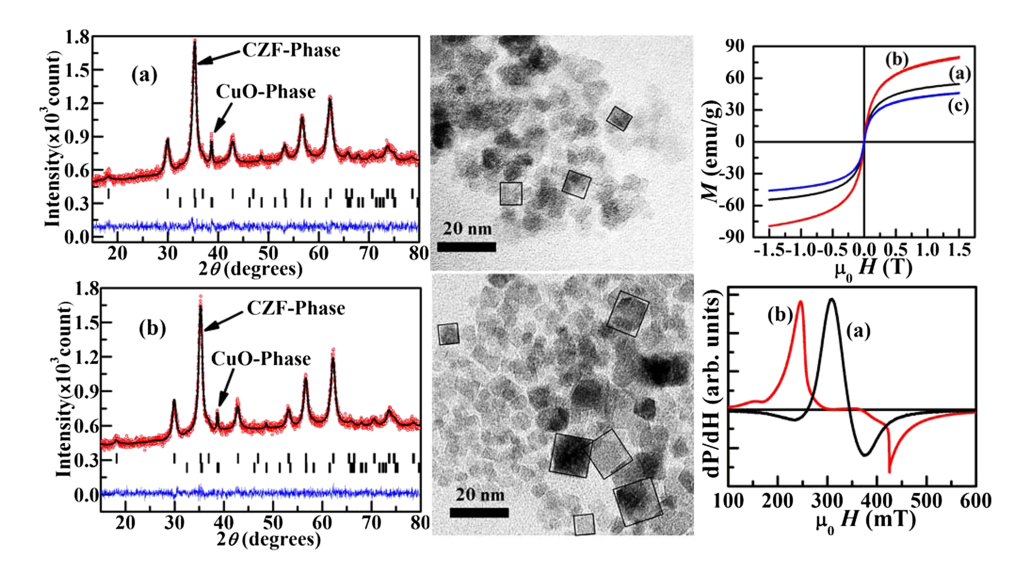


FIG. 1. X-ray diffraction pattern (left), TEM micrograph (middle), M vs H plot and FMR spectra at θ =0 (right) of the nanoparticles of Cu_{0.6}Zn_{0.4}Fe₂O₄ (a) and Cu_{0.4}Zn_{0.6}Fe₂O₄ (b) The curve (c) in M vs H plots is for coated nanoparticles of Cu_{0.4}Zn_{0.6}Fe₂O₄.

field. Here, this is related to the conversion of magnetic force on the nanoparticles into viscosity of the fluid.

For CZF1 ferrofluid, the viscosity increases rapidly followed by saturation in higher magnetic field region with hysteresis when the magnetic field is decreased gradually. The small sized magnetic nanoparticles can rotate and align easily in the magnetic field direction in the low applied magnetic field region. So the magneto-viscosity increases from 0.6 to 2.4 Pa-s in the low field region. As the magnetic field is increased, the formation of chains take place and the viscosity approaches saturation. In the higher field region, the viscosity hysteresis is due to breaking of formed chains (relaxation or lag) when the magnetic field is removed gradually. In low field region, the hysteresis is less due to the zero coercivity of the magnetic nanoparticles. The solid content by volume is about 25 % in the ferrofluid. The chain formation model, therefore is quite valid.

The magneto-viscosity plot of CZF2 does not saturate in the high field region and it shows more hysteresis compared to CZF1 as magnetic field is reduced. This indicates that high magnetic force is needed to rotate and align the nanoparticle suspension in the magnetic field direction. Magnetic field (>1.33 T) is required for the formation of long chains leading to saturation in viscosity. These results confirm that the size of magnetic nanoparticles influence the conversion of magnetic force on the nanoparticles into the magneto-viscosity of the ferrofluids.

Fig. 2 (middle) shows the flow curves of CZF1 and CZF2 at different magnetic fields. These curves show almost Newtonian behaviour in the absence of the magnetic field due to less disorder in the nanoparticles. When the magnetic field is applied, the abrupt change in viscosity is observed in low shear flow range and the viscosity is constant in the high flow region. The viscosity increases with increase in magnetic field as the magnetic force resists the flow. At higher flow rate, the magnetic chains break into smaller units and arrange along the flow direction. Apart from chain formation perpendicular to the flow, the lateral aggregation of chains (zippering) occurs in the ferrofluids which refers to the high shear thickening at higher magnetic fields. These plots are fitted with following power law equation: $\eta = K\dot{\gamma}^{n-1}$ Here K is the consistency coefficient and the exponent n is power law index. The *n*-value is in the range of 0.15 to 0.26 and 0.005 to 0.12 at different applied magnetic fields for CZF1 and CZF2. The power law behavior is due to the zippering of chains in the magnetic field. There is competition between hydrodynamic and magnetic forces acting in the ferrofluid which determines the behaviour of viscosity as a function of magnetic field. There is an equilibrium state when hydrodynamic and magnetic forces acting on the ferrofluid are equal. The viscosity variation with magnetic field is represented in terms of Mason number (Mn) which is the ratio of shear forces or hydrodynamic forces (F_H) to the magnetic forces (F_M) i.e. Ma= F_H/F_M . ^{10–13} The shear stress (τ) vs. shear rate plots (Fig. 2 (right)) at various applied magnetic field are as per predictions of Herschel-Bulkley (HB) model for non-Newtonian flow of fluids. ¹⁴ The variation observed in shear stress vs

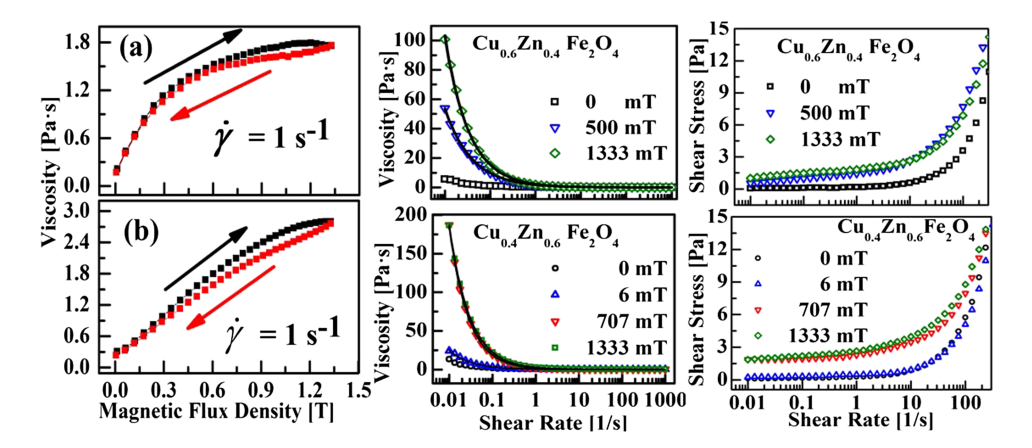


FIG. 2. Magneto viscosity hysteresis plots at the shear rate of 1 s⁻¹ (left), the flow curves at different magnetic fields (middle) and Shear stress vs. shear rate at various magnetic fields (right) of the ferrofluids of $Cu_{0.6}Zn_{0.4}Fe_2O_4$ (CZF1) (a) and $Cu_{0.4}Zn_{0.6}Fe_2O_4$ (CZF2) (b).

shear rate indicates that the torque cell in the rheometer is quite sensitive. It shows a resolution better than 0.3 Pa in shear stress measurements.

In conclusion, the size, shape and magnetic behaviour of the nanoparticles influence the magneto-viscosity of the synthesized ferrofluid.

ACKNOWLEDGMENTS

NG is grateful for the support under RGN Fellowship programme of UGC, India.

- ¹ A. Gangwar, S. K. Alla, M. Srivastava, S. S. Meena, E. V. Prasadrao, R. K. Mandal, S. M. Yusuf, and N. K. Prasad, J. Magn. Magn. Mater. 401, 559 (2016).
- ² M. Krishna Surendra, S. Annapoorani, E. B. Ansar, P. R. Harikrishna Varma, and M. S. Ramachandra Rao, J. Nanoparticle Res. 16 (2014).
- ³ J. Lu, S. Yang, K. M. Ng, C.-H. Su, C.-S. Yeh, Y.-N. Wu, and D.-B. Shieh, Nanotechnology 17, 5812 (2006).
- ⁴G. Zabow, S. Dodd, J. Moreland, and A. Koretsky, Nature **453**, 1058 (2008).
- ⁵ K. Nejati and R. Zabihi, Chem. Cent. J. **6**, 1 (2012).
- ⁶G. Wang, Y. Ma, X. Dong, Y. Tong, L. Zhang, J. Mu, Y. Bai, J. Hou, H. Che, and X. Zhang, Appl. Surf. Sci. **357**, 2131 (2015)
- ⁷N. Gautam, G. Thirupathi, and R. Singh, IEEE Trans.on Magnetics **52**(7), 4600204 (2016).
- ⁸ S. Kamali, M. Pouryazdan, M. Ghafari, M. Itou, M. Rahman, P. Stroeve, H. Hahn, and Y. Sakurai, J. Magn. Magn. Mater. 404, 143 (2016).
- ⁹ N. S. Mousavi, S. D. Khapli, and S. Kumar, J. Appl. Phys. **117**, 103907 (2015).
- ¹⁰ S. G. Sherman, A. C. Becnel, and N. M. Wereley, J. Magn. Magn. Mater. **380**, 98 (2015).
- ¹¹ J. de Vicente, M. T. López-López, J. D. G. Durán, and F. González-Caballero, Rheol. Acta 44, 94 (2004).
- ¹² D. Faivre and M. Bennet, Nature **535**, 235 (2016).
- ¹³ S. Odenbach and K. Raj, Magnetohydrodynamics **36**, 312 (2000).
- ¹⁴ W. H. Herschel and R. Bulkley, "Konsistenzmessungen von Gummi-Benzollösungen," Kolloid Zeitschrift 39, 291 (1926).

Magneto-viscosity of Stable colloidal solutions of Barium-Strontium Hexaferrite Ferrofluid

Nisha Gautam and Rajender Singh*

School of Physics, University of Hyderabad, Central University P.O., Hyderabad, Telangana-500046, India

Abstract We report the synthesis of ferrofluids (FF) based on Ba_{0.95}Sr_{0.05}Fe₁₂O₁₉ (BSM) ferrite platelet shaped nanoparticles. The structural and magnetic properties were studied to get the information about the particle shape and saturation magnetization. The magneto-viscosity measurements were undertaken on ferrofluids consisting of nanoparticles dispersed in water and silicone oil. The rheological properties of BSM ferrofluids were characterized as a function of field strength and shear rate. It is observed that the viscosity of both type of ferrofluids increases with increase in field strength. However, different hysteresis behavior is observed with different colloids in the magneto-viscosity plots at 1 and 10 s⁻¹ shear rates respectively. The power law behavior is observed at different fields. These magneto-viscosity properties are useful in magneto mechanical and heat absorber applications.

Keywords: Ba-Sr ferrite, platelets, ferrofluids, structural and magneto-viscosity properties

• Corresponding author: Prof R. Singh, email: rsinghsp@gmail.com

Introduction

Barium and strontium ferrites known as M-type magnetically hard ferrites with hexagonal crystal structures [1]. These ferrites show high coercive force, large magneto crystalline anisotropy, large saturation magnetization and mechanical resilience because of which they are demanded in various application such as multiple- state memory elements, magnetic bearings, magneto-therapy, purification and sensors etc [2]. Ferrofluids are the stable suspension of magnetic nanoparticle dispersed in suitable liquid solvent. Generally the ferrofluids are involved in various applications such as semiconductor, clutches, loudspeakers, sensors, micro-magnetic anti-seismic drug delivery, hyperthermia treatment etc. [3]. The behavior of plate shaped magnets dispersed in liquid crystals have also been reported in view of their applications in display devices [4]. Various methods have been introduced to improve the stability of ferrofluid considering their structural and magnetic response. In our earlier works we reported magnetoviscosity of paraffin based cubic shaped Cu-Zn nanoparticle ferrite ferrofluid [5]. We also reported magneto-viscosity of paraffin based Ba ferrite ferrofluids. These ferrofluids were synthesized by dispersing hexagonal shaped nanoplatelets of Ba ferrite of size (50-250 nm) in paraffin [12]. In the present work we report the magneto-viscosity of ferrofluids synthesized by dispersing BaSr ferrite hexagonal platelets shaped nanoparticles of size 20-25 nm in two different solvents i.e. water and silicone oil. This study is useful in understanding the effect of platelet size and nature of solvent on the magneto-viscosity of ferrofluids. It is found that the magneto-viscosity behavior of these ferrofluids is different from the behavior observed in our earlier work.

Experimental

The nanoparticles of hexaferrite of compositions $Ba_{0.95}Sr_{0.05}Fe_{12}O_{19}$ (BSM) were synthesized by hydrothermal process in autoclave at 210 °C for 20 hrs as described in our work [5]. The BSM nanoparticles were coated with DBSA (4-Dodecylbenzenesulfonic acid) and oleic acid to avoid the agglomeration and cluster formation and dispersed in water and silicone oil for the synthesis of ferrofluids. The respective volume ratio of BSM nanoparticles, DBSA/oleic acid and water/ silicone oil was taken as 0.5:0.5:1. The X-Ray diffraction (XRD) pattern of the BSM sample was recorded using powder X-ray diffractometer (Bruker) with Cu- k_{α} radiation. The micrograph of the BSM nanoparticles were recorded using a CARL ZEISS field emission scanning electron microscope and FEI Tecnai G2S-Twin 200 kV

transmission electron microscope (TEM). The distribution of particles and zeta potential were recorded using LitisizerTM 500 particle size analyzer (Anton Paar). For measuring the distribution and surface charge of BSM platelets, a very thin fluid (0.05% in volume) was used in water media. The magnetization as a function of applied field measurements were carried out using physical property measurement system (PPMS). The magneto-rheological data was investigated using oscillatory and rotational Rheometer (Anton-Paar MCR 501) at 303 K. The rheology measuring system was a 20 mm diameter parallel-plate geometry with 0.1 mm gap used in rotational mode. The Rheometer equipped with magnetic stage was used for the generation of magnetic field in the vertical direction.

Results and Discussion

X ray diffraction data of the synthesized nanocrystalline ferrite Ba_{0.95}Sr_{0.05}Fe₁₂O₁₉ (BSM) shown in fig 1 confirms the formation of hexagonal structure with space group (P63/mmc) as per standard JCPDS data file [6]. The lattice parameters are 5.896, 5.896 and 23.835 Å.

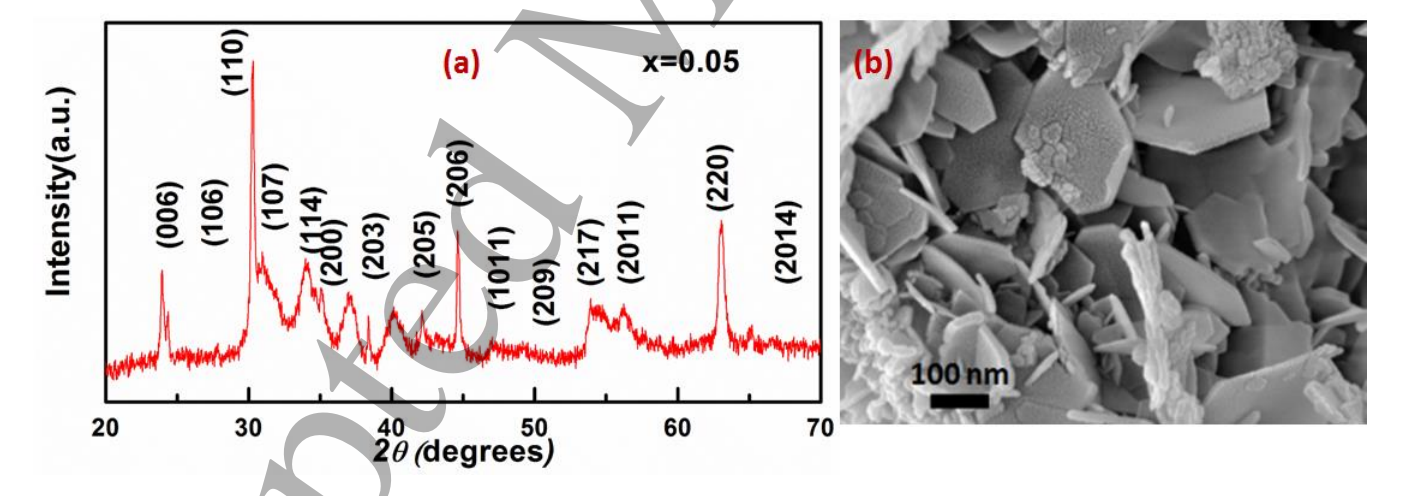


Figure 1. X-ray diffraction pattern (a), FESEM micrograph(b) of BSM nanoparticles respectively.

The FESEM micrograph for the synthesied nanoparticles is shown in Fig 1(b). It is observed that the nanoparticles are hexagonal disk shaped. The grains are homogenously distributed in well crystallized irregular shape [7].

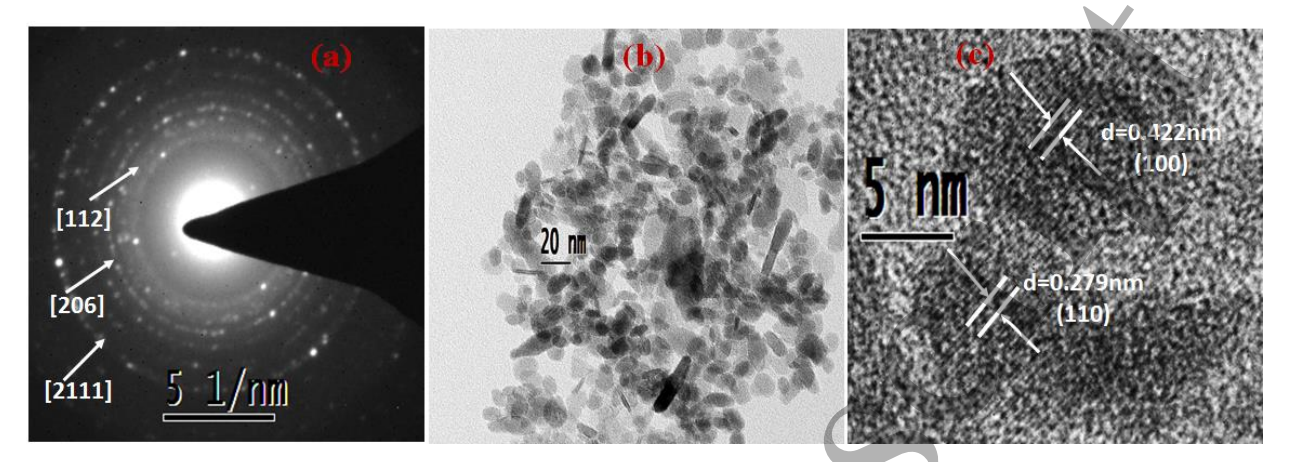


Figure 2. Electron diffraction pattern (a), TEM particle distribution (b), HR TEM micrograph (c), of BSM nanoparticles respectively.

TEM micrographs of BSM nanoparticles are shown in Figure 2. The electronic diffraction pattern (fig 2 (a)) confirmed the hexagonal structure [8]. The particle are hexagonal shaped with thickness of 3 to 5 nm and size distribution of 20-25 nm (fig 2(b)). The HR-TEM micrograph corresponds to hexagonal structure (fig2(c)).

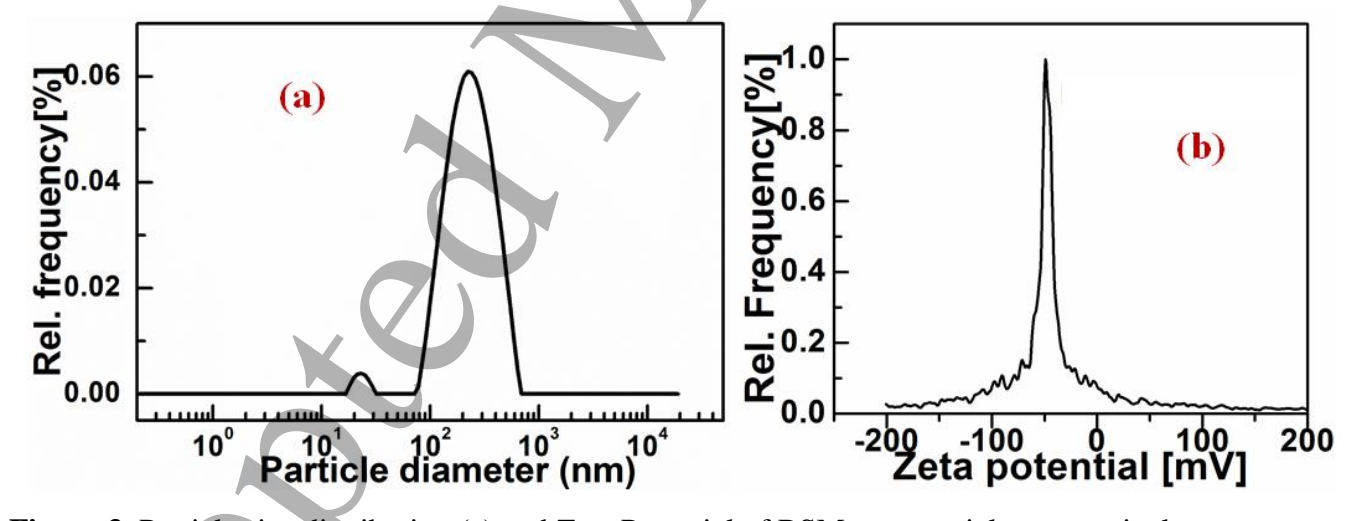


Figure 3. Particle size distribution (c) and Zeta Potential of BSM nanoparticles respectively.

Figure 3(a) and (b) show the hydrodynamic particle size distribution and zeta potential of BSM ferrofluid respectively. There are two distributions observed in particle size of the BSM platelets. The hydrodynamic size (Fig3 (a)) is recorded as 120 nm. The particle size analyzer distributions is high compared to TEM distribution because in the water based media the magnetic nanoparticles are forming clusters. The zeta

potential known as the surface collector charge from variation of particle zeta potential and heterogeneous distribution of surface charge. The characteristic of zeta potential of BSM nanoparticles in water is investigated. The mean zeta potential (Fig3 (b)) is found to be -49 mV for water based ferrofluid, indicating good stability of BSM platelets in water media. The zeta potential of particles may be changed by changing the ionic strength of a solution. An increase in ionic strength can compress the electric double layer and thereby decrease the zeta potential while a decrease of ionic strength can increase the zeta potential.

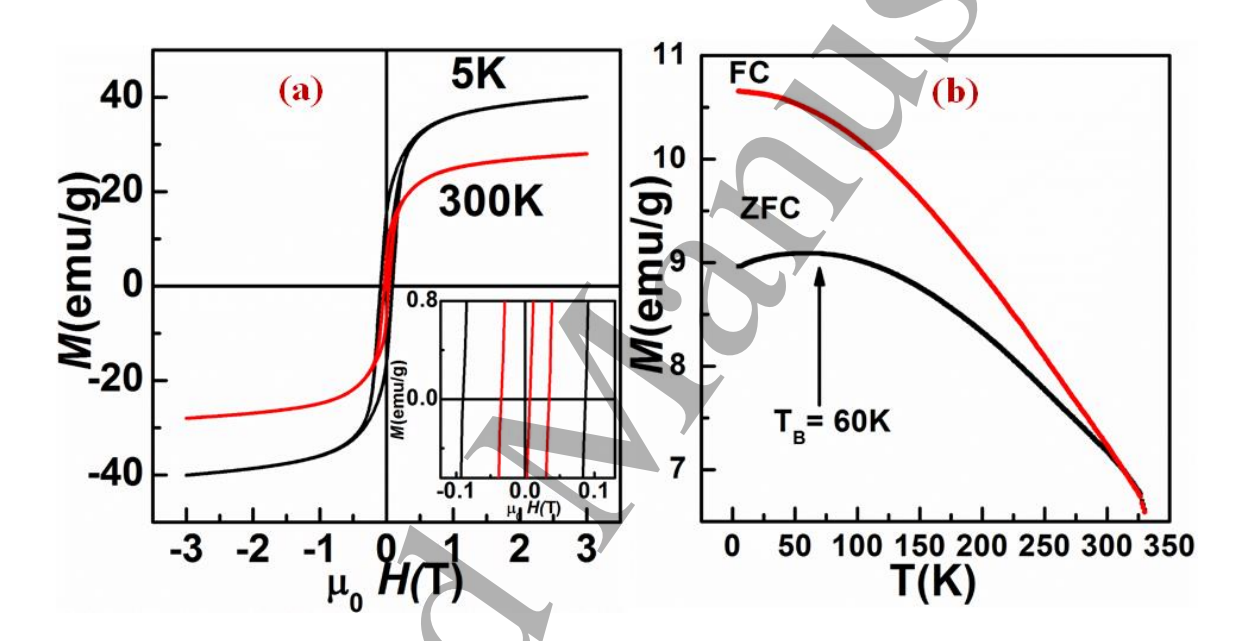


Figure 4. Magnetization as a function of applied magnetic field of BSM nanoparticles.

Figure 4 shows the M(H) plots for BSM nanoparticles. The data reveals the hard ferromagnetic behavior with the saturation magnetization (Ms) of \sim 28emu/g and 40 emu/g at 300 K and 5 K respectively which is close to reported by other groups [9]. The coercivity (Hc) values are 348 Oe and 890 Oe and remanence values (Mr) are 6 emu/g and 15 emu/g at 300 K and 5 K respectively.

Figure 3(b) shows the temperature dependence of magnetization for BSM nanoparticles in the temperature range of 2 to 350 K in applied magnetic field of 100 Oe under zero-field cooling (ZFC) and field-cooling (FC) modes. In ZFC mode, the BSM ferrite sample cooled from 375 K down to 2 K in the absence of magnetic field, then a magnetic field of 100 Oe was applied and the magnetization

measurement was made with increase in temperature [10]. Whereas, in FC mode the sample was cooled from 375 K down to 2 K in the presence of magnetic field and then magnetization measurement was recorded with increase in temperature [11]. The magnetization increases for both FC and ZFC modes with decrease in temperature and at high temperatures both follow the same path. In ZFC mode the magnetization of the sample increases with decrease in temperature. In the presence of a magnetic field if the nanoparticles are cooled to a very low temperature, the magnetization direction of each particle is frozen in the field direction. At blocking temperature (T_B) the ZFC magnetization will be maximum at which the relaxation time equals the time scale of the magnetization measurements. By decreasing the temperature further, while the FC curve continues to increase, the ZFC curve reaches a maximum magnetization at 230 K. The separation between the ZFC and the FC curves gives the information about the non-equilibrium magnetization.

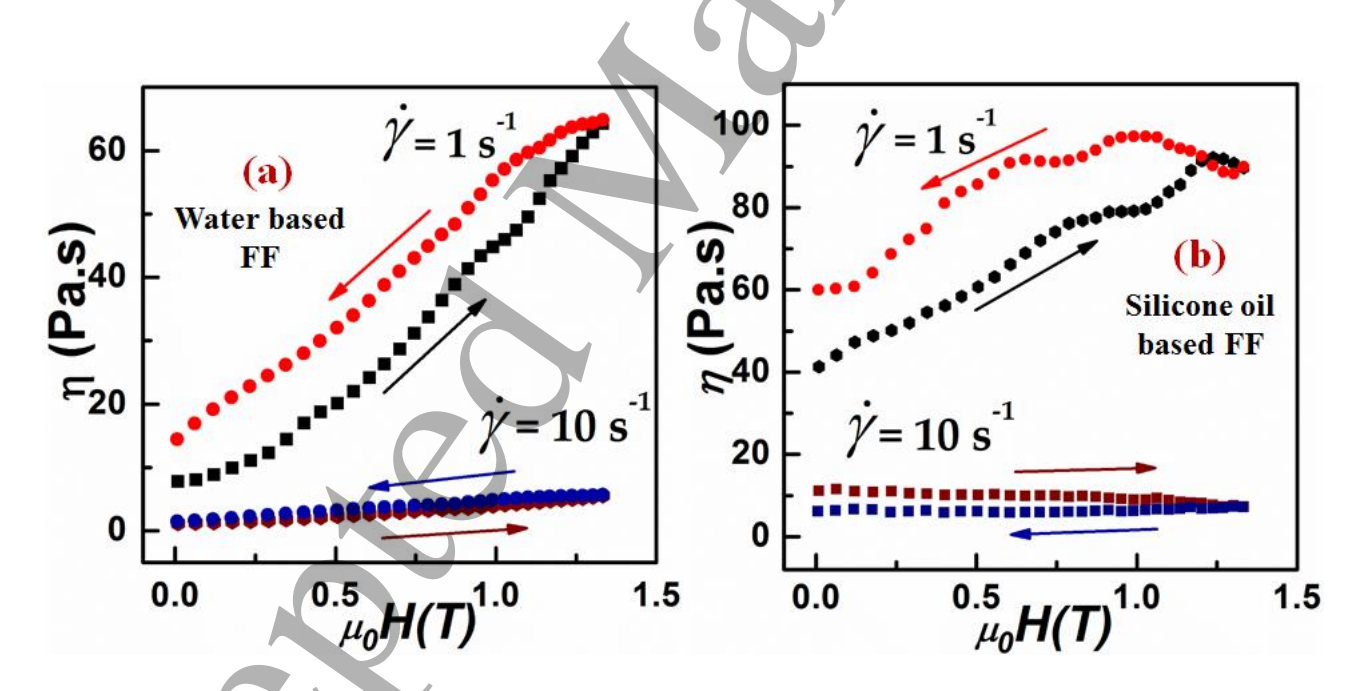


Figure 5. Magneto viscosity plots at different shear rates of BSM ferrofluid with increasing and decreasing magnetic field for water based FF and silicone oil based FF at 1 and 10 s⁻¹ respectively.

Figure 5 shows the measurements carried out to investigate the shear dependence of magneto-viscosity. The experiments were performed at shear rate of 1s⁻¹ and 10s⁻¹. The magnetic field strength ranged from 0

to 1.33T. The ferrofluids were maintained at 25 °C for all measurements. In the case of water based FF the viscosity increases rapidly from 20 to 68 P.s and does not saturate at the high fields at shear rate 1 s⁻¹ .Very small increase in viscosity with increase in magnetic field is observed at shear rate of 10 s⁻¹. No saturation in viscosity with increase in magnetic field is observed at both the shear rates. Whereas in the case of silicone oil based FF, slight saturation in viscosity with increase in magnetic field is observed above 1.25 T of magnetic field at shear rate of 10 s⁻¹. There is no significant change in viscosity with magnetic field at shear rate of 10 s⁻¹. A comparison of the magneto-viscosity of BSM FF shows that : (1) the viscosity is high in silicon based FF compared to water based FF. 2. The viscosity increases linearly with increase in magnetic field. (2) The rate of increase in viscosity with field is higher in water based FF compared to silicon oil based FF. 3. At shear rate of 1 s⁻¹ the viscosity is high as compared to at 10 s⁻¹ because at low shear rate the magnetic force dominates the hydrodynamic force which is the main cause for chain formation. 4. The shear force and magnetic force become comparable at higher shear rate and magnetic force contain the chain together. When the field is applied the alignment of magnetic platelets takes place towards the field direction and chain formation takes place [12]. The chain formation leads to increase in viscosity with increase in magnetic field [12]. These chains break at high shear rate, leading to very small increase in viscosity with increase in magnetic field at shear rate of 10 s⁻¹. When the field is removed, the chains are broken and platelets try to come back to their original position and give rise to hysteresis in viscosity vs field plot. The linear increase in viscosity with no saturation with increase in magnetic field is a new result which is not observed in our earlier studies [5,12]. This may be due to smaller size of the platelet nanoparticles in the present ferrofluids. The FF based on cubic shaped nano particle show saturation in viscosity at high magnetic field [5]. Whereas FF based on disc shaped nanoparticles of size 50-250 nm show saturation in viscosity at very low value of magnetic field [12].

The flow curves (shear rate vs viscosity) of BSM FF are shown in Figure 6. The plots are fitted with the power law equation $\eta = K\dot{\gamma}^{n-1}$. Here the K is consistency and n is power law index. The K value is between 17- 27 for various magnetic field values. The n- values are 0.55 to 0.59 as the field increases from 0.02 to 1.33 T. The small n- value indicates higher shear thinning at different fields.

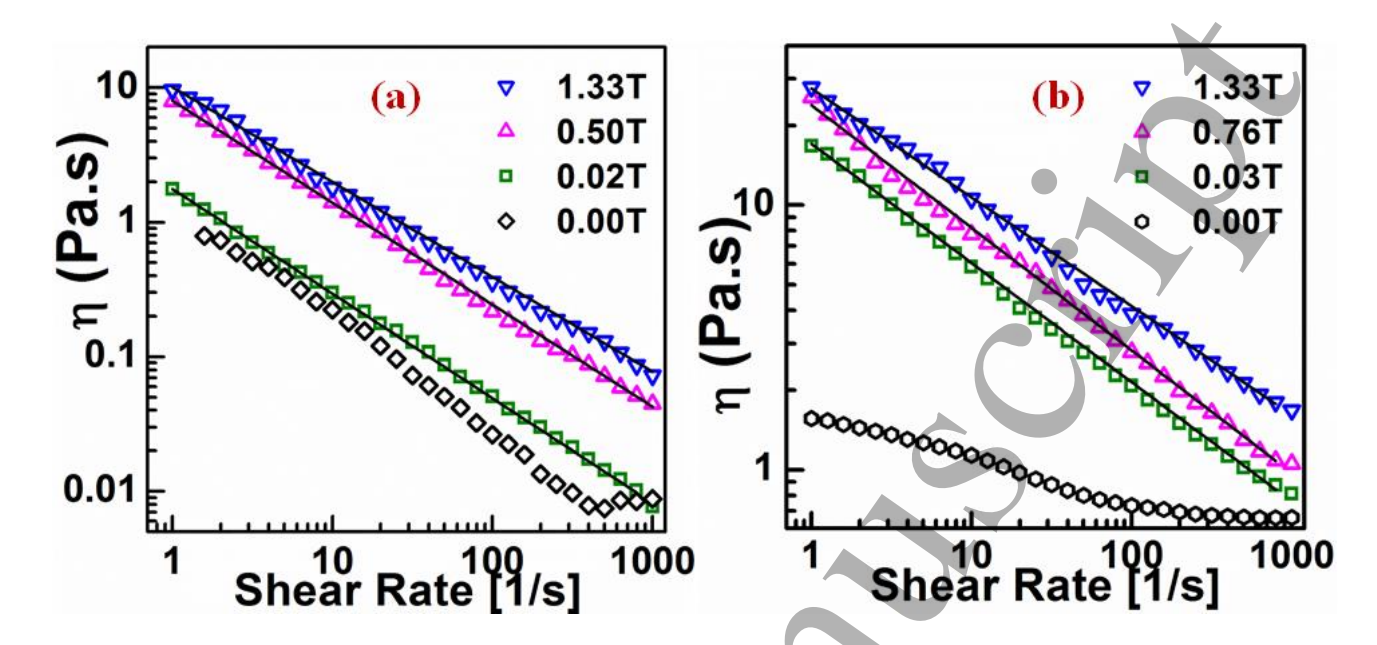


Figure 6 shows the Shear rate vs. viscosity (η) plots at some selected magnetic fields (H). These plots are fitted with following power law equation.

The power law behavior is due to the zippering of chains in magnetic field [5]. At different shear rate there is competition between the hydrodynamic forces (FH) and magnetic forces (FH) characterized by Mason number (Mn= FH/FM) [14]. The information regarding breaking and reformation of chains in the fluid can be determined by Mn value.

Conclusion

Ferrofluids (FF) based on Ba_{0.95}Sr_{0.05}Fe₁₂O₁₉ (BSM) ferrite platelet shaped nanoparticles were synthesized.. The magneto-viscosity measurements show that the viscosity increases in silicone oil based FF as compared to the water based FF. The flow curves show the power law behavior. Due to smaller size of platelets in the present ferrofluids, magneto-viscosity plots show different behavior as compared to other ferrofluids. The synthesized ferrofluids are useful for heat absorber and magneto-mechanical application.

Acknowledgements

Nisha Gautam is grateful for RGNF Fellowship by UGC, India

References

- 1. Bilel Grindia,b, Amor BenAlib, Cesar Magend, Guillaume Viau 2018 M-SrFe12O19 and ferrihydrite-like ultrathin nanoplatelets as building blocks for permanent magnets: HAADF-STEM study and magnetic properties *Journal of Solid State Chemistry* **264** 124–133
- 2. Esmail Kiani, Amir S.H. Rozatian, Mohammad H. Yousefi 2014 Structural, magnetic and microwave absorption properties of SrFe122x(Mn0.5Cd0.5Zr)xO19 ferrite *Journal of Magnetism and Magnetic Materials* **361** 25–2926
- 3. K.S. Martirosyana, E. Galstyanb, S.M. Hossainc, Yi-Ju Wangc, D. Litvinov 2011 Barium hexaferrite nanoparticles: Synthesis and magnetic properties *Materials Science and Engineering B* **176** 8–13
- 4. Alenka Mertelj, Darja Lisjak, Miha Drofenik & Martin Copic 2013 Ferromagnetism in suspensions of magnetic platelets in liquid crystal *Nature* **504** 237-241
- 5. Nisha Gautam, Gadipelly Thirupathi and Rajender Singh 2017 Magneto-viscosity of hydrothermal synthesized Cu-Zn ferrite ferrofluids AIP Advances **7** 056727
- 6. S. Shooshtary Veisia, M. Yousefia, M. M. Aminib, A. R. Shakeric, M. Bagherzadehd 2018 Magnetic and microwave absorption properties of Cu/Zr doped M-type Ba/Sr hexaferrites prepared via sol-gel auto-combustion method *Journal of Alloys and Compounds* S0925-8388
- 7. Jianxing Liu and Xiangxin Xue 2016 Morphology and magnetic properties of SrFe12O19 synthesized with oxidized scale *Materials Letters* **164** 579-582
- 8. D Prime, D Makovec, D Lisjak and M Drofenik 2009 Hydrothermal synthesis of ultrafine barium hexaferrite nanoparticles and the preparation of their stable suspensions *Nanotechnology* **20** 315605(9pp)
- 9. M.M. Rashad and I.A. Ibrahim 2011 Improvement of the magnetic properties of barium hexaferrite nanopowders using modified co-precipitation method *Journal of Magnetism and Magnetic Materials* **323** 2158–2164
- 10. Noel A. Clark 2013 Ferromagnetic ferrofluids Nature 504 229-230
- 11. Liang Zhao, Xiaoxia Lv, Yanshi Wei, Chong Ma, Lijun Zhao 2013 Hydrothermal synthesis of pure BaFe12O19 hexaferrite nanoplatelets under high alkaline system *Journal of Magnetism and Magnetic Materials* **332** 44–47
- 12. Nisha Gautam, Gadipelly Thirupathi and Rajender Singh 2016 Magneto-viscosity of Paraffin Based Barium Ferrite Ferrofluid *IEEE Transactions on Magnetics* **52** (7); 1-1

- 13. S. Masoud Hosseini, Alireza Fazlali, E. Ghasemi, H. Ahmadi Moghaddam, M. Salehi 2010 Rheological properties of a g-Fe2O3 paraffin-based ferrofluid *Journal of Magnetism and Magnetic Materials* **322** 3792–3796
- 14. Stephen G. Sherman, Andrew C. Becnel, Norman M. Wereley 2015 Relating Mason number to Bingham number in magnetorheological fluids *Journal of Magnetism and Magnetic Materials* 380 98–104